Organic thin films: a comparison of their electrical and gas sensitivity

R Casalini

ORGANIC THIN FILMS: A COMPARISON OF THEIR ELECTRICAL AND GAS SENSITIVITY

by

R.Casalini

A Thesis submitted in partial fulfilment
of the requirements for the degree of PhD

School of Engineering
University of Durham
1999

DECLARATION

I hereby declare that the work carried out in this thesis has not been previously submitted for any degree and is not currently being submitted in candidature for any other degree.

Signed.....
Candidate

The work in this thesis was carried out by the candidate

Signed.....
Director of Studies

Signed.....
Candidate

Acknowledgments

I have to thank many people for helping me during these years spent in Durham.

Regarding my scientific project I must first thank my supervisor, Prof. Mike Petty, who could always find the time to have helpful discussions and to encourage me. Then I would like to thank all the other members of the Molecular Electronics group that helped to make my work more enjoyable. In particular, Dr.C.Pearson for helping me with the technical problems encountered during my work and Dr.L.M.Goldenberg that taught me on the LB technique and helped to improve my tennis skills.

I also would like to thank all the people that with their friendship, helped me to have an enjoyable time in Durham. Among them (in random order) Jenifer, Eugenia, Bianca, Nomsa, J.G.Jung, Sabine, Karima, Carlos, Marcos, Simone, Celine and many others.

Finally, I thank the School of Engineering at the University of Durham for providing research funding.

Abstract

This thesis presents a study of the electrical properties and gas sensitivity of thin films of four different organic materials. These are: (i) Langmuir-Blodgett (LB) films of tetrabutylammonium Ni(dmit)$_2$ complex (Bu_4-Ni(dmit)$_2$ complex) mixed with tricosanoic acid (TA); (ii) thin films of polypyrrole (PPy) mixed with palmitic acid (PA) obtained using the LB technique followed by two solid state reactions; (iii) cast films of polycyanopropylmethylsiloxane (PCMS); and (iv) LB films of a co-ordination polymer 5,5´ methylenebis (N-hexadecylsalicydeneamine) (MBSH) (poly(CuMBSH)).

LB films of (Bu_4-Ni(dmit)$_2$ complex)/TA were characterised by electrical measurements (AC in the frequency range 10^2-10^6 Hz) at room temperature. For the other three types of films, characterisation of the structure and electrical behaviour (DC and AC in the frequency range 10^2-10^6 Hz) on varying the temperature (in the range 90 - 298 K) and during the exposure to benzene, ethanol, acetonitrile and water (concentrations in the range 10^2 - 10^5 ppm) was undertaken.

During exposure to vapours, reversible changes in the electrical properties of the films were observed. The electrical behaviour and the changes during exposure to vapours were interpreted in terms of models in the literature, assuming a bulk dissolution of the vapours in the organic films. In all cases an 'anomalous' response to water was observed. For poly(CuMBSH), this effect was interpreted in terms of a Low Frequency Dispersion.

The device characteristics for gas sensing applications are also discussed. Estimated minimum detectable concentrations were between 1-100 ppm for the three organic solvent vapours. Moreover, it is shown that the frequency behaviour for the admittance changes of the PCMS and poly(CuMBSH) devices could be exploited for the improvement of the sensitivity of a single device. The unique response of all the films to water vapour could be useful for its discrimination.

CONTENTS

Chapter 1

INTRODUCTION

The detection of chemical vapours, both in the workplace and in the environment, has been growing in importance in recent years. Exposure to certain chemicals has been related to the incidence of disease, which has led to legislation on exposure limits in many countries. Gas sensors have also been developed to monitor the quality of food, drinks and other industrial products. Problems in the development of these devices include poor sensitivity to low gas concentrations, cross-sensitivity to different gases and incomplete reversibility of the response.

Electrical impedance spectroscopy is a relatively simple and sensitive method for detecting the presence of gases and vapours. Many interaction mechanisms influence the permittivity of a material and the changes are generally frequency dependent. Impedance data collected at various frequencies can be used with pattern-recognition software or to train a neural network, increasing the selectivity of the single-element sensor [1]. However, before practical devices can be produced, it is important to understand fully the effects of the vapour on the electrical properties of the sensing material.

Organic compounds have been used successfully for gas sensing. An advantage of these materials is the wide range of physical properties obtainable by manipulating their chemical structures. Such features have been exploited in the realisation of arrays of different sensitive materials (electronic 'nose') [2-4].

In this thesis, the sensitivity of the admittance of organic thin films to vapours of organic solvents (benzene, ethanol and acetonitrile) and to water vapour has been investigated. The main aim of the work was the interpretation and understanding of the physics of the observed changes and not the optimisation of commercial gas sensing devices.

Chapter 2 gives an introduction to the electrical properties of organic materials, with a presentation of models and concepts used for the interpretation of the experimental results. Chapter 3 provides an overview of the devices used in gas sensing applications together with a description of the materials and some of the techniques available for the deposition of thin solid films.

A discussion of the principles of the experimental techniques together with a description of the experimental set up are found in chapter 4.

In the following four chapters (chapters 5 to 8) the results for each of the materials are given. Chapter 5 presents the characterisation of LB films of tetrabutylammonium $Ni(dmit)_2$ complex mixed with tricosanoic acid. In chapters 6 to 8, the results for thin films of polypyrrole (PPy) mixed with palmitic acid, for polycyanopropylmethylsiloxane (PCMS) and for a co-ordination polymer 5,5′ methylenebis (N-hexadecylsalicydeneamine) (MBSH), respectively, are given. The first part of each chapter concerns a study of the structure and the electrical properties on varying the temperature. This is followed by the vapour response, and finally a discussion of the sensing characteristics of the devices.

In the final chapter, some conclusions are drawn and suggestions for further work given.

References

[1] M.E.H.Amrani, R.M.Dowdeswell, P.A.Payne, K.C.Persaud, *Sensors and Actuators B*, **44** (1997) 512-516.

[2] See Aromascan catalogue, model A32/8.

[3] M.Haug, K.D.Schierbaum, H.E.Endres, S.Drost, W.Göpel, *Sensors and Actuators A*, **32** (1992) 326-332.

[4] K.Buhlmann, B.Schlatt, .Cammann, A.Shulga, *Sensors and Actuators B*, **49** (1998) 156-165.

Chapter 2

ELECTRICAL PROPERTIES OF THIN ORGANIC FILMS

2.1 Introduction

The four materials used in this thesis belong to different classes of organic compounds (i.e. charge transfer salts, polar polymers, conducting polymers and co-ordination polymers), each possessing different electrical properties. In this chapter, an overview of the electrical properties of organic films is given. For the materials used (as for most organic materials), the electrical behaviour is influenced by the disorder in their solid-state structure. Appropriate models used for the interpretation of the experimental data are presented.

First (in section 2.2), a definition of the electrical polarisation in time dependent fields is given noting how this is related to the electrical properties of materials where charge carriers are bound (i.e. permanent dipoles). This is followed by: (i) a description of the Debye model for the interpretation of the dielectric relaxation of non-interacting dipoles (paragraph 2.2.2); (ii) an introduction to empirical relaxation functions often used for the interpretation of dielectric spectra (paragraph 2.2.3); and (iii) a general overview of the dielectric response observed in polymers (paragraph 2.2.4).

The electrical transport in disordered media is then reviewed starting with the basic physical concepts (paragraph 2.3.1), and progressing to a description of the Variable Range Hopping model for both d.c. conductivity (paragraph 2.3.2) and for a.c. conductivity (paragraph 2.3.3).

In section 2.4, interfacial polarisation phenomena are introduced, together with the polarisation of heterogeneous dielectrics. Section 2.5 provides a brief discussion of Low Frequency Dispersion. Finally, in sections 2.6 and 2.7 an overview of the two important

classes of electrical conductive organic materials - conducting polymers and charge-transfer complexes - is presented.

2.2 Electric polarisation in time dependent fields

In this section, an introduction to the basic concepts of electrical polarisation is given. The ideas are developed to include a discussion of the electric polarisation due to charges that are locally bound in atoms or molecules or in the structure of solids and liquids. A description of the polarisation due to charge carries that can migrate for some distance through the dielectric is presented later in the chapter.

2.2.1 Basic concepts of electrical polarisation

Two electric charges of opposite polarity, $\pm q$, separated by a distance d, represent an electric dipole of moment

$$\mu = q\,d \qquad (2.1)$$

This dipole moment is symbolised by a vector of magnitude $|\mu|$ pointing from the negative to the positive pole.

Matter is made up of charged particles (electrons, protons, ions etc.) whose motion and position can be altered by applying an external electric field. This produces a distortion in the localised charge distribution, thereby creating a polarisation. This distortion is generally very small and, to a first approximation, can be considered linearly dependent on the electric field strength. To test the validity of this hypothesis, consider a dipole moment of 1 Debye, corresponding to two electronic charges separated by a distance of

about one fifth of an Angstrom unit (1 Debye = $(1/3)\times10^{-29}$ C m). To have an electrostatic energy of the order of the thermal energy at room temperature (~ 1/40 eV) or of a typical binding energy of atoms in a molecule (~ 10 eV), this dipole moment needs to be in an electric field of $E \sim 10^{9}$ V m^{-1} or $E \sim 10^{11}$ V m^{-1}, respectively. Such fields are greater than the typical breakdown strength of materials: generally the electric fields used in this experimental work were not larger than 10^{8} V m^{-1}.

The macroscopic effect observed when a dielectric material is placed in an electric field is the creation of a second electric field that tends to oppose to the original field. Microscopically, the polarisation arises from two main phenomena: induced and orientational polarisation. The former is present when the applied electric field causes a displacement of the electronic cloud relative to the nuclei in each atom (electronic polarisation) or when there is a displacement of the atomic nuclei relative to one another (atomic polarisation). Orientational polarisation is related to the orientation of molecules or to part of them. Chemical bonding between atoms of different electronegativity in a molecule can create an asymmetric charge distribution (i.e. so that the centres of positive and negative charge are not coincidental) forming a permanent dipole moment. Such moments experience a torque in an applied electric field that tends to orient them in the field direction (molecular polarisation). Molecules possessing a permanent dipole moment are termed polar.

When changes in the time-dependent electric field **E**(t) occur slowly compared with the motions of the microscopic particles, there is enough time to establish a time-dependent polarisation **P**(t) that is in equilibrium with the electric field at any moment. This is called the quasi-static case. For a linear, isotropic dielectric we can write

$$\mathbf{P}(t) = \chi\, \mathbf{E}(t) \qquad (2.2)$$

where χ is the electrical susceptibility. From this follows the well known relation between the electric displacement **D**(t), the electric field **E**(t) and the permittivity ε

$$\mathbf{D}(t) = \mathbf{E}(t) + \mathbf{P}(t) \tag{2.3}$$

$$\mathbf{D}(t) = \varepsilon\, \mathbf{E}(t) \tag{2.4}$$

$$\varepsilon = \chi + 1 \tag{2.5}$$

In contrast, for rapidly changing electric fields, the polarisation cannot be considered as instantaneous, because the motions of the microscopic particles required to reach a stable value of polarisation have characteristic times. These times are: for electronic polarisation about 10^{-17} s; for atomic polarisation 10^{-14} s; and for molecular polarisation greater than 10^{-12} s (figure 2.1).

When the electric field strength varies within a period of the same order of the characteristic time, the motions of the microscopic particles will not be sufficiently rapid to build up the equilibrium polarisation, and the actual value of the polarisation **P**(t) will lag behind the changing electric field **E**(t) and equation (2.2) will be no longer be valid. In this case, for linear and isotropic dielectrics the polarisation **P**(t) can be expressed as a function of the electric field by

$$\mathbf{P}(t) = \chi_0 \int_{-\infty}^{t} \left[-\frac{\delta F(t-t')}{\delta (t-t')} \right] \mathbf{E}(t')\, dt' \tag{2.6}$$

where F(t-t′) is called the step-response function, which describes the polarisation response to an unit step electric field [1]. Introducing the pulse-response function of the polarisation defined as

$$f(t) = -\frac{dF(t)}{dt} \tag{2.7}$$

it is possible to rewrite equation (2.6) as [1]

$$\mathbf{P}(t) = \chi_o \int_{-\infty}^{t} \mathbf{E}(t')\, f(t-t')\, dt' = \chi_o \int_{0}^{+\infty} \mathbf{E}(t-t')\, f(t')\, dt' \qquad (2.8)$$

Applying the Laplace transformation to equation (2.8) with respect to iω, a linear relation between the electric field and the polarisation can be found in the frequency domain. This allows the redefinition of susceptibility

$$\mathbf{P}(\omega) = \chi_o\, f(\omega)\, \mathbf{E}(\omega) = \chi(\omega)\, \mathbf{E}(\omega) \qquad (2.9)$$

where $\chi(\omega)$, apart from the case of static susceptibility, coincides with the transform of f(t)

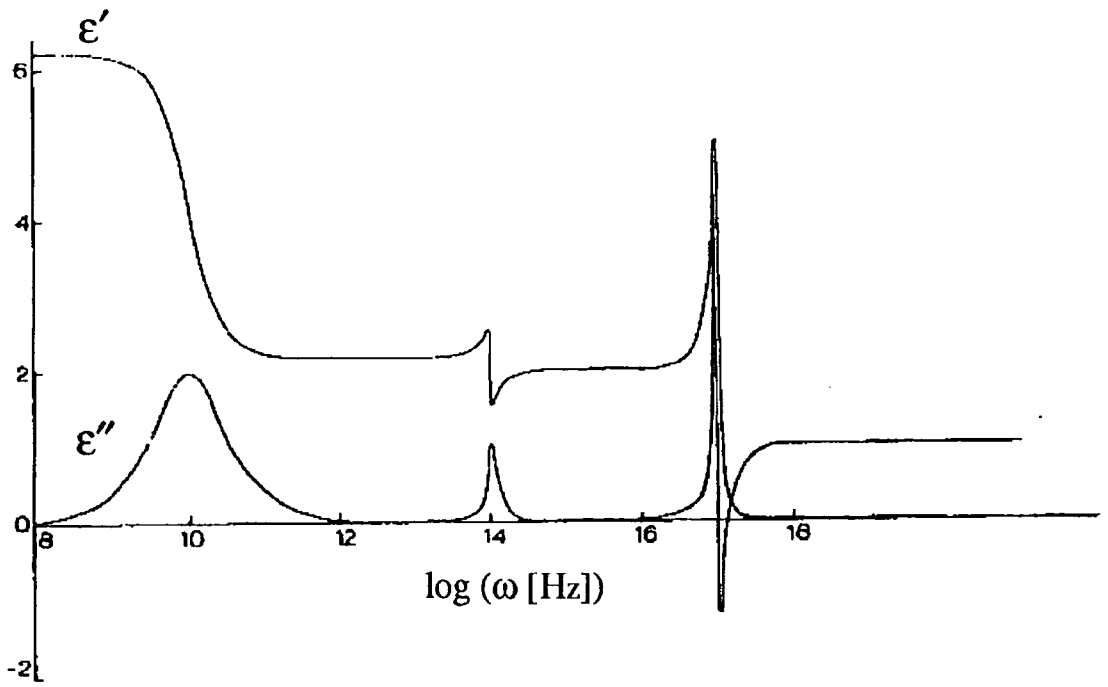

Figure 2.1: Dielectric dispersion ε′ and loss ε″ for a polar compound in the condensed phase [1].

$$\chi(\omega) = \chi'(\omega) - i\chi''(\omega) = \chi_o \int_0^{+\infty} f(t)\, e^{-i\omega t} dt \qquad (2.10)$$

The permittivity can be redefined as a complex quantity

$$\varepsilon(\omega) = 1 + \chi(\omega) = \varepsilon'(\omega) - i\,\varepsilon''(\omega) \qquad (2.11)$$

Moreover, because f(t) represents the response function of a linear system, the casuality principle is valid. This leads to the Kronig-Kramers relations which link the real and imaginary parts of the permittivity [1]. The behaviour of $\varepsilon'(\omega)$ and $\varepsilon''(\omega)$ as a function of the frequency are shown in figure 2.1.

When studying orientational polarisation, however, one often neglects the time required for intramolecular motions by which the induced polarisation adapts itself to the electric field. In this approximation, the induced polarisation is

$$\mathbf{P}_{in}(t) = \mathbf{E}(t)(\varepsilon_\infty - 1) \qquad (2.12)$$

where ε_∞ is the permittivity of induced polarisation (i.e. high frequency limit). Considering $\mathbf{P}(t) = \mathbf{P}_{or}(t) + \mathbf{P}_{in}(t)$ and substituting equation (2.12) in equation (2.3)

$$\mathbf{D}(t) = \varepsilon_\infty \mathbf{E}(t) + \mathbf{P}_{or}(t) \qquad (2.13)$$

In the case of the response function for orientational polarisation $f_{or}(t)$, equation (2.8) can be written in the form

$$\mathbf{P}_{or}(t) = (\varepsilon_s - \varepsilon_\infty) \int_0^{+\infty} f_{or}(t')\, \mathbf{E}(t - t')dt' \qquad (2.14)$$

where ε_s is the static permittivity (i.e. for $\omega = 0$).

The relation between the permittivity $\varepsilon(\omega)$ and the $f_{or}(t)$ can be found by substituting equation (2.14) into equation (2.13) and calculating the Laplace transform

$$\varepsilon(\omega) = \varepsilon_\infty + (\varepsilon_s - \varepsilon_\infty)\, L_{i\omega}(f_{or}) \qquad (2.15)$$

where $L_{i\omega}$ indicates the Laplace transform.

The response of a dielectric may also be described in terms of a complex conductivity. As $\mathbf{J} = d\mathbf{D}/dt$, it follows

$$\sigma(\omega) = \sigma'(\omega) + i\sigma''(\omega) = \mathbf{J}(\omega)/\mathbf{E}(\omega) = i\omega\,\varepsilon_o\,\varepsilon(\omega) \qquad (2.16)$$

$$\sigma'(\omega) = \omega\,\varepsilon_o\,\varepsilon''(\omega) \quad ; \quad \sigma''(\omega) = \omega\,\varepsilon_o\,\varepsilon'(\omega) \qquad (2.17)$$

In materials showing a measurable DC conductivity σ_{DC}, $\varepsilon(\omega)$ is associated only with the AC losses

$$\sigma'(\omega) = \sigma'(0) + \omega\,\varepsilon_o\,\varepsilon''(\omega) = \sigma_{DC} + \omega\,\varepsilon_o\,\varepsilon''(\omega) \qquad (2.18)$$

2.2.2 Debye model for dielectric relaxation

The first model for dielectric relaxation was presented by Debye [2,3] for the interpretation of the dielectric response of polar liquids. Debye supposed the existence of a system of N non-interacting dipoles in a viscous medium. He neglected dipole-dipole interactions and any other interactions dependent on the molecular arrangement, considering instead an average interaction in the form of a friction with the medium. The dipoles were imagined as rotating under the torque **T** of an electric field with an angular velocity $d\theta/dt$ proportional to this torque, or

$$T = \zeta \frac{d\theta}{dt} \tag{2.19}$$

where the friction factor ζ depends on the shape of the molecule and on the type of interaction it encounters.

In a static field, the dipoles will have a slight preferential orientation parallel to the field. A sudden removal of the field will cause an exponential decay of this ordered state due to the randomising of the Brownian movement. The relaxation time τ measures the time required to reduce the order to e^{-1} of its original value. Debye was able to calculate this time statistically by deriving the space orientation under the counteracting influences of the Brownian motion of a time-dependent electric field and found [2,3]

$$\tau = \frac{\zeta}{2k_B T} \tag{2.20}$$

giving an average dipole moment

$$\mu = \frac{\mu^2 E}{3k_B T} \frac{1}{1 + i\omega\tau} \tag{2.21}$$

from which he was able to calculate the macroscopic polarisation

$$P = N\mu \tag{2.22}$$

and the susceptibility, from which followed the important Debye equation

$$\chi(\omega) = \frac{N\mu^2}{3k_B T} \frac{1}{1 + i\omega\tau} = \chi_o \frac{1}{1 + i\omega\tau} \tag{2.23}$$

It should be noted that, in this calculation, the electric field acting on the dipoles was considered to be the external (applied) field. The problem of calculating the field effectively acting on an individual dipole, the internal field, is discussed extensively in the literature [1].

2.2.3 Phenomenological description of the dielectric relaxation

Debye's result, in the time domain, corresponds to having a step relaxation function of the form

$$F(t) = e^{-t/\tau} \tag{2.24}$$

where τ is termed relaxation time. In the frequency domain the relationship is usually found in the form

$$\varepsilon(\omega) = \varepsilon_\infty + (\varepsilon_s - \varepsilon_\infty)\frac{1}{1+i\omega\tau} \tag{2.25}$$

Separating the real and imaginary parts of the permittivity as in equation (2.11) it is possible to obtain the Debye-Pellat equations [1 - 4]

$$\varepsilon'(\omega) = \varepsilon_\infty + (\varepsilon_s - \varepsilon_\infty)\frac{1}{1+\omega^2\tau^2} \tag{2.26}$$

$$\varepsilon''(\omega) = (\varepsilon_s - \varepsilon_\infty)\frac{\omega\tau}{1+\omega^2\tau^2} \tag{2.27}$$

A plot of ε' against ε'' (Cole-Cole plot[1]), for a Debye relaxation produces a semicircle of diameter (ε_s - ε_∞) and centre ((ε_s - ε_∞)/2, 0).

The Debye equation has been found adequate to describe the orientational polarisation for a large number of simple condensed materials (e.g. solvents). However, for more complex systems, such as macromolecules, deviations are observed. These take the form of a broader and asymmetric peak in the ε'' versus frequency curve, or in a depressed and asymmetric semicircle in a Cole-Cole plot.

To describe these responses, the Debye equation has been modified empirically by introducing other parameters. In this way, new phenomenological relaxation functions are derived, allowing the dielectric relaxation of most dielectrics materials to be mathematically described. Three examples of modified Debye responses are listed below.

The Cole-Cole equation [1, 4, 5]

$$\varepsilon(\omega) = \varepsilon_\infty + (\varepsilon_s - \varepsilon_\infty)\frac{1}{1+(i\omega\tau)^{1-\alpha}} \qquad 0 < \alpha \le 1 \tag{2.28}$$

This describes a symmetrical Cole-Cole plot, with respect to $\varepsilon'(\omega = \tau^{-1})$, but depressed.

The Cole-Davidson equation [1, 4, 5]

$$\varepsilon(\omega) = \varepsilon_\infty + (\varepsilon_s - \varepsilon_\infty)\frac{1}{(1+i\omega\tau)^{\beta}} \qquad 0 < \beta \le 1 \tag{2.29}$$

This gives an asymmetric curve respect to $\varepsilon'(\omega = \tau^{-1})$ in the Cole-Cole plot.

The Havriliak-Negami equation [1, 4 - 6]

$$\varepsilon(\omega) = \varepsilon_\infty + (\varepsilon_s - \varepsilon_\infty)\frac{1}{\left(1+(i\omega\tau)^{1-\alpha}\right)^{\beta}} \qquad 0 < \beta \le 1;\, 0 < \alpha \le 1 \tag{2.30}$$

This is more general, being a combination of equations (2.28) and (2.29).

The classical description underlying equations (2.28) - (2.30) is based on a superposition of independent Debye relaxation functions with different relaxation times. In this case, equation (2.24) will become

$$F(t) = \int_0^{+\infty} w(\tau)\, e^{-\frac{t}{\tau}}\, d\tau \qquad (2.31)$$

where $w(\tau)$ is the distribution function. The expression $w(\tau)$ for the different relaxation functions can be found using equations (2.7) and (2.15).

From a physical point of view, the approach is unsatisfactory because it does not provide an explanation of the different parameters (i.e. α and β) in terms of the physical properties of the dielectric materials.

More recently, several authors, in particular A.K.Jonscher [7 - 9], have shown how, in a very large number of disordered materials (polymers, glasses, etc.), the frequency dependence of the susceptibility follows an 'universal' law. This consists of a power law dependence of the susceptibility for frequencies higher and lower of the characteristic frequency $\omega_m = \tau^{-1}$ (corresponding to the maximum of the loss peak for a symmetric relaxation function, i.e. a Debye or a Cole-Cole equation)

$$\chi'(\omega) \propto \chi''(\omega) \propto \omega^{-n} \qquad \text{for } \omega \gg \omega_m \qquad \text{with } 0 < n < 1 \qquad (2.32)$$

$$\chi'(0) - \chi'(\omega) \propto \chi''(\omega) \propto \omega^{m} \qquad \text{for } \omega \ll \omega_m \qquad \text{with } 0 < m < 1 \qquad (2.33)$$

From this work there has been considerable interest in finding theoretical models that give an interpretation of the power law exponents [10 - 12]. In the case of the Havriliak-Negami function (2.30), it is possible to estimate the exponents in terms of the

parameters α and β using the following equations

$$m = 1 - \alpha \quad ; \quad n = (1 - \alpha)\beta \tag{2.34}$$

2.2.4 Dielectric relaxation in polymers

Because of their complexity, polymers usually exhibit more than one power loss peak. These are denoted using the Greek letters α, β, γ etc. At a fixed temperature, α corresponds to the lowest frequency relaxation, and the others, β and γ, describe those observed progressively at higher frequencies. Generally, the α relaxation originates from the main chain and is referred to as 'structural' relaxation. It has been shown that, for the same polymer, changes in the parameters (ie, τ, α, β, $\varepsilon_o - \varepsilon_\infty$,...) of the structural relaxation are directly related to structural changes of the polymer. This can be observed, for example, during the glass-transition of a polymer or during a polymerisation process. The glass transition temperature may be defined by dielectric measurements as the temperature for which the relaxation time τ is equal to 100 s. However, a direct relation between the observed macroscopic response and the microscopic motion of the molecules has not yet been found. Several models have been proposed [10 - 12], but none has been universally accepted.

The relaxation functions for polymers are non-Debye and are described by the more complicated relaxation functions given by equations (2.28)-(2.30). In fact, equation (2.30) was introduced for the first time by Havriliak and Negami [6] to describe the behaviour of polymers.

To estimate the frequency width Δf of a dielectric relaxation, we can first consider that of a Debye-type relaxation measured at half height of the loss peak. This is the smallest (for the same value of $\varepsilon_o - \varepsilon_\infty$) between all the relaxation functions described in section 2.2.3,

and it is equal to

$$\Delta f = \frac{\sqrt{3}}{\pi}\frac{1}{\tau} \tag{2.35}$$

Using a relaxation time $\tau = 10^{-11}$ s, $\Delta f = 4.6$ GHz. Therefore, it is essential to measure the dielectric properties over a wide range of frequencies, even more important when there is more than one relaxation.

The dependence of the relaxation time τ on temperature, for secondary relaxations (β,γ,..), is usually described by an Arrhenius type equation.

$$\frac{1}{\tau} = A \exp\left(-\frac{\Delta E}{RT}\right) \tag{2.36}$$

where ΔE is termed the activation energy, R is the gas constant (8.314 J K^{-1} $mole^{-1}$) and A is a constant characteristic of the system. The Vogel-Fulcher equation usually describes a 'structural' (or α) relaxation

$$\frac{1}{\tau} = C \exp\left(-\frac{B}{T - T_o}\right) \tag{2.37}$$

where B is termed the pseudo activation energy, C is a constant and T_o corresponds to the temperature for which τ becomes infinite, often called the Kauzmann temperature.

The first equation in an Arrhenius plot (i.e. $\log(\tau^{-1})$ versus $1000\ T^{-1}$) is a straight line. In contrast, equation (2.37) is a curve that for high temperature tends to straight line and whose derivative increases with a decrease of the temperature.

The Arrhenius equation can be derived using a simple physical model based on two states separated by an energy barrier energy (paragraph 2.3.3). The system then oscillates

between these states with a frequency ν [13]

$$\nu = \frac{kT}{h} \exp\left(-\frac{\Delta G}{RT}\right) \tag{2.38}$$

where ΔG is the height of the energy barrier, k is the Boltzmann constant and h is Planck's constant.

The Vogel-Fulcher relationship has a similar physical basis, but the height of the barrier increases with decreasing of temperature.

2.3 Electrical transport in disordered media

2.3.1 Hopping conduction

The Hamiltonian H describing the conductivity in a solid should contain the following terms [14]

$$H = H_e + H_{ph} + H_{e\text{-}e} + H_{e\text{-}ph} + H_V \tag{2.39}$$

H_e describes the non-interacting electron system (i.e. from a tight-binding model), H_{ph} is the phonon term, $H_{e\text{-}e}$ the electron-electron interaction, $H_{e\text{-}ph}$ the electron-phonon interaction and the last term H_V describes the potential seen by the electrons when they move through the lattice. To find the solution of this Hamiltonian is a formidable and maybe impossible task, so that approximations are necessary.

One simplification is that in which the electrons are considered free to move in a periodic potential (i.e. $H_e \neq 0$). This was the approach used for the first time by Bloch and

allowed the interpretation of the conductivity in crystalline materials. Bloch solved the Schrödinger equation finding wavefunctions representing plane waves modulated by the crystal field and not showing any scattering [15]. The resistivity of a material originates from deviations from the perfect crystal lattice, resulting either from thermal vibration or from the presence of impurities.

Bloch also showed how the possible energies of an electron were divided into zones (Brillouin zones) with gaps between them [15]. As a consequence, for material in which one or more zones, corresponding to the same energy but different momentum, are partially occupied by electrons, electrons can easily move between them and the material shows high conductivity (metals). In the case in which all zones are completely full or empty, there is an energy gap (E_{gap}) between the highest occupied band (valence band)

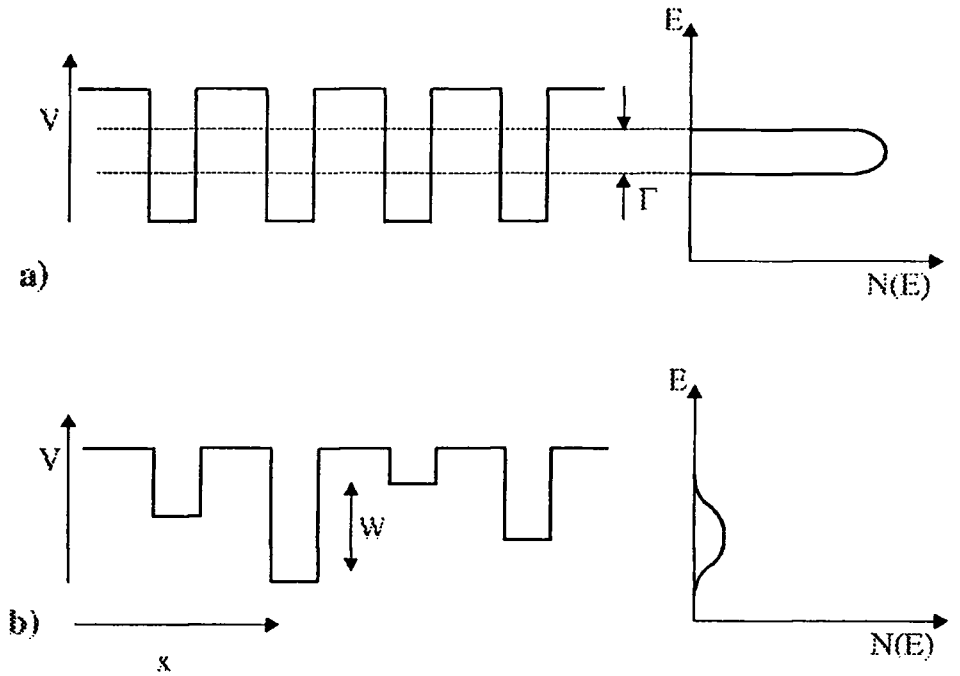

Figure 2.2: (a) Potential wells for a crystalline lattice. (b) The same with a random potential energy at each well as in Anderson model. V is the potential energy function, W is a random potential at each well (i.e. the spread of energies), Γ is the band width, and N(E) is the density of states.

and the first empty band (conduction band). Electrons need additional energy to move between the two zones and the material exhibits a low conductivity, which decreases with an increasing energy gap. For semiconductors, $E_{gap} \sim k_B T$, while for insulators $E_{gap} >> k_B T$.

An efficient way to solve the Schrödinger equation is by introducing the density of states function N(E). This is defined so that N(E)dE is the number of eigenstates per unit volume for electrons in the system with given spin direction and energy between E and E + dE. At temperature T, the number of electrons in the energy range dE is, for each spin direction, $N(E) f(E) dE$, where $f(E)$ is the Fermi distribution function.

In disordered systems, impurities and defects introduce substantial scattering of the electron wave function. This may lead to localisation, which means that each wavefunction is confined to a small region of space, falling off exponentially with distance and with a quantized energy value. Anderson demonstrated [16] that electronic wave functions can be localised if the random component of the disorder potential W is large compared to the electronic bandwidth Γ, as sketched in figure 2.2

The associated broadening of the density of states (vs. energy) due to the random potential is shown in figure 2.2. According to Anderson, states will become localised throughout the band for a critical value of W/Γ that is estimated to be of the order of unity in three dimensions [17]. If $\Gamma = 0$ the problem is the same as that resolved by Bloch, and the electronic states are delocalised over all the lattice, with a narrow energy band W (figure 2.2a). When the critical value of W/Γ is approached, the states become localised with a wide energy distribution. For intermediate situations, some of the states will be localised and some delocalised.

Later Mott [17, 18] showed that band tails are more easily localised than states in the centre of the band. Consequently, there exists a critical energy separating the localised states in the band tails from the extended states in the centre of the band. This is called

the mobility edge E_C. The resulting electronic behaviour of a material depends on where the Fermi energy E_F lies relative to E_C. If E_F lies in the range of the extended states, then σ_{DC} is finite as $T \rightarrow 0$ (metallic behaviour). However, if the disorder is strong enough to cause E_F to be in the range of localised states, then the material will be non-metallic, with $\sigma_{DC} \rightarrow 0$ as $T \rightarrow 0$, even though there is a finite density of states at E_F. In this case there is a transition from the metallic state to a non-metallic state. Mott called this disorder induced M-I (Metal-Insulator) transition the 'Anderson transition'.

When E_F approaches E_C on the insulating side of the M-I transition, the localisation length diverges as the electronic wave function becomes delocalised through the material. However, because of the strong disorder, the mean free path is still very short. Ioffe and Regel [18] proposed that the lower limit for the metallic mean free path is the interatomic spacing. This condition led Mott to propose a 'minimum metallic conductivity' $\sigma_{min} \sim 0.03e^2/3\hbar a \sim 10^2$ S cm^{-1} in three dimensions (where a is the interatomic spacing and e the electronic charge). The scaling theory of Abrahams [19] demonstrated however that the M-I transition is continuous in three dimensions. Consequently, the conductivity goes smoothly to zero as $E_F \rightarrow E_C$, and σ_{min} does not exist.

On introducing the lattice vibrations (terms H_{ph} and $H_{e\text{-}ph}$ in equation 2.39), there is a decrease of the mean free path due to the phonon scattering. At the same time other mechanisms of conduction are possible between localised states. At a sufficiently high temperature, charge transfer by thermally activated hopping becomes another possible conduction mechanism. The lattice provides (or adsorbs) energy for the charges necessary to hop over the potential barriers which are randomly distribute between localised states.

2.3.2 Variable range hopping (VRH)

When the Fermi level lies in the localised states, the conductivity at zero temperature is zero, even for a system with a finite density of states. The conduction mechanism may be of two kinds. First, by electrons excited to the mobility edge E_C, so that the conductivity behaves as

$$\sigma_{DC} = \sigma_o \exp\{-(E_C - E_F)/k_B T\} \tag{2.40}$$

with $\sigma_o \sim 0.03\, e^2/\hbar L$ [18], where L is the diffusion length. This form of conduction is normally predominant at high temperatures or when $E_C - E_F$ is small. Secondly, if $N(E_F)$ is finite thermally activated hopping can be important. This is a process in which an electron in an occupied state with energy below E_F receives energy from a phonon, enabling it to move to a nearby state above E_F. A process of this kind was first described by Miller and Abrahams, and is called 'nearest-neighbour' hopping. Because of a very strong localisation, the hopping of the electrons is limited only by the distance and electrons are supposed always to move to the nearest empty centre. The resulting expression for the conductivity is

$$\sigma_{DC} = \sigma_{nn} \exp(-E_{nn}/k_B T) \tag{2.41}$$

where E_{nn} is expected to be of the order of the band width

$$E_{nn} \sim 1/N(E_F)a^3 \tag{2.42}$$

a is the distance between nearest neighbours.

Mott [17, 18] first pointed out that at low temperatures ($\Delta E/k_B T \gg 1$) the most frequent hopping process would not be to the nearest neighbour, the process also limited by the spread of the energy values. It could be more convenient to hop to a site at longer

distance R but having a smaller ΔE, than to a closer one with a greater ΔE. Therefore, the maximum hopping rate will be for a combination of the optimal difference in energy ΔE and distance R. The argument, in its simplest form, is as follows. Within a range R of a given site, the density of states per unit energy range n(E), near the Fermi energy, is

$$n(E_F) = (4\pi/3)\, R^3\, N(E_F) \tag{2.43}$$

For hopping through a distance R with the lowest activation energy, ΔE will be

$$\Delta E = \frac{1}{(4\pi/3)R^3\, N(E_F)} \tag{2.44}$$

The further the electron hops the smaller will be ΔE. Hopping over a large distance involves quantum mechanical tunnelling and the probability will contain the factor $\exp(-2\alpha R)$, where α^{-1} is the decay length of the localised wave function. So there will be an optimum hopping distance R, for which the hopping probability

$$\nu_{hop} = \nu_{ph} \exp(-2\alpha R) \exp(-\Delta E/K_B T) \tag{2.45}$$

has a maximum. Here ν_{ph} is the phononic frequency. This will occur when (using equation (2.44)

$$2\alpha R + 1/\{(4\pi/3)R^3\, N(E)\, k_B T\}$$

has its minimum value, that is when

$$R = \{9/[8\pi N(E)\alpha k_B T]\}^{1/4} \tag{2.46}$$

Substituting for R in equation (2.45) the hopping probability is obtained and the conductivity (for the three-dimensional problem) is of the form [17, 18]

$$\sigma_{DC} = \sigma_{vr} \exp\left[-\left(\frac{T_o}{T}\right)^{1/4}\right] \tag{2.47}$$

where

$$T_o = B_o^4 \left\{\frac{\alpha^3}{k_B N(E_F)}\right\} \quad ; \quad B_o = 2\left(\frac{3}{2\pi}\right)^{1/4} = 1.66 \tag{2.48}$$

$$\sigma_{vr} = D\left(\frac{T_o}{T}\right)^{\frac{1}{2}} \quad ; \quad D = \left(\frac{3}{2^4}\right)^{\frac{1}{2}} \left[e^2 \nu_{ph} N(E_F)/\alpha^2\right] \tag{2.49}$$

The value of the factor B_o varies considerably, but is generally found in the range 2.5 - 1.7 [18]. In the two-dimensional and one-dimensional cases, the factor 1/4 in equation (2.47) is replaced by 1/3 and 1/2, respectively.

2.3.3 Hopping conduction for alternating currents

The electrical conductivity in disordered solids is characterised by a strong dispersion. At low frequency, a constant conductivity is observed while at higher frequencies the conductivity becomes strongly frequency dependent, varying approximately as a power of the frequency, $\sigma'(\omega) \propto \omega^s$ (as shown in figure 2.3), with the exponent s between 0.7 and 1.0. The increase of conductivity usually continues up to phonon frequencies. This frequency behaviour corresponds to a superposition of a broad dielectric loss peak, having a characteristic frequency ω_m, with a conductivity value $\sigma'(0)$ that is independent of frequency (equation (2.18)). Such effects are seen in a wide variety of non-metallic disordered solids. Classes of disordered solids investigated in the last 40 years include amorphous semiconductors, ionic conductive glasses, conducting polymers and organic semiconductors [8, 20 - 23].

All disordered solids show similar behaviour for the temperature dependence of the ac properties. Experiments reveal that: (i) the ac conductivity ($\sigma'(\omega)$) depends much less on temperature than σ_{DC} and becomes almost temperature independent as $T \rightarrow 0$; (ii) the exponent s increases on decreasing the temperature, tending to 1 as $T \rightarrow 0$; and (iii) the characteristic frequency ω_m shows an Arrhenius temperature dependence (equation (2.36)).

The frequency maximum of the loss peak ω_m and $\sigma'(0)$ are often related [20, 21]

$$\sigma'(0) = p\, \Delta\varepsilon\, \varepsilon_o\, \omega_m \qquad (2.50)$$

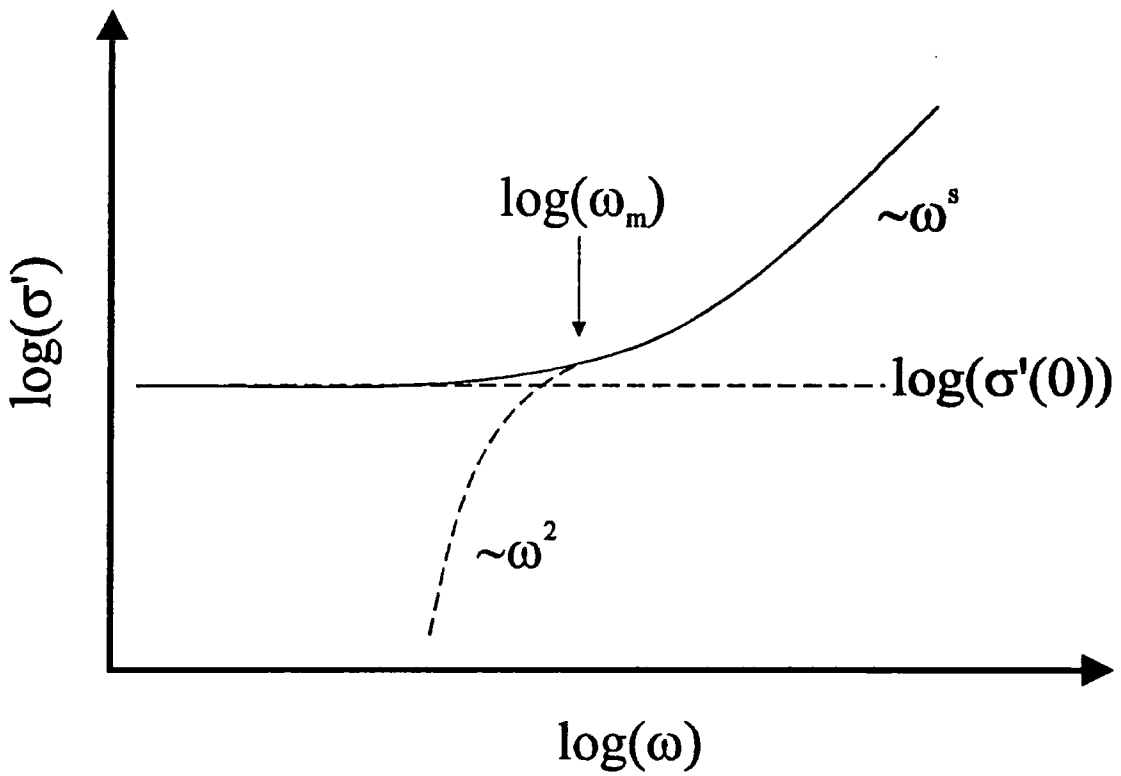

Figure 2.3: Real part of the frequency-dependent conductivity in a disordered solid (solid line). The two dotted lines show how this curve can be obtained as a superposition of the dc conductivity $\sigma'(0)$ and of a loss peak.

Here, $\Delta\varepsilon$ is the dielectric relaxation strength (i.e. $\Delta\varepsilon = \varepsilon_o - \varepsilon_\infty$) and p is a temperature independent constant close to unity. Equation 2.50 implies that $\sigma'(\omega)$ and $\sigma'(0)$ are closely correlated and must originate from the same mechanism. Therefore, the dc conductivity $\sigma'(0)$ corresponds to the limit of $\sigma'(\omega)$ for $\omega \rightarrow 0$.

In the last 40 years, several models have been developed to relate the observed ac electrical behaviour to the microscopic properties [23 - 25]. Currently none of these is universally accepted. The most thoroughly studied models for ac conduction in disordered solids are probably based on hopping. A quite common feature is to assume the hopping process is Markovian, i.e. the charge carrier jump probabilities are assumed to be time independent. This leads to a simple exponential decays for the probability of a charge carrier staying at a given site [20]. The observed frequency dispersion of the conductivity is then attributed to spatial and energy disorder in the solid resulting in a broad distribution of relaxation times (waiting times). The relaxation function is of the form of equation (2.31).

The simplest model is probably that proposed by Mott [18], the so called "pair approximation". This assumes that the loss is due to independent pairs of sites in the solid, where each pair provides two possible positions for a localised charge carrier. A charge hopping between two sites is equivalent to a dipole D oscillating between two opposite directions with an energy difference ΔE between the two configurations. If the angle between the direction of the dipole and of the field F is θ, the conductivity becomes [18]

$$\sigma'(\omega) = \frac{\left(nD^2\cos^2(\theta)/k_BT\right)\left\{1+\exp\left(\Delta E/k_BT\right)\right\}^{-1}\omega^2\tau}{1+\omega^2\tau^2} \qquad (2.51)$$

where τ is the mean jump time and n is the number of dipoles (i.e. number of pairs per site) per unit volume. If we average $\cos^2(\theta)$ over all angles, we obtain a factor 1/3. If close to $\Delta E = 0$ there are N dE dipoles with ΔE in the range dE, then the integration over

ΔE, assuming N is fairly constant in the range $\Delta E = 0$, yields [18]

$$\sigma'(\omega) = \frac{1}{3}\frac{(\ln 2)ND^2\omega^2\tau}{1+\omega^2\tau^2} \tag{2.52}$$

This corresponds, apart from a numerical factor, to a Debye-like frequency (eq.(2.27)) behaviour.

If the process involves an electron surmounting a barrier of height U, so that

$$\tau^{-1} = \nu_{ph} \exp(-U/k_BT) \tag{2.53}$$

and B(U) is the probability that a barrier has height between U and dU, then writing $d\tau/\tau = dU/k_BT$, and calculating the average of $\omega^2\tau/(1+\omega^2\tau)$, the conductivity is

$$\sigma'(\omega) = \frac{1}{3}\ln(2)ND^2k_BT\omega^2\int_0^\infty B(U)\left(1+\omega^2\tau^2\right)^{-1}d\tau \tag{2.54}$$

This is a general expression from which is evident that, assuming different distributions B(U), it is possible to obtain all the possible phenomenological relaxation functions. This is practically equivalent to equation (2.31).

Applying these ideas to an electron hopping between two localised states at a distance R from each other, the hopping rate is [18]

$$\tau^{-1} = \nu_{ph} \exp(-2\alpha R) \exp(-\Delta E/k_BT) \tag{2.55}$$

Assuming that only hops of energy ~ k_BT make an important contribution, that the important hops are those for which $\omega\tau \sim 1$ and that the number of vacancies where the electrons can hop are $N(E_F)k_BT$, gives [18]

$$\sigma'(\omega) = A\left(\frac{e^2}{\alpha^5}\right)\{N(E_F)\}^2\, k_B T\omega\left\{\ln\left(\frac{\nu_{ph}}{\omega}\right)\right\}^4 \qquad (2.56)$$

where $A = (\pi^2/24)\ln 2 \sim 0.3$. With the approximations made, this equation describes the dependence of the conductivity at high frequency (not the full relaxation). Equation (2.56) gives an approximate power law conductivity with an exponent s given by

$$s = 1 + 4 / \ln(\omega\tau_{ph}) \qquad (2.57)$$

where τ_{ph} is the phonon time ($\sim 10^{13}$ Hz). For a typical experimental frequency, $s \approx 0.8$, a value close to that obtained experimentally.

The pair approximation derivation has several problems and cannot be used as a valid model to interpretate all experimental data: (i) equation (2.56) does not provide an expression for σ_{DC}, which is considered an independent phenomena, in disagreement with equation (2.50); (ii) the value $s = 0.8$ is not universally valid, and higher values of s lead to unreasonable values of ν_{ph} (i.e. $s = 0.96 \rightarrow \nu_{ph} = 10^{39}$ Hz for $\omega = 10^4$ Hz); and (iii) the model predicts s to be a weakly decreasing function of frequency whereas experimentally s increases slowly with increasing frequency.

Improved results may be found by hopping models that include a random walk of charge carriers in a disordered structure. Here, the jump rate between two sites is usually taken to be a function of an activation energy or distance, and to be nonzero only for nearest-neighbour jumps. Such models provide a natural explanation of the increase in conductivity with the frequency. By hopping backward and forward at places with a high jump probability, a charge carrier may significantly contribute to the ac conductivity. In contrast, the dc conductivity is determined by overcoming the unfavourable hops for the formation of a continuous percolation path between the electrodes. The higher the frequency, the larger is the ac conductivity because better use is made of places with very

large jump probability. Hopping models are complex and cannot be resolved analytically. To evaluate $\sigma(\omega)$, either one has to use a computer simulation or to rely on analytical approximations [20, 23 - 25].

In this thesis, specific models for the ac conductivity are not elaborated any further. The discussion will be limited to the interpretation of the permittivity in terms of a superposition of an empirical relaxation function (such as described by equations (2.28) - (2.30)) with a conductivity independent from the frequency $\sigma'(0)$. We also note the correlation between $\sigma'(0)$ and the relaxation time τ of the relaxation function (equation 2.50).

2.4 Interfacial and space charge polarisation

Since the early theoretical studies of Maxwell [26] and Lord Rayleigh [27] on heterogeneous dielectrics, extended later by Wagner [28], it was evident that, in general, a heterogenous medium exhibits frequency-dependent dielectric and conductive properties that differ from those of the constituent components. Such dielectric

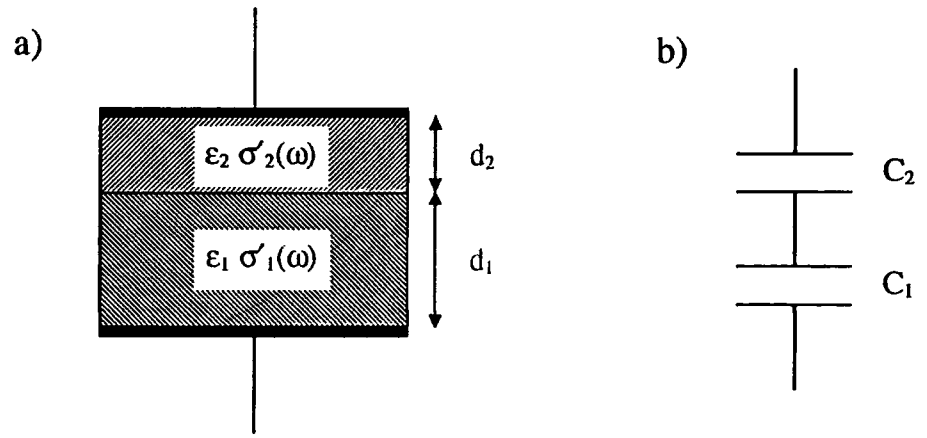

Figure 2.4: a)Two-layer heterogeneous system; b) equivalent circuit.

dispersions have become to be known as Maxwell-Wagner or interfacial polarisation.

The simplest heterogenous system is that of the two-layer capacitor shown in figure 2.4. This consists of two parallel slabs of differing dielectrics, with dielectric constants ε_1 and ε_2, and thickness d_1 and d_2, respectively. The two layer model can be represented as two capacitors connected in series, each with a complex capacitance given by

$$C_i = A\varepsilon_o (\varepsilon_i - i\, \sigma'_i(0)/\omega\varepsilon_o)/d_i \tag{2.58}$$

where the subscript i can be 1 or 2, A is the area of the two slabs and $\sigma'(0)$ is the dc conductivity. The total complex capacitance is

$$\frac{1}{C} = \frac{1}{C_1} + \frac{1}{C_2} \tag{2.59}$$

This gives the following expression for the total capacitance C [4, 29]

$$C = [\varepsilon_\infty + (\varepsilon_s - \varepsilon_\infty)/(1 + i\omega\tau) - i\sigma/(\omega\varepsilon_o)]\, A/d \tag{2.60}$$

Equation (2.60) corresponds to a Debye-like relaxation, plus a term related to the conductivity, in which the parameters ε_s and ε_∞ in the Debye equation (equation 2.26) are related to conductivity, dielectric constant and thickness of the two layers by

$$\varepsilon_s = \frac{d\left(\varepsilon_1 d_1 \sigma_2(0)^2 + \varepsilon_2 d_2 \sigma_1(0)^2\right)}{\left(\sigma_1(0) d_2 + \sigma_2(0) d_1\right)^2} \tag{2.61}$$

$$\varepsilon_\infty = \frac{d\varepsilon_1\varepsilon_2}{(\varepsilon_1 d_2 + \varepsilon_2 d_1)} \tag{2.62}$$

and

$$\tau = \frac{\varepsilon_0(\varepsilon_1 d_1 + \varepsilon_2 d_2)}{\sigma_1(0)d_2 + \sigma_2(0)d_1} \tag{2.63}$$

$$\sigma = \frac{d\sigma_1(0)\sigma_2(0)}{\sigma_1(0)d_2 + \sigma_2(0)d_1} \tag{2.64}$$

The underlying physical origin of such dielectric behaviour is associated with the non-uniform distribution of free electronic charges across the interface between dissimilar dielectric materials. This can be best envisaged by considering the situation under dc equilibrium conditions where there must be electrical current continuity across the boundary between materials 1 and 2 of figure 2.4. Each material will have its own free charge carrier concentration and associated charge mobility. To achieve current continuity through the materials there will have to be a carrier concentration discontinuity across the interface. It is essentially the dynamic behaviour of this interfacial charge build-up or polarisation, as a function of frequency, that gives rise to the dielectric dispersion exhibited by inhomogeneous systems. Therefore, interfacial polarisation results when contiguous dielectrics differ in conductivity.

A system composed of a number of layers of one material (ε_1,$\sigma'_1(0)$) alternated with layers of another material (ε_2,$\sigma'_2(0)$) will have the same dielectric characteristics as the two-layer system. A multilayer system of many materials will have limiting permittivities in the Debye equations given by [4, 29]

$$\begin{cases} \varepsilon_s = d\left(\sum_i d_i\varepsilon_i / \sigma_i(0)^2\right) / \left(\sum_i d_i / \sigma_i(0)\right)^2 \\ \varepsilon_\infty = d / \left(\sum_i d_i / \varepsilon_i\right) \end{cases} \tag{2.65}$$

Another important heterogenous model is that shown in figure 2.5. For such system, with $\sigma'_2(0) \gg \sigma'_1(0)$, the dispersion is characterised by the dielectric parameters [4, 30]

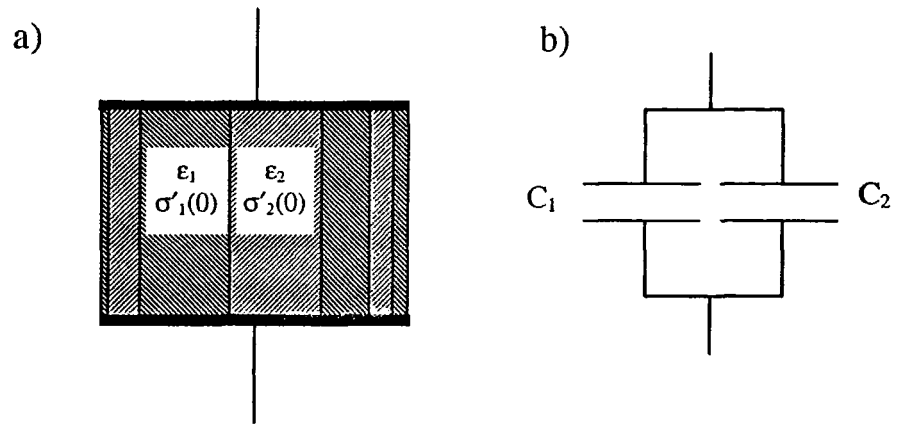

Figure 2.5: a) Heterogeneous system of slabs perpendicular to the electrodes; b) its equivalent circuit.

$$\varepsilon' = (1-v)\,\varepsilon_1 + v\,\varepsilon_2 \tag{2.66}$$

$$\varepsilon'' = \sigma'_2(0) / \varepsilon_o\omega \tag{2.67}$$

where v is the volume fraction occupied by medium 2. In this case, a loss peak would not be observed, only the effect of the dc conductivity. The discussion of a more general case, in which the heterogeneous system consists of inclined layers with different local conductivities, can be found in the literature [31]. This also provides a Debye-like response.

The models shown in figures (2.4) and (2.5) can be considered as extreme cases. Most models of heterogenous systems will be somewhere between. The most general case of one component dispersed in the form of particles inside a second component can be considered as a continuous medium. It has been shown how the frequency behaviour of the response would be the same (Debye-like) but, for the same volume fraction (i.e. the ratio between the volume of the dispersed component to that of the second component), with a difference in the amplitude and characteristic time τ depending on the shape of the particles [32]. This is related to a depolarisation factor, whose value can be found in the

literature for different particle shapes [4].

From the above results, it can be envisaged how more complicated frequency responses could be obtained by a distribution of relaxation processes (i.e. equation 2.31). This could be achieved by (i) a distribution of the particles' shapes or (ii) a distribution of the particles' conductivities [31, 33, 34].

For a mixture of two components of permittivity ε_1 and ε_2, but with negligible conductivities, the problem is easier. The best known formula to find the permittivity ε_m of a mixture is that first derived by Maxwell for spherical particles (with permittivity ε_2) dispersed randomly in a dielectric medium with a low volume fraction ($v < 0.1$) [4, 35]

$$\varepsilon_m = \varepsilon_1 \frac{\left[1 - 2\,v\,\frac{(\varepsilon_1 - \varepsilon_2)}{(2\varepsilon_1 + \varepsilon_2)}\right]}{\left[1 + v\,\frac{(\varepsilon_1 - \varepsilon_2)}{(2\varepsilon_1 + \varepsilon_2)}\right]} \tag{2.68}$$

If the term $(\varepsilon_1 - \varepsilon_2)v/(2\varepsilon_1 + \varepsilon_2)$ is small compared to unity, we have the approximation

$$\varepsilon_m = \varepsilon_1\left[1 - 3\,v\,\frac{(\varepsilon_1 - \varepsilon_2)}{(2\varepsilon_1 + \varepsilon_2)}\right] \tag{2.69}$$

2.5 Low Frequency Dispersion

The phenomenon of Low-Frequency Dispersion (LFD) is a form of dielectric response widely found at low frequencies in materials in which the polarisation is dominated by slowly mobile charge carriers [8,9]. In many cases, it has been associated with the presence of water inside the material [36 - 40]. The classical definition of LFD involves

two fractional power law terms for the complex susceptibility

$$\chi(\omega) = A_l(i\omega)^{n_2-1} + A_h(i\omega)^{n_1-1} \tag{2.70}$$

where the low frequency term has a pre-exponential factor A_l and an exponent n_2 which is close to zero (from the literature $0 < n_2 < 0.5$), while the high frequency term has the factor A_h and exponent n_l close to unity (from the literature $0.5 < n_l < 1$). An immediate consequence of the power law dependence is the frequency independence of the ratio of the real and imaginary parts of the susceptibility. This has been termed the "universal" response [9] (equations (2.32) and (2.33)). The frequency dependence of LFD, as shown in figure 2.6, is characterised by the transition between two fractional power laws of the same kind (i.e. ω^{-n} with $n < 1$) with different exponents. The physical significance is that two independent parallel processes exist. One of these, dominating at high frequencies, is due to the normal dielectric response of the material, while the strongly dispersive

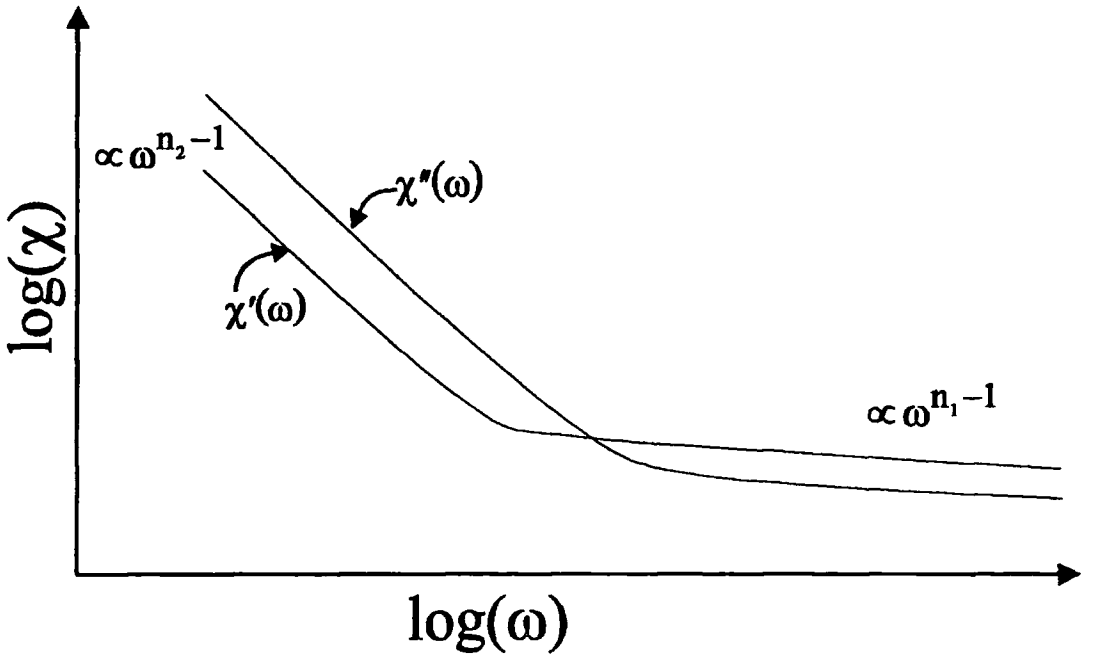

Figure 2.6: Representation of the low-frequency dispersion.

process dominating at low frequency is due to a "transport-like" phenomena. The frequency response of the dc conductivity (equations (2.17) and (2.18)) is clearly different to that observed in figure 2.6. In fact in that case, $\chi'(\omega)$ tends to a constant and $\chi''(\omega)$ is proportional to $\sigma_{DC}\ \omega^{-1}$ when the frequency approaches zero.

Similarly, Maxwell-Wagner interfacial polarisation (equation (2.60)) predicts a limiting behaviour of a power law form but with a higher-frequency region in which $\chi'(\omega)$ and $\chi''(\omega)$ are proportional, respectively, to ω^{-1} and ω^{-2}, so that their ratio is not independent of frequency. For a description of LFD in terms of a polarisation effect, it would be necessary to envisage a superposition of Maxwell-Wagner processes with a distribution of the characteristic times. Such evidence led Jonscher [41] to consider LFD as a separate phenomenon, generated by an imperfect charge transport.

A few models have been proposed that give a microscopic insight into LFD. Among those is that developed by Dissado and Hill [42]. This considers that LFD is associated with the hopping of charges between clusters and whose movement is restricted by the site occupancy or by the low dimensionality of the system. The model is an extension of their theory of cluster vibrations [43], which attempted to interpret the "universal" fractional power law response (i.e. equations (2.32), (2.33) and (2.70)) on the basis of many-body interactions. The approach considers the modifications to the vibrational spectrum of a perfect lattice arising as a result of imperfections such as dipoles and charge carriers. This leads to the appearance of long "tails" in the spectrum which follow fractional power laws. The model explains the power laws in terms of interactions between the defects. Defining clusters as local groupings of interacting defects, intracluster interactions are shown to be responsible for the short-time response (high-frequency) while intercluster interactions account for the long-time response (low-frequency).

2.6 Electric properties of conducting polymers

Electrically conductive polymers represent one class of organic materials that have attracted considerable interest since the discovery by Chiang et al. [44] in 1977 that upon treatment (doping) with iodine or other acceptors, polyacetylene (a good insulator in its undoped form) converts into a quasi-metal. Since this time, other polymers with similar

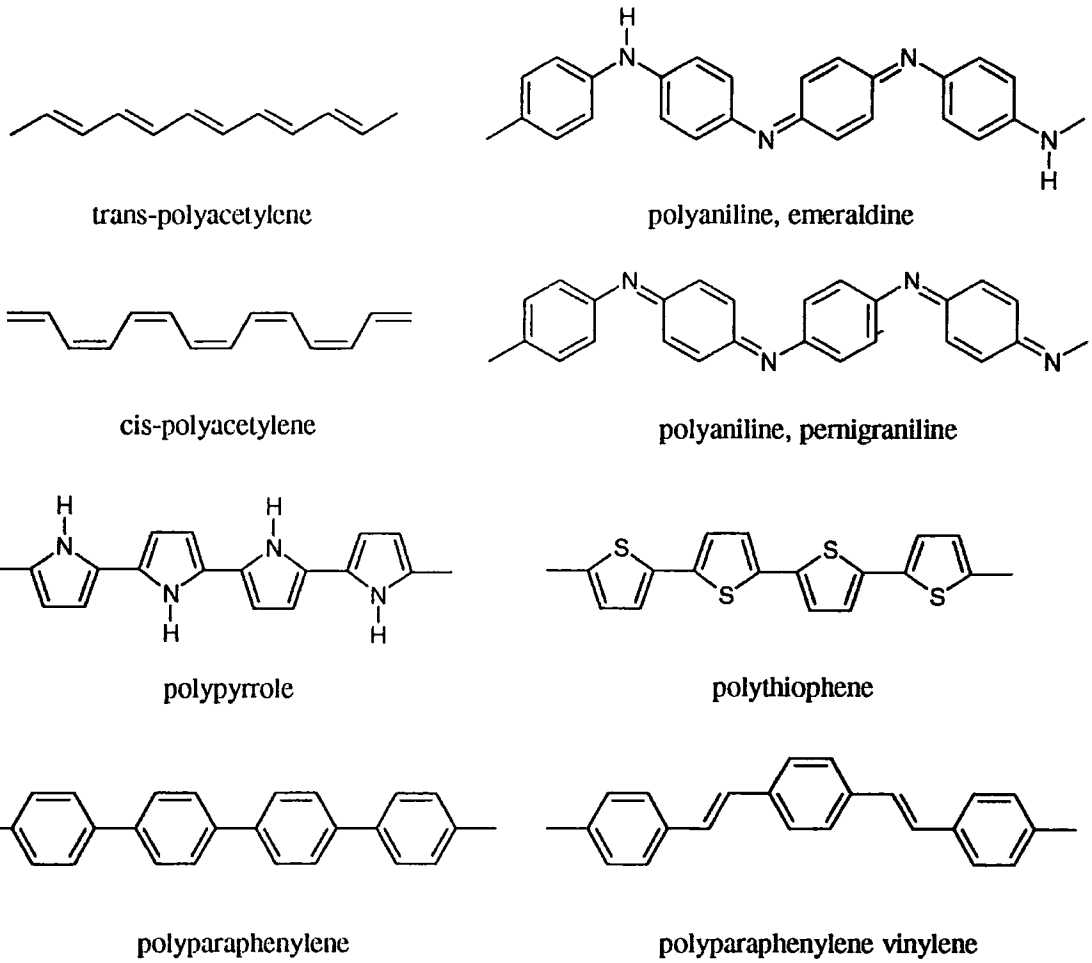

Figure 2.7: Chemical structure of some important conjugated polymers, which become conductive upon doping.

properties have been discovered, some of these are shown in figure 2.7.

A common feature of all conductive polymers is the existence of an extended system of conjugated double bonds (regular alternation of double and single bonds). In fact the conjugated structure is the origin of the intriguing electronic properties of these polymers. In trans-polyacetylene, σ-bonds connecting neighbouring carbon atoms in the polymer chain are formed by sp^2-hybrid orbitals. A σ-bond also binds the hydrogen atoms. In addition, every carbon atom forms a π-bond with the single electron in its p_z orbital. As the electrons in the π bonds are less tightly bonded to the carbon nuclei, the electrons require less energy to be perturbed into excited states.

If all bond lengths between carbon atoms were equal, trans-polyacetylene would be an organic unidimensional metal with a half-filled π-band and the π electrons would be delocalised on the polymer chain. In reality, the ground state has alternating shorter double and longer single bonds, which opens a gap at the Fermi energy, transforming trans-polyacetylene into a semiconductor. This band gap has been found to be around 1.4 eV for trans-polyacetylene and is often in the range 1 - 4 eV for other conducting polymers.

The rather large band gap gives rise to a small intrinsic carrier concentration at room temperature. This intrinsic conductivity is generally lower than 10^{-8} S cm^{-1}. Carriers can be created by adding electron donating (reduction) or accepting (oxidation) species to the polymer, causing electron (n-type) or hole (p-type) conductivity. This procedure is called doping, as in the case of inorganic semiconductors. The dopant materials are typically molecules (or occasionally atoms) with a large electron affinity or a small ionisation potential for acceptors and donors, respectively.

As discussed in section 2.3.1, disorder introduces localised states in the energy gap. For polymers with conjugated double bonds, there are two main types of localised states, soliton and polaron states (figure 2.8). A soliton states occurs when there is bond

mismatch with two adjacent bonds of the same length, which results in an unpaired π electron. From symmetry reasons [45] the localised state is exactly at midgap. Polarons are introduced when new charges are added to the polymer, as shown in figure 2.8. A polaron can be envisaged as a 'molecule' of two solitons. Because of the interaction between these, the degeneracy of the two midgap states is lifted and one is pushed towards the valence band, the other towards the conduction band, as shown in figure 2.8. When these defects are doubly charged, they are termed bipolarons. Soliton and polaron states play an important role in the conductivity of conjugated polymers since they serve as hopping sites for the charge carriers. But due to disorder, solitons and polarons lose many of their characteristic features in real polymer samples.

When a sample with neutral solitons is treated with an oxidising agent (acceptor doping) the electrons sitting in the soliton states are the first to be removed. When all neutral solitons have been used up, further electrons can only be taken out from the polymer if

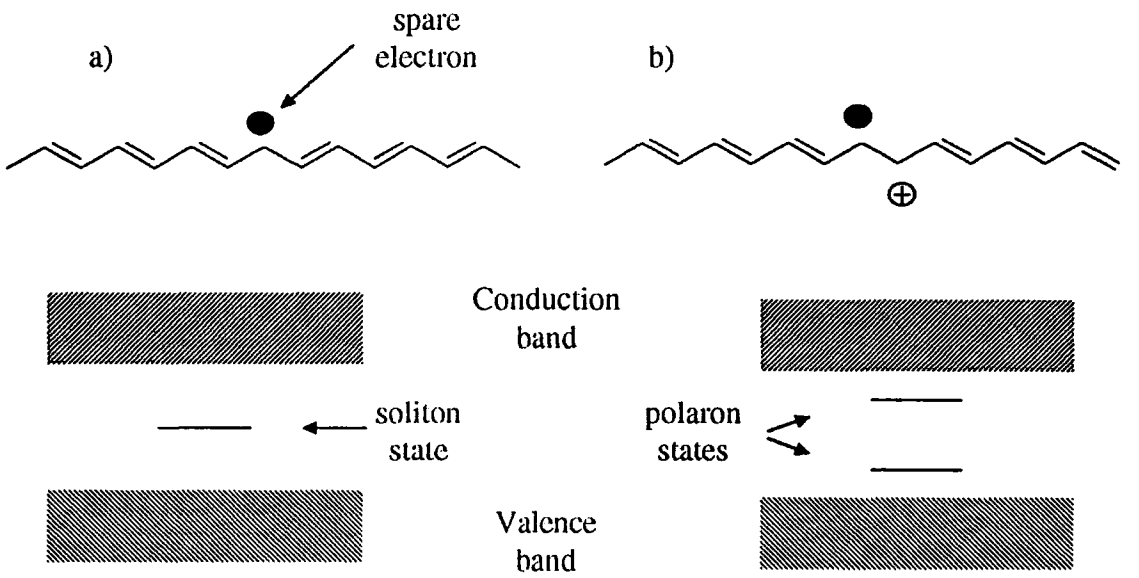

Figure 2.8: a) Soliton and b) polaron states in trans-polyacetylene.

bonds are broken. This creates new solitons and polarons. Thus the process of doping not only consists of the introduction of charge but also in the generation of localised states in the gap, until finally the band structure of the conjugated system is severely disrupted and the polymer behaves like a disordered metal.

The disorder in a doped conducting polymer originates from the random distribution of doping ions, or the clustering of doping ions. Other causes include structural defects such as fibrillar morphology, crystalline and amorphous regions, chains of finite length, and defects within a chain. Consequently, the fundamental electronic structure of a heavily doped conductive polymer is that of a metal with a continuous density of states. However, because polymeric systems are inherently disordered, states in the band tails are localised and there exists a mobility edge that separates the region of the extended states in the interior of the band from the region of localised states. Whether the doped system behaves as a metal or as an insulator is determinated by the relative position of the Fermi energy with respect to the mobility edge.

For conducting polymers in the insulating state, the conductivity decreases upon cooling. Due to the disorder, the states in the band gap are localised and the conduction is by hopping. A typical temperature dependence observed for the conductivity in conducting polymers is the exponential law behaviour characteristic of the hopping transport (equation (2.47)). Various values of the exponent ($\ln \sigma_{DC} \sim T^{1/4}$, $T^{1/3}$, $T^{1/2}$, T) have been reported.

Only recently has improvement in the sample quality sufficiently reduced the dominant role of disorder-induced localisation (although it certainly remains important even in the best materials) to allow metallic behaviour to be observed, with conductivities in the range 10^2 S cm^{-1} < σ_{DC} < 10^5 S cm^{-1} and a negative $\delta\sigma_{DC}/\delta T$ for low temperature. Detailed studies have been undertaken on the metal-insulator transition at low temperature. Results show the presence of a critical regime in which the conductivity has a dependence [46]

$$\sigma_{DC}(T) \propto T^{\beta} \tag{2.71}$$

with $0.3 < \beta < 1$.

Moreover, it has been shown how the transition through the disorder induced critical regime of the metal-insulator transition into the metallic or insulating regimes can be induced by pressure and magnetic field, respectively [47, 48]. The first is explained with a decrease of the interchain spacing due to the high pressure, with a consequent higher overlap of the π-electron wavefunction. In the second case, the magnetic field is supposed to shrink the wavefunction, i.e. increasing the localisation of the states, inducing the transition to the insulating regime (hopping).

2.7 Conductive charge-transfer complexes

The other class of organic materials that possess high electrical conductivity are the charge-transfer (CT) complexes. Some of these are shown in figure 2.9. In such organic systems, intermolecular charge-transfer interactions between the constituent molecules of the salt or complex are the source of the unpaired electrons, giving rise to the conductivity.

Such organic solids are formed by the combination of two (or more) types of neutral molecules, one of which is an electron donor (i.e. has a low ionization potential and can be easily oxidised) and the other is an electron acceptor (i.e. has a high electron affinity and can be easily reduced). The reaction between donor (D) and acceptor (A) molecules in these salts can be illustrated as follows

$$D + A \rightarrow [D^{+\bullet}] + [A^{-\bullet}]$$

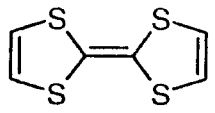

TTF (d)

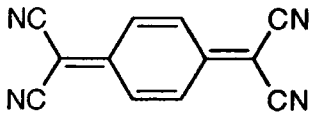

TCNQ (a)

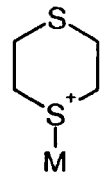

MDT (d)

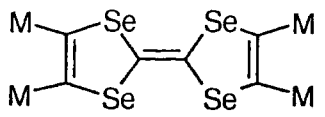

TMTSF (d)

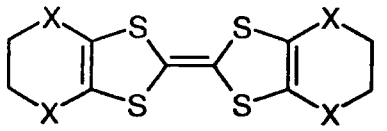

X = S BEDT-TTF (d)
X = O BEDO-TTF (d)

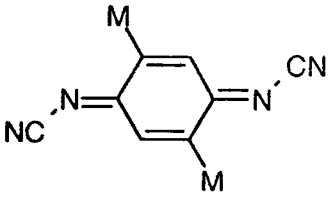

DM - DCBQI (a)

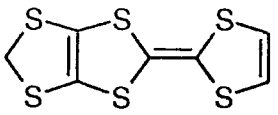

MDT - TTF (d)

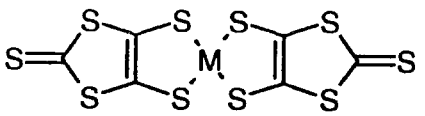

$M(dmit)_2$ (a)

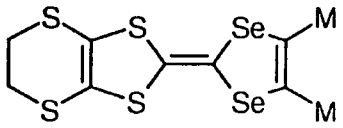

DMET (d)

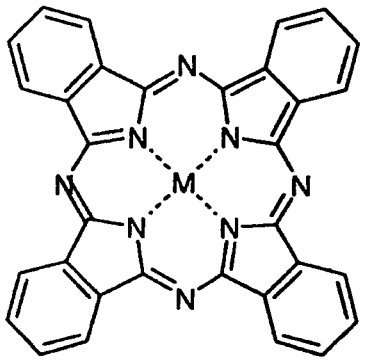

M(Pc) (d)

Figure 2.9: Formulae of some common (d) donor and acceptor (a) molecules that form charge transfer-complexes. M indicates a generic metal element.

where $[D^{+}\bullet]$ and $[A^{-}\bullet]$ are a cation and an anion radical, respectively. As a consequence of this reaction, each molecule has a 'free' electron and a 'free' hole that can contribute to the conduction.

To obtain an organic conductor, other electronic and structural criteria need to be fulfilled. Typically, either the acceptor or donor molecules (or both species) are planar (or nearly planar) in shape. This favours crystallisation in the form of highly ordered stacks. Stacks arrangement can be of two types: (i) segregated stacks, in which the donors and acceptors form separated stacks as shown in figure 2.10a; or (ii) mixed stacks, in which the donor (D) and acceptor (A) stack alternately face-to-face as shown in figure 2.10b.

Molecular compounds with mixed stacks are not highly conductive because of electron localisation on acceptor species. For charge-transfer complexes that form segregated stacks, high conductivity can be observed. If there is an effective overlap of the π-electronic systems (the p_z orbitals) above and below the molecular planes of each molecule, then there is extensive electronic delocalisation along the stacks. Consequently, a high conductivity is observed in the direction along the stacks (indicated by the arrow in figure 2.10b). The conductivity is highly anisotropic, with a value in the stack direction that can be 2 - 3 orders of magnitude higher than that in the direction perpendicular to the stacks.

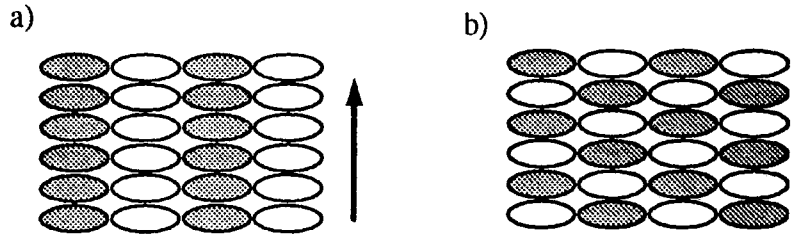

Figure 2.10: (a) segregated and (b) mixed donor-acceptor stacks. The different shadings correspond to acceptors and donors molecules, respectively.

Another important factor in a CT compound is the degree of charge-transfer ρ, i.e. the average number of electrons transferred from the donor to the acceptor molecule. This is important because conduction can occur down the stack only if a mixed valence state is realised. Consider the general case in which the donor to acceptor stoichiometry is 1 : n. For n = 1, if the charge transfer is complete (i.e. ρ = 1), the salt is an insulator because the conduction can only occur down the stacks at a cost of a large Coulombic energy (due to the interaction between electrons on the same molecule). However, if ρ < 1, the unpaired electron can move along the stack without having to overcome large Coulombic interactions and a highly conductive solid can be formed. For TTF - TCNQ complex (molecular structures in figure 9) ρ has been determined to be 0.59 [49] (i.e. 59 electrons per 100 molecules of TCNQ). In the case in which n > 1, for ρ = 1 the resulting solid is conducting, but the conduction is limited by the weaker Coulombic interactions between electrons on neighbouring molecules. In the case of incomplete charge transfer (i.e. $\rho < n^{-1}$), a higher conductivity can also be observed for n > 1 [50].

The first stable highly-conducting organic CT compound was reported by workers at Dupont laboratories in 1962. The key material was TCNQ [51], which in combination with many monovalent cations formed salts showing a conductivity as high as 10^3 S cm^{-1} at room temperature and semiconducting behaviour on varying the temperature [50]. Later [52], a 1 : 1 salt was formed by combining TCNQ with the donor TTF. This was the first molecular crystal exhibiting metallic behaviour. TTF-TCNQ possesses a conductivity of about 550 S cm^{-1} at room temperature which increases on decreasing the temperature, until 54 K when a metal-insulator transition is observed. In 1979, it was observed that if a conductive salt was subject to a pressure of 10 kbar and then cooled, very high conductivity resulted at low temperature [53], i.e. it was possible to suppress the metal-insulator transition to lower temperature. Superconductivity was first observed in TMTSF (molecular structure in figure 9) salts at low temperature (~ 1 K) and high pressure (8 - 12 kbar) [54]. $(TMTSF)_2ClO_4$ was the first superconductive material at ambient pressure when slowly cooled (T_c = 1.3 K). More recently, the use of BEDT-TTF (molecular structure in figure 9) has yielded a new class of superconductive organic

materials with much higher transition temperatures (as high as 10.4 K) at ambient pressure.

Bibliography

- C.J.F.Böttcher, *Theory of electric polarization vol.1 & 2*, 1978, Elsevier, Amsterdam.
- R.Pethig, *Dielectric and electronic properties of biological materials*, 1979, John Wiley & Sons, Chichester.
- A.R.Von Hippel, *Dielectrics and waves*, 1954, John Wiley & Sons, New York
- A.R.Blythe, *Electrical properties of polymers*, 1979, Cambridge University Press, Cambridge.
- A.K.Jonscher, *Dielectric relaxation in solids*, 1983, Chelsea Dielectric Press, London.
- A.K.Jonscher, *Universal relaxation law*, 1996, Chelsea Dielectric Press, London.
- N.F.Mott, *Conduction in non-crystalline materials*, 1987, Clarendon Press, Oxford.
- N.F.Mott, E.A.Davis, *Electronic processes in non-crystalline materials*, 1979, Oxford University Press, Oxford.
- T.A.Skotheim, R.L.Elsenbaumer, J.R.Reynolds, *Handbook of conducting polymers (second edition)*, 1998, Marcel Dekker Inc., New York.
- M.C.Petty, M.R.Bryce, D.Bloor, *An introduction to molecular electronics*, 1995, Edward Arnold, London
- J.R.Ferraro, J.M.Williams, *Introduction to synthetic electrical conductors*, 1987, Academic Press Inc., Orlando.
- G.J.Ashwell, *Molecular electronics*, 1992, Research Studies Press Ltd, Taunton.
- M.Pollak, B.I.Shklovskii, *Hopping transport in solids*, 1991, Elsevier Science Publishers, Amsterdam.
- B.I.Shklovskii, A.L.Efros, *Electronic properties of doped semiconductors*, 1984, Springer-verlag, Berlin.

References

[1] C.J.F.Böttcher, *Theory of electric polarization vol.2*, 1978, Elsevier, Amsterdam, Chapter VIII.

[2] P.Debye, *Z.Physik.*, **13**(1912), 97.

[3] P.Debye, *Polar molecules*, 1929, Dover Publ. Inc., New York.

[4] R.Pethig, *Dielectric and electronic properties of biological materials*, 1979, John Wiley & Sons, Chichester, Chapter 1.

[5] A.R.Blythe, *Electrical properties of polymers*, 1979, Cambridge University Press, Cambridge.

[6] S.Havriliak Jr., S.Negami, *J.Polym.Sci. C*, **14** (1966) 99.

[7] A.K.Jonscher, *Nature*, **267** (1977), 673.

[8] A.K.Jonscher, *Dielectric relaxation in solids*, 1983, Chelsea Dielectric Press, London.

[9] A.K.Jonscher, *Universal relaxation law*, 1996, Chelsea Dielectric Press, London.

[10] L.A.Dissado, R.M.Hill, *Chemical Physics*, **111** (1987), 193.

[11] K.Weron, *Acta Physica Polonica*, **A70** (1986), 529.

[12] A.Schönhals, A.Schlosser, *Colloid.Polym.Sci.*, **267** (1989) 125.

[13] N.G.McCrum, B.E.Read, G.Williams, *Anaelastic and dielectric effects in polymeric solids*, 1967, John Wiley & Sons, New York.

[14] H.Böttger, V.V.Bryksin, *Hopping conductivity in solids*, 1985, Akademie-Verlag, Berlin.

[15] C.Kittel, *Introduction to solid state physics*, 1986, Wiley, New York.

[16] P.W.Anderson, *Phys.Rev.*, **109** (1958) 1492.

[17] N.F.Mott, *Conduction in non-crystalline materials*, 1987, Clarendon Press, Oxford.

[18] N.F.Mott, E.A.Davis, *Electronic processes in non-crystalline materials*, 1979, Oxford University Press, Oxford.

[19] E.Abrahams, P.W.Anderson, D.C.Licciardello, T.V.Ramakrishnan, *Phys.Rev.Lett.*, **42** (1979) 695.

[20] J.C.Dyre, *J.Appl.Phys.*, **64** (1988) 2456.

[21] J.C.Dyre, *Physical Review B*, **48** (1993) 12511.

[22] B.Wessling, in *Handbook of conducting polymers (second edition)* (T.A.Skotheim, R.L.Elsenbaumer, J.R.Reynolds, eds.), 1998, Marcel Dekker Inc., New York.

[23] M.P.J.van Staveren, H.B.Brom, L.J.de Jongh, *Physics Reports*, **208** (1991) 1.

[24] H.Böttger, V.V.Bryksin, *Phys.Stat.Sol.(b)*, **113** (1982) 9.

[25] H.Böttger, V.V.Bryksin, *Phys.Stat.Sol.(b)*, **78** (1976) 415.

[26] J.C.Maxwell, *A treatise on electricity and magnetism vol.1*, 1881, Clarendon Press, Oxford.

[27] Lord Rayleigh, *Phil.Mag.*, **34** (1892) 481.

[28] K.W.Wagner, *Arch.Elektrotech.*,**2** (1914) 378; **3** (1915) 100.

[29] A.R.Von Hippel, *Dielectrics and waves*, 1954, John Wiley & Sons, New York

[30] L.K.H. van Beek, *Progress in Dielectrics*, **7** (1960) 69.

[31] K.Yamamoto, H.Namikawa, *Jap. J. Appl. Phys.*, **28** (1989) 2523.

[32] R.W.Sillars, *J.Inst.Elec.Engrs.*, **80** (1937) 378.

[33] K.Yamamoto, H.Namikawa, *Jap.J.Appl.Phys.*, **27** (1988) 1845.

[34] K.Yamamoto, H.Namikawa, *Jap.J.Appl.Phys.*, **31** (1992) 3619.

[35] B.K.P.Scaife, *Principles of dielectrics*, 1989, Clarendon Press, Oxford.

[36] A.R.Haidar, A.K.Jonscher, *J.Chem.Soc.Faraday Trans.1*, **82** (1986) 3535.

[37] A.K.Jonscher, T.Ramdeen, *IEEE Transactions*, **EI-22** (1987) 35.

[38] T.Ramdeen, L.A.Dissado, R.M.Hill, *J.Chem.Soc.Faraday Trans. 2*, **80** (1984) 325.

[39] E.F.Owede, A.K.Jonscher, *J.Mater.Sci.*, **27** (1992) 1672.

[40] A.K.Jonscher, Berjees Nafis Ayub, *J.Mater.Sci.*, **28** (1993) 1879.

[41] A.K.Jonscher, *Philos.Mag. B*, **38** (1978) 587.

[42] L.A.Dissado, R.M.Hill, *J.Chem.Soc.Faraday Trans. 2*, **80** (1984) 291.

[43] L.A.Dissado, R.M.Hill, *Proc.Roy.Soc.Lond. A*, **390** (1983) 131.

[44] C.K.Chiang, C.Z.Fincher, Y.W.Park, A.J.Heeger, H.Shirakawa, E.J.Louis, S.C.Gau, A.G.MacDiarmid, *Phys. Rev. Lett.*, **39C** (1997) 1098.

[45] A.P.Monkman, in *An introduction to molecular electronics* (M.C.Petty, M.R.Bryce, D.Bloor, eds.), 1995, Edward Arnold, London.

[46] R.Menon, C.O.Yoon, D.Moses, A.J.Heeger, in *Handbook of conducting polymers (second edition)* (T.A.Skotheim, R.L.Elsenbaumer, J.R.Reynolds, eds.), 1998, Marcel Dekker Inc., New York.

[47] M.Reghu, K.Vakiparta, CO.Yoon, Y.Cao, D.Moses, A.J.Heeger, *Synthetic Metals*, **65** (1994) 167.

[48] M.Reghu, K.Vakiparta, Y.Cao, D.Moses, *Physical Review B-Condensed Matter*, **49** (1994), 16162.

[49] M.R.Bryce, in *An introduction to molecular electronics* (M.C.Petty, M.R.Bryce, D.Bloor, eds.), 1995, Edward Arnold, London.

[50] J.R.Ferraro, J.M.Williams, *Introduction to synthetic electrical conductors*, 1987, Academic Press Inc., Orlando.

[51] L.R.Melby, R.J.Harder, W.R.Hertler, W.Mahler, R.E.Benson, W.E.Mochel, *J.Am.Chem.Soc.*, **84** (1962) 3374.

[52] J.Ferraris, D.O.Cowan, V.V.Walatka, J.H.Perlstein, *J.Am.Chem.Soc.*, **95** (1973) 948.

[53] A.Andrieux, C.Duroure, D.Jérome, K.Bechgaard, *J.Phys.Lett.*, **40** (1979)381.

[54] K.Bechgaard, C.S.Jacobsen, K.Mortensen, H.J.Pedersen, N.Thorup, *Solid State Commun.*, **33** (1980) 1119.

Chapter 3

GAS SENSING OVERVIEW: SENSORS AND MATERIALS

3.1 Introduction

In this chapter, an overview of the main types of gas sensing devices is first given (section 3.2), followed by a discussion of some of the materials used for gas sensing (section 3.3). Finally, a description of thin film deposition techniques is provided (section 3.4).

3.2 Gas sensing devices

In this first section, the four main types of gas sensors are discussed: (i) electrochemical sensors; (ii) optical sensors; (iii) thermal sensors; and (iv) mass sensors. For each type, some examples are given.

3.2.1 Electrochemical gas sensors

There are three main types of electrochemical sensors. These can be conveniently categorised by the physical parameter being measured: (i) Potentiometric - voltage measurements; (ii) Amperometric - current measurements; and (iii) Conductimetric - conductivity measurements.

Potentiometric gas sensors

In potentiometric gas sensors, a potential change is obtained from the interaction of electrically neutral gas molecules with the sensor. To produce a potential difference, a charge separation is required. Therefore, this type of sensor needs a mechanism to generate ions or electrons at an interface within the sensor.

Within any electrochemical sensor there is a transfer of charge from an electrode to another phase, which can be either a solid or a liquid electrolyte. During this process, chemical changes occur at the electrodes, allowing the charge to be conducted through the electrolyte phase.

An example is the classical potentiometric oxygen sensor in which a solid electrolyte separates two electrodes placed in regions of oxygen partial pressures $(p_{O_2})_1$ and $(p_{O_2})_2$. The reactions taking place at the electrodes might be

Cathode $O_2 + 4e^- \rightarrow 2O^=$

Anode $2O^= + 2H_2 \rightarrow 2H_2O + 4e^-$

and the potential across the membrane V is then given by the Nernst equation [1]

$$V = \frac{RT}{4F} \ln\left[\frac{(p_{O_2})_1}{(p_{O_2})_2}\right] \qquad (3.1)$$

where R is the gas constant, F is the Faraday constant and T is the absolute temperature. Is it clear that the two reactions at the electrodes can only proceed if they are supported by a flux of oxygen ions through the electrolyte and an electronic current through an external load (the total current has to be zero). The best known solid electrolyte used for oxygen sensors is zirconia. This material exhibits a high ionic conductivity while

remaining electronically insulating.

Amperometric gas sensors

An amperometric gas sensor uses the variation in current, induced by a gas, to evaluate the concentration or type of gas. Similar to other types of gas sensors, these devices use semi-permeable membranes through which the gas can diffuse into the electrolyte. The gas is then either oxidised or reduced, resulting in a change in the steady state current over a scanned potential range.

Amperometric gas sensors using solid electrolytes generally operate in the limiting current mode. An example is an oxygen sensor, where the device is used to pump oxygen from the cathode to the anode. The cathode compartment allows access of oxygen gas from the test atmosphere through a small aperture that behaves as a diffusion barrier. If a sufficient voltage is applied between the electrodes, the partial pressure of oxygen in the cathode compartment is reduced to a value near to zero. Under this condition, the current passed by the cell is limited by diffusion through the aperture. The limiting current is then directly proportional to the partial pressure of oxygen outside the cathode compartment [1].

Conductometric gas sensors

The chemiresistor is one of the simplest types of chemical sensor available, and is a classic example of a conductometric gas sensor. A simple chemiresistor, illustrated in figure 2.1, comprises of two electrodes on an inert substrate. The chemically-sensitive thin film is then deposited over the electrode structure. A variety of materials have been exploited including metal oxides [2 - 13], organic crystals [14 - 17] and conductive polymers [18 - 38].

When a voltage is applied to the electrodes, the conduction electrons or holes travel

through the thin film between the two electrodes. On exposure to an electroactive gas, a reduction or oxidation reaction takes place, changing the electrical conductivity of the active material. For example, a tin-oxide sensor exposed to 10 ppm of NO_2 can experience a fall in conductance of three orders of magnitude [2]. Such changes may be due to surface or bulk reactions and are required to be reversible for a practical sensor. Factors affecting the response of these devices include the quality and thickness of the sensitive material as well as the geometry of the electrode structure [3, 39].

Most chemiresistors operate in a DC mode. When applying a periodically changing excitation, it is possible to have a better insight in the equivalent circuit of the device with a discrimination of the electrode effects [40]. In this case the output signal will be related to the changes of the permittivity of the sensitive layers. Therefore, it is not necessary for the sensing material to be conducting and changes of the impedance can be observed without any charge transfer reaction taking place between the gas and the sensitive layer [41 - 56]. Often this type of sensor is referred to as a dielectric sensor.

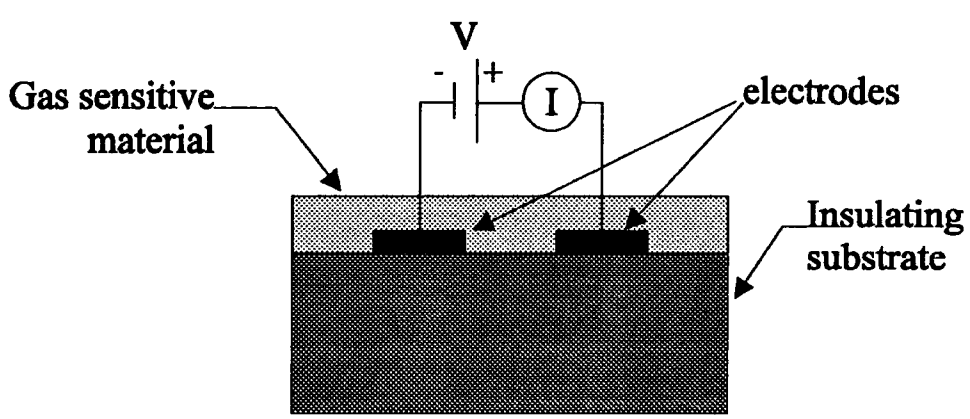

Figure 3.1: General structure of a chemiresistor gas sensor.

3.2.2 Optical sensors

Optical fibres and waveguides are able to transmit light over long distances with a minimal loss of intensity, allowing the development of remote sensors, with the data being propagated as a light pulse. This is useful in situations where the use of electric powered sensors would be hazardous. These sensors can be based on evanescent waves, fluorescence measurements, infrared or ultraviolet-visible absorption and surface plasmon resonance.

Fibre optical devices

Fibre optical devices are normally based on the evanescent wave principle. If focused light is directed into a glass fibre (core) which is encased in a material of a lower refractive index (cladding), part of the beam will be transmitted to the end of the fibre by total reflection at the core/cladding interface. The resulting standing wave in the fibre core will penetrate a small distance into the cladding. The adsorption or dispersion of energy within the cladding is determined by the optical constants of the cladding material. Therefore any optical changes in the cladding, due to a gas, will change the amount (and/or the speed of propagation) of light transmitted down the fibre. For example, one method used is to coat, with a gas sensitive layer, one of two interferometric arms of an integrated optical Mach-Zehnder interferometer [57]. The absorption of light over a range of frequencies in unclad fibres has been recorded on exposure to acetone, ethanol, sulphuric acid [58], ammonia [59], octane, heptane and tetrachloroethane [57]. Optical fibres have also been used to detect pollutants in water, e.g. polydimethylsiloxane clad fibres to detect trichloroethene, dichloromethane and chlorobenzene [60].

Fluorescence devices

Fluorescence-based sensors have been developed for the simultaneous detection of oxygen and carbon dioxide [61]. The tip of a fibre optic cable is coated with both oxygen and carbon dioxide sensitive materials, entrapped in a polymer matrix. The two gases can be detected, and differentiated, by the two distinct emission bands generated by the excitation of the fluorescence indicators. This fibre optic device is a convenient sensor for internal medical monitoring.

Infra-red absorption devices

Infra-red absorption sensors operate on the principle that any compound with a covalent bond or net dipole moment will interact with infrared radiation at a characteristic frequency. When a gas reacts with a chemically sensitive layer, the characteristic spectrum of the layer will change, with the formation of new and/or the suppression of old absorption bands. The sensitivity of this system is high and the selectivity can be enhanced by using narrow band optical filters or by restricting the wavelength region scanned. Infra-red gas sensors have been used to detect H_2S, NO_x, CO, CH_4 [62,63].

Surface plasmon resonance (SPR) devices

When a thin film of a metal is irradiated with a p-polarised light source at a specific angle of incidence, collective oscillations in the free electron plasma are induced at its surface [64]. These are called non-radiative surface plasmons. The effect is observed as a minimum on a plot of the intensity of the reflected light as a function of the angle of incidence. By coating the metal layer with a gas-sensitive film, an optical gas sensor can be fabricated. Exposure to a gas results in a change in the refractive index or thickness of the overlayer, and hence, a shift in the point of resonance. SPR has been used to

successfully detect NO_x [65,66], and hydrocarbons [67,68] (as toluene and benzene) at room temperature.

3.2.3 Thermal gas sensors

Thermal chemical sensors detect the heat ΔE_h that is released or absorbed during a chemical reaction between a gas and the selective layer. This change in enthalpy causes a change in the temperature ΔT which can be monitored. For a thermally insulated system, the temperature change is given by

$$\Delta T = -\frac{\Delta E_h}{C_p} \tag{2.2}$$

where C_p is the heat capacity of the system at constant pressure. The two common types of thermal gas sensors are pyroelectric devices and catalytic gas sensors.

Pyroelectric devices

The pyroelectric effect is the property of certain crystalline, ceramic and polymeric materials to produce an electric charge when they undergo a variation of the temperature. A gas sensor can be fabricated by evaporating two electrodes onto the measurement surface of a pyroelectric material (e.g. $LiTaO_3$ or the β phase of polyvinylene difluoride). One of these electrodes is coated with a chemically sensitive material, allowing the second electrode to be used as a reference. A heater element is attached to the reverse side, allowing complete control of the temperature on one side of the pyroelectric material. The heat loss (or gain) associated with the reaction of the gas with the chemically sensitive material can be assessed by measuring the change in the electrical response.

Catalytic devices (pellistors)

Conventional catalytic gas sensors, often referred as pellistors, operate by the catalytic oxidation of combustible gases. These consist of a catalytic surface constructed around a temperature sensor, and a heater that maintains the catalyst at a sufficiently high temperature to ensure rapid combustion of any flammable gas molecules present. Usually the heating and temperature measurement functions are combined: a platinum coil is embedded in a refractory bead of alumina which is maintained at 500 °C by a current through the wire. The sensor detects the gas by monitoring changes in the resistance of the wire resulting from temperature increases produced by the combustion. Catalytic devices are used for the detection of explosive mixtures of methane or other flammable gases with air. The response of a pellistor is not selective but depends on the product of the flammable gas concentration and its heat of combustion as well as the rate of diffusion of the flammable gas to the gas sensor. So this device gives approximately a universal measure of all flammable gases expressed as a percentage of the lower explosive limit and can be used to monitor the 'explosiveness' of an atmosphere.

3.2.4 Mass gas sensors

The most common gas sensors utilising a change in mass that occurs during a chemical reaction are the quartz crystal microbalance (QCM) and surface acoustic wave (SAW) devices. In each case, metal transducers on a piezoelectric substrate convert r.f. electrical energy into mechanical energy in the form of an acoustic wave. For sensor applications, the device is usually placed in an oscillator circuit where it functions as the resonant element, and the resonance frequency is monitored. Shifts in the frequency Δf are observed when the mass on the surface changes. The basic equation that relates the change of mass Δm to Δf is known as the Sauerbrey equation [40]

$$\Delta f = -\frac{1}{\rho_m k_f} f_o^2 \frac{\Delta m}{A} \tag{2.3}$$

where A is the crystal surface area, ρ_m is the density of the gas sensitive coating on top of the piezoelectric substrate, f_o is the resonance frequency of the uncoated crystal and k_f is the frequency constant.

Quartz crystal microbalance devices

A piezoelectric crystal (e.g. α-quartz) has a resonant frequency that is directly proportional to its mass. By coating a sensitive material onto its upper surface a simple mass gas sensor can be created. The adsorption and desorption of gas molecules, resulting in a change in the overall mass of the sensor, alters the resonant frequency of the crystal according to equation (2.3). This shift in frequency Δf is characteristic of the species and concentration of gas absorbed. By using an array of piezoelectric sensors with different coatings and pattern recognition software, gases including toluene, chloroform and pentane have been successfully detected [70]. Exposing QCMs coated with polymers to various organic solvent molecules (ethanol, benzene, acetone, toluene, dichloromethane etc.), shows how the sensitivity of this devices to specific vapours depends on the functional groups in the polymers [71, 72].

Surface acoustic wave devices

A SAW sensor is a transmission (or delay) line in which an acoustic Rayleigh wave is piezoelectrically generated from a transmitter, propagated along the surface of the substrate, and is transformed back into an electrical signal at the receiver. Interactions of gaseous molecules with the selective material leads to an increase in the layer's mass, modulating the acoustic wave. This can be detected at the receiver as a variation in the

amplitude ΔA, a shift in the frequency Δf, or as a phase shift $\Delta\phi$ in the electrical signal. Any of these parameters can be measured and expressed as a function of the gas concentration. The most common technique is to measure the change in the frequency Δf.

The selectivity of a SAW device is determined by the choice of chemically sensitive material used on the delay line. Using Langmuir-Blodgett films or self-assembled monolayers as coatings, SAW devices offer clear advantages due to their high surface sensitivity. Various polymer and phthalocyanine compounds have been applied to SAW sensors, for the detection of NO_2 [73], ethanol and hexane [74], n-octane and tetrachloethene [75]. The main problems with SAW sensors are poor long-term stability, a high dependence on the temperature and a high sensitivity to ambient moisture. However, with signal processing and compensation techniques, these problems can be minimised.

3.3 Gas sensing materials

The sensitive materials used in gas sensors can be subdivided into two important categories: inorganic and organic materials. Examples of these are presented in the following sections.

3.3.1 Inorganic materials

Metal oxides

Gas sensors (mainly chemiresistors) based on metal oxides (especially SnO_2) are currently the predominant solid-state devices used in commercial sensors [76].

The adsorption of a gas onto the surface of a semiconducting material generates, or modifies, existing surface states. As a result the electrical properties of these surfaces, e.g. conductivity, change. This effect has been observed in many metal oxides including ZnO [4], TiO_2 [6], WO_3 [5], SnO_2 [3, 7-9], $Cr_{2-x}Ti_xO_{3+z}$ (with $0.01 < x < 0.45$) [10], Fe_2O_3 [12], In_2O_3 [13].

Such materials are considered to act as semiconductors with a large band gap. In a metal oxide crystal (e.g. SnO_2) there is a finite density of electron donors (e.g. adsorbed hydrogen) and/or electron acceptors (e.g. oxygen) bound to the surface. These represent surface states that can exchange electrons with the interior of the semiconductor, forming a space-charge layer situated close to the surface. Inside the sensor, current flows through the micro crystallites. At grain boundaries, adsorbed acceptors form a potential barrier (Schottky barrier) which prevents carriers from moving freely (figure 2.2(a)). The electrical resistance of the sensor is attributed to this potential barrier. Thus, by changing the surface concentration n of the donors/acceptors the conductivity is modulated. In the presence of an acceptor gas, the surface density of the negatively charged acceptors decreases, so the barrier height in the grain is reduced (figure 2.2(b)) with a consequent decrease of the sensor resistance.

In conclusion, n-type metal oxides show an increase in conductivity in the presence of reducing gases, and a conductivity decrease due to oxidising gases: p-type oxides exhibit the opposite behaviour. Metal oxides sensors needs to work at elevated temperature. When heated to a certain temperature (~500 °C) there is the reversible reaction of atmospheric oxygen with lattice vacancies in the metal oxide leading to a reduction in the electron concentration n_i. This reaction produces various oxygen species (denoted by the constant m) at different temperatures and oxygen pressures, i.e. O_2^-, O^-, O^{2-}, which can then react reversibly with certain gas (X). Typically, these are reducing agents, gases that are oxidised by atmospheric oxygen, and those such as H_2, CO, hydrocarbons, and other organic gases and vapours. The following reaction scheme applies

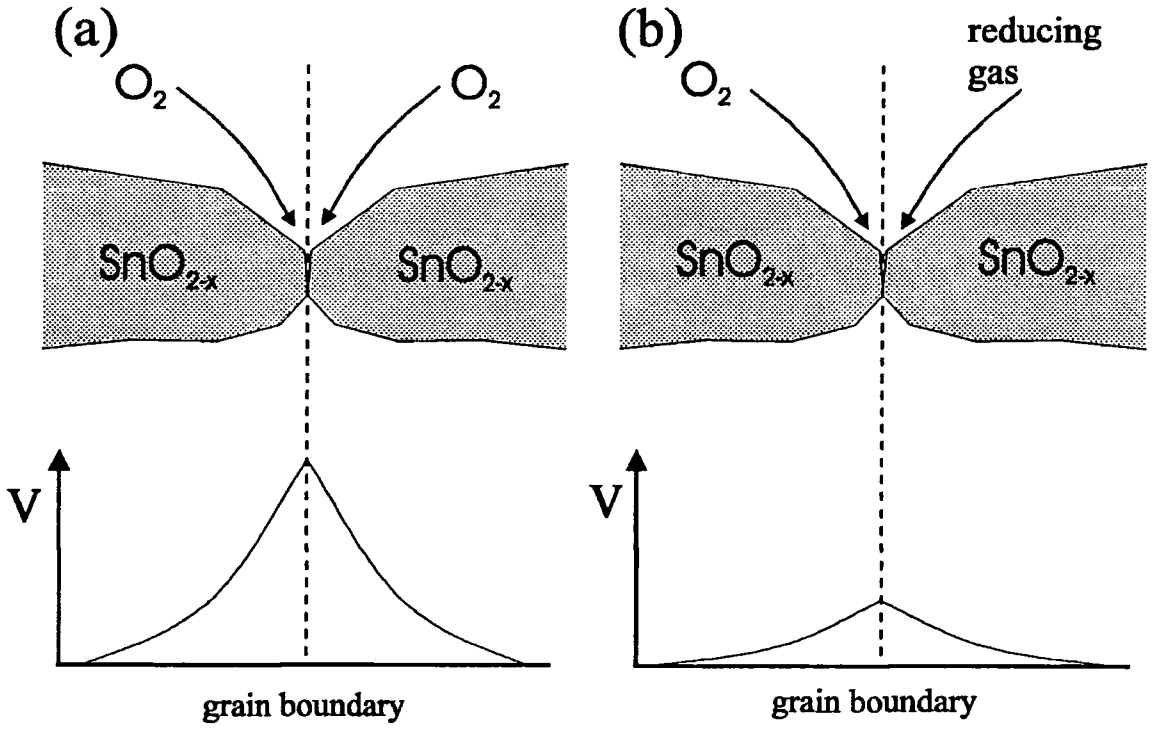

Figure 3.2: Model of inter-grain potential barrier for SnO_2 (a) in the presence only of oxygen (oxidising gas), (b) in the presence of oxygen and a reducing gas.

$$\frac{m}{2}O_2 + [\text{vacant site}] + e^- \xrightarrow{k_1} \left(O_m^-\right)_{site}$$

$$X + \left(O_m^-\right)_{site} \xrightarrow{k_2} \left(XO_m\right)_{site} + e^-$$

Where k_1 and k_2 are the equilibrium constants of the two reactions. For example, the reaction between CH_4 and the oxygen lattice generates water vapour and CO_2 with an increase in the carrier concentration to n_f. Theory predicts an increase in the electrical conductivity $\Delta\sigma$ of the material which can be related to the change in the carrier concentration Δn (n_f - n_i) and, from simple reaction kinetics, to a fractional power λ of the gas concentration [X],

$$\Delta\sigma = \mu_n e \Delta n \propto [X]^{\lambda} \text{ ; where } 0.5 < \lambda < 1$$

where e is the electron charge and μ_n is the electron mobility.

Metal oxides (e.g. SnO_2) generally show a low selectivity and a high sensitivity to water. To improve their response, various techniques have been adopted including: pre-treatment of the material with certain gases (e.g. SO_2 [77]); use of molecular filters [78,79]; and the choice of a optimum temperature (i.e. high temperature for hydrocarbons, low for CO). However, the most common method to improve specificity and rate of response is to add a small percentage of a catalytic metal such as platinum, palladium, aluminium or gold to the metal oxide film [2,80] (this is discussed in the following paragraph).

Catalytic metals

Catalysts alter the rates at which chemical reactions approach equilibrium, without themselves undergoing any permanent change. Catalysts that find use in gas sensors are usually solids that hasten the reactions of molecules in liquids or gases. They provide a means of allowing molecular detection at lower temperatures than would be possible in their absence and they also represent a means to enhancing selectivity. A large proportion of the materials used as catalyst are metals, usually deployed in a high-surface-area form.

A catalytic metal when used in a pellistor (paragraph 3.2.3) allows a decrease of the operating temperature from 800 - 1000 °C (typical of a bare coil) to around 500 °C. However, problems can arise from irreversible 'poising' of the catalyst by, for example, halogenated hydrocarbons.

The addition of particles of precious metal such platinum in a metal oxides sensors can give rise to an increase in the baseline resistance. The mechanism here is similar to the formation of a Schottky barrier from oxygen surface states, except that the charge withdrawal is now due to the high work function of the metal. The oxide is now less susceptible to changes in the moisture content of the atmosphere and responds to reducing gases at lower temperature.

Other uses of catalytic metals are as electrodes in electrochemical cells and in calorimetric sensors [81].

3.3.2 Organic materials

Organic materials generally offer the advantage of being more sensitive at room temperature than their inorganic counterparts, reducing problems of power consumption and enhancing the portability. Moreover, their sensitivity and selectivity can be tailored by modifications to their chemical structure (i.e. a change of functional groups in polymers).

Organic molecular crystals

(i) Phthalocyanines

Phthalocyanines are an important group of charge transfer complexes, offering good thermal stability (up to 200 °C) together with chemical stability (resistant to weak acids and bleaches).

The molecular structure of a metal phthalocyanine is shown in figure 2.9. Several derivatives have been synthesised: with different central metal atoms (i.e., Pb, Cu, Mg, Fe, Ni, Pd, Zn); with various substituted organic side chains to improve their solubility

and improve film deposition (i.e. using the LB technique, spin coating or spray coating); they have also been incorporated in polymers.

The sensitivity of phthalocyanines to gases has been investigated using various techniques: electrical [17, 36, 37]; optical [65, 67]; and mass [82, 83]. The change of the electrical properties of the phthalocyanines during exposure to gases has been related to a charge transfer interaction between the phthalocyanine and the gas. For the majority of phthlocyanines, an increase of the conductivity is observed when exposed to electron acceptor gases (i.e. oxidising gases) such as NO_2, and a decrease when exposed to electron donor gases (i.e. reducing gases) such as ammonia. The increase of conductivity during exposure to NO_2 can be as large as eight orders of magnitude [84] and has been explained by the formation of charge transfer complexes in which electrons are delocalised over the π bonding of the NO_2 and the holes are delocalised over the phthalocyanine structure. This charge transfer reaction has been shown to depend on the central metal ion.

(ii) Porphyrins

Porphyrins compounds are related to phthalocyanines. These comprise a hydrocarbon ring structure with a central metal ion and substituent organic groups around the periphery. Many of these compounds occur naturally. The mechanism for their interaction with gases is similar to that observed for phthalocyanines. When exposed to electron accepting/donating gases (i.e. NO_2, NO and NH_3) they show significant changes in their electrical conductivity [85,86], optical properties [87] and mass [88]. Studies undertaken on these compounds have shown their interactions with gaseous molecules to be largely dependent on the electronegativity of the central metal ion [89]. It has also been demonstrated that the utilisation of porphyrins as gas sensing materials is dependent on factors such as the film thickness and the peripheral substituents on the porphyrin ring [88, 90].

Polymers

Polymers consist of repeat units (monomers) that are joined together to form long chains or reticles depending on the number of monomer functional groups (i.e. if monomers have only two functional groups they will form a chain). The physical and chemical properties of polymers can be varied by changing the monomer, and the molecular dimension (i.e. chain length). This characteristic is maybe one of the most attractive characteristic of these materials: i.e. the possibility of synthesising materials possessing very different physical properties.

For gas sensing, two main classes of polymers are considered: (i) conducting polymers (whose electrical properties have been discussed in paragraph 2.6); and (ii) non-conducting polymers.

(i) Conducting polymers

Since their discovery conducting polymers have attracted considerable interest for their possible applications in gas sensing device. Electrochemical sensors (i.e. chemiresistors) have been widely investigated, also studies of mass [34] and optical changes [91] have been undertaken to gain a better understanding of the polymer/gas interactions. The electrical properties (discussed in paragraph 2.6) can be greatly influenced by interactions with oxidizing/reducing agents. Generally, the effects are not fully reversible for exposure to high concentrations of strong oxidant/reducing agents (e.g. NO_2, NH_3) [23], but show reversible changes for exposure to high concentration of organic vapours (e.g. ethanol, methanol, etc.) [18-20]. The interaction can be explained in terms of a charge transfer reaction between the gas molecules and the polymer [34]. However, other mechanisms, such as film swelling, can be important [92].

Derivatives of the 'basic' conducting polymers have been synthesised to increase their processability in the form of thin films. At present, conducting polymer films can be

formed by electrochemical growth, the Langmuir-Blodgett technique, spin coating, spray coating and thermal evaporation [93].

(ii) Non-conducting polymers

Non-conducting polymers (i.e. non-conjugated polymers) have been used in mass sensors [41 - 43, 55, 71, 72, 75], thermal sensors [42, 43, 55], optical sensors [41, 43, 55] and dielectric sensors [41 - 43, 55]. The detection principle is usually based on a bulk-dissolution of the gas into the polymer film with a consequent change of physical properties such as: (i) mass; (ii) permittivity; (iii) refractive index; (iv) thickness etc. To monitor such quantities, a transducer is required that is more complicated than a simple resistance. However, the advantage of not requiring a chemical reaction between the gas and the polymer molecules can provide improved reversibility and stability. This class of polymer is more wide-ranging than that of conducting polymers, offering more potential for chemical modification to tailor the gas/polymer interaction.

An example is the 'family' of polysiloxanes, characterised by a repeat unit (-RR′-Si-O) where R and R′ are generic functional groups. Studies of the mass changes of different polysiloxane thin films, exposed to organic vapours, has shown that the differences in sensitivities depend on the specific functional groups in the polymer [71, 72]. This can be exploited for the optimisation of the sensitivities to certain organic vapours and for the selection of appropriate materials for sensor arrays.

3.4 Thin film deposition techniques

3.4.1 Langmuir-Blodgett deposition

The Langmuir-Blodgett (LB) technique was first introduced by Irving Langmuir and applied extensively by Katharine Blodgett. This allows the deposition of very thin films onto a solid substrate, with thickness control at the molecular level. The method is based on the transfer of a monomolecular layer (called a monolayer) floating on the surface of a liquid subphase (generally high purity water) to a substrate. Only certain types of molecules have the ability to form such a monolayer. These are generally composed of two parts: one that by itself would mix with water (hydrophilic) and another that by itself

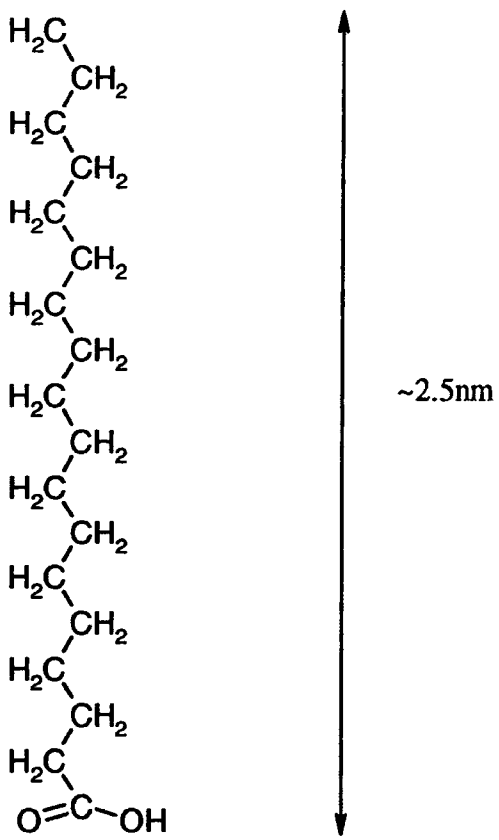

Figure 3.3: Chemical formula for n-octadecanoic acid (stearic acid).

would not (hydrophobic). Such molecules are called amphiphilic: a typical example is octadecanoic acid (stearic acid), shown in figure 3.3. This molecule consists of 16 CH_2 groups forming a long hydrocarbon chain with a methyl CH_3 group at one end and a polar carboxylic acid COOH group at the other. The latter group confers water solubility while the hydrocarbon chain prevents it.

To prepare the monolayer, the organic material is first dissolved in a solvent and the solution spread over the subphase surface. After evaporation of the solvent, the organic molecules remain as a monolayer floating on the subphase, with the hydrophilic part immersed in the water and the hydrophobic parts remaining outside.

The monolayer is enclosed by a barrier system capable of varying its area. When the area is reduced, the monolayer is compressed and, as a consequence, it passes through varies phases analogous to a two-dimensional 'gas', 'liquid' and 'solid'. These phases can be observed by measuring the surface pressure of the monolayer while varying the area (isotherm plot). The surface pressure is defined as the reduction of the pure liquid surface tension due to the presence of the film. The 'gaseous' phase corresponds to the initial situation in which the distance between the molecules is large so that their interaction is negligible. When the area, and therefore the distance between the molecules, is reduced, the hydrophobic chains begin to interact (with a corresponding increase in the pressure) with a transition to a 'liquid' phase, which is characteristic of a random orientation of the hydrophobic chains. As the area is progressively reduced, another increase in the pressure is observed, corresponding to an arrangement in which the molecules form close-packed solid-like phases, with oriented hydrophobic chains pointing away from the water surface.

When the film is in a close-packed state, monolayers can be transferred to a suitable substrate. In the LB deposition method [94], a substrate is coated by moving it up and down through the monolayer/air interface. As material is transferred from the subphase surface to the substrate, a surface pressure sensor is used to control the barriers to maintain the surface pressure constant.

In the most frequently encountered mode of deposition, a monolayer is transferred during each traversal of the monolayer/air interface. These layers arrange in a head-to-head and tail-to-tail pattern, this deposition mode is called Y-type (figure 3.4(a)). Although this is the most frequently encountered situation, instances in which the floating monolayer is only transferred to the substrate surface as it is being inserted into the subphase, or only as it is being removed, are often observed. These deposition modes are called X-type (figure 3.4(b)) (monolayer transfer on the downstroke only) and Z-type (figure 3.4(c)) (transfer on the upstroke only).

Using specialised deposition equipment, films may also be prepared that consist of layers of different molecules. For example, alternate-layer structures can be produced by dipping a substrate through a monolayer of one material (monolayer A) and withdrawing it through a monolayer of a second substance (monolayer B). In this fashion, a monolayer structure of the form ABABAB.. can be built up, as illustrated in figure 3.5.

It is also possible to deposit complex monolayers in which the two components are spread as a mixture onto the subphase surface. To improve the film transfer properties, a fatty acid may be combined with a material that would normally be impossible to deposit

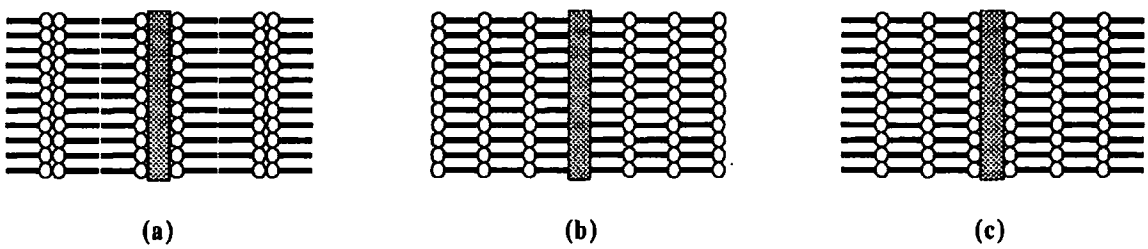

Figure 3.4: Schematic representation of the structures of LB multilayers deposited by three different modes of dipping. (a) Y-type, (b) X-type and (c) Z-type.

reliably on its own. The components in complex monolayers may be completely miscible, as illustrated in figure 3.6(a) or immiscible, in which case the different molecules will aggregate (figure 3.6(b)).

The discussion so far has been confined to monolayers of neutral molecules that bear no electrical charge. This would be the situation for a long-chain fatty acid at a pH of 4 or less. However, on making the subphase more alkaline, ionisation of the polar head groups will occur to form hydrogen ions in the subphase and carboxylate ions in the film, i.e.

$$C_nH_{2n+1}COOH \rightleftharpoons C_nH_{2n+1}CO_2^- + H^+$$

The pH at which half the molecules of an acid are ionised is known as the pK_A of the acid. For example the expected pK_A for n-octadecanoic acid on a water surface is 5.6 [95]. LB films of long-chain fatty acids are often prepared by deliberately adding divalent ions to the subphase to improve the deposition characteristics of the monolayer film. The floating layer will be a mixture of the fatty acid and the fatty acid salt. The salt concentration in the monolayer will depend upon the pH. In a subphase containing cadmium chloride, the following reaction will take place

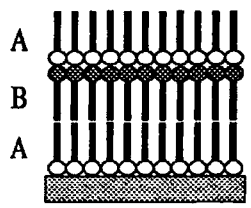

Figure 3.5: An alternate-layer LB film built up from monolayers of compound A and monolayer of compound B.

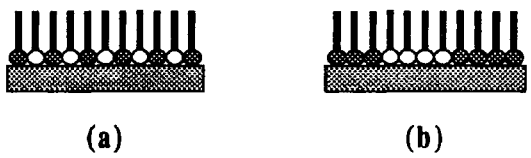

Figure 3.6: Schematic diagram showing the two possible arrangements of molecules in a two-component monolayer: (a) miscible components, (b) immiscible components.

$$2C_nH_{2n+1}COOH + CdCl_2 \rightleftharpoons (C_nH_{2n+1}CO_2)^-{}_2Cd^{2+} + 2HCl$$

The salt formation is favoured by high subphase pH. In the specific case of a floating monolayer of n-eicosanoic acid (arachidic acid) on a subphase at room temperature containing a cadmium salt in a concentration of 10^{-4} M and having a pH = 5.7, a monolayer comprising about 50% cadmium eicosanoate and 50% eicosanoic acid will be formed [96]. By adjusting the pH to 6.5 (for example by addition of sodium bicarbonate $NaHCO_3$) a monolayer of 100% cadmium eicosanate will be formed [97]. The formation of the salt monolayer converts the floating monolayer into a more condensed solid as the head groups are drawn closer together and the tails move nearer to the vertical [98]. LB films of salts of other metal ions, either doubly charged (e.g. Ca^{2+} and Ba^{2+}) or triply charged (e.g. Fe^{3+} and Al^{3+}), have been successfully obtained [99].

3.4.2 Spin coating

The spin-coating technique is currently used in many practical applications to deposit thin films of soluble polymers. For example, it is used extensively in photolithography, to apply the photoresist to a semiconductor wafer surface. The method allows the deposition of thin films, of thickness of the order of microns, which can be controlled by varying parameters such as the spin speed of the substrate and the viscosity of the spun liquid (dependent on the material/solvent ratio). This technique consists of several steps:

(i) the substrate is placed on a spinning plate;
(ii) the solution is dispensed on the substrate while it is stationary;
(iii) the spin speed of the substrate is accelerated to a low speed (~300 rpm) to spread the solution on the substrate (sometimes the solution is directly dispensed when the substrate is already spinning);

(iv) the spin speed is then increased to a high value (of the order of 10^3 rpm). In this way most of the solution is spun off the edge leaving a thin film on the substrate;
(v) the rotating plate is slowly decelerated; and finally
(vi) the film is baked to remove all the solvent (not always used).

3.4.3 Thermal evaporation

Thermal evaporation is a commonly used technique for the preparation of thin films of inorganic as well as organic materials. The process is carried out in a vacuum system. The use of low pressure serves to lower the evaporation temperature as well as reducing the amount of oxides and other impurities in the deposited film. In addition, under vacuum, straight line propagation of the evaporant is favoured, making it possible to reproduce finely defined patterns by the introduction of a shadow mask between the source and the substrate. For best results, the vacuum chamber is held at a pressure below 10^{-4} mbar for the duration of the process, with an ideal pressure for normal working of around 10^{-5} mbar.

A variety of materials are suitable for use as substrates and the properties of the deposited film can be adjusted by heating or cooling the substrate. Deposition rates are variable over a wide range by control of the source temperature. A typical value is 1 nm s^{-1}, but rates as high as 10^3 nm s^{-1} can be achieved. The deposition rate and overall film thickness can be monitored during the evaporation experiment by measuring the shift in the oscillation frequency of a quartz crystal, which is also located in the vacuum chamber and exposed to the evaporation source. The condensed molecules coalescence to form stable nucleation sites which act as centres for film growth. The monolayer grows to form a film covering the entire substrate. The film may not be continuous until many monolayers thick. This contrasts markedly to the LB technique in which complete coverage of the substrate can be achieved by a single monolayer.
Compound films can be produced by the co-evaporation of two or more components

from separate sources. There are two common types of evaporation source: (a) wire filaments or metal foil boats which are directly heated by the passage of an electric current; and (b) non-metallic crucibles (oxides, nitrides, etc) where heat can be supplied by a separate resistive heater or an RF coil wound around the crucible. Alternatively, the evaporation can be directly heated with a focused beam of electrons or a laser.

Bibliography

- J.Janata, *Principles of chemical sensors*, 1989, Plenum, New York.
- J.W.Gardner, *Microsensors: principles and applications*, 1994, Wiley, New York.
- P.T.Moseley, A.J.Crocker, *Sensor materials*, 1996, IOP Publishing Ltd, Bristol.
- J.W.Grate, M.H.Abraham, *Review paper: 'Solubility interactions and the design of chemically sensitive sorbent coatings for chemical sensors and arrays'*, Sensors and Actuators B, **3** (1991) 85-111.
- P.T.Moseley, *Review paper: 'Solid state gas sensors'*, Meas.Sci.Technol., **8** (1997) 223-237.

References

[1] P.T.Moseley, Solid state gas sensors, *Meas.Sci.Technol.*, **8** (1997) 223.

[2] G.Sberveglieri, S.Groppelli, P.Nelli, V.Lantto, H.Torvela, P.Romppainen, S.Leppävuori, *Sensors and Actuators B*, **1** (1990) 79.

[3] W.Göpel, K.D.Schierbaum, *Sensors and Actuators B*, **26-27** (1995) 1.

[4] T.Seymana, A.Kato, K.Fulishi, M.Nagatani, *Anal.Chem.*, **34** (1962) 1502.

[5] D.J.Dwyer, *Sensors and Actuators B*, **5** (1991) 155.

[6] P.J.Shaver, *Appl.Phys.Lett.*, **11** (1967) 255.

[7] G.Wiegleb, J.Heitbaum, *Sensors and Actuators B*, **17** (1994) 93.

[8] L.I.Popova, S.K.Andreev, V.K.Gueorguiev, N.D.Stoyanov, *Sensors and Actuators B*, **19** (1994) 543.

[9] R.Romppainen, V.Lantto, S.Leppävuori, *Sensors and Actuators B*, **1** (1990), 73.

[10] G.S.Henshaw, D.H.Dawson, D.E.Williams, *J.Materials Chem.*, **5** (1995) 1791.

[11] U.Weimar, W.Göpel, *Sensors and Actuators B*, **26-27** (1995) 13.

[12] A.S.Poghossian, H.V.Abovian, V.M.Aroutiounian, *Sensors and Actuators B*, **18-19** (1994) 155.

[13] T.Takada, K.Suzuki, M.Nakane, *Sensors and Actuators B*, **13-14** (1993) 404.

[14] A.Cole, R.J.McIlroy, S.C.Thorpe, M.J.Cook, J.McMurdo, A.K.Ray, *Sensors and Actuators B*, **13** (1993) 416.

[15] B.Bott, S.C.Thorpe, *Techniques and mechanism in gas sensing* (ed. P.T.Moseley et al), 1991, Hilger, Bristol

[16] J.Souto, M.L.Rodríguez-Méndez, J.deSaja-González, J.A.deSaja, *Thin Solid Films*, **284-285** (1996) 888.

[17] R.Rella, P.Siciliano, D.Manno, A.Serra, A.Taurino, A.Tepore, L.Valli, A.Zocco, *Sensors and Actuators B*, **44** (1997) 585.

[18] P.N.Bartlett, S.K.Ling-Chung, *Sensors and Actuators*, **19** (1989) 141.

[19] P.N.Bartlett, P.B.M.Archer, S.K.Ling-Chung, *Sensors and Actuators*, **19** (1989) 125.

[20] P.N.Bartlett, S.K.Ling-Chung, *Sensors and Actuators*, **20** (1989) 125.

[21] H.V.Shurmer, P.Corcoran, J.W.Gardner, *Sensors and Actuators B*, **4** (1991) 29.

[22] J.W.Gardner, P.N.Bartlett, *Synthetic Metals*, **55-57** (1993) 3665.

[23] G.Gustafsson, L.Lundström, *Synthetic Metals*, **21** (1987) 203.

[24] O.N.Timosfeeva, B.Z.Lubentsov, Ye.Z.Sudakova, D.N.Chernyshov, M.L.Khidekel, *Synthetic Metals*, **40** (1991) 111.

[25] J.W.Gardner, M.Vidic, P.Ingleby, A.C.Pike, J.E.Brignell, P.Scivier, P.N.Bartlett, A.J.Duke, J.M.Elliott, *Sensors and Actuators B*, **48** (1998) 289.

[26] M.Angelopoulos, A.Ray, A.G.MacDiarmid, A.J.Epstein, *Synthetic Metals*, **21** (1987) 21.

[27] S.Sukeerthi, A.Q.Contractor, *Indian Journal of Chemistry*, **33A** (1994) 565.

[28] P.D.Harris, W.M.Arnold, M.K.Andrews, A.C.Partridge, *Sensors and Actuators B*, **42** (1997) 177.

[29] F.Musio, M.C.Ferrara, *Sensors and Actuators B*, **41** (1997) 97.

[30] F.Musio, M.E.H.Amrani, K.C.Persaud, *Sensors and Actuators B*, **23** (1995) 223.

[31] E.Milella, F.Musio, M.B.Alba, *Thin Solid Films*, **284-285** (1996) 908.

[32] E.Stussi, R.Stella, D.DeRossi, *Sensors and Actuators B*, **43** (1997) 180.

[33] A.C.Partdridge, P.Harris, M.K.Andrews, *Analyst*, **121** (1996) 1349.

[34] K.Nigorikawa, Y.Kunugi, Y.Harima, K.Yamashita, *Journal of Electrochemical Chemistry*, **396** (1995) 563.

[35] D.L.Ellis, M.R.Zakin, L.S.Bernstein, M.F.Rubner, *Anal. Chem.*, **68** (1996) 817.

[36] T.Moriizumi, *Thin Solid Films*, **160** (1988) 413.

[37] S.Baker, G.G.Roberts, M.C.Petty, *IEE Proceedings*, **130** (1983) 260.

[38] M.Penza, E.Milella, M.B.Alba, A.Quirini, L.Vasanelli, *Sensors and Actuators B*, **40** (1997) 205.

[39] P.Ingleby, J.W.Gardner, P.N.Bartlett, *EUROSENSOR XII* (ed. J.N.White), 1998, IOP Publishing, Bristol.

[40] J.Janata, *Principles of chemical sensors*, Chapter 3, 1989, Plenum Press, New York.

[41] F.L.Dickert, U.P.A. Bäumler, G.K.Zwissler, *Synthetic Metals*, **61** (1993) 47.

[42] K.D.Schierbaum, A.Gerlach, M.Haug, W.Göpel, *Sensors and Actuators A*, **31** (1992) 130.

[43] M.Haug, K.D.Schierbaum, G.Gauglitz, W.Göpel, *Sensors and Actuators B*, **11** (1993) 383.

[44] M.E.Nicholas, D.E.Pitkanen, C.F.Lavine, J.D.Zook, G.P.Hagen, *Journal of Applied Physics*, **47** (1976) 2191.

[45] E.C.M.Hermans, *Sensors and Actuators*, **5** (1984) 181.

[46] F.L.Dickert, M.Keppler, G.K.Zwissler, E.Obermeier, *Ber. Bunsenges Phys. Chem.*, **100** (1996) 1312.

[47] F.L.Dickert, M.Keppler, *Advanced Materials*, **7** (1995) 1020.

[48] F.L.Dickert, G.K.Zwissler, E.Obermeier, *Ber. Bunsenges. Phys. Chem.*, **97** (1993) 184.

[49] F.Josse, R.Lukas, R.Zhou, S.Schneider, D.Everhart, *Sensors and Actuators B*, **35-36** (1996) 363.

[50] K.Alberti, F.Fetting, *Sensors and Actuators B*, **21** (1994) 39.

[51] C.Cornilia, A.Hielermann, R.Lenggenhager, P.Malcovati, H.Baltes, G.Noetzel, U.Weimar, W,Göpel, *Sensors and Actuators B*, **24-25** (1995) 357.

[52] M.Haug, K.D.Schierbaum, H.E.Endres, S.Drost, W.Göpel, *Sensors and Actuators A*, **32** (1992) 326.

[53] H.E.Endres, S.Drost, *Sensors and Actuators B*, **4** (1991) 95.

[54] H.E.Endres, S.Drost, F.Hutter, *Sensors and Actuators B*, **22** (1994) 7.

[55] K.D.Schierbaum, *Sensors and Actuators B*, **18-19** (1994) 71.

[55] J.J.Sprague, O.Porat, H.L.Tuller, *Sensors and Actuators B*, **35** (1996) 348.

[57] G.Gauglitz, J.Ingenhoff, *Sensors and Actuators B*, **11** (1993) 207.

[58] J.Heo, M.Rodrigues, S.J.Saggese, G.H.Sigel, *Applied Optics*, **30** (1991) 3944.

[59] J.F.Giuliani, H.Wohltjen, N.L.Jarvis, *Opt.Lett.*, **8** (1983) 54.

[60] J.Bürck, J.P.Conzen, B.Becknaus, H.J.Ache, *Sensors and Actuators B*, **18-19** (1994) 291.

[61] O.S.Wolfbeis, L.J.Weis, M.J.P.Leiner, W.E.Zeigler, *Anal. Chem.*, **60** (1988) 2028.

[62] T.Hanawa, S.Kuwabata, H.Hashimoto, H.Yoneyama, *Synthetic Metals*, **30** (1989) 173.

[63] J.P.Li, R.H.Tredgold, R.Jones, *Thin Solid Films*, **160** (1990) 167.

[64] C.Nylander, B.Liedberg, T.Lind, *Sensors and Actuators*, **3** (1982), 79.

[65] J.P.Lloyd, C.Pearson, M.C.Petty, *Thin Solid Films*, **160** (1988) 431.

[66] D.G.Zhu, M.C.Petty, *Sensors and Actuators B*, **2** (1990) 265.

[67] C.Granito, J.N.Wilde, M.C.Petty, S.Houghton, P.J.Iredale, *Thin Solid Films*, **284-285** (1996) 98.

[68] J.N.Wilde, J.Nagel, M.C.Petty, *Thin Solid Films*, in press.

[69] E.Jones, *Solid state gas sensors* (ed. P.T.Moseley, B.C.Tofled), 1987, Hilger, Bristol.

[70] J.Auge, P.Hauptmann, J.Hartmann, S.Rösler, R.Lucklum, *Sensors and Actuators B*, **26** (1995) 181.

[71] R.Zhou, U.Weimar, K.D.Schierbaum, K.E.Geckeler, W.Göpel, *Sensors and Actuators B*, **26-27** (1995) 121.

[72] J.W.Grate, M.H.Abraham, *Sensors and Actuators B*, **3** (1991) 85.

[73] C.Yuquan, Z.Wuming, L.Guang, *Sensors and Actuators B*, **20** (1994) 247.

[74] M.Ohnishi, C.Ishimoto, J.Seto, *Thin Solid Films*, **210** (1992) 455.

[75] K.Bodenhöfer, A.Hielermann, G.Noetzel, U.Weimar, W.Göpel, *Anal.Chem.*, **68** (1996) 2210.

[76] See, for example, Figaro Inc. , Japan Tech. Reps. or Capteur Sensors, UK.

[77] R.Lalauze, N.Bui, C.Pijolat, *Sensors and Actuators B*, **26** (1995) 24.

[78] G.Tournier, C.Pijolat, R.Lalauze, B.Patissier, *Sensors and Actuators B*, **26** (1995) 24.

[79] S.Strathmann, M.Schweizer-Berberich, A.Seube, R.Sharma, A.Peyre-Lavigne, W.Göpel, *Eurosensors XII* (ed. N.M.White), 1998, IOP Publishing Ltd, Bristol.

[80] W.M.Sears, K.Colbow, F.Consadori, *Semicond.Sci.Technol.*, **4** (1989) 351.

[81] P.T.Moseley, A.J.Crocker, *Sensor materials*, 1996, IOP Publishing Ltd, Bristol.

[82] K.D.Schierbaum, R.Zhou, S.Knecht, R.Dieing, M.Hanack, W.Göpel, *Sensors and Actuators B*, **24** (1995) 69.

[83] C.Fietzek, K.Bodenhöfer, M.Hees, P.Haisch, M.Hanack, W.Göpel, *Eurosensors XII vol. 1* (ed. N.M.White), 1998, IOP Publishing, Bristol.

[84] R.L.van Ewyk, A.V.Chadwick, J.D.Wright, *J.Chem.Soc.: Faraday Trans. I*, **76** (1980) 2194.

[85] C.Z.Gu, L.Y.Sun, T.Zhang, T.J.Li, *Thin Solid Films*, **285** (1996) 863.

[86] A.Tepore, A.Serra, D.Manno, L.Valli, G.Micocci, D.P.Arnold, *Journal of Applied Physics*, **84** (1998) 1416.

[87] V.C.Smith, T.Richardson, H.L.Anderson, *Supramolecular Science*, **4** (1997) 503.

[88a] C.Di Natale, A.Macagnano, F.Davide, A.D'Amico, R.Paolesse, T.Boschi, M.Faccio, G.Ferri, *Sensors and Actuators B*, **44** (1997) 521.

[88b] R.Paolesse, C.Di Natale, A.Macagnano, F.Davide, T.Boschi, A.D'Amico, *Sensors and Actuators B*, **47** (1998) 70.

[88c] C.Di Natale, R.Paolesse, A.Macagnano, A.Mantini, A.D'Amico, *Eurosensors XII vol.2* (ed. N.M.White), 1998, IOP Publishing, Bristol.

[89] M.M.Catalano, M.J.Crossley, M.M.Harding, L.G.King, *J.Chem.Soc.: Chem. Commun.*, 1984, 1535.

[90] R.H.Tredgold, M.C.J.Young, P.Hodge, A.Hoorfar, *IEE Proocedings*, **132** (1992) 486.

[91] D.Blackwood, M.Josowicz, *J.Phys.Chem.*, **95** (1991) 493.

[92] J.M.Slater, E.J.Watt, N.J.Freeman, I.P.May, D.Weir, *Analyst*, **96** (1992) 1265.

[93] M.F.Rubner, *Molecular electronics* (ed.G.J.Ashwell), p.89 , 1992, Research Studies Press Plc, Taunton.

[94] K.B.Blodgett, *J.Am.Chem.Soc.*, **56** (1934) 495.

K.B.Blodgett, *J.Am.Chem.Soc.*, **57** (1935) 1007.

[95] J.J.Betts, B.A.Pethica, *Trans. Farad. Soc.*, **52** (1956) 1581.

[96] K.B.Blodgett, I.Langmuir, *Phys.Rev.*, **51** (1937) 964.

[97] R.Viswanathan, D.K.Schwartz, J.Garnaes, J.A.N.Zasadzinski, *Langmuir*, **8** (1992) 1603.

[98] M.C.Shih, T.M.Bohanon, J.M.Mikrut, P.Zschack, P.Dutta, *J.Chem.Phys.*, **96** (1992) 1556.

[99] R.A.Hann, *Langmuir-Blodgett films* (ed. G.G.Roberts), 1990, Plenum Press, New York.

Chapter 4

EXPERIMENTAL TECHNIQUES

4.1 Introduction

In this chapter, is given a description of the experimental techniques and the apparatus used in the research undertaken.

The chapter is divided in for four main sections: (i) Electrical characterisation (section 4.2); (ii) X-ray characterisation; (iii) Surface profiling; and (iv) Gas sensing.

4.2 Electrical characterisation

Depending on the electrical conductivity of the samples, measurements were taken in either, or both, the in-plane and out-of-plane directions. Descriptions of the electrode configurations and experimental apparatus are provided in the following sections.

4.2.1 DC characterisation

The measurement of the DC conductivity (σ_{DC}) was undertaken using the two probe method. Using this, σ_{DC} is given by the following relationship

$$\sigma_{DC} = \frac{I}{V}\frac{d}{A} \qquad (4.1)$$

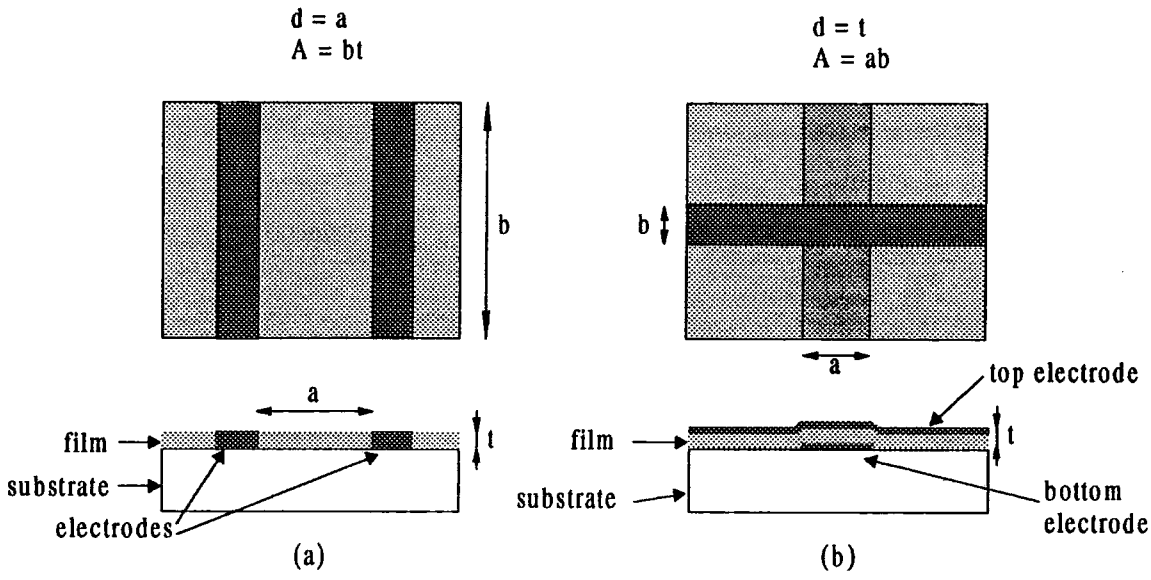

Figure 4.1: Electrode configuration for the measurement of the conductivity (a) in the in-plane and (b) out-of-plane direction. In both diagrams, t indicates the film thickness, d the distance between the electrodes and A their area.

where I is the current flowing in the sample due to an applied bias V, d is the distance between the electrodes and A is their area of overlap. The relationship between the measured σ_{DC} and the film thickness will depend on the electrode configuration, as shown in figure 4.1.

To measure the conductivity in the in-plane direction (figure 4.1 (a)) two electrode configurations were used. The first consisted of interdigitated electrodes (figure 4.2) on which the film was deposited. These were made with: (i) gold (undercoated with chromium) on glass fabricated using photolithography; and (ii) gold/platinum blend printed on an alumina substrate (CorinTech Ltd). The other configuration used was silver paint (Acheson Colloids Electrodag 1415M high conductivity silver paint) electrodes applied to the film after deposition. The silver paint was deposited by hand with a thin wire and 10 minutes were allowed for the paint to dry before any measurement were made.

For the measurement of the conductivity in the out-of-plane direction (figure 4.1 (b)) the electrodes were deposited by thermal evaporation. Metals used were gold, silver and aluminium. Generally, the aluminium was preferred for the top contact because it showed less diffusion into the film.

The experimental circuit for the two probe measurement is shown in figure 4.3. Measurements were made under vacuum (~ 10^{-2} mbar) in a sealed and electrically grounded metal chamber. Contacts to the sample under test were established using gold ball probes.

All electrical connections between the sample chamber, the variable source voltage and the picoammeter were screened to minimise noise interference. Voltages were supplied by a Time Electronics type 2003S voltage calibrator. Current flow was measured using a Keithley Instruments 410A picoammetter.

The experimental set-up for the measurement of σ_{DC} during exposure to gases was similar to that described above, however a different chamber (described in the section 4.6.2) and a different picoammeter were used. For these measurements, a Keithley Instruments 617 was connected to a computer, via an IEEE488 interface, allowing the data to be stored directly. Because of the small dimensions of the chamber, the electrical contacts to the sample were established using silver paint.

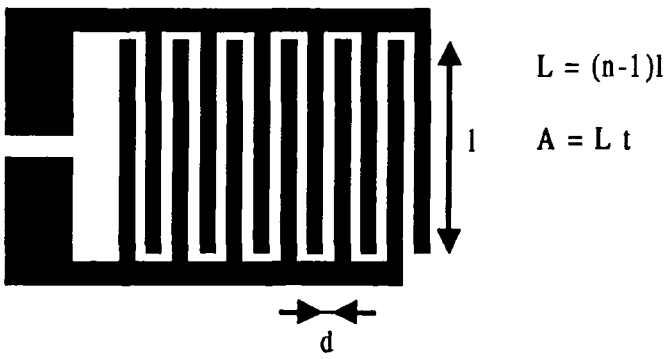

Figure 4.2: Schematic diagram (not to scale) of the interdigitated electrodes used for the measurement of the conductivity in the in-plane direction. n is number of fingers (i.e. 12 in the picture), L is the total length of the electrodes and t is the film thickness.

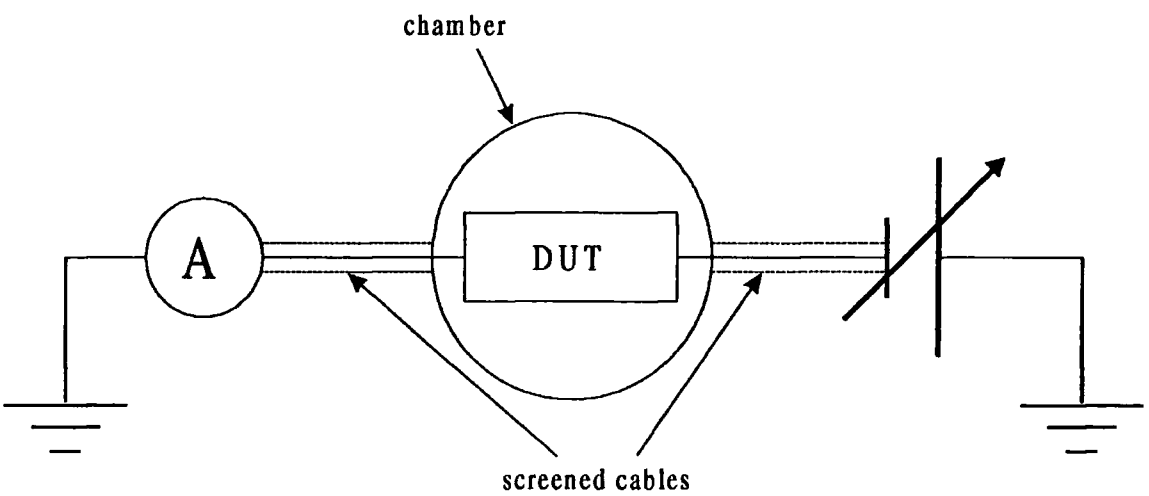

Figure 4.3: Electrical circuit for two-probe measurement. DUT indicates the device under test.

4.2.2 AC characterisation

Principles

The measurement of AC conductivity at different frequencies is a powerful method known as Impedance Spectroscopy (IS). This may be used to investigate the dynamics of bound or mobile charge in the bulk or interfacial regions of a solid or liquid material. These may be ionic, semiconducting, mixed electronic-ionic or dielectric.

The general approach is to apply a perturbation through an electrical stimulus (a known voltage or current) to the electrodes and observe the response (the resulting current or voltage). It is always assumed that the properties of the electrodes/material system are time invariant, and it is one of the purposes of IS to determine their dependence on other controllable variables such as temperature, concentration of gases, applied static voltage, etc.

There are several methods of applying the electrical stimulus. In the frequency domain, the approach consists of using a single frequency voltage $V(t) = V_0 \sin(\omega t)$ (where the signal frequency in Hz is $\nu = \omega / 2\pi$) to the electrodes and measuring the amplitude and the phase shift of the resulting current $I(t) = I_0 \sin(\omega t+\phi)$. The measurement is then repeated at different frequencies.

The impedance at a fixed frequency is defined

$$Z(\omega) = V(\omega)/I(\omega) \tag{4.2}$$

where $Z(\omega)$ is a complex quantity having a real and imaginary part

$$Z(\omega) = Z'(\omega) + i Z''(\omega) = |Z(w)| (\sin(\phi) + i\cos(\phi)) \tag{4.3}$$

The physical properties of the material are generally described by the complex susceptibility $\chi(\omega)$

$$\chi(\omega) = \chi'(\omega) - i\chi''(\omega) \tag{4.4}$$

which is related to the admittance $Y(\omega)$ (the reciprocal of the impedance) by

$$Y(\omega) = \varepsilon_o C_g \chi(\omega) \tag{4.5}$$

where ε_o is the permittivity of free space and C_g is the geometrical capacitance, related to the geometrical structure of the electrodes material system (C_g = A/d, for the structure shown in figure 4.1). The admittance $Y(\omega)$ is often described in terms of its real and imaginary parts

$$Y(\omega) = G(\omega) + iB(\omega) \tag{4.6}$$

where $G(\omega)$ is the conductance and $B(\omega)$ is the susceptance. The response of the system may also be described in terms of a complex conductivity $\sigma(\omega)$

$$\sigma(\omega) = i\omega\varepsilon_o \chi(\omega) \tag{4.7}$$

or in terms of a complex permittivity $\varepsilon(\omega)$

$$\varepsilon(\omega) = \varepsilon_o [1 + \chi(\omega)] \tag{4.8}$$

Equation (4.7) is normally used to describe a system in which a measurable DC conductivity is present, while the equation (4.8) is preferred when dealing with dielectric

materials.

To analyse the results, it is necessary to represent the sample (material plus electrodes, wires, etc.) with an equivalent circuit and to extract the contribution related to the physical properties of the material itself. A mathematical model can then be applied. In our frequency range (10^2 - 10^7 Hz), the system comprises a voltage generator, wires and the electrode/sample system. This can be represented using a equivalent circuit involving ideal elements [1]. Experimental impedance data for a given electrode/material system may be analysed by using an exact mathematical model based on a plausible physical theory, or by a relatively empirical equivalent circuit. An analysis of the charge transport process often suggests an equivalent circuit of ideal resistors and capacitors [1].

The electrical equivalent circuit for our devices include contributions from the film (Z_S), insulating oxide(s) on the electrodes (Z_{ox}), electrodes' resistance (R_e) and the resistance (r) and inductance (L) of the measuring leads (figure 4.4).

The contribution of the inductance was found to be negligible for frequencies less than 10^6 Hz. Furthermore, the contribution from the oxide impedance was much smaller than that of the sample. Therefore the main problem was an estimation of the series resistance r. If we consider a resistance r in series with a sample of admittance G_S and capacitance C_S (both frequency independent), the total admittance is

Figure 4.4: The general equivalent circuit for impedance measurements using the electrode configuration shown in figure 4.1. Z_{OX} and Z_S are the impedances of the metallic oxide(s) and of the film, respectively, R_e the electrodes' resistance and r and L resistance and inductance of the wires, respectively.

$$G(\omega)=\frac{G_S(1+rG_S)+(\omega C_S)^2 r}{(1+rG_S)^2+(\omega C_S r)^2} \quad ; \quad B(\omega)=\frac{\omega C_S}{(1+rG_S)^2+(\omega C_S r)^2} \tag{4.9}$$

Considering, as typical values, $C_S = 50$ pF, $r = 10\ \Omega$ and $G_S \ll r^{-1}$ ($rG_S \ll 1$), we can see that the condition $(\omega C_S r)^2 \ll 1$ is always satisfied in our frequency range and the denominator in equations (4.9) can be considered unity. As a consequence, the contribution of the resistance r will be important only at high frequency ($\nu \geq (2\pi C_S)^{-1}(G_S/r)^{1/2}$). A variation of $G \propto \omega^2$ will then be apparent.

Experimental apparatus

To measure the impedance of our sample we used an HP4192A Impedance Analyzer, controlled by a PC, was used. The software used to control the PC is reported in Appendix A. The measurement function of the 4192A is based on the vector-voltage-current ratio measurement method. Here, the impedance of the Device Under Test (DUT) is determined by measuring the vector ratio between the applied test voltage and the current flowing through the DUT. A method to measure this ratio is based on a range resistor amplifier, as shown in figure 4.5. A voltage to current converter amplifier with a range feedback resistor is used to detect the DUT vector current i_X. The I-V converter causes a current i_R to flow through the range resistor R_R equal to the current through the DUT. Thus the DUT current i_X and the DUT impedance can be found from

$$i_X = e_R / R_R \quad \text{and} \quad Z_X = e_S / i_X = R_R \times e_S / e_R \tag{4.10}$$

Where e_R is the output voltage of the I-V converter and e_S the test signal voltage.

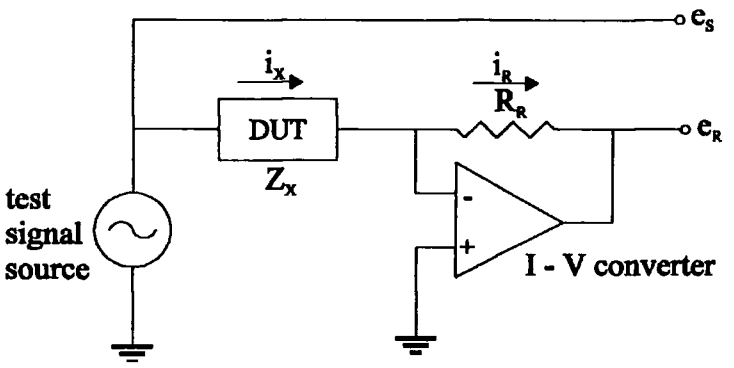

Figure 4.5: Vector-voltage-current ratio measurements using the range resistor amplifier.

This method has a frequency limitation due to the bandwith of the I-V converter so it cannot be used for high frequency impedance measurements.

The 4192A uses an auto-balance bridge circuit [2] that permits the vector voltage across the range resistor to be accurately proportional to the DUT current. In figure 4.6 the basic configuration of the auto-balance bridge circuit is given. The test signal source applies a signal e_S to the DUT and causes a current i_X to flow. This provides the current i_R through R_R. The variable amplitude-phase oscillator applies a signal e_R of the same frequency as the test signal to R_R. Currents i_X and i_R can be balanced varying e_R. The null detector detects the difference i_D between i_X and i_R ($i_D = i_X - i_R$) and gives an output used as the feedback control of the variable amplitude-phase oscillator. When e_R is adjusted for $i_D = 0$, the impedance Z_X of the DUT is calculated from the vector voltages e_S and e_R, in fact

$$i_X = e_S / Z_X , \quad i_R = e_R / R_R , \quad i_X = i_R \tag{4.11}$$

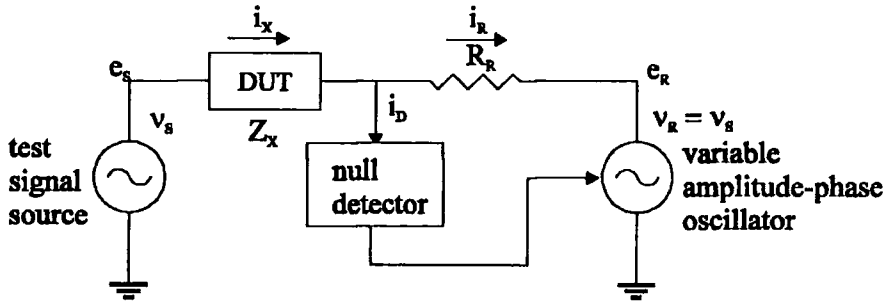

Figure 4.6: Two oscillator model of the auto-balancing bridge.

then

$$e_S / Z_X = e_R / R_R \qquad \text{and} \qquad Z_X = R_R\, e_S / e_R \tag{4.12}$$

so the impedance of the DUT is known by measuring the ratio between the vector voltages.

4.2.3 Low temperature conductivity

To investigate temperature induced variations in the DC and AC conductivity of samples, an Oxford Instruments DN704 liquid nitrogen exchange gas cryostat was used. The unit was constructed around a simple tube with an internal diameter of 20 mm to which a copper heat exchanger was attached. This heat exchanger was cooled with liquid nitrogen fed from a stainless steel reservoir vessel via a supply tube. Nitrogen gas leaving the heat exchange block could exit from the cryostat through an exhaust valve in the top plate. The reservoir was regularly topped up during the course of an experiment to ensure a continuous supply of coolant. A vacuum system consisting of a rotary vane backing pump and an oil vapour diffusion pump was used for evacuation of the equipment. Also, an activated charcoal 'sorb' that would cryopump when cooled was

incorporated in the equipment ensuring a good insulating vacuum for the liquid nitrogen in the reservoir.

The samples were cut approximately 1 cm^2 in size and held in position on the sample holder with air drying silver paint. Electrical contacts to the electrodes on the sample film were made using silver paint, as for the gas sensing experiment. The exchange gas was helium and, after insertion of the sample, the tube was evacuated and flushed out with this gas to ensure complete removal of any water vapour.

The heat exchange block was fitted with a platinum resistance thermometer and a 39 Ω resistive heater, allowing the temperature to be measured and controlled. Temperature variation was achieved by balancing the heat input against the cooling power available, which could be regulated by opening and closing the exhaust valve. The required temperature was set and held constant by an Oxford Instruments DCT2 precision temperature controller.

Using this apparatus, it was possible to measure the DC and AC conductivity in the range 77 K to 300 K.

4.3 X-ray characterisation

When electromagnetic radiation is incident on the surface of a material, some of it will be reflected specularly. For crystalline materials, constructive and destructive interference between the radiation reflected from successive crystal planes will occur when the wavelength λ of the incident radiation is of the same order as the lattice spacing (0.1-5 nm), as shown in figure 4.7. The condition for maxima in the reflected radiation is provided by Bragg's law

$$n\lambda = 2d \sin\theta \qquad (4.12)$$

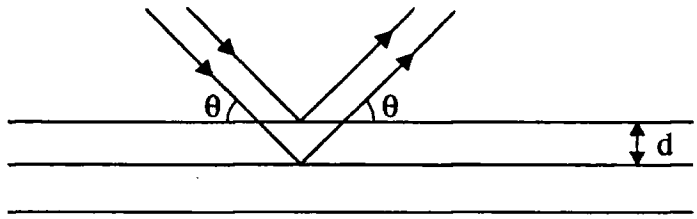

Figure 4.7: Bragg reflection from crystalline planes with spacing d.

where θ is the angle of incidence (conventionally measured from the plane of reflection), d is the interplanar spacing and n is an integer known as the order of the reflection. In the LB films, the distance d will correspond to the distance between the hydrophilic head groups [3], ie, to the thickness of two monomolecular layers for Y-type LB films.

If we consider a typical LB film of a fatty acid, the interplanar space d is approximately 5.0 nm. Using equation (4.12) with an X-ray wavelength of 0.154 nm, gives $\theta \approx 1°$ for the first order Bragg peak. Therefore, low-angle measurements are necessary for X-ray studies of LB films of long-chain compounds.

Our measurements were undertaken on films deposited on a silicon substrate (orientation 100) with X-ray radiation of wavelength $\lambda = 1.3926 \times 10^{-10}$ m.

4.4 Surface profiling

The stylus profilometer is a mechanical instrument that has been used to measure the thickness of LB films. In this technique, a stylus is moved slowly across the surface of

the sample under test. The upward force on the stylus varies with the height of the surface and therefore a graph of the pressure, measured electronically, against stylus position provides a profile of the surface which can be calibrated to give height measurements. Since the profilometer detects changes in height, a step must be provided in the film. For the measurement of the LB films thickness, multilayer structures were deposited onto polished silicon substrates and a step created by carefully wiping away a portion of the film using a tissue soaked in a suitable organic solvent, usually chloroform. Additionally, to prevent the stylus from penetrating the surface of the film, a layer of aluminium, 200 nm thick, was deposited by thermal evaporation over the step between the film and the area of cleaned substrate.

The stylus profilometer used was a Tencor Instruments Alpha-step 200. A stylus force of 11 ± 1 mg was used, together with a scan length 1-2 mm and a sample frequency of 1 per μm.

4.5 Atomic force microscopy

Atomic force microscopy (AFM) is a technique used to provide direct images of surfaces with nanometre resolution [4]. AFM measures the interatomic forces between a cantilever spring tip and the sample surface. The image contrast is achieved by probing the elastic response of the molecules to the force exerted by the scanning tip. AFM can damage the surface of the sample if no care is taken to limit the force exerted by the cantilever tip on the sample. Forces used in AFM range from 10^{-6} N in air to 10^{-11} N while imaging in liquids.

AFM has been successfully used to provide details of the submolecular packing of the hydrophobic surface of LB films [5], but obtaining molecular resolution is not trivial and depends on different factors such as the film fragility.

4.6 Gas sensing

In our experiments, the samples were exposed to four different types of vapour: benzene (C_6H_6), acetonitrile (CH_3CN), ethanol (C_2H_5OH) and water (H_2O). Because of the different sensitivity of the materials used, it was necessary to control the vapour concentration from a few parts per million (ppm) to a few percent by volume. To achieve this, two different methods were used. The diffusion technique allowed vapour generation in the ppm range, while the evaporation method provided concentrations of few percent by volume. In the following paragraphs these two methods will be described, together with the rest of the gas sensing system. The main physical properties of the different used vapours are also briefly reviewed.

4.6.1 Vapour generator

Diffusion method

Gases and vapours have the property of diffusing through tubes at a uniform rate if the temperature, concentration gradients and tube geometry remain unchanged. This phenomenon is a convenient method of producing concentrations of solvent vapours in the low parts per million range. In figure 4.8 the diffusion system is illustrated. Here a metered nitrogen stream was brought to the desired experimental temperature (T = 393 K) by passing it through a constant-temperature bath. The preconditioned nitrogen then passed over the diffusion cell (figure 4.9) and mixed with the vapour of interest at a constant rate. The resultant concentration was controlled by varying the flow rate of either the primary (vapour) or secondary diluent gas (nitrogen). The flow rate of the nitrogen could be controlled using the needle valve of the flowmeter, while that of the vapour could be varied using the temperature (controlled to ± 0.1 °C) of the constant-temperature bath in which the diffusion cell was immersed.

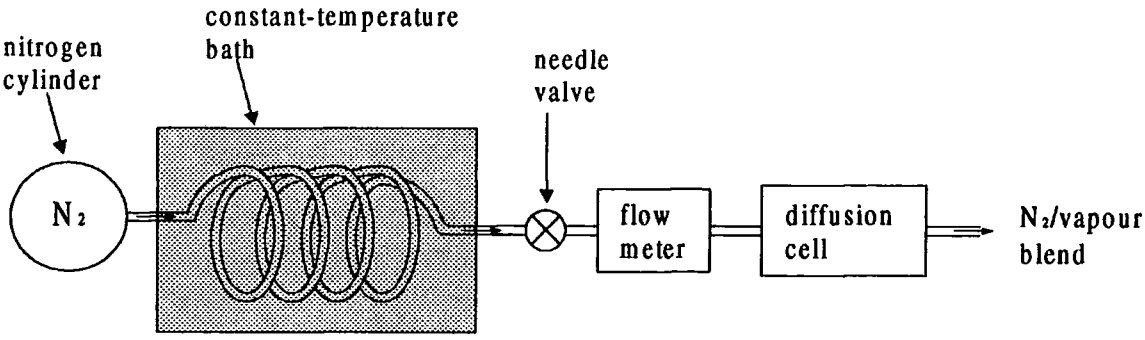

Figure 4.8: Schematic diagram of the dynamic diffusion system.

Figure 4.9 shows a diagram of the diffusion cell. The apparatus consists of two flasks, connected by a length of straight glass tubing (diffusion tube). The inlet and outlet of the upper flask are designed to promote mixing of the vapour with the nitrogen. Ground glass joints connect the upper and lower flasks to the tube, so that tubes of different sizes can be interchanged. In operation, the lower flask is partially filled with a liquid and submerged in a constant temperature bath. The space above the liquid in the lower flask becomes saturated with its vapour. This diffuses through the tube into the upper flask, where it mixes with the gas stream, and is carried away. For a given tube and a given liquid, the diffusion rate depends only on the total gas pressure and the vapour pressure of the liquid in the flask. If the total pressure is constant, the diffusion rate is a function of the temperature only and can be controlled by regulating the bath temperature [6,7].

To calculate the diffusion rate, both the length (L) and the cross-sectional area ($\pi d^2/4$, where d is the diameter of the tube) of the tube must be accurately known. The ratio of area to length should be maintained at less than 0.3 for accurate results [6]. Tubes should be between 2 and 20 mm in diameter. Diameters smaller than 2 mm make tube filling a problem while diameters above 20 mm lead to excessive turbulence. In our experiments,

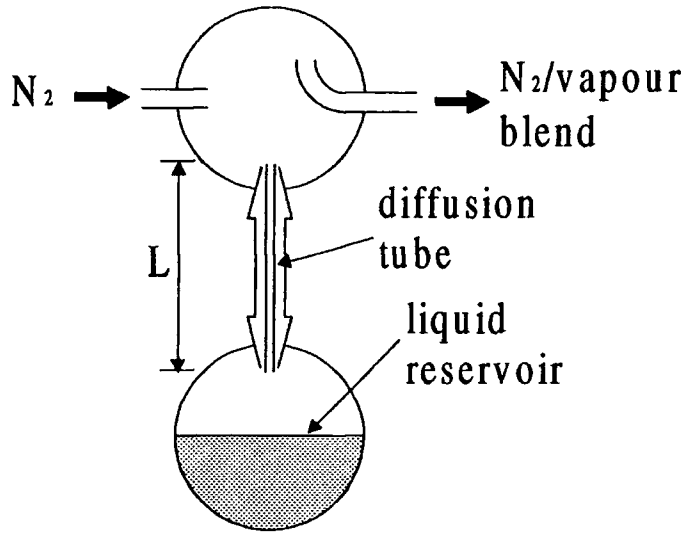

Figure 4.9: Schematic diagram of the used diffusion cell.

we used 2 and 5 mm diameter tubes, with a length of 10 cm (ratios of area to length = 0.03 and 0.20, respectively).

A calibration of our diffusion tubes was made gravimetrically. The liquids in the reservoir were weighed (± 1 mg) before and after a sufficiently long time (generally about 12 hours) of diffusion. A weight loss greater than 100 mg was needed to minimise weighing errors. Before exposing the sample to the N_2 / vapour blend, a period of at least one hour was allowed for the system to settle.

The concentration of a dynamic diffusion system can be expressed by

$$C_{ppm} = \frac{10^6 q_d}{q_N} \qquad (4.14)$$

where C_{ppm} is the concentration in ppm, q_d is the diffusion rate (mL min^{-1}), and q_N is the dilution flow rate i.e. the nitrogen flow rate (mL min^{-1}).

An estimation of the diffusion rate can be found as a function of the size of the tube and of the physical properties of the liquid. Assuming that the concentration of vapour at the tube exit is maintained at nearly zero by the dilution gas and that the vapour in the tube is saturated, then q_d can be calculated from [6,7]

$$q_d = \frac{DMPA \ln\left(\frac{P}{P - p_V}\right)}{LRT} \tag{4.15}$$

where q_d is the diffusion rate (g s^{-1}), D is the diffusion coefficient (cm^2 s^{-1}), M is the molecular weight of the diffusing vapour (g mol^{-1}), P is the pressure in the diffusion cell (mmHg), A is the diffusion tube cross-sectional area (cm^2), L is the length of the diffusion tube (cm), R is the molar gas constant (ml·mmHg (mol K)$^{-1}$), T is the temperature (K) and p_V is the partial pressure of the diffusing vapour (mmHg). If the volumetric flow rate (in mL s^{-1}) is desired it can be obtained by multiplying the previous equation by RT/MP.

Diffusion coefficients at standard conditions (298 K and 1 atm) can be found in the literature [6,8]. At other temperatures and pressures these can be calculated from

$$D = D_{298}\left(\frac{T}{298}\right)^n\left(\frac{760}{P}\right) \tag{4.16}$$

D is the diffusion coefficient at a new pressure P (mmHg) and temperature T (K), D_{298} is the diffusion coefficient at 298 K and 760 mmHg (cm^2 s^{-1}), and n is a coefficient that depends on the vapour and its value is usually in the range 1.5-2.0.

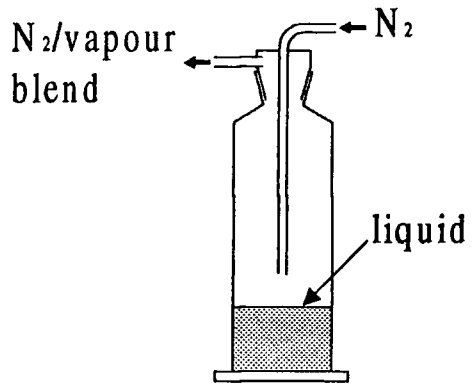

Figure 4.10: Schematic diagram of the evaporation cell.

Evaporation method

Evaporation techniques comprise one of the most generally useful dynamic methods to produce gas mixtures. A diluent gas is passed in a close proximity to the liquid to be vaporised by either dispersing it through or passing it over the liquid of interest. The vapour generator system using the evaporation method was similar to that used with the diffusion method shown in figure 4.8. The difference is the flow of the nitrogen in the evaporation cell, as shown in figure 4.10.

The resultant concentration was controlled by varying either the nitrogen flow rate or the evaporation rate. The latter was accomplished by varying the temperature of the constant-temperature bath (controlled to ± 0.1 K) in which the cell was immersed.

The concentration of vapour in the N_2/vapour blend is calculated from [6]

$$C_{ppm} = \frac{22.4 \times 10^6 \left(\frac{T}{273}\right)\left(\frac{760}{P}\right) W_t}{M(q_N + q_V)} \tag{4.17}$$

where C_{ppm} is the concentration (ppm), T is the experimental temperature (K), P is the experimental pressure (mmHg), W_t is the weight loss per unit time (g min^{-1}), M is the molecular weight (g mol^{-1}), q_N is the flow rate of the nitrogen (L min^{-1}) and q_V is the flow of the contaminant vapour (L min^{-1}). The flow of the contaminant vapour at room temperature can be calculated from

$$q_V = \frac{24.5 W_t}{M} \tag{4.18}$$

The vapour concentration may also be calculated directly from vapour pressure if it is assumed that the diluent gas stream has reached the theoretical saturation at a known temperature.

In our experiment, we calculated the concentration gravimetrically by measuring the quantity of liquid evaporated from the cell. Before starting a calibration, the lower part of the evaporation cell (the flask) was left sealed in the constant temperature bath for a period of more than 15 minutes (to ensure that the liquid was at the same temperature as the bath). Generally, a period of 2 hours was sufficient to have a weight loss of the order of 1 g. Before exposing the sample to the N_2/vapour blend, a period of about 1 hour was allowed for the system to settle.

4.6.2 Gas chamber

The gas sensing circuit (figure 4.11) was the same for both types of vapour generator. A metered nitrogen stream, from a cylinder, was brought to the desired experimental temperature (T = 293 K) by passing it through a constant-temperature bath. The preconditioned nitrogen was then split into two flows, f_1 and f_2. The first, f_1, passed through the vapour generator cell (described above) while the other, f_2, passed directly to the chamber (or to the exhaust). The flows of the two streams were controlled using two different flow-meters in series with a needle valve. By using a four-connector valve, it was possible (with a single rotation of $\pi/2$) to direct f_1 to the gas chamber and f_2 to the exhaust, or vice versa. With this method, a continuous and constant flow through the vapour generator was established, avoiding any change in concentration due to a variation of the flow, e.g. resulting from an accumulation of vapour in the top flask of the diffusing cell (figure 4.9).

In our experiments, f_1 and f_2 were chosen to have the same flow rate, 100 cc min^{-1}. The tubing used was PVC (diameter 8 mm) apart from that from the vapour generator to the

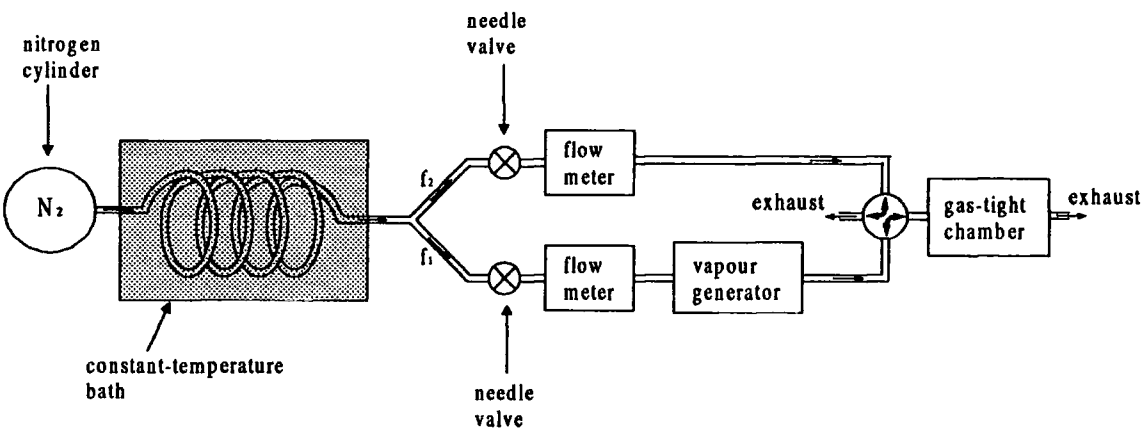

Figure 4.11: Schematic diagram of the gas distribution system.

gas-tight chamber, which was PTFE.

The gas-tight chamber was designed specifically for this work. There were two main requirements. First, the chamber needed to be small so that the time taken to fill with vapour was negligible with respect to the interaction time of the vapour with the sample. Secondly the thermal mass should be sufficient that any change in the electrical properties due to the change of temperature could be negligible. To satisfy the first requirement, a cell was designed with a volume of 14.7 cc, that would be filled in about 9.5 s with a flow of 100 cc min^{-1}. For the thermal stabilisation it was possible to obtain a stable temperature using a water circulator connected to the same constant-temperature bath which was used to thermalise the nitrogen flow. The sample was fixed on the bottom of the gas chamber using a heat sink compound (RS 554-311), which allowed heat exchange between the sample and the chamber. The chamber was made using stainless steel.

4.6.3 Chemical structure and properties of the solvents

The gas sensitivity to four different vapours was investigated. Three of these were organic solvents (acetonitrile, ethanol and benzene) and the other was water. The main physical properties and the molecular structures of these molecules are given in table 4.1. The choice of the organics was based on the following criterea. First, similar boiling points and vapour pressures were needed, so that it was possible to generate similar values of vapour concentration. It was also decided to choose materials with different dipole moments. Acetonitrile is highly polar, benzene is non-polar (on grounds of molecular symmetry) while ethanol has a dipole moment that is in between these two. The use of the water vapour was to the assess the response of the sensing films under practical conditions.

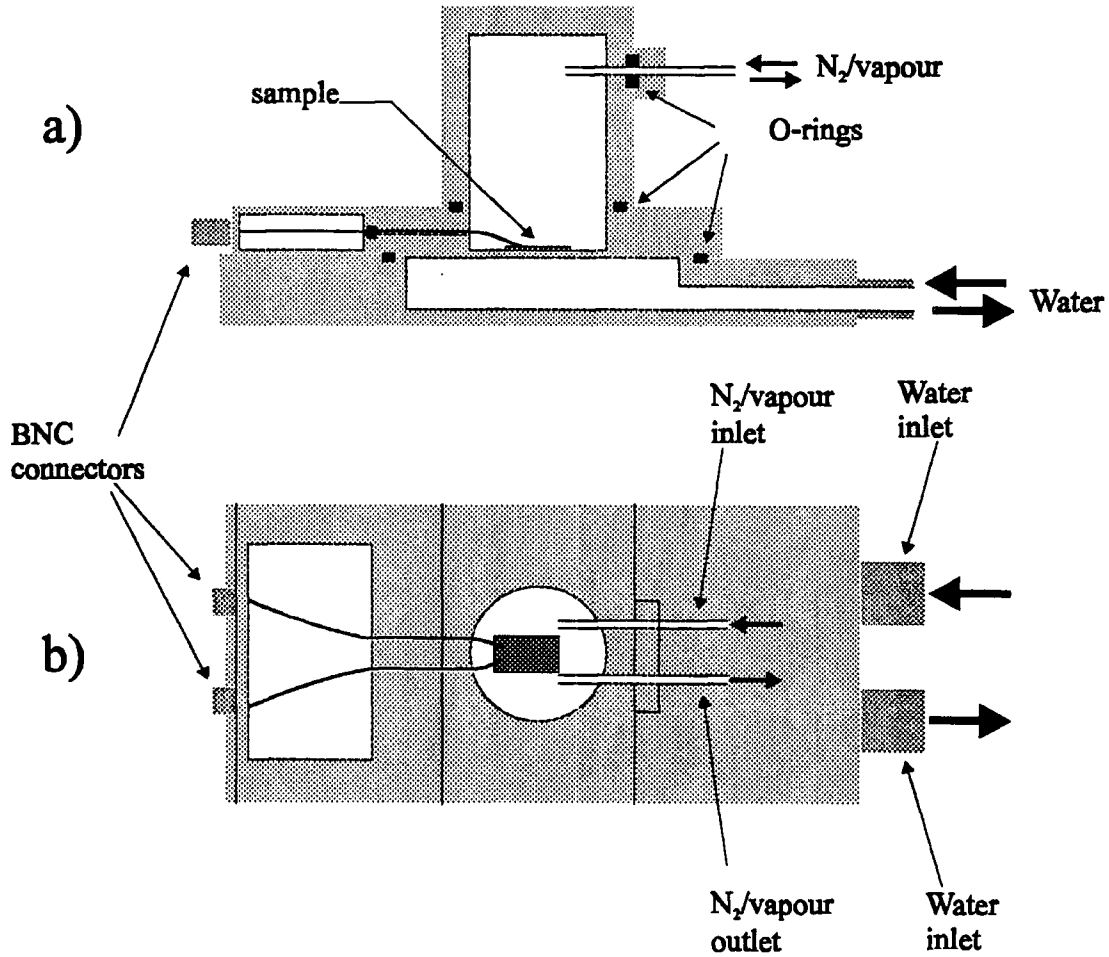

Figure 4.12: Schematic diagram of the gas-tight chamber: (a) side view; (b) top view.

Acetonitrile (Cyanomethane)			
Molecular structure	**boiling point (°C)**	**Formula weight (g mol^{-1})**	**dipole moment (Debyes)**
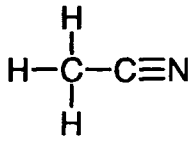	82	41.05	3.92 ± 0.04

Ethanol (Ethyl alcohol)			
Molecular structure	**boiling point (°C)**	**Formula weight (g mol^{-1})**	**dipole moment (Debyes)**
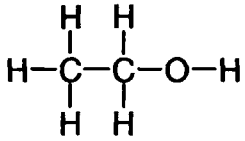	78	46.07	1.69 ± 0.03

Benzene			
Molecular structure	**boiling point (°C)**	**Formula weight (g mol^{-1})**	**dipole moment (Debyes)**
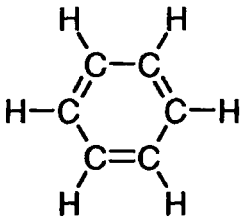	80	78.07	0

Water			
Molecular structure	**boiling point (°C)**	**Formula weight (g mol^{-1})**	**dipole moment (Debyes)**
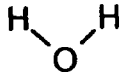	100	18.02	1.85 ± 0.03

Table 4.1: Molecular structure and physical properties of the vapours used in this work.

References

[1] J.R.Macdonald, *Impedance Spectroscopy*, 1987, J.Wiley & Sons, New York

[2] Hewlett Packard 4192A LF Impedance Analyzer Operation and Service Manual (1986)

[3] M.C.Petty, *Langmuir-Blodgett films: an introduction*, 1996, Cambridge University Press, Cambridge.

[4] W.M.Heckl, *Thin Solid Films*, **210/211** (1992) 640.

[5] M.Flörsheimer, A.J.Steinfort, P.Günter, *Thin Solid Films*, **244** (1994) 1078.

[6] G.O.Nelson, *Gas Mixtures 'Preparation and Control'*, 1992, Lewis Publishers, London

[7] J.M.McKelvey, H.E.Hoelscher, *Anal.Chem.*, **29** (1957) 123.

[8] *International Critical Tables*, 1929, Mc Graw Hill Book Company Inc., New York

Chapter 5

Characterisation of organometallic complex LB films

5.1 Introduction

In this chapter, the structural and electrical characterisation of multilayer films containing tetrabutylammonium $Ni(dmit)_2$ complex (figure 5.1) mixed with tricosanoic acid are discussed. The films were built up using the LB deposition technique. Details of the film preparation and the study of its structure are given first (sections 5.2 and 5.3). The electrical measurements in the in-plane and out-of-plane directions are then presented and discussed (section 5.4).

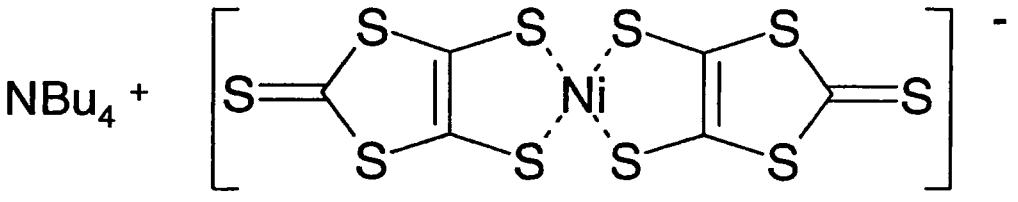

Figure 5.1: The tetrabutylammonium $Ni(dmit)_2$ complex.

5.2 Experimental techniques

Tricosanoic acid (TA) was obtained from Sigma and tetrabutylammonium $Ni(dmit)_2$ complex (Bu_4-$Ni(dmit)_2$ complex) (figure 5.1) from Tokyo Organic Chemicals; both chemicals were used as received. The solution of Bu_4-$Ni(dmit)_2$ complex in dichloromethane (0.5 g l^{-1}) and TA in chloroform (1 g l^{-1}) were used for the preparation of the spreading solutions. For the spreading and deposition of Bu_4-$Ni(dmit)_2$ mixed with TA, the solutions were mixed in the appropriate ratio before spreading on the surface of ultrapure water, at pH 5.8 ± 0.2.

The substrates for film deposition were glass microscope slides. These were cleaned in an ultrasonic bath in a 5% Decon 90 solution, rinsed in ultrapure water and dried with a flow of nitrogen gas.

For electrical measurements in the out-of-plane direction, the electrodes were in a sandwich configuration as shown in figure 4.1. The base electrode strip was aluminium (width 1.4 mm, thickness 400 nm) and the top electrode strip was silver (width 0.6 mm, thickness 50 nm), both deposited by thermal evaporation under high vacuum conditions (≅ 10^{-5} mbar). For the measurements in the in-plane direction, interdigitated (figure 4.2) gold electrodes (undercoated with chromium) with a separation of 20 μm and a total length of 4 cm were used. The electrode patterns were fabricated on glass substrates using standard photolithography techniques. Silver paste (Acheson Electrodag 915) was used to establish electrical contacts to both types of electrode arrangements.

Impedance measurements in the frequency range 10 - 10^6 Hz were made using the HP 4192A impedance analyzer. The RMS amplitude of the ac voltage applied was 1.1 V, no effects were observed for lower applied voltages. Electrical measurements were recorded with the samples under vacuum (≅ 10^{-2} mbar) and the temperature was maintained, using a Peltier element, at 288 ± 0.5 K. Measurements were undertaken both in the in-plane and in the out-of-plane directions.

5.3 Film deposition

Studies of monolayers on the water surface, the film deposition conditions and film morphology have been undertaken previously in Durham [1, 2]. Their results are summarised below.

Condensed pressure versus area isotherms could be obtained for floating films of pure Bu_4-Ni(dmit)$_2$ complex, or mixed with TA. Figure 5.2 shows examples for pure complex, and two different molar concentrations of the mixture with TA. The isotherms were reproducible (within 5%) for subsequent expansions and compressions. No dependence on the time that the film was left on the subphase before compression was observed. This contrasts with the results observed for amphiphilic Ni(dmit)$_2$ analogues, where true monolayers were obtained only if the floating film was kept for several hours on the subphase in its uncompressed state [3, 4].

The average molecular area per Bu_4-Ni(dmit)$_2$ complex can be calculated by extrapolating the high-pressure regions of the isotherms (> 30 mN m^{-1}) in figure 5.2 to zero pressure and subtracting the average area occupied by the fatty acid molecules (assuming the TA molecules are all in contact with the subphase surface and have a cross-sectional area of 0.20 nm^2). Figure 5.3 shows the resulting dependence upon fatty acid concentration. The Ni(dmit)$_2$ moiety may be modelled by a box of dimensions 1.61 nm $\times$ 0.623 nm $\times$ 0.366 nm [3] while the tetrabutylammonium cation will be more similar to a sphere of approximate diameter 1.3 nm. At low TA concentration, figure 5.2 indicates that the organometallic complex is almost certainly in the form of a multilayer on the water surface. As the proportion of fatty acid increases, the average molecular area per complex also increases, indicating that more of the Ni(dmit)$_2$ molecules and/or the counter ions are incorporated in the plane of the fatty acid monolayer.

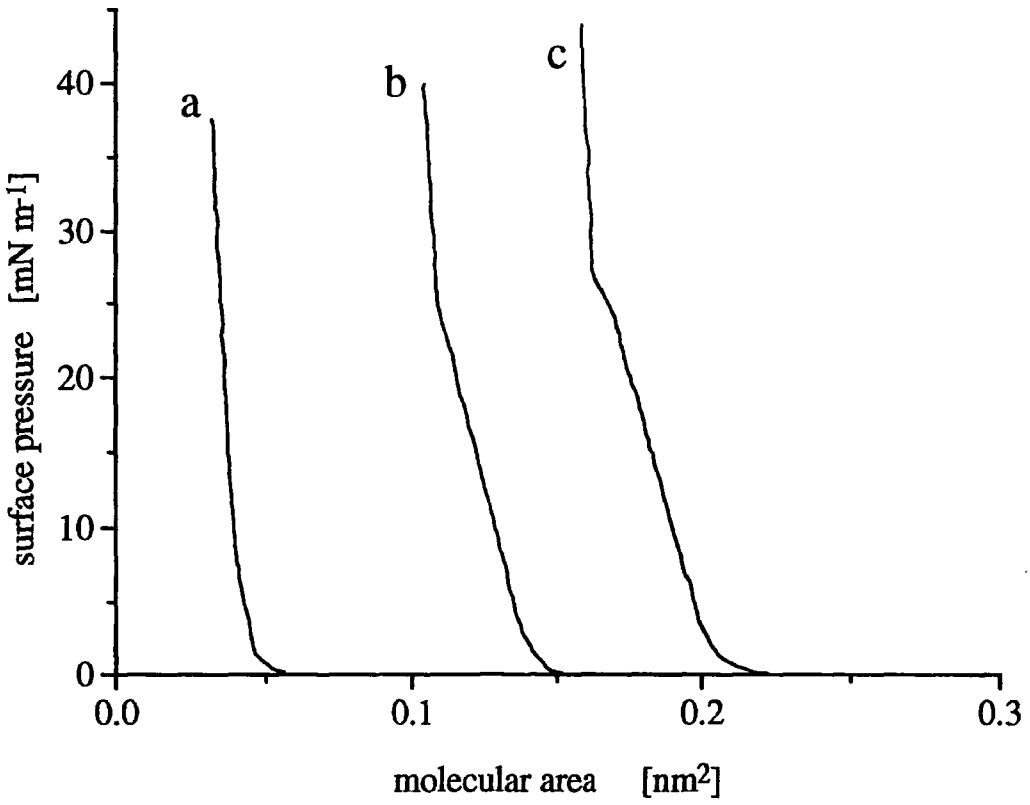

Figure 5.2: Pressure versus area isotherms of Bu_4-Ni(dmit)$_2$ complex mixed with different concentrations of TA. Subphase pH 5.8 ± 0.2, monolayer compression rate ca. 4×10^{-2} nm^2 complex^{-1} s^{-1} : a, 0% TA; b, 24% TA; c, 66% TA. After L.M.Goldenberg et al. [1].

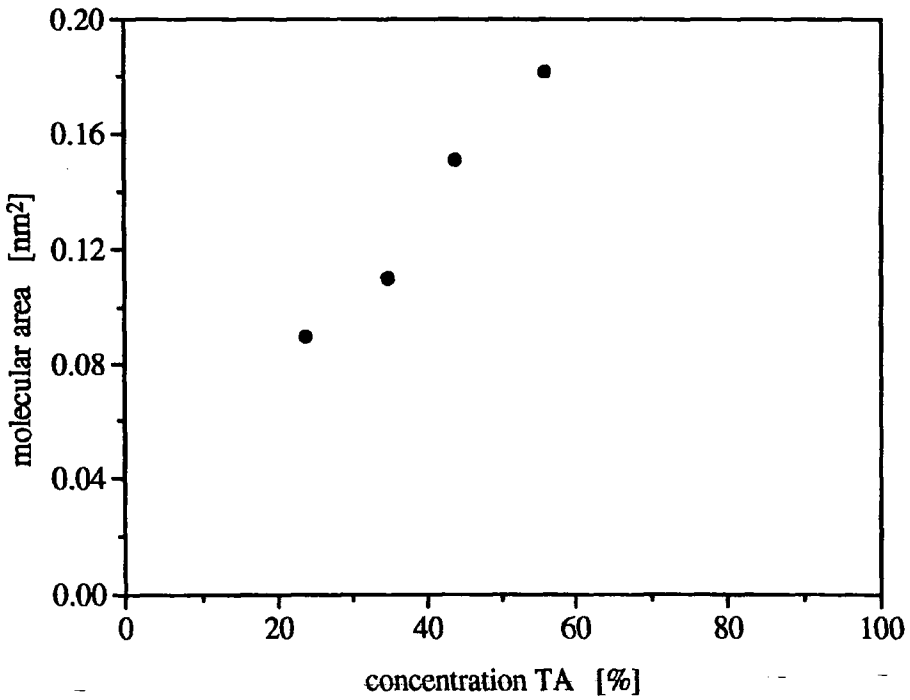

Figure 5.3: Area per Bu_4-Ni(dmit)$_2$ complex, calculated assuming the cross-section of TA as 0.2 nm^2 versus concentration of TA. Subphase pH 5.8 ± 0.2, monolayer compression rate ca. 4×10^{-2} nm^2 complex^{-1} s^{-1}. After L.M.Goldenberg et al. [1].

LB film deposition was undertaken at a surface pressure of 30 - 35 mN m^{-1}. Pure Bu_4-Ni(dmit)$_2$ complex exhibited Z-type deposition. For mixtures with fatty acid, the film transfer started as a Z-type deposition but reverted to Y-type after several (1 - 4, depending on the exact composition) dipping cycles. The deposition ratio was 1.0 ± 0.1 for both the Z and Y cycles. Multilayers assembled from pure Bu_4-Ni(dmit)$_2$ appeared reasonably uniform to the eye but their quality improved with increasing fatty acid content.

A plot of the average thickness per layer, measured with the surface profiling Alpha-Step versus TA concentration is shown in figure 5.4. The large values of thickness obtained with low fatty acid concentrations confirm the suggestion above that the floating film is more than one molecule (complex) in thickness. With increasing TA content, the average thickness per transferred layer decreases and approaches a constant value of 5 nm. This is considerably greater than the longest side of the Ni(dmit)$_2$ anion (1.61 nm) but is consistent with a film in which the Ni(dmit)$_2$ anion is mixed within the fatty acid matrix (thickness 3.0 nm) and the tetrabutylammonium cation is on the top. This would give a total thickness of ca. 3.0 nm + 1.3 nm = 4.3 nm. This model results in the calculated average area per complex equal to that of the Ni(dmit)$_2$ cross-section (ca. 0.23 nm^2), which corresponds well with the observed value of 0.18 nm^2 at high TA concentration (figure 5.2).

Scanning electron microscopy of a 26 layers LB film of Bu_4-Ni(dmit)$_2$ complex mixed with TA (44%) after I_2 doping reveals that the film consists of two phases, with lighter aggregates randomly distributed in a darker matrix [1]. The dimension of the aggregates is < 1 μm. These data are consistent with the LB films containing separated phases of Bu_4-Ni(dmit)$_2$ complex and TA.

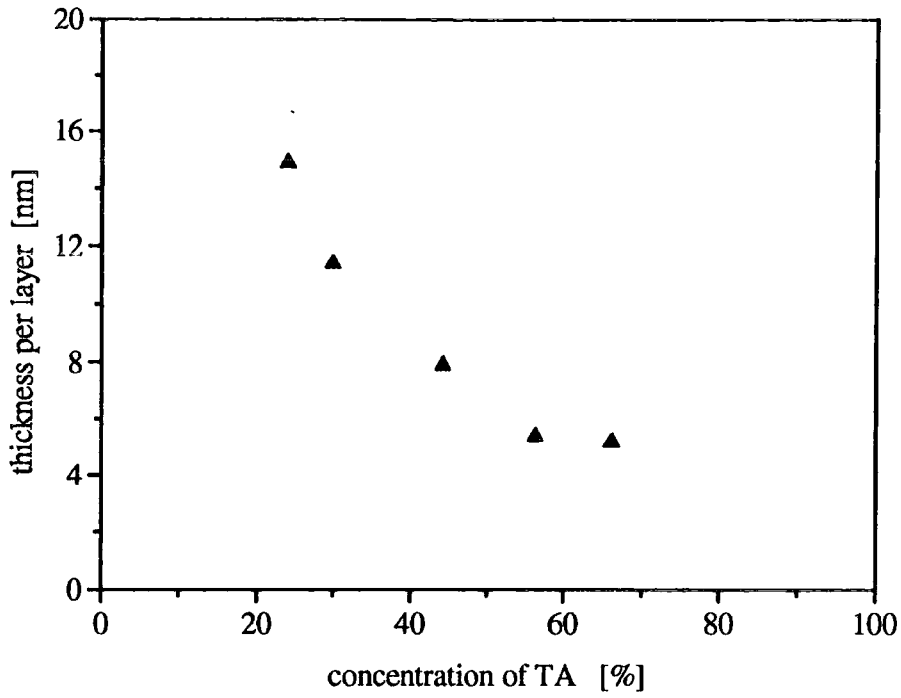

Figure 5.4: Single layer thickness of films of Bu_4-Ni(dmit)$_2$ complex determined by Alpha-Step profiling versus TA concentration. After L.M.Goldenberg et al. [1].

5.4 Electrical characterisation

An investigation of the in-plane DC conductivity for LB film of mixed TA : Bu_4-Ni(dmit)$_2$ complex after post-deposition electrochemical (with four different anions) and chemical (with iodine vapour) doping has been undertaken previously by other workers in Durham [1]. A conductivity $\sigma_{DC} = 10^{-2}$ S cm^{-1} and thermal activation energy $\Delta E = 0.08$ - 0.1 eV over the temperature range 300 - 100 K were reported.

In this section, the electrical measurements on undoped mixed TA : Bu_4-Ni(dmit)$_2$ LB films are reported.

5.4.1 Measurements perpendicular to the film plane

The electrical equivalent circuit of the device will include contributions from the LB film, from insulating oxide(s) on the top and bottom electrodes and from the resistance and inductance of the measuring leads, as indicated in figure 5.5 (discussed in paragraph 4.1.2). Impedance measurements were made for structures both with and without the LB film between the top and bottom electrodes; i.e. the latter 'control' sample simply consisted of $Ag/Al_2O_3/Al$. Figures 5.6 and 5.7 reveal the real (Z') and imaginary (Z'') components of the impedance of these samples over the frequency range $10 - 10^6$ Hz. The LB sample consisted of 15 layers of the mixed TA : Bu_4-Ni(dmit)$_2$ complex with 0.31 molar fraction of fatty acid.

Using the equivalent circuit in figure 5.5 (without any contribution from the LB film), the real and imaginary components of the impedance of the control sample are given, respectively, by

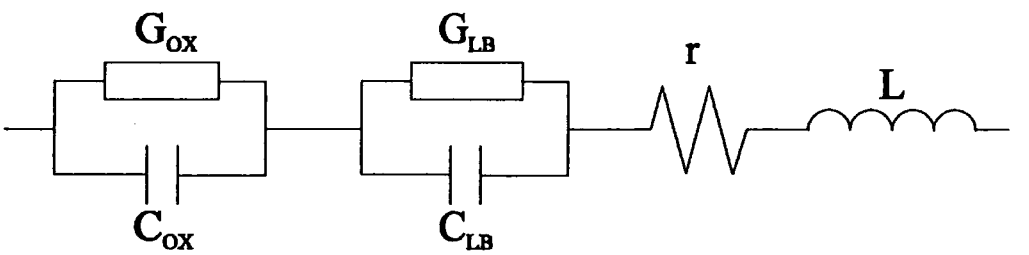

Figure 5.5: The equivalent circuit for the out-of-plane structure. C_{ox} and G_{ox} are the capacitance and conductance, respectively, of the metallic oxide layer(s), C_{LB} and G_{LB} are the capacitance and conductance, respectively, of the LB film, r and L are the resistance and inductance, respectively, of the electrodes and connecting leads.

$$Z' = \frac{G_{ox}}{G_{ox}^2 + \omega^2 C_{ox}^2} + r \qquad (5.1)$$

$$Z'' = \omega L - \frac{\omega C_{ox}}{G_{ox}^2 + \omega^2 C_{ox}^2} \qquad (5.2)$$

where C_{ox} and G_{ox} are the capacitance and conductance, respectively, associated with the oxide layers on the metallic electrode(s), and r and L are the resistance and inductance, respectively, of the electrodes and connecting leads.

For the control sample, in the frequency range 10 - 10^4 Hz, Z′ (figure 5.6) decreased as the frequency increased. The frequency dependence was approximately $Z' \propto \omega^{-2}$, which is consistent with equation (5.1) for the case $\omega C_{ox} \gg G_{ox}$ and $r \ll G_{ox}/(\omega^2 C_{ox}^2)$. Above 10^4 Hz, Z′ approached a constant value of 8 Ω, which we attribute to the series resistance r. Over most of the frequency range studied, the imaginary part of the impedance Z" (figure 5.7) for the control sample decreased approximately as ω^{-1}, according to equation (5.2) with $\omega C_{ox} \gg G_{ox}$ and $\omega L \ll (\omega C_{ox})^{-1}$. Some control samples exhibited a more rapid decrease in Z" above 10^5 Hz due to a finite value of inductance in the measuring circuit (approaching resonance).

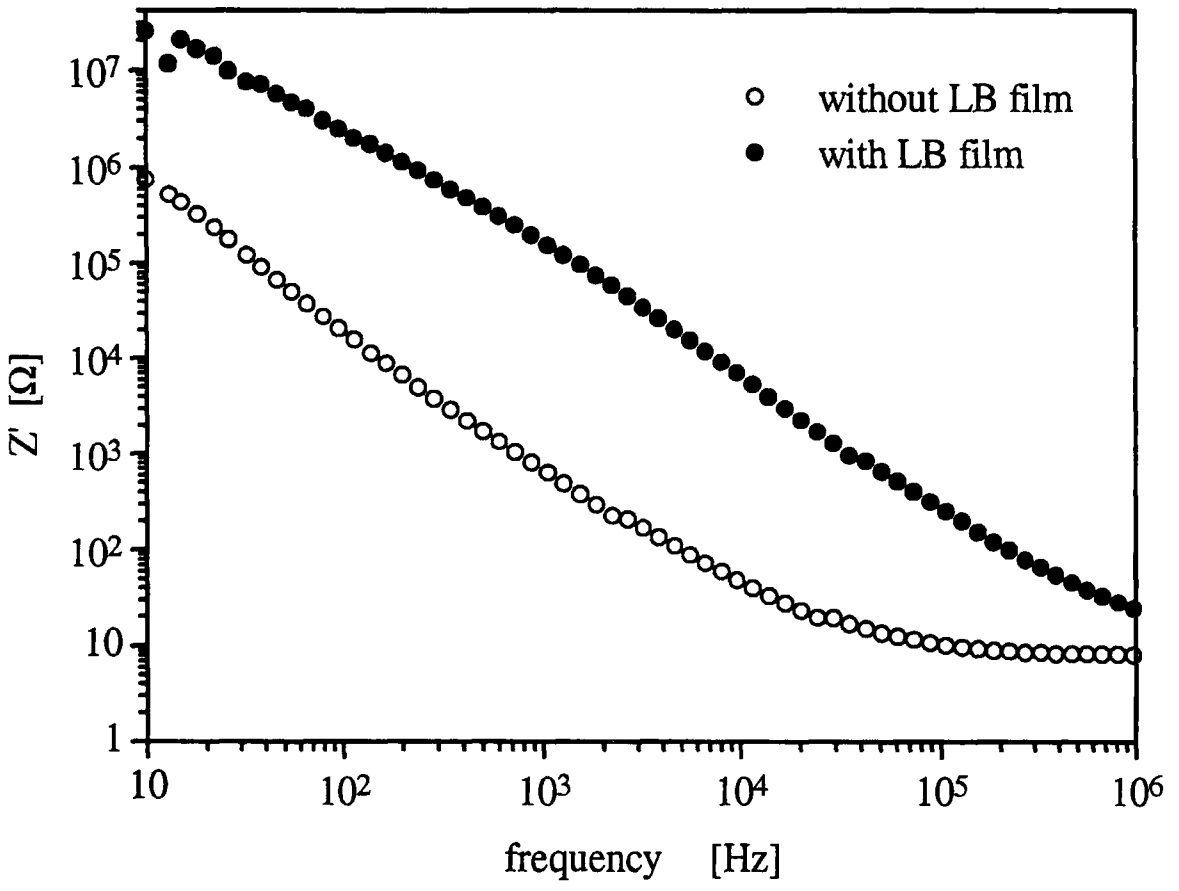

Figure 5.6: The real part of the impedance Z', with and without the LB sample, as a function of the frequency. The LB film consisted of 15 layers of Bu_4-Ni(dmit)$_2$ complex mixed with TA containing a 0.31 molar fraction of fatty acid.

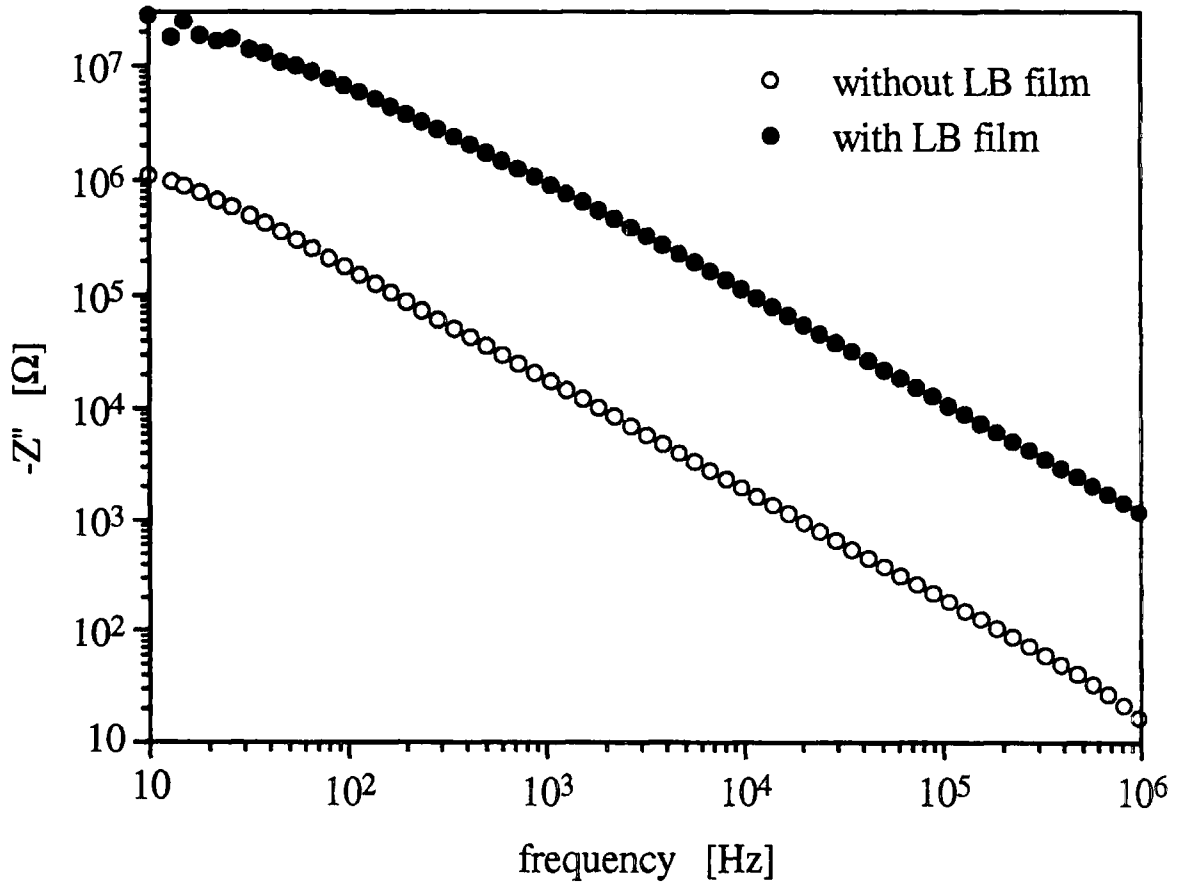

Figure 5.7: The imaginary part of the impedance Z″, with and without the LB sample, as a function of the frequency. The LB film consisted of 15 layers of Bu_4-Ni(dmit)$_2$ complex mixed with TA containing a 0.31 molar fraction of fatty acid.

The impedance behaviour for the LB sample was qualitatively similar to that for the control. It is evident from figures 5.6 and 5.7 that, over the frequency range 10 - 10^5 Hz, both Z' and Z" for the LB sample were between one and two orders of magnitude greater then the control values, suggesting that the metallic oxide(s), contacts and connecting leads may be neglected in the calculation of the LB film's conductivity σ_{AC}. This was therefore evaluated from the measured conductance values and the sample dimensions.

Figure 5.8 shows conductivity versus frequency data for three TA : Bu_4-Ni(dmit)$_2$ complex compositions. It is evident that the conductivity follows a frequency relationship of the form

$$\sigma_{AC} = A\,\omega^n \qquad (5.3)$$

where A and n are constants with n less than unity. The n values obtained from these curves are 0.63 ± 0.004, 0.59 ± 0.003 and 0.51 ± 0.004 for samples with fatty acid molar fractions of 0.93, 0.46 and 0.31, respectively. These results are consistent with the 'universal' model for the AC response of dielectric materials [5] (paragraph 2.3.3). Langmuir-Blodgett assemblies often exhibit this behaviour and the conductance has been interpreted in terms of the trapping of charge carriers between localised states in the multilayer array. For pure fatty acid films, reported n values are generally close to unity [6, 7]. The smaller values measured in this work are almost certainly associated with the more conductive organometallic component in the mixed multilayer films. There is little published data on LB films containing more than one component. Sugi and Iizima have predicted a frequency dispersion for each superstructure in a homogeneous multilayer assembly [8]. The same authors subsequently noted such behaviour in mixed LB films of fatty acid salts [9]. However, the frequency dispersion occurred at very low frequencies (10^{-1} - 10^{-4} Hz), beyond the range of the measurements in this work.

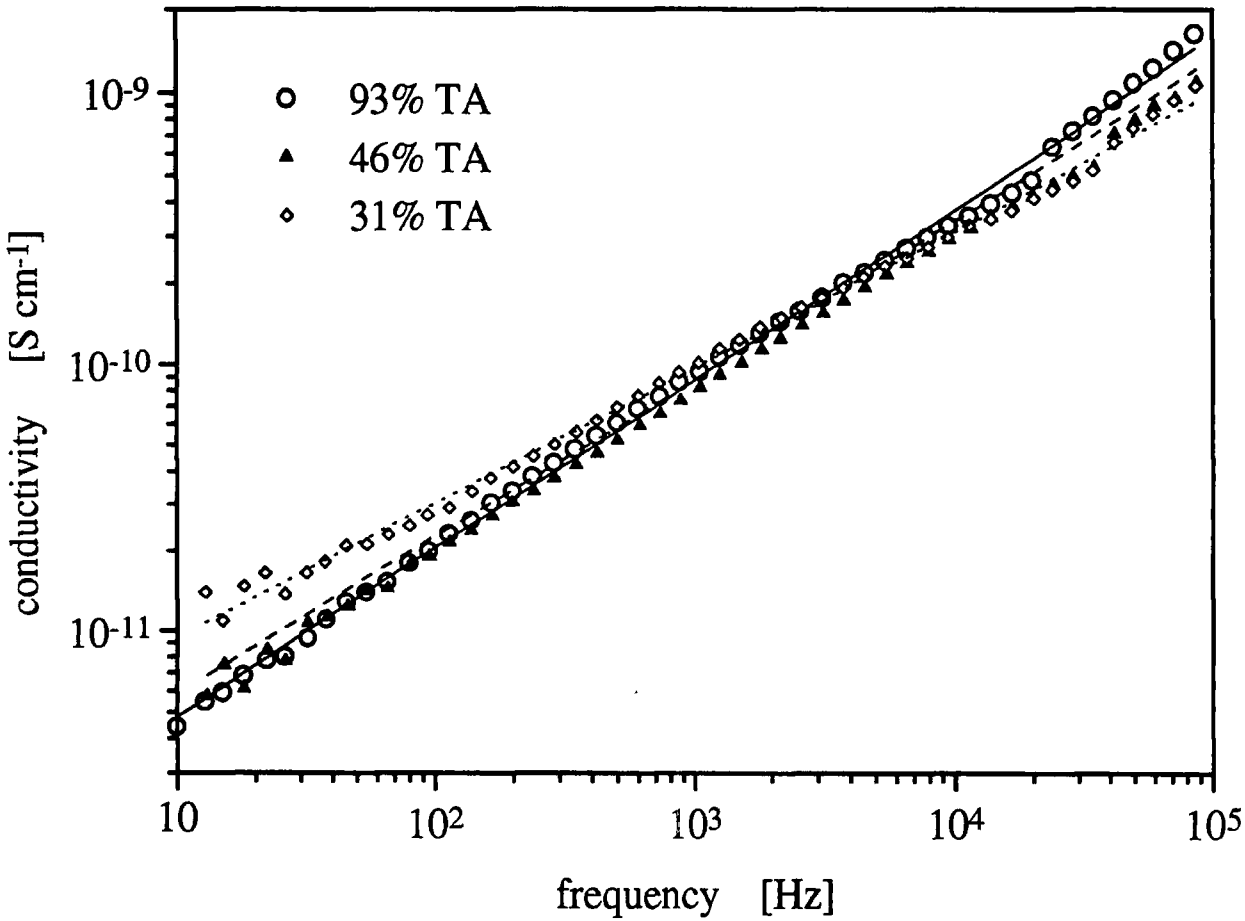

Figure 5.8: The conductivity in the out-of-plane direction versus the frequency for three mixed Bu_4-Ni(dmit)$_2$ / TA LB films with varying fatty acid content. In all cases the LB films consisted of 15 layers. Points are experimental, lines are theoretical fit using equation (5.3).

5.4.2 In-plane measurements

The equivalent circuit for the interdigitated gold electrodes arrangement is different from that of the previous case. Here, there is no contribution from an oxide on the electrodes: furthermore, because of the smaller capacitance (≅ 4 pF), the effects of the inductance at high frequency (in our frequency range) are negligible. However, there are several conductance components that must be considered. Figure 5.9 shows a cross section of the interdigitated structure, with an indication of the lines of electric field. As well as a conduction path through the LB sample, there will be contributions from the conductivity of the upper (air) and lower (glass substrate) semi-planes. In the case under study, both these contributions are likely to be negligible compared with that of the

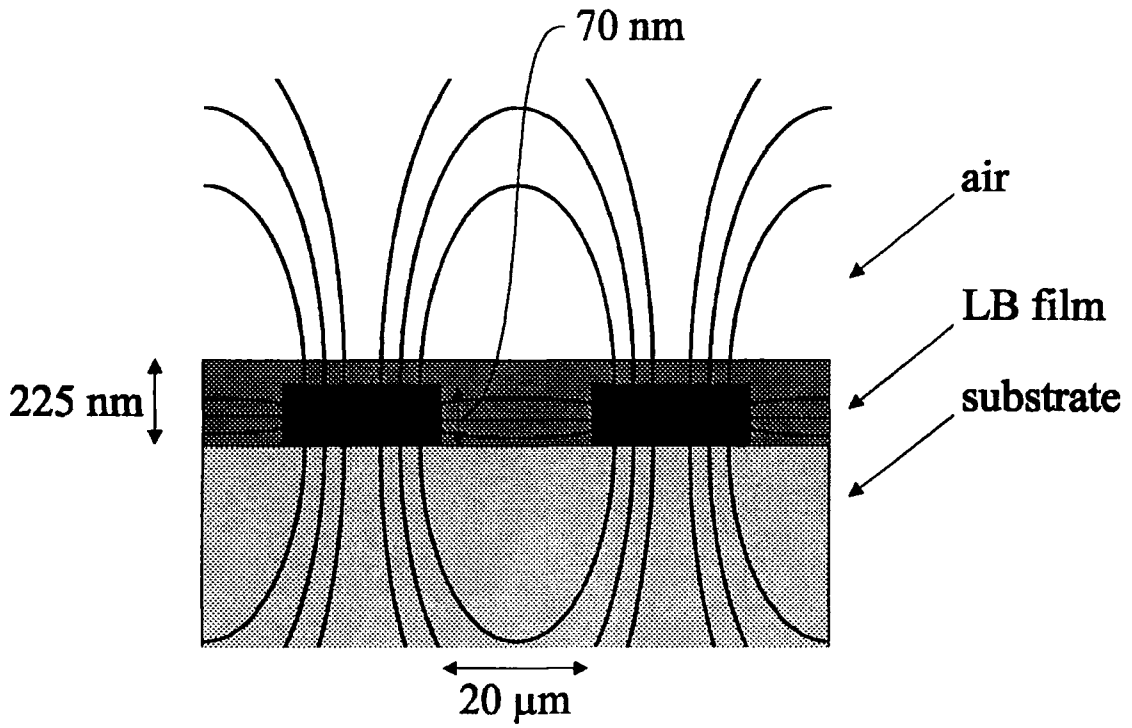

Figure 5.9: A schematic diagram (not to scale) showing a cross section of the interdigitated electrode structure. The lines of electric field are indicated.

organic layer. Most of the current through the LB film will be parallel to the substrate surface. However, because the LB film is thicker than the metal electrodes, there may also be a perpendicular component. Further discussion of the equivalent circuit for interdigitated electrodes will be given in chapter 6.

The conductivity of the LB film was calculated from the measured conductance using

$$\sigma_{AC}(\omega) = G(\omega)\frac{d}{lt} \qquad (5.4)$$

where d is the distance between the electrodes (20 μm), l is the total length of their overlap (4 cm) and t is the LB film thickness (225 nm). The data are shown in figure 5.10. The measured conductivity is independent of the frequency, suggesting that any out-of-plane contribution to the conductivity is negligible (it was shown in the previous section that this is highly frequency dependent). The constant value $\sigma_{AC} \cong 10^{-7}$ S cm^{-1} is similar to that reported previously for the DC conductivity of undoped films of TA : Bu_4-Ni(dmit)$_2$ complex [1]. The large anisotropy of the conductivity in the in-plane and out-of-plane directions in the structures studied here is consistent with there being a high degree of order in the multilayer film, probably related to the presence of the fatty acid.

Further investigations of the electrical properties on varying the temperature and during the exposure to vapours were not undertaken because of difficulties in reproducing the electrical data over an extended period (a year). In some cases, undoped LB films were obtained with a DC conductivity of about 10^{-2} S cm^{-1} after deposition. This was attributed to inadvertent doping of the organometallic complex, probably on the water surface, due to the presence of undetermined ions in the water subphase. A similar phenomenon has also been observed for amphiphilic Ni(dmit)$_2$ materials [10].

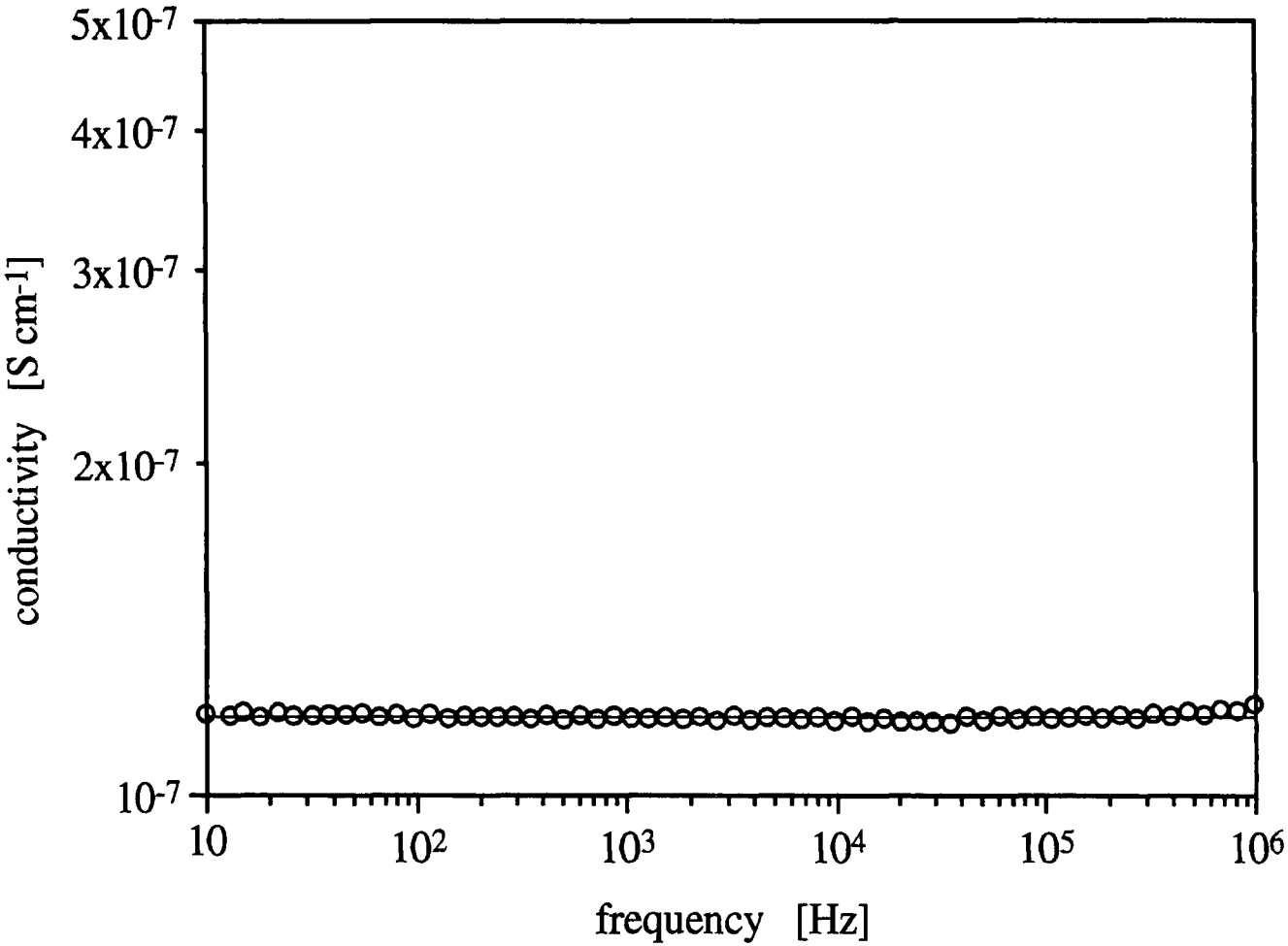

Figure 5.10: The in-plane conductivity versus the frequency for 15 LB layers of Bu_4-Ni(dmit)$_2$ complex mixed with TA with a 0.31 molar fraction of fatty acid.

5.5 Exposure to vapours

Due to problems of reproducibility over a long period, investigations on vapour sensing were not undertaken using this material.

5.6 Summary

Mixed multilayer assemblies containing a tetrabutylammonium $Ni(dmit)_2$ complex and tricosanoic acid have been assembled on solid substrates using the Langmuir-Blodgett technique. The AC conductivity of these films has been studied over the frequency range 10 Hz to 1 MHz using both in-plane and out-of-plane electrode configurations. A high anisotropy in the conductivity was observed ($\cong 10^{-11}$ S cm^{-1} for the out-of-plane conductivity and $\cong 10^{-7}$ S cm^{-1} for the in-plane conductivity, both measured at 10 Hz). This was attributed to the presence of the fatty acid film. A power law relationship between the AC conductivity σ_{AC} and the frequency ω of the form $\sigma_{AC} \propto \omega^n$ was noted for the out-of-plane measurements. The n values (0.52 - 0.63 for the range of samples studied) were found to decrease with an increase in the amount of the charge-transfer compound in the film and were generally lower than those reported for homogeneous fatty acid films. For the in-plane measurements, the conductance was constant over the frequency range studied and was dominated by the DC conductivity of the sample.

References

[1] L.M.Goldenberg, C.Pearson, M.R.Bryce, M.C.Petty, *J.Mater.Chem.*, **6** (1996) 699.

[2] M.R.Bryce, A.J.Moore, A.S.Batsanov, J.A.K.Howard, L.M.Goldenberg, C.Pearson, M.C.Petty, B.K.Tanner, *Synthetic Metals*, **86** (1997) 1839.

[3] D.M.Taylor, S.K.Gupta, A.E.Underhill, C.E.Wainwright, *Thin Solid Films*, **210/211** (1992) 287.

[4] C.Pearson, A.S.Dhindsa, L.M.Goldengerg, R.A.Singh, R.Dieing, A.J.Moore, M.R.Bryce, M.C.Petty, *J.Mater.Chem.*, **5** (1995) 1610.

[5] A.K.Jonscher, *Universal relaxation law*, 1996, Chelsea Dielectrics Press, London.

[6] M.C.Petty in *Langmuir-Blodgett films* (G.G.Roberts ed.), Plenum Press, New York.

[7] M.Careem, A.K.Jonscher, *Philosophical Magazine*, **35** (1977), 1489.

[8] M.Sugi, S.Iizima, *Phys.Rev.B*, **15** (1977) 574.

[9] M.Sugi, S.Iizima, *Appl.Phys.Lett.*, **34** (1979) 290.

[10] C.Pearson, Z.A.Ibrahim, A.S.Dhindsa, A.S.Batsanov, M.R.Bryce, J.A.K.Howard, M.C.Petty, A.E.Underhill, *J.Mater.Chem.*, **8** (1998) 387.

Chapter 6

POLYPYRROLE LB FILMS: CHARACTERISATION AND VAPOUR RESPONSE

6.1 Introduction

In this chapter, the structural and electrical characterisation, and the vapour response for multilayer films containing polypyrrole are discussed. The films were built up using a technique based on LB deposition followed by two solid state reactions. Details of the film preparation and a study of its structure by X-ray diffraction and thickness measurements are given at the beginning of the chapter (sections 6.2 and 6.3). The electrical measurements (DC and AC) in the in-plane and out-of-plane directions on varying the temperature are then discussed (section 6.4). Finally, the electrical characterisation of multilayer films deposited on interdigitated electrodes during exposure to vapours and an evaluation of the gas sensing properties of these devices are presented (sections 6.5 and 6.6).

6.2 Film deposition

The sample preparation has been documented previously [1, 2] and consists of three steps (shown in figure 6.1). First, a monolayer of ferric palmitate (FP) was formed on the surface of an LB trough by spreading a solution of palmitic acid (PA) in chloroform ($1\ g\ l^{-1}$) on a subphase of ferric chloride ($FeCl_3$) dissolved in ultrapure water (concentration $2\ mg\ l^{-1}$). The pH of the subphase was controlled by adding some ammonia solution (Aristar), to be $5.00 \pm .05$. The layer was left for 15 min so that the

solvent could evaporate. Using the LB technique, monolayers were transferred to glass or single crystal silicon substrates. The deposition was Z-type for the first few layers (~3) and Y-type, with a transfer ratio of 1 ± 0.1, for all subsequent layers. Optimum film transfer was obtained with quite slow dipping rates (2 - 3 mm min^{-1}) and a drying time of about 1 hour. This film was then exposed to saturated HCl vapour at room temperature for about five minutes. During this process, a solid state reaction transforms the FP multilayer film to a structure that consists of layers of $FeCl_3$ separated by bilayers of FP. In the third and final step, the film was exposed to pyrrole (Py) vapour in a partially evacuated desiccator and left for two days. Here, a reaction occurs between the pyrrole vapour and the ferric chloride producing polypyrrole within the multilayer assembly. The final, ideal result of the preparation should be layers of PPy separated by bilayers of PA. All the preparation steps were undertaken in a microelectronics clean room.

6.3 Film structure

To characterise the film structure, the following experiments were undertaken: (i) grazing incidence specular X-ray measurements in the range 0° - 3.33° with the same sample of 61 monomolecular layers deposited on a silicon substrate; and (ii) thickness measurements using the surface profiling Alfa-step.

As discussed in paragraph 4.3, when a sample has a periodic structure, constructive and destructive interference between the radiation reflected from the crystal planes takes place, and maxima in the reflected radiation will be found when the following relationship (Bragg's law) is satisfied

$$n\lambda = 2d\sin\theta \qquad (6.1)$$

where θ is the angle of incidence, d is the interplanar spacing and n is an integer known as the order of the reflection.

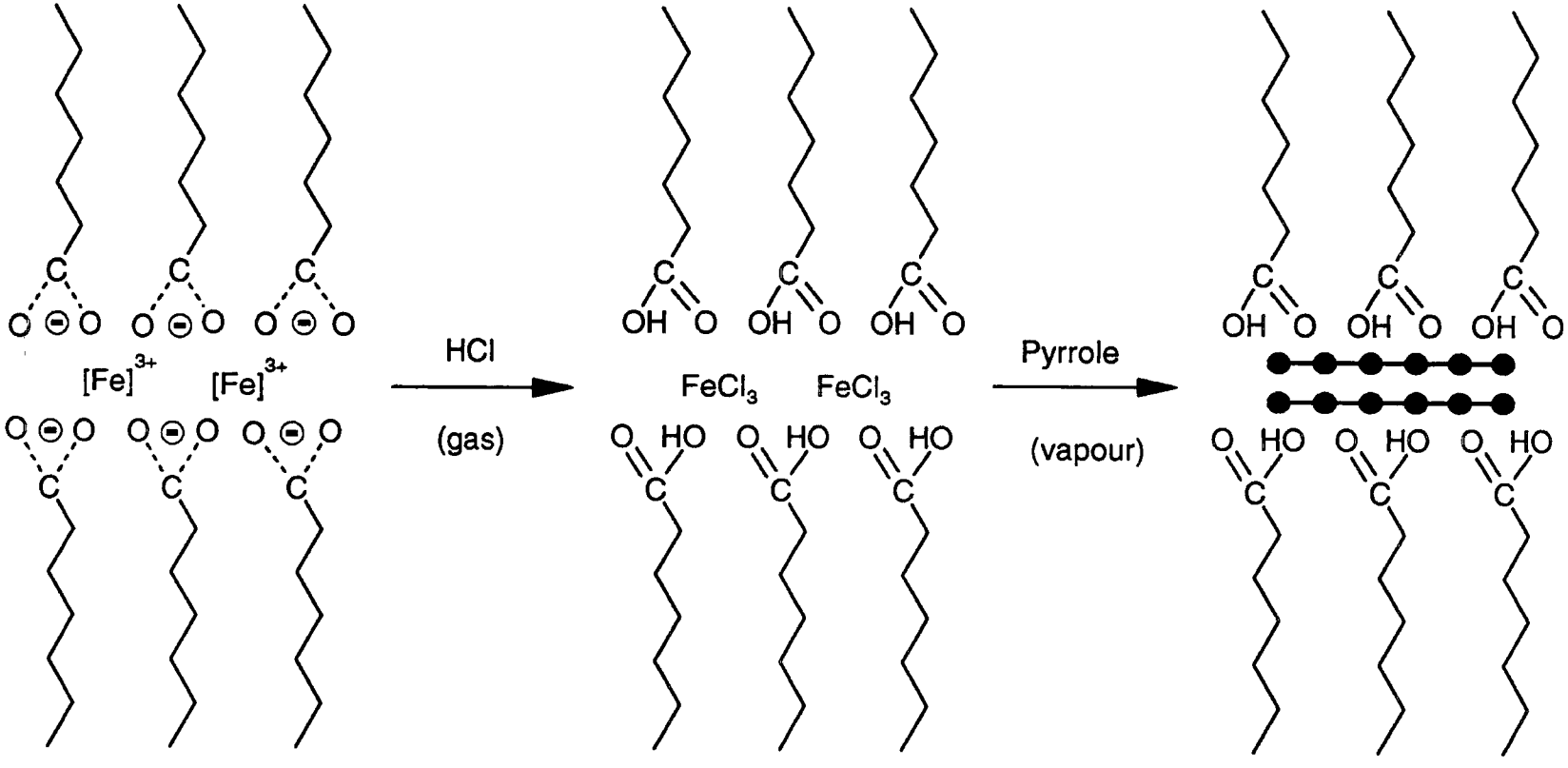

Figure 6.1: Idealised scheme showing the solid-state reactions of ferric palmitate multilayers with hydrogen chloride gas and pyrrole vapour to form conductive polypyrrole. Connected black dots symbolise polypyrrole.

In the case of LB films, d will correspond to the distance between the hydrophilic head groups [3], i.e. to the thickness of two monomolecular layers for Y-type LB films.

From the quality of the FP film X-ray spectrum (figure 6.2a), it was evident that the film possessed a well-ordered structure. In this spectrum, there were two main Bragg peaks, with the first showing a double maximum at angles 2690 and 2860 sec. of arc, and the second with a maximum at 5460 sec. of arc. The Bragg peak doublet suggests the presence of two phases in the multilayer film - possibly the free acid (palmitic acid) and its salt (ferric palmitate). From equation (6.1) using both maxima for the first-order peak and the single maximum for the second-order peak, and assuming that our LB film was Y-type, we obtained the following bilayer thicknesses

$$d_1^{(1)} = 1.3926 \times 10^{-10} / (2\ sin\,(2860/3600)) = 5.0 \pm 0.6 \text{ nm}$$

$$d_1^{(2)} = 1.3926 \times 10^{-10} / (2\ sin\,(2690/3600)) = 5.4 \pm 0.6 \text{ nm}$$

$$d_2 = 1.3926 \times 10^{-10} / (2\ sin\,(5460/3600)) = 5.2 \pm 0.6 \text{ nm}$$

where $d_1^{(1)}$, $d_1^{(2)}$ represents the bilayer thickness calculated from the first and second doublet peaks of the first-order Bragg reflection, respectively, and d_2 is that calculated from the second-order Bragg peak.

The estimated thicknesses are all greater than twice the known length for PA (barium palmitate = 2.3 nm, cadmium palmitate = 2.26 nm [4]). This may be explained by the presence of bilayers of ferric ions between the head group of the fatty acid. A similar discrepancy has been reported for a ferric stearate LB film [5], which possessed a bilayer thickness 0.4 nm greater than twice the known length for the stearic acid.

Using the Alphastep, a thickness of 2.5 nm per transferred LB layer was obtained for the PA/FP films, in agreement, within experimental error, with the X-ray data.

A significant change in the X-ray diffraction spectrum of the sample was observed after exposure to HCl vapour (figure 6.2b). Only one Bragg peak (double maximum) of relatively low intensity, is evident. This is a clear indication that the structure in not as well ordered as for the FP. The maximum was observed at an angle $\theta = 4120$ sec. of arc, corresponding to $d = 3.5 \pm 0.6$ nm. This suggests that the alkyl chains in the multilayer structure have reorganised, with their long axes tilted with respect to the substrate normal. A similar effect has been reported by Rosner and Rubner for ferric stearate exposed to HCl [5]. From our Alphastep thickness measurements, an increase in the roughness of the film was now evident. The average layer thickness was 5.8 ± 1 nm, more than double that observed before HCl exposure, suggesting that this treatment leads to considerable swelling in the organic film. However, as seen from the X-ray studies, some of the underlying multilayer structure is preserved. The difference between the third (figure 6.2c) and the second X-ray spectrum was relatively small. The Bragg peak, now 3230 sec. of arc, corresponds to $d = 4.4 \pm 0.6$ nm. The slight increase of d can be explained by the formation of PPy inside the film. A similar increase in the thickness was also observed in the Alphastep measurements, from which a value of 6 ± 1 nm was estimated for the layer thickness.

Further investigations of the film structure were undertaken using AFM by Dr. L.M.Goldenberg, Dr. V.Geskin, Dr. R.Lazzaroni and Prof. J.L.Bredas at the Service de Chimie des Materiaux Nouveaux, Universite de Mons-Hainaut (Belgium) [6]. The samples used for the AFM measurements were deposited on mica. The preparation was undertaken in Durham using the same conditions as for the films deposited previously. Two samples, each comprising three steps of different thickness (5, 11 and 21 layers), were deposited simultaneously. One was studied as deposited, while the other was investigated after undergoing all the PPy preparation steps.

In figure 6.3, an AFM scan of a ferric palmitate LB film 21 monolayers thick is shown. Good order in the film structure is evident, but measurements on a smaller scale (molecular resolution) were not possible due to the fragility of the film. In figure 6.4 an

AFM image of a polypyrrole/palmitic acid LB film 21 monolayer thick is shown. It is clear that, following the solid state reactions, a significant change in the structure has occurred. The chemical changes also affected the mechanical properties of the films, which were found to be more robust compared to the ferric palmitate LB. It was not possible to make any holes in the film by applying the maximum force to the tip. The AFM measurements confirm the X-ray and thickness measurements, indicating a change in the film structure during the chemical reactions.

From the AFM measurements, the presence of polypyrrole on the surface suggests that the polymer is located close to the tails of the fatty acid (i.e. the top of the film) and not just near the head groups. The reason of this is still unclear. Possible explanations could be: (a) a diffusion of the ferric ions to the surface during the exposure to HCl; or (b) a partial reorientation of the fatty acid during exposure to HCl so that some head groups of the fatty acid would be outermost.

The observed structure in figure 6.4 is clearly related to the polypyrrole (not present in the FePA LB film (figure 6.3)). This agrees with a molecular model proposed in which the polypyrrole is supposed to form a two dimensional structure [7]. The model was mainly supported by experimental results obtained by XPS (X-ray-induced photoelectron spectroscopy) [7]. In our case, the lower conductivity in the out-of-plane direction with respect to that in the in-plane direction (discussed in section 6.4) provides a further evidence for this model. Therefore, it seems likely that the polymer is arranged in two dimensional structures and not in the ideal (linear) arrangement depicted in figure 6.1.

6.4 Electrical behaviour with the temperature

In-plane and out-of-plane conductivity (DC and AC) studies were undertaken using a two probe technique. Ohmic current versus voltage behaviour was noted in both cases.

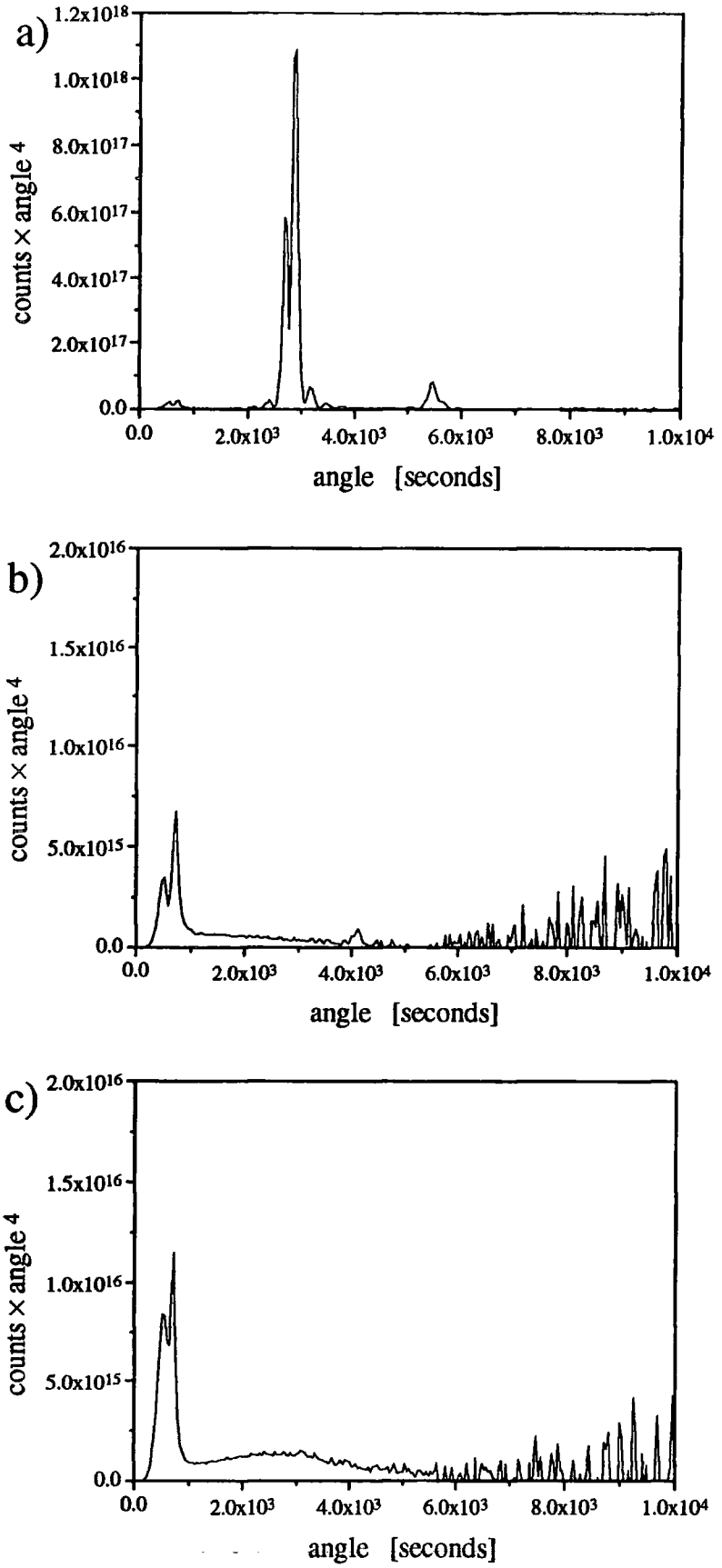

Figure 6.2: X-ray diffraction data for a ferric palmitate LB film, 61 monomolecular layers thick: (a) immediately after deposition; (b) after exposure to HCl vapour; and (c) after exposure to polypyrrole vapour.

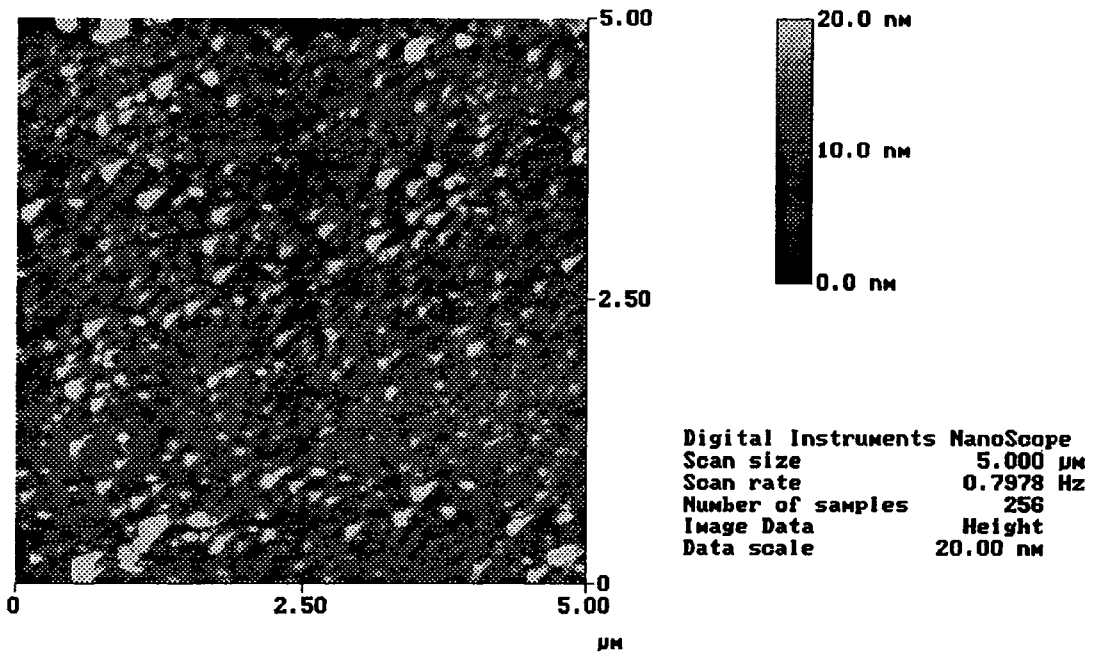

Figure 6.3: AFM measurement of a ferric palmitate LB film 21 monomolecular layer thick.

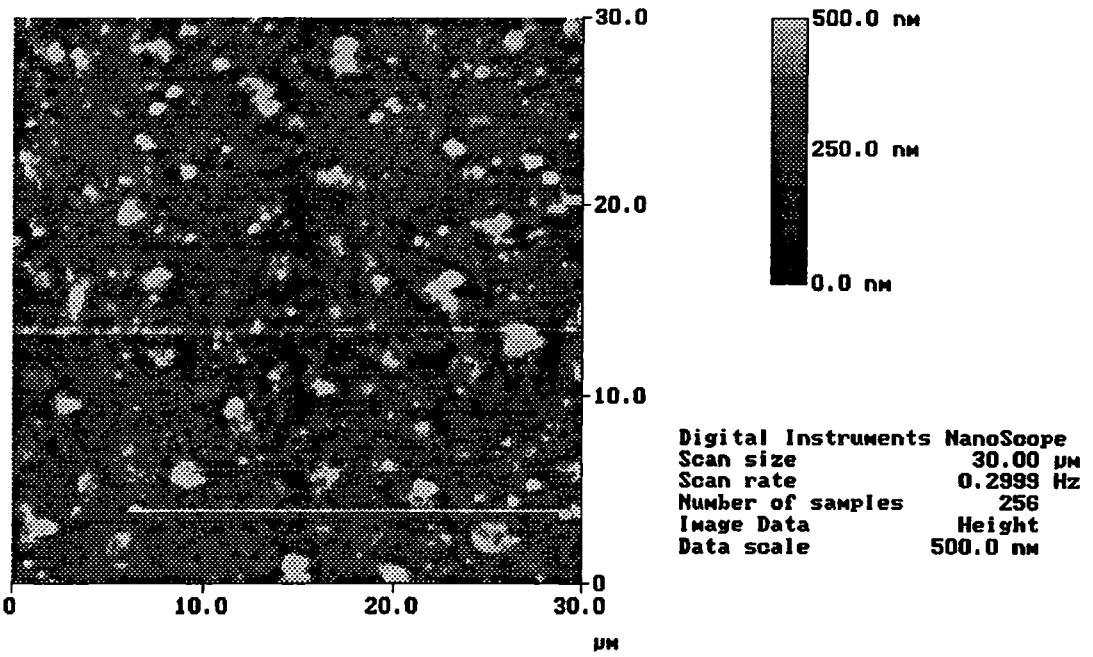

Figure 6.4: AFM measurement for a polypyrrole+palmitic acid LB film 21 monomolecular layers thick.

For measurements in the in-plane direction, the electrical contacts were silver paint and the substrates were glass slides. By varying the distance between the contacts, it was established that the contact resistance was negligible. In the case of experiments in the direction normal to the film surface, the substrate was metal-coated with gold stripes (width 1.4 mm, thickness 600 nm). A second metal strip was deposited on top of the organic film to obtain a sandwich configuration (shown in figure 4.1(b)). This second strip was silver (width 0.6 mm, thickness 50 nm). The metals were deposited by thermal evaporation under high-vacuum conditions (~ 10^{-5} mbar).

Electrical conductivity measurements over the temperature rage 90-300 K were made in helium, as described in paragraph 4.2.3.

6.4.1 DC conductivity

The conductivity of the sample exhibited a large anisotropy in the in-plane and out-of-plane directions ($\sigma_{//}/\sigma_{\perp} \sim 10^{7}$). At room temperature, the values of the in-plane and out-of-plane DC conductivity were 20 $S\,cm^{-1}$ and 3×10^{-6} $S\,cm^{-1}$, respectively. The conductivity of the sample was also monitored during the previous stages of preparation. The conductivity in the in-plane direction was found to be out of the range of our instruments (lower than 10^{-8} $S\,cm^{-1}$) for the first two preparation steps. The out-of-plane DC conductivity for the FP was $\sigma_{\perp} = 10^{-13}$ $S\,cm^{-1}$. After exposure to HCl it was not possible to measure the conductivity because of the extremely disordered and non compact structure (evident from the X-ray and thickness measurements) in which the metal easily infiltrated the organic layers during evaporation of the top contact.
An analysis of the DC conductivity σ versus temperature T was undertaken using the Variable Range Hopping (VRH) model [8] discussed in paragraph 2.3.2. The best fit was found using the equation corresponding to three-dimensional hopping (equation (2.48))

$$\sigma = \sigma_{vr} \exp\left[-\left(\frac{T_o}{T}\right)^{1/4}\right] \tag{6.2}$$

where $\sigma_{vr} = D\,(T_o/T)^{1/2}$.

The best-fit parameters were as follows

(i) In-plane conductivity (figure 6.5)

$$T_o = (1.23 \pm 0.08) \times 10^5 \text{ K} \quad ; \quad D = 79 \pm 4 \text{ S cm}^{-1}$$

(ii) Out-of-plane conductivity (figure 6.6)

$$T_o = (1.00 \pm 0.01) \times 10^7 \text{ K} \quad ; \quad D = (1.17 \pm 0.04) \times 10^{-2} \text{ S cm}^{-1}$$

To see if the VRH model gave a reasonable physical picture of the conduction mechanism, we have extracted the microscopic parameters from equations (6.2) and used the equation for the optimum hopping distance R (equation (2.46)) to find the average hopping distance

$$\langle R \rangle = 3/4\, R = 3/4 \left\{9/\left[8\pi\, N(E_F)\, \alpha k_B T\right]\right\}^{1/4} \tag{6.3}$$

where $N(E_F)$ is the density of states at the Fermi energy, k_B is the Boltzmann constant, α^{-1} is the decay length of the localised wave function. Hence

$$\alpha \langle R \rangle = 1/2\ (3/4)\ (T_o/T)^{1/4} \tag{6.4}$$

$$N(E_F) = (24/\pi)\ \alpha^3/(k_B T_o) \tag{6.5}$$

$$\nu_{ph} = (2^4/3)^{1/2}\ \{D\,\alpha^2 / [e^2\, N(E_F)]\} \tag{6.6}$$

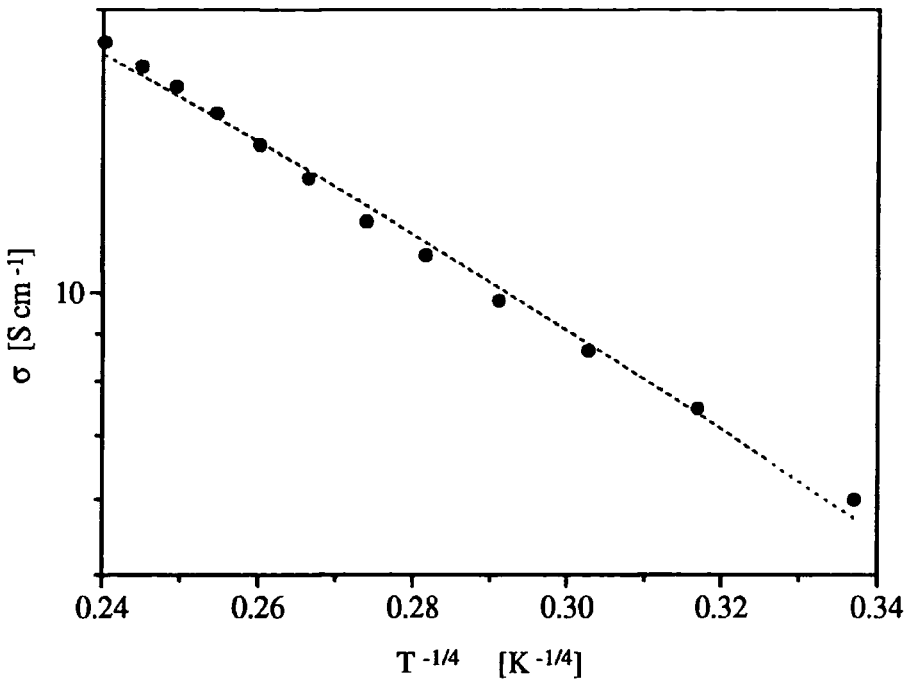

Figure 6.5: In-plane DC conductivity versus $T^{-1/4}$ for a polypyrrole+palmitic acid LB film 21 monomolecular layers thick. Points are experimental data. The dashed line is the best fit obtained with equation (6.2).

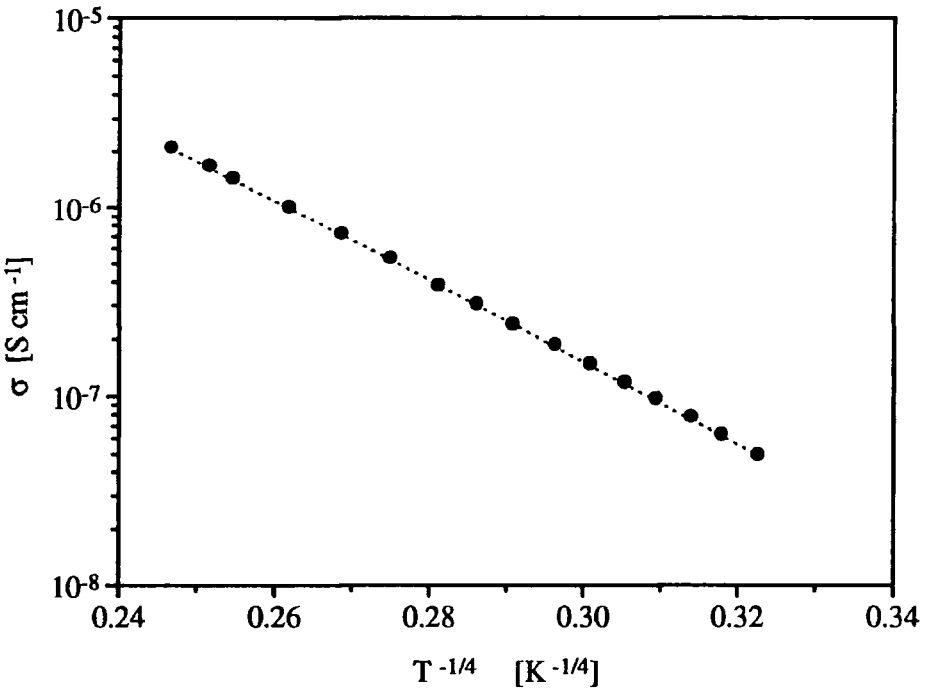

Figure 6.6: Out-of-plane DC conductivity versus $T^{-1/4}$ for a polypyrrole+palmitic acid LB film 115 monomolecular layers thick. Points are experimental data. The dashed line is the best fit obtained with equation (6.2).

where ν_{ph} is the phonon frequency.

With three equations and only two known parameters (T_o, D), we have estimated α, $N(E_F)$ and ν_{ph} for hopping distances of 1 Å and 10 Å. The values are given in tables 6.1 and 6.2 for the in-plane and out-of-plane conductivities, respectively. For the in-plane conductivity the values obtained were in reasonable agreement with typical values for solids: $\nu_{ph} \sim 10^{13}$ Hz, $N(E_F) \sim 10^{22} - 10^{23}$ $cm^{-3}eV^{-1}$, $\alpha \sim 10^8 - 10^7$ cm^{-1}. Slightly smaller values of ν_{ph} and $N(E_F)$ were estimated for the out-of-plane conductivity.

From figures 6.5 and 6.6, it is evident that the fit of the VRH hopping model to the experimental data for DC conductivity in the in-plane direction it is not as good as for the data in the out-of plane direction.

An acceptable fit to the DC conductivity data in the in-plane direction was also obtained using the model, known as fluctuation-induced tunnelling, of Sheng et al. [9]. Here, the conductivity is assumed to be dominated by tunnelling of electrons across small potential barriers that separate conductive regions (≅20 nm). We would expect such a model to apply to our films (which consists of islands of conductive polymer separated by insulating fatty acid molecules). The DC conductivity is given by

$$\sigma = \sigma_o \exp[-T_1/(T + T_2)] \qquad (6.7)$$

where σ_o, T_1 and T_2 are constants. For $T \ll T_2$, the conductivity is temperature independent and equation (6.7) reduces to the form expected for quantum mechanical tunnelling through a parabolic barrier [9]. However, at high temperatures the electrical conductivity is thermally activated with an energy $k_B T_1$. The Sheng model includes three unknowns, rather than the two of the VRH approach and was rather easier to fit to the experimental data as shown in figure 6.7. The best-fit parameters were

$\sigma_o = 58 \pm 4$ S cm^{-1}; $T_1 = 520 \pm 50$ K; $T_2 = 150 \pm 15$ K

$\langle R \rangle$ [Å]	α [cm^{-1}]	$N(E_F)$ [$cm^{-3} eV^{-1}$]	ν_{ph} [Hz]
1	$(1.6 \pm 0.1)\times10^{8}$	$(3.0 \pm 0.6)\times10^{24}$	$(10 \pm 2)\times10^{12}$
10	$(1.6 \pm 0.1)\times10^{7}$	$(3.0 \pm 0.6)\times10^{21}$	$(10 \pm 2)\times10^{13}$

Table 6.1: Values from VRH model for the in-plane conductivity, calculated using equations (6.4)-(6.6) from the parameters estimated with the best fit using equation (6.2). Measurements for a polypyrrole+palmitic acid LB film 21 monomolecular layers thick.

$\langle R \rangle$ [Å]	α [cm^{-1}]	$N(E_F)$ [$cm^{-3} eV^{-1}$]	ν_{ph} [Hz]
1	$(4.7 \pm 0.05)\times10^{8}$	$(9.2 \pm 0.3)\times10^{23}$	$(4.1 \pm 0.2)\times10^{10}$
10	$(4.7 \pm 0.05)\times10^{7}$	$(9.2 \pm 0.3)\times10^{20}$	$(4.1 \pm 0.2)\times10^{11}$

Table 6.2: Values from VRH model for the out-of-plane conductivity, calculated using equations (6.4)-(6.6) from the parameters estimated with the best fit using equation (6.2). Measurements for a polypyrrole+palmitic acid LB film 115 monomolecular layers thick.

The last two values should be contrasted to figures of $T_1 = 225$ K and $T_2 = 8.3$ K, obtained by Rosner and Rubner using stearic acid as the host fatty acid [5], although these results very close to the values $T_1 = 600$ K and $T_2 = 170$ K, obtained by Paasch et al. for two-dimensional polypyrrole films (electrochemical deposition) [10].

6.4.2 AC conductivity

In the in-plane direction, the imaginary part of the permittivity ε'' ($= \sigma_{DC}\, \omega^{-1}$) was dominated by the DC conductivity. No information could be found from ε' because of

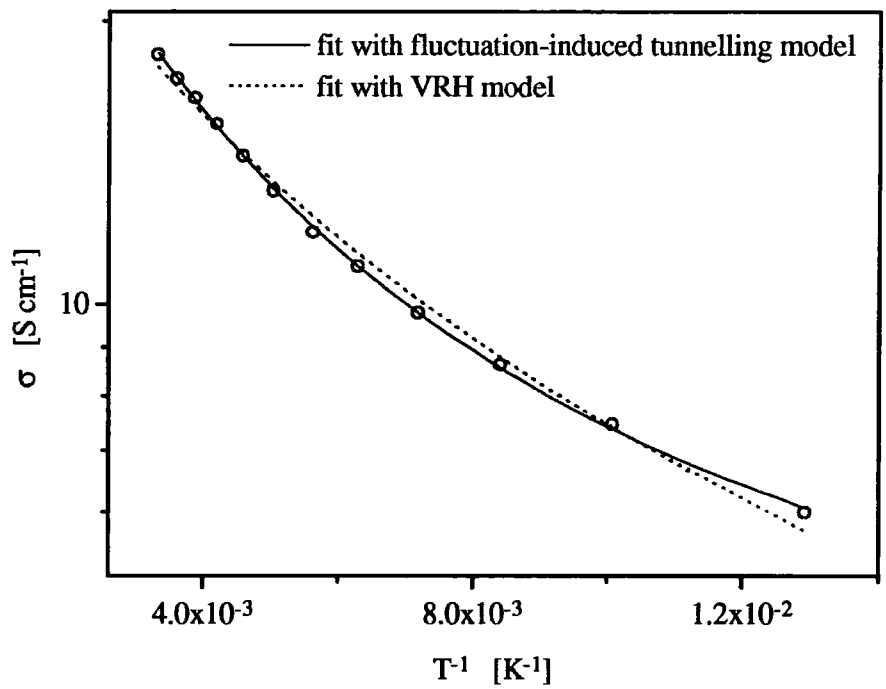

Figure 6.7: The in-plane DC conductivity versus T^{-1} for a PPy plus PA LB film 21 monolayers thick. Points are experimental. Lines are the best fits obtained with the VRH model (equation (6.2)) and the fluctuation-induced tunnelling model (equation (6.7)).

the very small capacitance of the silver paint electrodes (~10^{-5} pF).

The equivalent circuit used for the interpretation of our results in the out-of-plane direction includes contributions only from the LB film and the electrodes. Other contributions from oxide and leads were negligible (as discussed in paragraph 4.1.2). The LB film was modelled as a capacitance C_{LB} in parallel with a conductance G_{LB}, both frequency dependent. The electrodes were assumed to contribute a resistance r in series with the sample. For the frequency under consideration, the following conditions were satisfied

$$r\,G_{LB} \ll 1 \qquad \omega r\,C_{LB} \ll 1 \tag{6.8}$$

Using equation (4.9) the measured conductance G and capacitance C are given to a good approximation by

$$G(\omega) \cong G_{LB} + (\omega C_{LB})^2\, r \qquad C(\omega) \cong C_{LB} \tag{6.9}$$

Moreover, since $G_{LB} \gg (\omega C_{LB})^2 r$, it follows that the measured conductance $G(\omega)$ and capacitance $C(\omega)$ were, to a good approximation, equal to G_{LB} and C_{LB}, respectively.

G_{LB} and C_{LB} are related, respectively, to the real and imaginary part of the permittivity (as discussed in paragraph 4.1.2), by the geometrical capacitance of the electrodes C_G

$$G_{LB} = C_G\,\omega\varepsilon''(\omega) \qquad C_{LB} = C_G\,\varepsilon'(\omega) \tag{6.10}$$

In the out-of-plane direction, the permittivity was in good agreement with a Cole-Davidson function [11] (equation (2.28)), including a contribution from the DC conductivity (σ_{DC}), i.e.

$$\varepsilon(\omega) = \varepsilon_\infty + (\varepsilon_S - \varepsilon_\infty)\frac{1}{(1+i\omega\tau)^\beta} - i\frac{\sigma_{dc}}{\omega\varepsilon_o} \tag{6.11}$$

where ε_S is the static permittivity, ε_∞ is the high frequency value, τ is the relaxation time and β is a number in the range $0 < \beta \leq 1$. The Cole-Davidson relaxation function is asymmetric with respect to the characteristic frequency $\omega_m = \tau^{-1}$, and shows two power law relationships for $\omega \ll \omega_m$ and $\omega \gg \omega_m$ with exponents 1 and β (as can be found from equation (2.33) for $\alpha = 0$) respectively, with $\varepsilon'(\omega)$ tending to ε_S and ε_∞, respectively.

The analysis of the experimental data, over the temperature range 160-300 K, was based on the fit of both the real $\varepsilon'(\omega)$ (figure 6.8) and imaginary parts $\varepsilon''(\omega)$ (figure 6.9) of the permittivity $\varepsilon(\omega)$. It should be noted that the analysis for $\varepsilon'(\omega)$ was more accurate because $\varepsilon''(\omega)$ was dominated by the DC conductivity. For temperatures lower than 160 K, the relaxation time τ became large and the relaxation was out of the measurement frequency range.

The parameters estimated from the best fit are given in table 6.3. The high frequency permittivity ε_∞ is approximately constant over the temperature range. In contrast, the static permittivity ε_S increases with decreasing temperature, while the relaxation time τ was found to increase with decreasing temperature.

On plotting the relaxation time τ as a function of T^{-1}, we note that the behaviour is in good agreement with the Arrhenius law (figure 6.10)

$$\frac{1}{\tau} = A \exp\left(-\frac{\Delta E}{RT}\right) \qquad (6.12)$$

where A^{-1} is the relaxation time at $T \rightarrow \infty$ and ΔE is the activation energy. From the fit of our data, we found $A^{-1} = (1.0 \pm 0.1) \times 10^{-7}$ s and $\Delta E = = (8.9 \pm 0.2) \times 10^{-2}$ eV. As discussed in paragraph 2.3.3, the relaxation time and $\sigma'(0)$ are often related [12, 13].

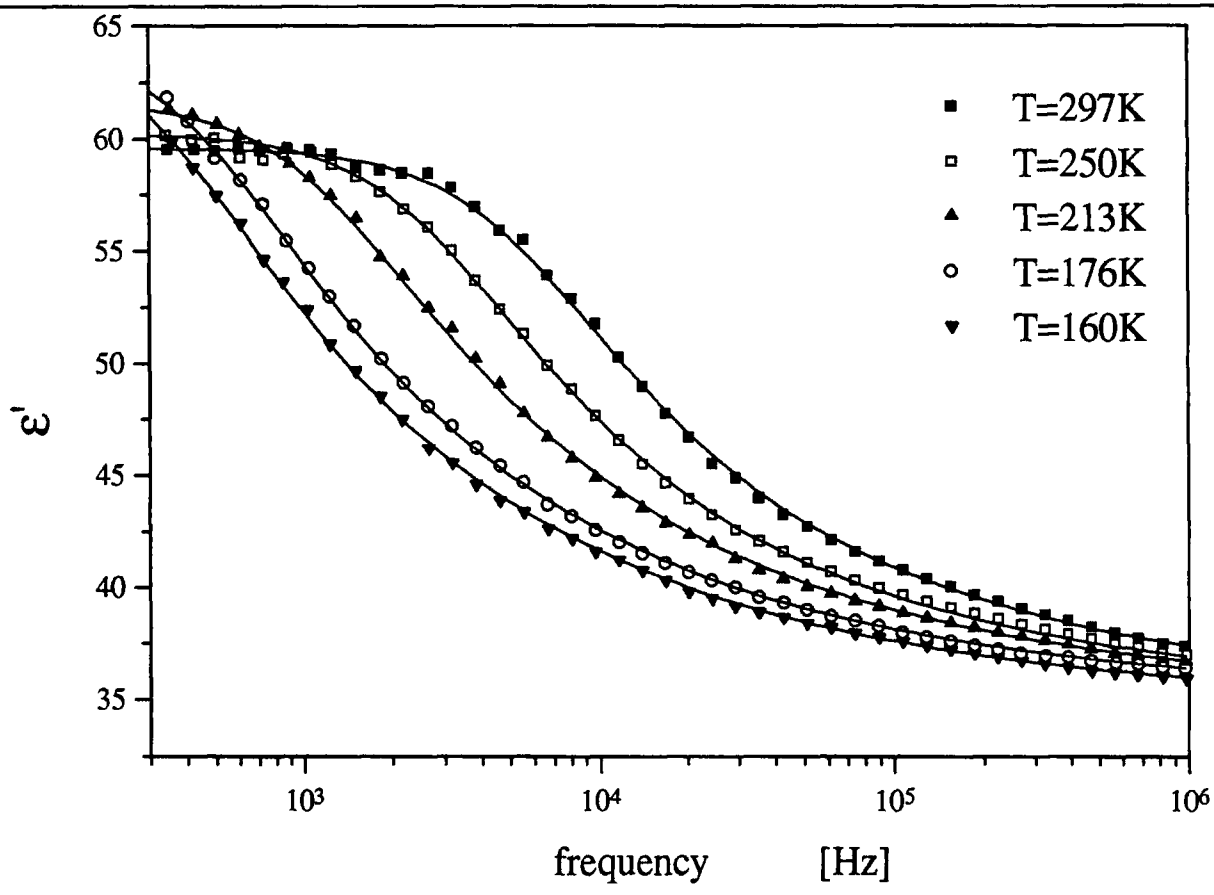

Figure 6.8: Real part of the permittivity ε'(ω) as a function of frequency for five different temperatures. Measurement in the out-of-plane direction for a polypyrrole+palmitic acid LB film 115 monomolecular layers thick. The full lines are the best fits obtained using equation (6.11).

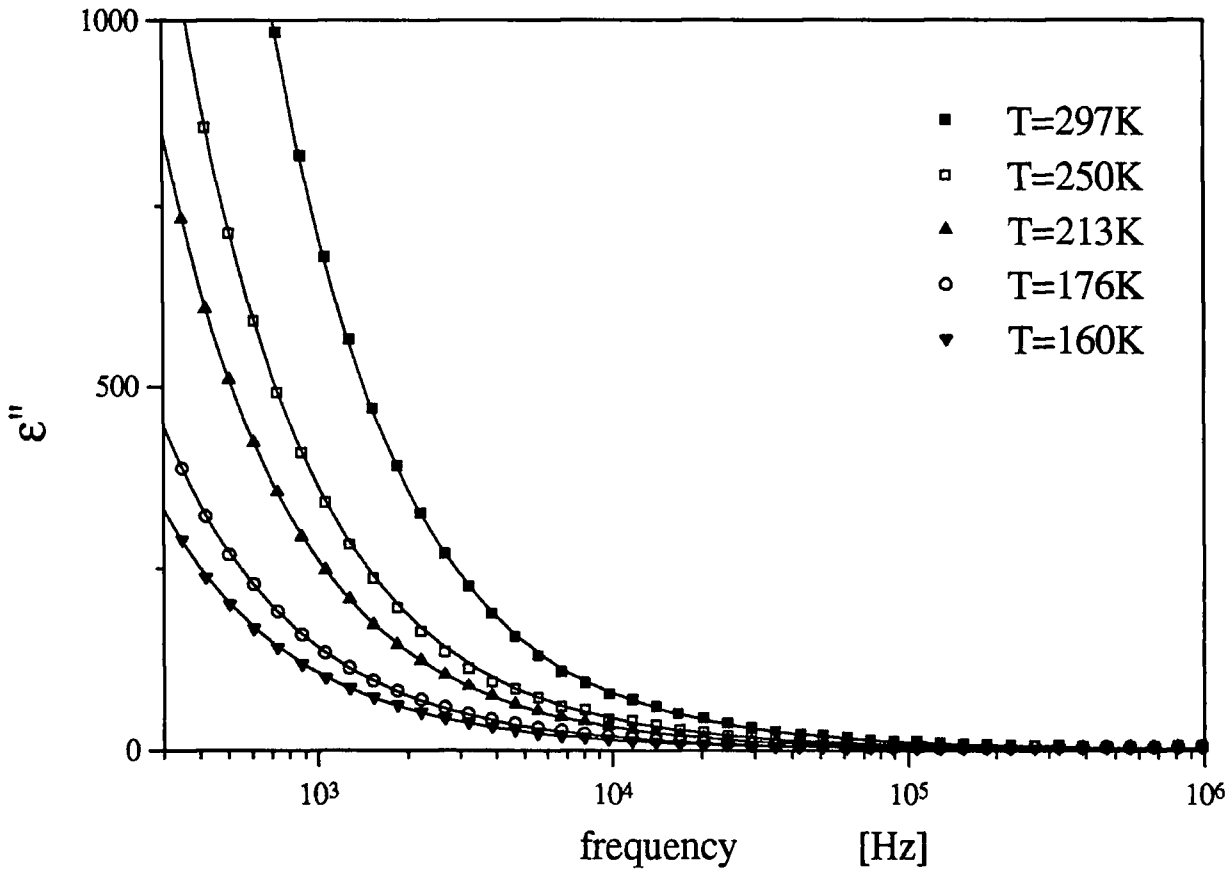

Figure 6.9: Imaginary part of the permittivity $\varepsilon''(\omega)$ as a function of frequency for five different temperatures. Measurement in the out-of-plane direction for a polypyrrole+palmitic acid LB film 115 monomolecular layers thick. The full lines are the best fits obtained using equation (6.11).

In this case the relaxation time τ was compared with that estimated using equation (2.49)

$$\tau_m = (p\,\Delta\varepsilon\,\varepsilon_o) / \sigma'(0) \qquad (6.13)$$

where $\Delta\varepsilon$ is the dielectric relaxation strength (i.e. $\Delta\varepsilon = \varepsilon_o - \varepsilon_\infty$) and p is a temperature independent constant. By plotting τ_m from equation (6.13) as a function of T^{-1}, good agreement with equation 6.12 (Arrhenius law) was found with $A^{-1} = (5 \pm 1) \times 10^{-8}$ s and $\Delta E = (7.3 \pm 0.4) \times 10^{-2}$ eV. However, the behaviour of τ_m was dissimilar to that of τ (i.e. that estimated with the fit) in the following respects: (i) τ_m was between 38 and 65 times smaller than τ (depending on the temperature); and (ii) the activation energy for τ_m was significantly smaller than that for τ.

From the parameter β, obtained by the fit to the experimental data, it is possible to obtain the exponent of the power law ($\sigma'(\omega) \propto \omega^s$) typically observed in disordered solids at high frequency, i.e. $s = 1 - \beta$ (from equation (2.18)). It can be seen from the values of β in table 6.3 that s first increases with decreasing temperature: at T = 298 K $s = 0.57 \pm 0.01$ and at T = 160 K $s = 0.61 \pm 0.02$. The first result is in agreement with the literature (as discussed in paragraph 2.3.3) but the value of s is smaller than that usually observed (generally s is found between 0.7 and 1).

The behaviour of PA plus PPy samples was compared to that of the FP, figure 6.11. The permittivity is $\varepsilon'(\omega) \approx 4$ over the frequency range studied, with no loss peak evident. However, there is a slight decrease in $\varepsilon'(\omega)$ with a decrease in temperature. The real part of the permittivity is larger than that reported for PA, probably because of the presence of ions inside the film. This could also explain the temperature dependence. Decreasing the temperature will increase the orientation of the dipoles (giving an increase in the static permittivity) and may also decrease the distance between the ions, with a consequent decrease in the associated dipole.

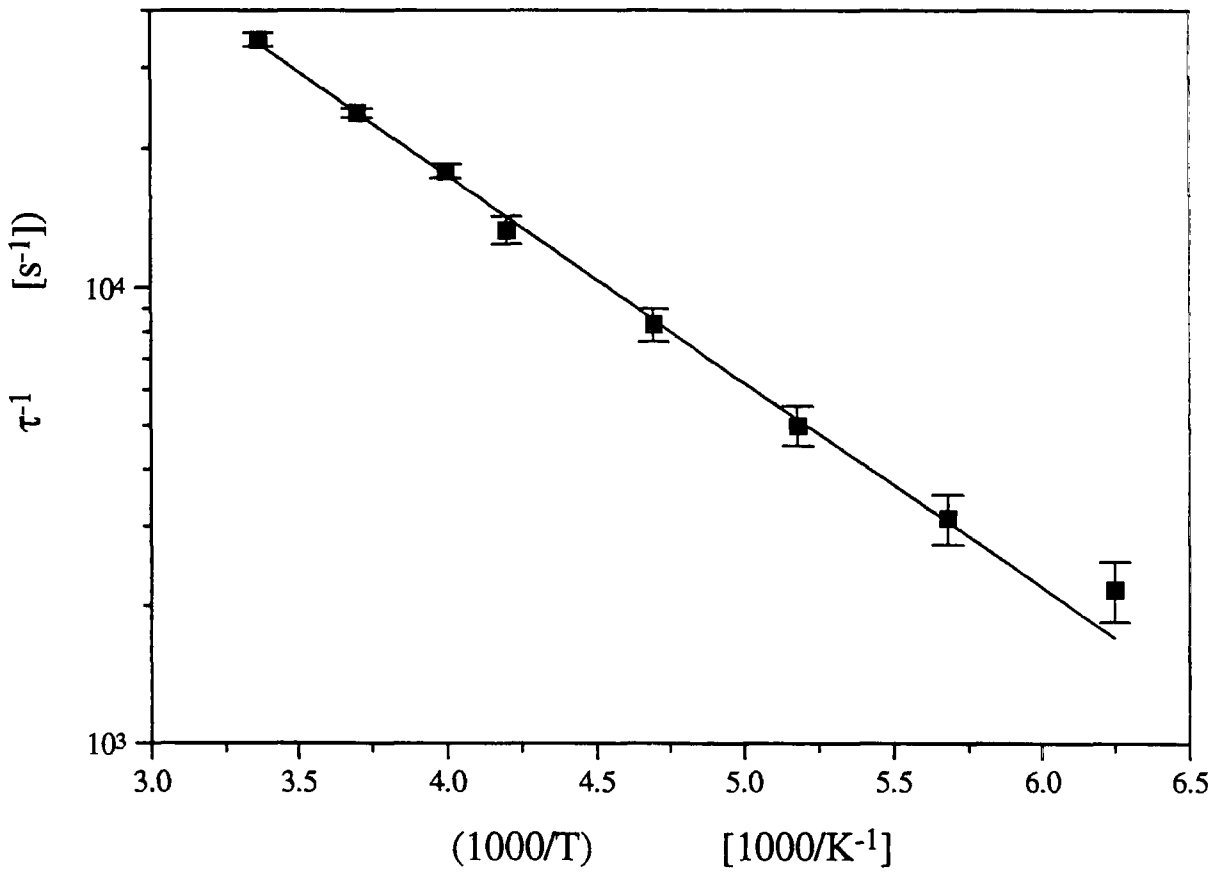

Figure 6.10: The inverse of the relaxation time τ, obtained from the best fit of equation (6.11) to the experimental data, versus 1000/T. The full line is the best fit using equation (6.12).

T [K]	ε_0	ε_∞	τ [s]	β	σ_{DC} [S cm^{-1}]
297 ± 0.2	59.6 ± 0.1	35.4 ± 0.3	(2.9 ± 0.1) × 10^{-5}	0.43 ± 0.01	(3.1 ± 0.04) × 10^{-6}
270 ± 0.2	59.7 ± 0.1	35.5 ± 0.2	(3.9 ± 0.1) × 10^{-5}	0.44 ± 0.02	(2.1 ± 0.02) × 10^{-6}
250 ± 0.2	60.2 ± 0.2	35.4 ± 0.3	(5.6 ± 0.2) × 10^{-5}	0.43 ± 0.01	(1.7 ± 0.02) × 10^{-6}
238 ± 0.2	61.1 ± 0.4	35.4 ± 0.5	(7.5 ± 0.2) × 10^{-5}	0.41 ± 0.01	(1.4 ± 0.02) × 10^{-6}
213 ± 0.2	61.8 ± 0.7	35.4 ± 0.2	(1.2 ± 0.2) × 10^{-4}	0.40 ± 0.02	(1.0 ± 0.01) × 10^{-6}
176 ± 0.2	64.5 ± 1	35.2 ± 0.3	(3.2 ± 0.3) × 10^{-4}	0.40 ± 0.02	(5.4 ± 0.05) × 10^{-7}
160 ± 0.2	65.2 ± 3	34.9 ± 0.4	(4.6 ± 1) × 10^{-4}	0.39 ± 0.02	(3.8 ± 0.04) × 10^{-7}

Table 6.3: Best fit parameters of the permittivity $\varepsilon(\omega)$ obtained using equation (6.11) for seven different temperatures. Measurement in the out-of-plane direction for a polypyrrole+palmitic acid LB film 115 monomolecular layers thick.

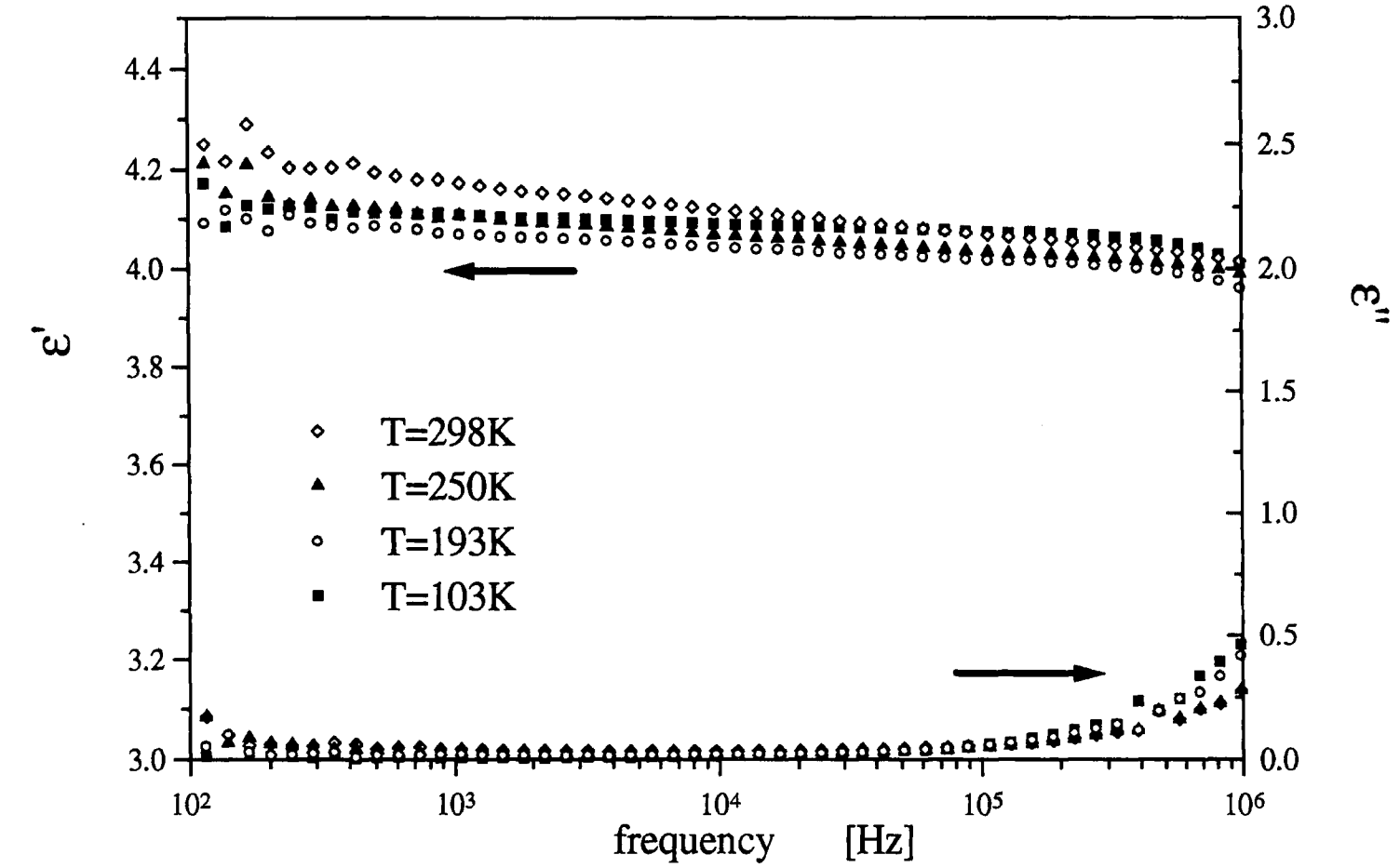

Figure 6.11: Real and imaginary parts of the permittivity for ferric palmitate LB film measured at four different temperatures. Measurement in the out-of-plane direction for a film 75 monolayers thick.

It is clear that the main contribution to the permittivity of the PPy plus PP film originates from the presence of the conductive polymer inside the multilayer structure. However, it is difficult to discern the precise mechanism of the observed relaxation. One interpretation could be related simply to the relaxation of the dipole in the presence of the counterion. In fact, the charges are separated by relatively large distances and may be able to move inside the film. The relaxation time characteristic of this process would need to be small for it to be observed in our frequency range. Another explanation could be related to the presence of delocalised charges that can move, jumping between localised states as discussed in paragraph 2.3.3. This would agree with the DC conductivity behaviour described by the VRH model, but not with the observed temperature dependence. As noted above (i) the value and behaviour of τ does not compare well with that of τ_m, and (ii) the value of s is smaller than what observed in the literature.

6.5 Effect of vapours

In this section, the change in the electrical properties during exposure to the four vapours is discussed. For these measurements the LB films were deposited on interdigitated electrodes (IDE) (figure 4.2) with a separation gap of 240 μm, a total length of 13.2 cm and a thickness of 80 nm. These were made of gold (undercoated with chromium) on glass fabricated using photolithography. The LB films used in this study were 19 monolayers thick, i.e. 100 ± 15 nm. The RMS amplitude of the AC voltage was 1.1 V; no changes in the samples' impedance were observed on applying lower voltages.

The equivalent circuit of the IDE covered with an LB film takes into account contributions from the substrate and from the medium above the LB film (figure 6.12), which were considered to be in parallel with that of the LB film. The former was modelled as a capacitance C_{SUB} in parallel with a conductance G_{SUB}, and the latter as a simple capacitance C_{AIR}. The contribution from the electrodes' resistance was negligible.

To evaluate the contribution of Y_{LB} to the measured admittance, the admittance of an IDE structure without any film deposited and that of an IDE covered with an LB film 19 monolayers thick were compared. The result are shown in figure 6.13. From figure 6.13(a), it is evident that the conductance of the LB film is at least two orders of magnitude greater than G_{SUB} over the entire frequency range (about four orders of magnitude at 100 Hz). For the capacitance (figure 6.13(b)), the contribution of the LB film at 100 Hz is about two orders of magnitude greater than $C_{SUB} + C_{AIR}$ and decreases on increasing the frequency, becoming comparable with $C_{SUB} + C_{AIR}$ for frequencies greater than 10 kHz. Therefore, by choosing a measuring frequency of 1 kHz, the change of the LB film admittance alone was measured during exposure to the vapours and the other contributions were negligible.

Because of the electric field distribution for the IDE and the large anisotropy of the LB film in the in-plane and out-of-plane directions, there is not a simple relationship between

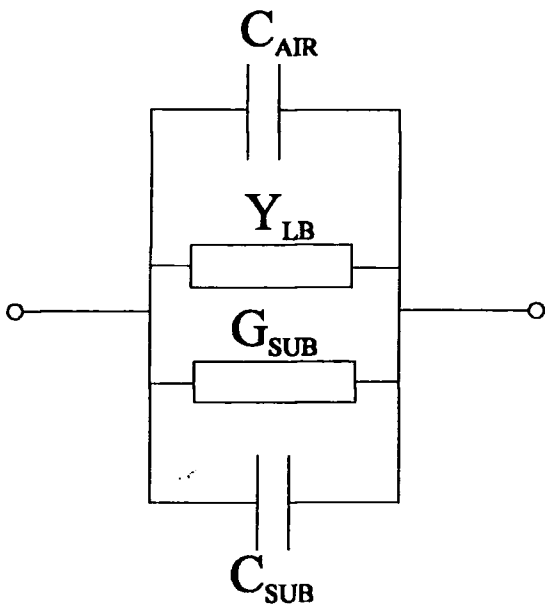

Figure 6.12: Equivalent circuit of an IDE covered with an LB film. C_{AIR} is the capacitance related to the medium above the LB film, Y_{LB} is the admittance related to the LB film and C_{SUB} and G_{SUB} are the capacitance and conductance due to the substrate, respectively.

the measured admittance and the film permittivity. An approximate model can be given in terms of the equivalent circuit shown in figure 6.14(a). Here, the LB film admittance is considered as the sum of two contributions related, respectively, to the permittivity in the in-plane and out-of-plane directions. The former is designated by $C_{LB//}$ and $G_{LB//}$, and the latter by $C_{LB\perp}$ and $G_{LB\perp}$. These are related to the LB film permittivity by

$$G_{LB//} = C_{geom//}\,\omega\varepsilon''_{//}(\omega) \qquad C_{LB//} = C_{geom//}\,\varepsilon'_{//}(\omega) \tag{6.14}$$

and

$$G_{LB\perp} = C_{geom\perp}\,\omega\varepsilon''_{\perp}(\omega) \qquad C_{LB\perp} = C_{geom\perp}\,\varepsilon'_{\perp}(\omega) \tag{6.15}$$

where $\varepsilon''_{\perp}(\omega)$ and $\varepsilon'_{\perp}(\omega)$ are, respectively, the imaginary and real parts of the permittivity in the out-plane-direction, $\varepsilon''_{//}(\omega)$ and $\varepsilon'_{//}(\omega)$ the imaginary and real part of the permittivity in the in-plane direction, and $C_{geom//}$ and $C_{geom\perp}$ the geometrical capacitance of the IDE in the in-plane and out-of-plane direction, respectively.

The geometrical capacitance in the in-plane direction can be calculated as

$$C_{geom//} = \frac{l\,t}{d}\varepsilon_o \tag{6.16}$$

where l is the total length, t is the thickness and d is the spacing of the IDE. Substituting the geometrical dimensions of the IDE into equation (6.16) $C_{geom//} = 3.9 \times 10^{-4}$ pF.

The geometrical capacitance in the out-of-plane direction can be calculated by the use of conformal mapping by the following expression found in the literature [14, 15]

$$C_{geom\perp} = l\,\varepsilon_o\,\frac{1}{2}\,\frac{K\left\{\left[1-\left(\frac{d}{w+d}\right)^2\right]^{\frac{1}{2}}\right\}}{K\left(\frac{d}{w+d}\right)} \tag{6.17}$$

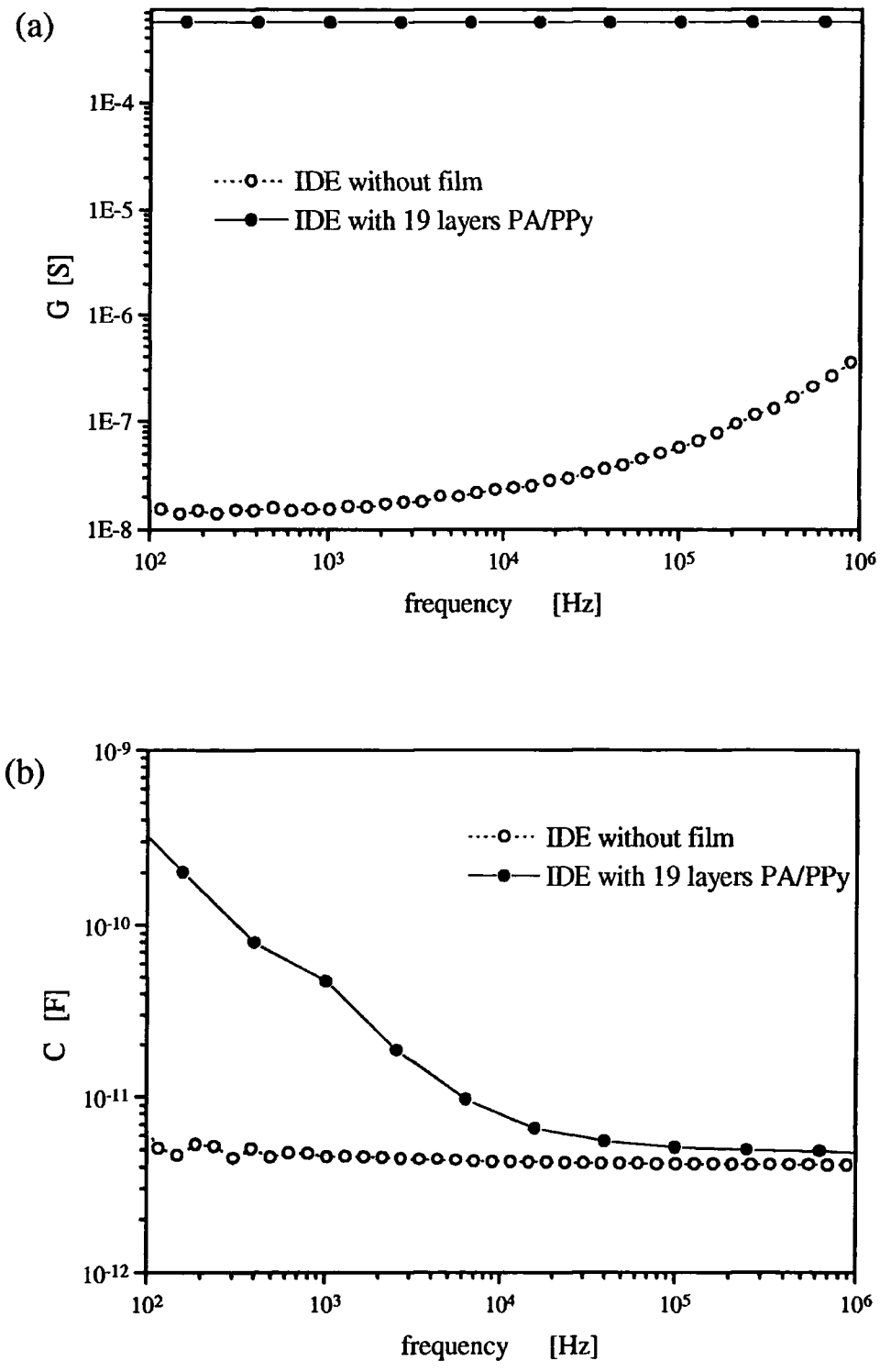

Figure 6.13: (a) Conductance measured for an IDE with and without an LB film, as a function of the frequency; (b) Capacitance measured for an IDE with and without an LB film, as a function of the frequency. In both cases the LB film consisted of 19 monolayers of PA/PPy.

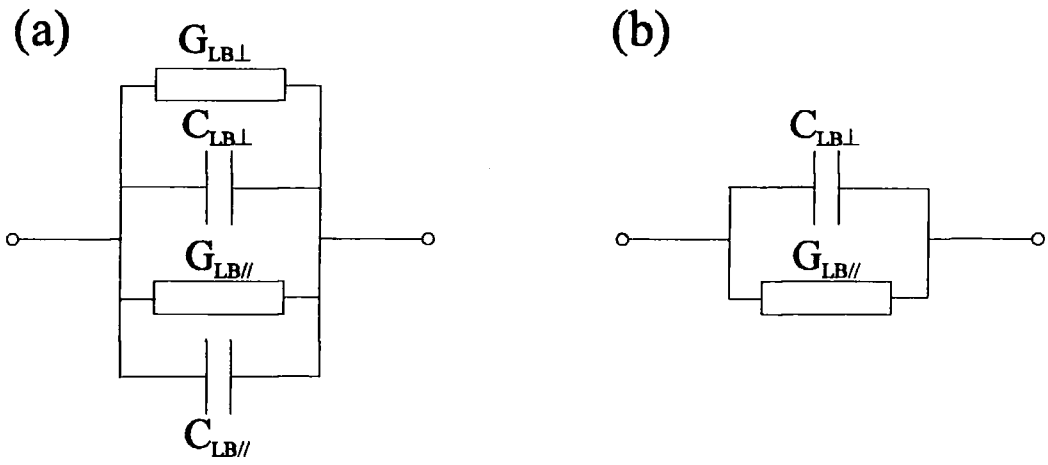

Figure 6.14: (a) Equivalent circuit for the admittance of a PA/PPy LB film on an IDE.(b) Simplified equivalent circuit for the admittance of a PA/PPy LB film on an IDE by estimating the absolute value of the elements. $C_{LB\perp}$ and $G_{LB\perp}$ are the capacitance and conductance related to the out-of-plane permittivity, respectively. $C_{LB//}$ and $G_{LB//}$ are the capacitance and conductance related to the in-plane permittivity, respectively.

where w is the width of the electrodes and K(x) is a complete elliptic integral of the first kind [16]. Substituting the geometrical dimensions of the IDE (the width was 240 μm) in equation (6.17), and using the values of K(x) found in the literature [16], $C_{geom\perp}$ was estimated to be 0.8 pF. This value is consistent with that of the IDE capacitance C_{IDE} without any film , given by

$$C_{IDE} \cong C_{geom\perp}(\varepsilon'_{glass} + 1) \qquad (6.18)$$

where ε'_{glass} is the real part of the glass permittivity. Using $\varepsilon'_{glass} = 4$, the estimated value of $C_{geom\perp}$ is found $C_{IDE} \cong 4$ pF, in agreement with our experimental results (figure 6.13).

Assuming that $\varepsilon''_{LB//}/\varepsilon''_{LB\perp} \sim 10^7$ ($\sigma_{//}/\sigma_{\perp} \sim 10^7$), and that $C_{G//}/C_{G\perp} \sim 5 \times 10^{-4}$, then $G_{LB//}/G_{LB\perp} \sim 5\times 10^3$. The ratio $\varepsilon'_{LB//}/\varepsilon'_{LB\perp}$ has not been measured but it seems sensible to expect this to be no greater than 10^2. In this case, $C_{LB//}/C_{LB\perp} \sim 5\times 10^{-2}$. From these calculations, it is evident that the following conditions are satisfied

$$G_{LB//} \gg G_{LB\perp} \qquad C_{LB//} \ll C_{LB\perp}. \tag{6.19}$$

Consequently, the equivalent circuit for the admittance of LB film on IDE can be simplified as shown in figure 6.14(b).

The value of $\sigma'_{LB//}$, obtained by dividing Y'_{LB} by $C_{geom//}$, is ~ 1 S cm^{-1}, in good agreement with the DC conductivity measured in the in-plane direction (discussed in section 6.4.1). In contrast, the value of $\varepsilon'_{LB\perp}$ estimated by dividing Y''_{LB} by $C_{geom\perp}$ does not compare well with the results in section 6.4.2. It is evident (i) the value of $\varepsilon'_{LB\perp}$ is large for low frequencies (~ 4×10^3 at 10^2 Hz), and (ii) there is a power law dependence of $\varepsilon'_{LB\perp}$ on the frequency with exponent -0.96 ± 0.04 at low frequency. A similar behaviour for capacitance at low frequency for thin films deposited on IDEs was found by other workers for polypyrrole [17] (not LB layers), polysiloxanes [18, 19] and zeolites [20].

An explanation of this result can be given by considering the more complicated equivalent circuit shown in figure 6.15. In this case, it is assumed that the capacitor above the IDE is partially filled by the LB film and the rest is filled by air. Therefore, the admittance in the out-plane direction is given by the series of the contribution of the LB film in the out-of-plane direction ($Y_{LB\perp}$) and the capacitance of the medium above the LB film $C^{(2)}_{AIR}$. The latter capacitance is designed as $C^{(2)}_{AIR}$ to distinguish it from the capacitance C_{AIR} for an IDE with no deposited film. This situation is analogous to a capacitor of capacitance C_{AIR} partially filled with a dielectric (the LB film). It is evident that the geometrical capacitance of the empty space (i.e. $C^{(2)}_{AIR}$) will be greater than C_{AIR}. For the same reason, the geometrical capacitance of the filled part, $C_{geom\perp}$ in equations (6.15), will be larger than that estimated using equation (6.17) (i.e. C_{AIR}). The conditions (6.19) will be still valid but $C_{LB\perp}$ and $G_{LB\perp}$ will be replaced by the total capacitance and conductance of the series combination of $Y_{LB\perp}$ and $C^{(2)}_{AIR}$, respectively.

The admittance $Y_{\perp}$ of the series combination of $Y_{LB\perp}$ and $C_{AIR}^{(2)}$ is

$$Y_{\perp} = i\omega C_{AIR}^{(2)} \frac{1+\omega^2\tau_1\tau_o}{1+\omega^2\tau_o^2} + \frac{R_{LB\perp}\left(\omega C_{AIR}^{(2)}\right)^2}{1+\omega^2\tau_o^2} \tag{6.20}$$

where

$$\tau_o = R_{LB\perp}(C_{LB\perp} + C_{AIR}^{(2)}) \qquad \text{and} \qquad \tau_1 = R_{LB\perp}C_{LB\perp} \tag{6.21}$$

This gives the following values for the capacitance at low and high frequency

$$C_{\perp} \cong C_{AIR}^{(2)} \qquad (\text{for} \quad \omega \to 0) \tag{6.22}$$

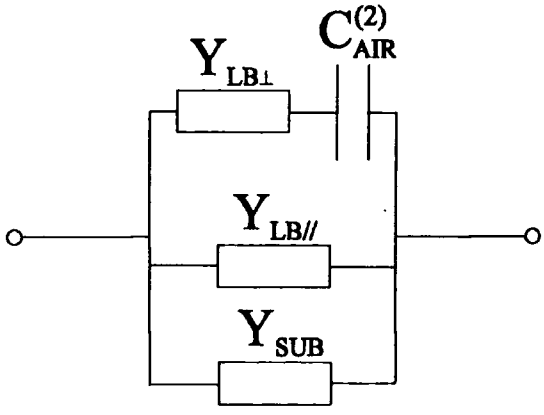

Figure 6.15: Equivalent circuit of an IDE covered with an LB film. $Y_{LB\perp}$ and $Y_{LB//}$ are the admittance related to LB film permittivity in the out-of-plane direction and in-plane direction, respectively, $C_{AIR}^{(2)}$ is the capacitance related to the medium above the LB film and Y_{SUB} is the admittance due to the substrate.

$$C_{\perp} \cong \frac{C_{AIR}^{(2)} C_{LB\perp}}{C_{AIR}^{(2)} + C_{LB\perp}} \qquad (\text{for} \quad \omega \to \infty) \qquad (6.23)$$

Therefore, the observed high value of capacitance at low frequency will require a large value of $C_{AIR}^{(2)}$. Further discussion would necessitate an estimation of $C_{AIR}^{(2)}$ to compare it to the experiments. Because of the dependence of the electric field geometry on the film thickness (that in this case has also the complication due to the film anisotropy), this would involve computer simulation, not undertaken in this preliminary study.

6.5.1 Exposure to organic solvent vapours

On exposure to organic solvent vapours, the samples all showed similar behaviour. A change in the conductance, dependent on the vapour concentration, was noted, but no change in the capacitance was seen (apart from an effect, attributed to the instrument, discussed in the final part of this section).

As the conductance was not dependent on frequency (even after exposure to the vapours), it was monitored at a fixed frequency of 1 kHz. The concentrations of the vapours were varied in the range between hundreds of ppm and tens of thousands of ppm (i.e. per cent).

The effect of pulses of ethanol vapour on the sample conductance is shown in figures 6.16(a) and (b). The following features are evident: (i) a decrease of the conductance when the sample is exposed to ethanol; (ii) a fast initial response that gradually becomes slower with the conductance tending to a stable value; (iii) a reasonable reversibility when the sample is exposed to N_2; and (iv) a good reproducibility on subsequent exposures. Similar features can be observed in figures 6.17(a) and (b) showing the changes of the conductance during exposure to acetonitrile vapour. During

exposure to benzene, the changes of the conductance were smaller than those observed for the other two organic solvent vapours (data not shown).

In figure 6.18, the absolute value of the fractional change in the conductance (measured at 1 kHz) $|\Delta G|/G_o$ versus the concentration of the three organic vapours and water (this will be discussed in a later section) is shown. Similar behaviour is noted for acetonitrile and ethanol, with a much smaller sensitivity to benzene. In all cases, it was possible to describe the dependence of the change of conductance on concentration with a power law

$$|\Delta G|/G_o = A\, c^b \qquad (6.24)$$

where A and b are constants and c is the vapour concentration. The best fits of the experimental data are shown in figure 6.18 (lines), and the estimated parameters A and b in table 6.4. It is evident that the parameter b is always smaller than 1.

Another possible function to describe the depedence of $\Delta G/G_o$ on vapour concentration is an adsorbtion isotherm. In this case, the changes are considered related to an adsorption of the vapour molecules on the film surface. The fractional coverage (θ) of a surface depends on the pressure of the overlying gas (p), and the variation of θ with p at a chosen temperature is called the adsorption isotherm. The simplest adsorption isotherm is the Langmuir isotherm [21]

$$\theta = \frac{Kp}{1+Kp} \qquad (6.25)$$

This isotherm is based on three assumptions

(i) Adsorption cannot proceed beyond monolayer coverage.

(ii) All sites are equivalent and the surface is uniform.

(iii) The ability of a molecule to adsorb at a given site is independent of the occupation of neighbouring sites.

To see if this function can be used to describe the observed behaviour it is necessary to relate the absorbed molecules to the change of conductivity. A possible hypothesis is that the decrease of charge carriers is equal to the adsorbed molecules, as discussed in paragraph 6.5.3, therefore the observed change of conductivity would be proportional to θ. A first analysis done using this hypothesis shown that in our case, the experimental data were not in good agreement with the behaviour described by the Langmuir isotherm. Therefore, the observed change of the conductivity seems to not be related to a simple adsorption of the gas molecules on the film surface and further investigation would be necessary to better understand this phenomenon.

During exposure to high concentrations of ethanol and acetonitrile vapours, a change in the capacitance was also noted. In figure 6.19, the change of the capacitance and conductance for a sample exposed to 5.4% of acetonitrile are shown. It is evident that there is a change of the capacitance only during the initial and final transient, corresponding to the rapid change of the conductance. It was observed that the change in capacitance was proportional to the rate of change of the conductance and not related to the presence of the vapour. This was shown by comparing the rate of change of the conductance and the measured capacitance during the exposure to ethanol vapour and also during a temperature transient (figure 6.20).

There is evidently a direct correlation between the rate of change of the conductance (calculated as the difference between two consecutive measurements of conductance) shown in figure 6.20(b) and the behaviour of the capacitance shown in figure 6.20(c). Therefore, the observed transient changes in the capacitance during the exposure to ethanol and acetonitrile were attributed to an instrumental effect and not to an effect related to the vapours. An explanation of this instrumental effect remains unclear.

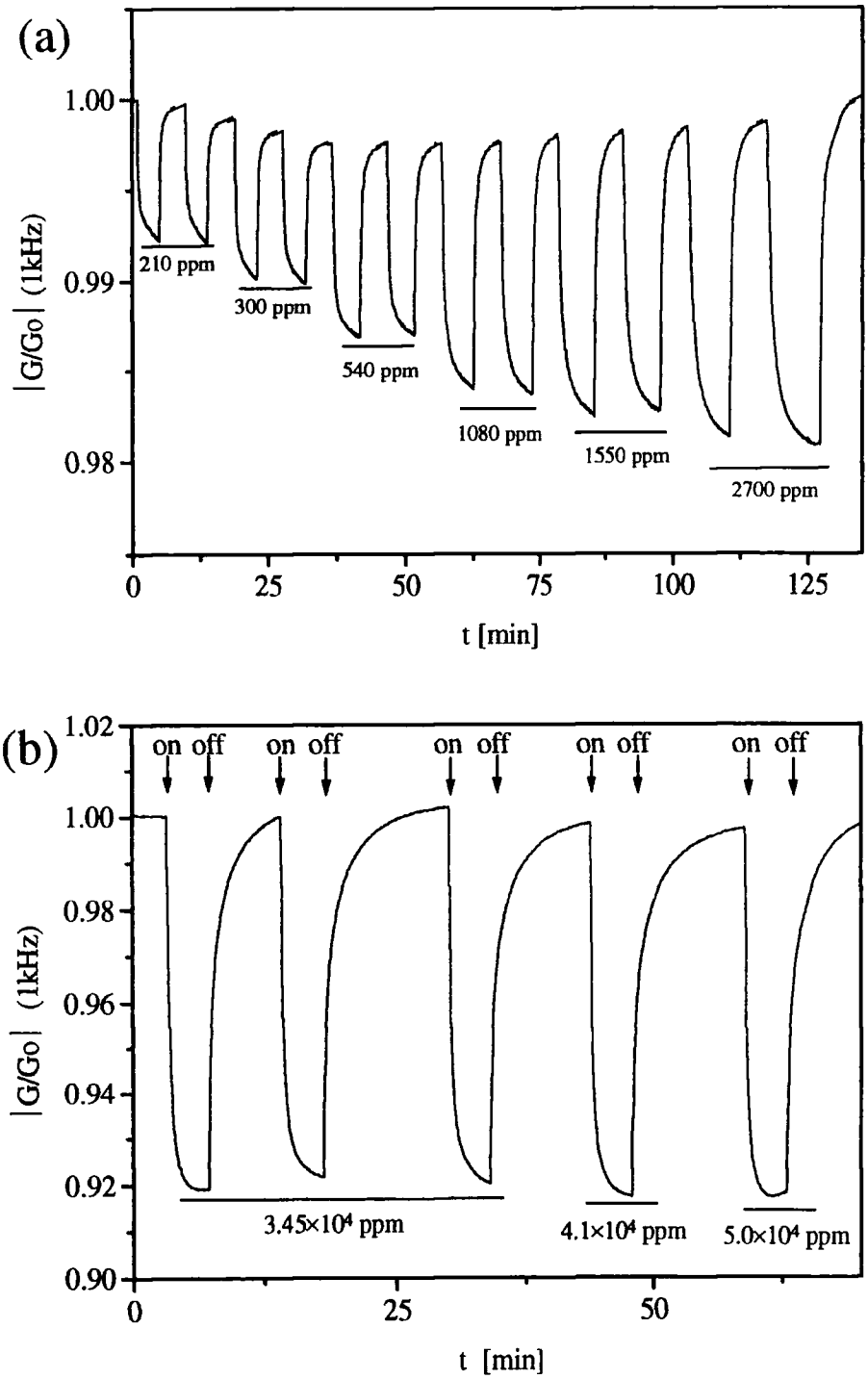

Figure 6.16:(a) & (b) The effect of pulses of increasing concentration of ethanol vapour diluted in N_2 on the conductance (measured at 1 kHz) for a PA/PPy film 19 monolayers thick deposited on an IDE. The data are presented in the form (conductance after exposure)/(conductance before exposure at t = 0) versus time. The concentration is indicated in the graph.

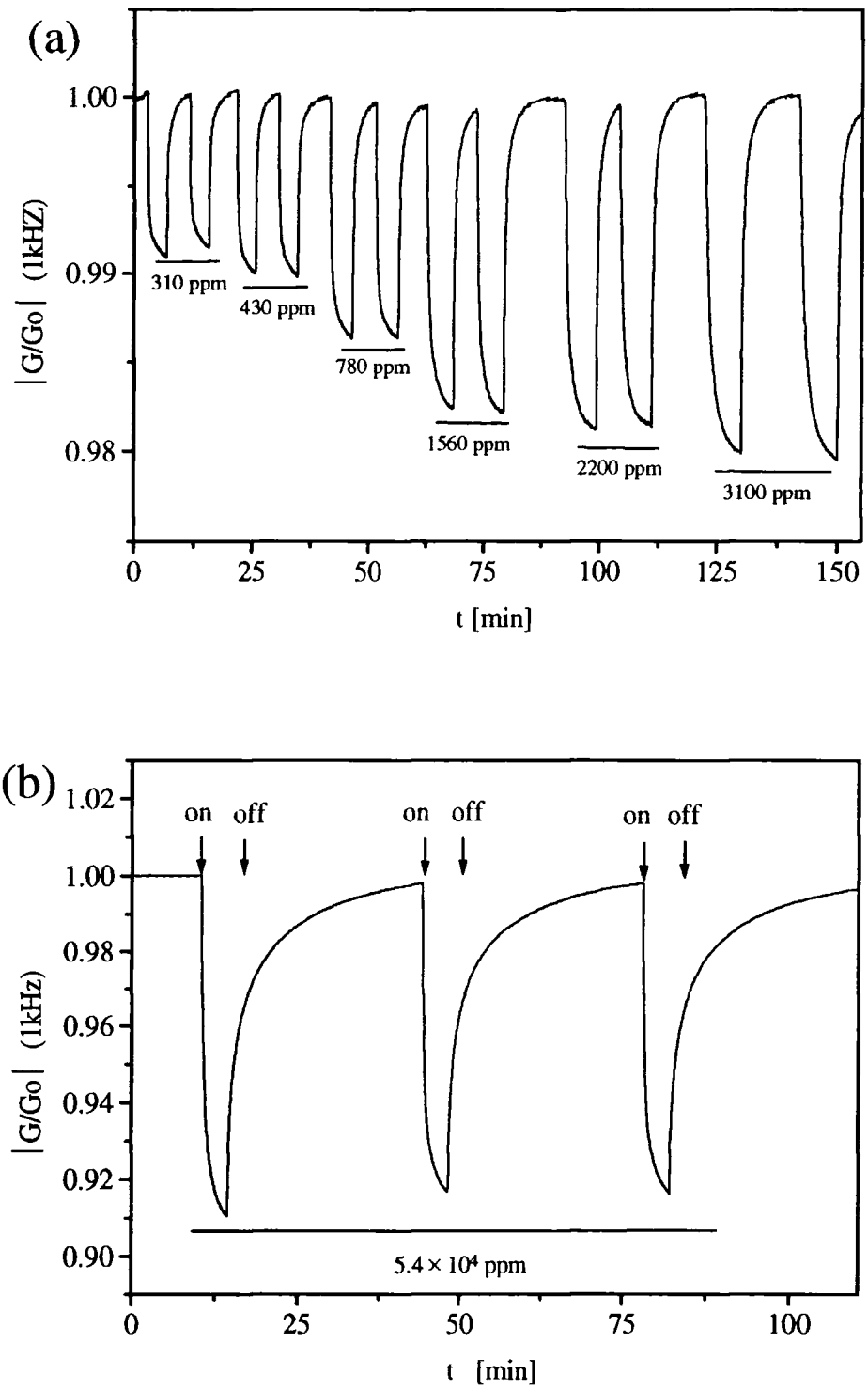

Figure 6.17: (a) & (b) The effect of pulses of increasing concentration of acetonitrile vapour diluted in N_2 on the conductance (measured at 1 kHz) for a PA/PPy film 19 monolayers thick deposited on an IDE. The data are presented in the form (conductance after exposure)/(conductance before exposure at t = 0) versus time. The concentration is indicated in the graph.

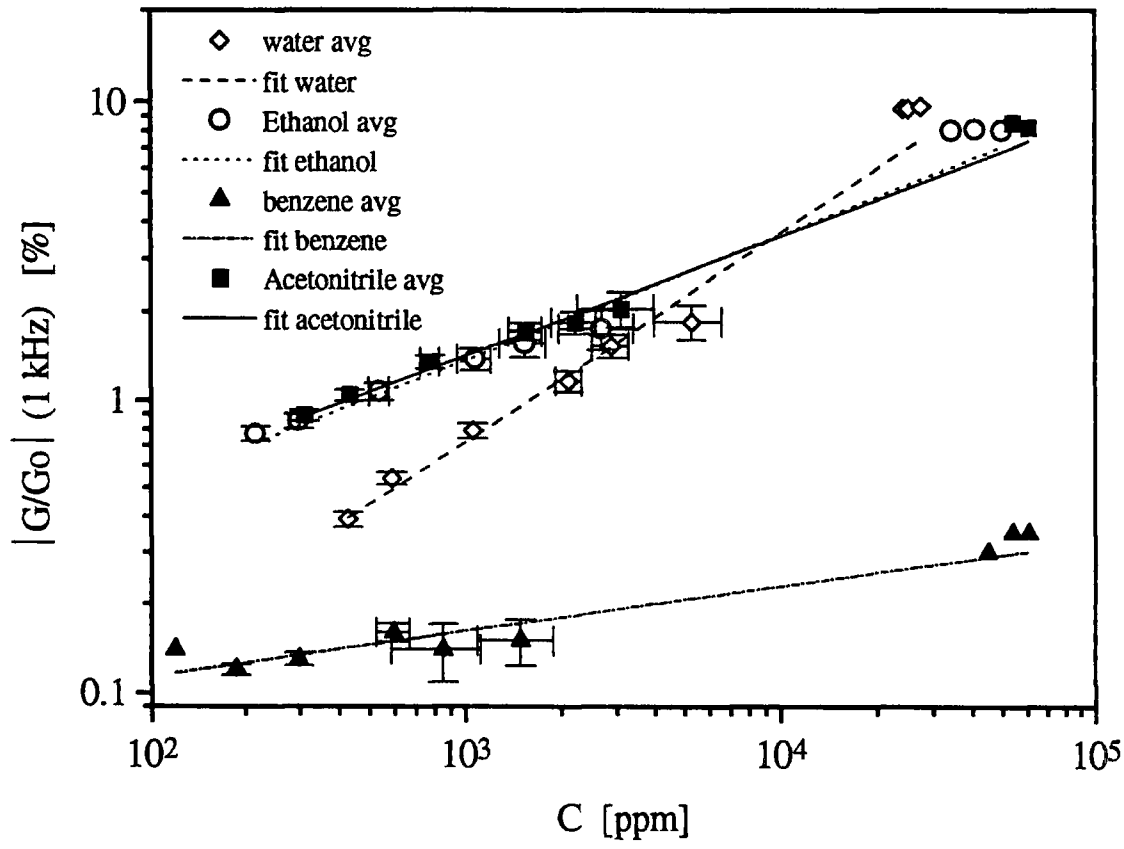

Figure 6.18: The absolute value of the fractional change in the conductance (measured at 1 kHz) $|\Delta G/G_o|$ versus the concentration of vapour (ethanol, acetonitrile, benzene and water) for a PA/PPy film 19 monolayers thick deposited on an IDE. The lines are best fits using equation (6.24), the estimated parameters are reported in table 6.4. Where the errors are not shown, these were smaller than the size of the data points.

Vapour	A	b
Ethanol	$(7 \pm 1) \times 10^{-2}$	0.42 ± 0.03
Acetonitrile	$(9 \pm 1) \times 10^{-2}$	0.40 ± 0.02
Benzene	$(6 \pm 0.9) \times 10^{-2}$	0.15 ± 0.02
Water	$(5 \pm 1) \times 10^{-3}$	0.71 ± 0.04

Table 6.4: Best fit parameters estimated by fitting the change of the conductance versus the concentration for the four different vapours with equation (6.24).

6.5.2 Exposure to water vapour

During exposure to water vapour, a change in the conductance dependent on the vapour concentration was seen together with a change in the capacitance observable only for high water concentrations.

In figures 6.21(a) and (b) the effect of pulses of water vapour on the sample conductance is shown. The behaviour is similar to that observed during the exposure to organic vapours. The dependence of the absolute value of the fractional change in the conductance (measured at 1 kHz) $|\Delta G|/G_o$ versus the water concentration is shown in figure 6.18 together with the data for the organic solvents. The dependence on the concentration can also be described by equation (6.24). The exponent of the power law, estimated by fitting the experimental data to equation (6.24) (reported in table 6.4), is greater than for the organic vapours. Moreover, the sensitivity to high concentrations of water is also greater than to high concentrations of the organic vapours

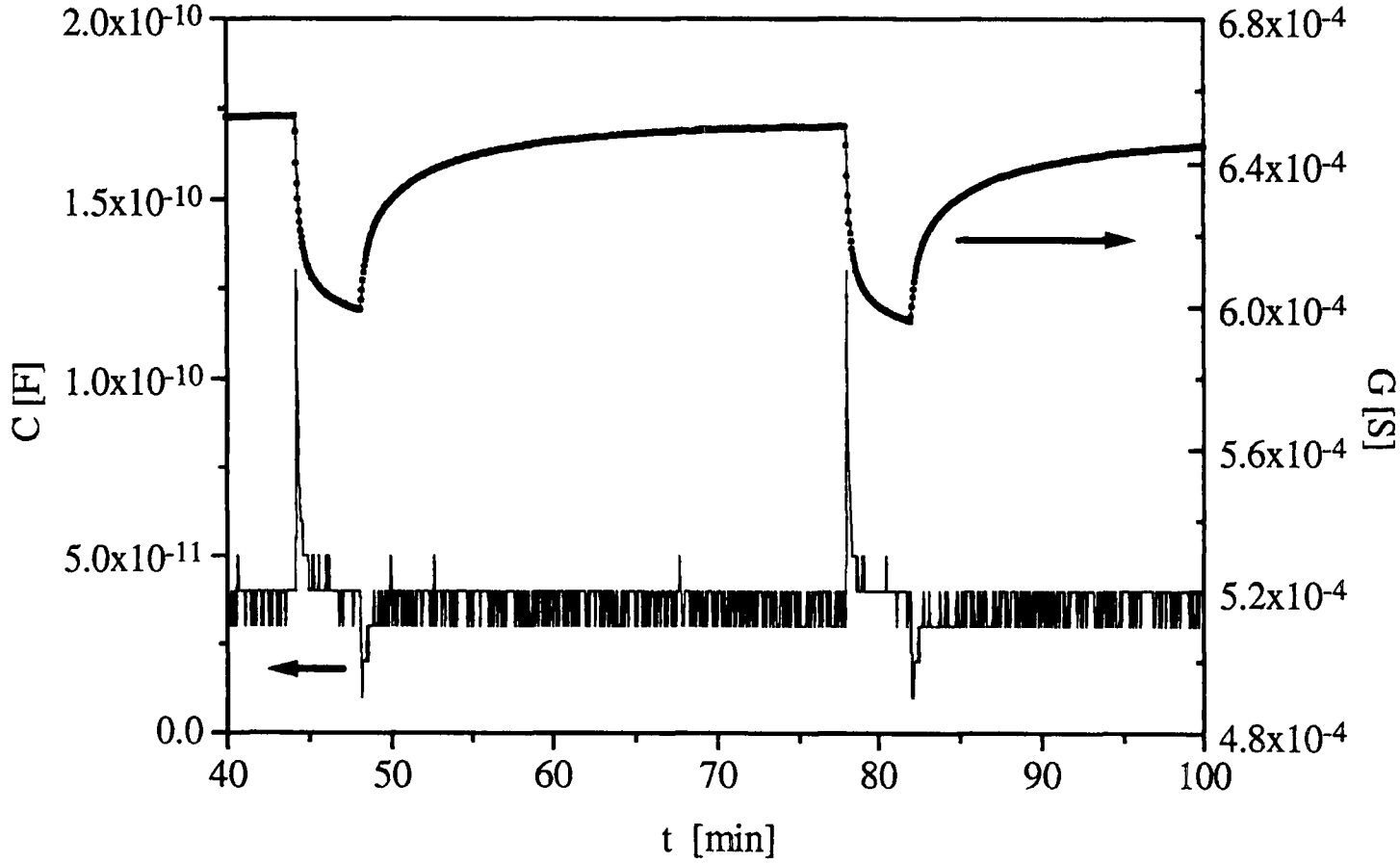

Figure 6.19: The effect of pulses of 5.4% acetonitrile vapour diluted in N_2 on the conductance and capacitance (measured at 1 kHz) for a PA/PPy film 19 monolayers thick deposited on an IDE. The data are presented in the form of measured conductance and capacitance versus time.

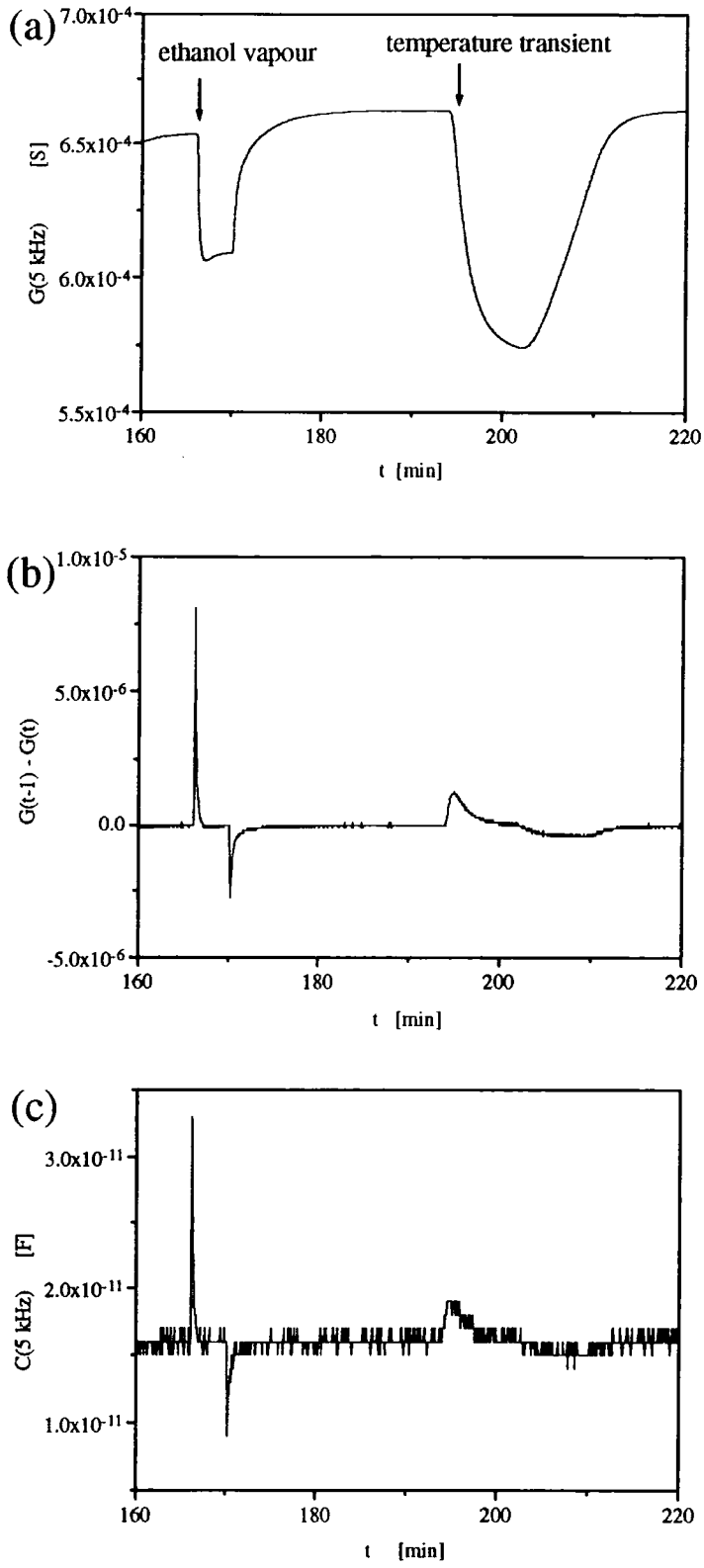

Figure 6.20: The effect of a pulse of 5.9% ethanol vapour diluted in N_2 and of two temperature transients (the first from T = 294 K to T = 280 K and the second from T = 280 K to T = 294 K) (a) on the conductance, (b) on the rate of change of the conductance and (c) on the capacitance measured at 5 kHz for a Pa/PPy film 19 monolayers thick deposited on an IDE. The data are presented versus time. The rate of change of the conductance was calculated as the difference between two consecutive measurements of the conductance, with $\Delta t = 3$ sec.

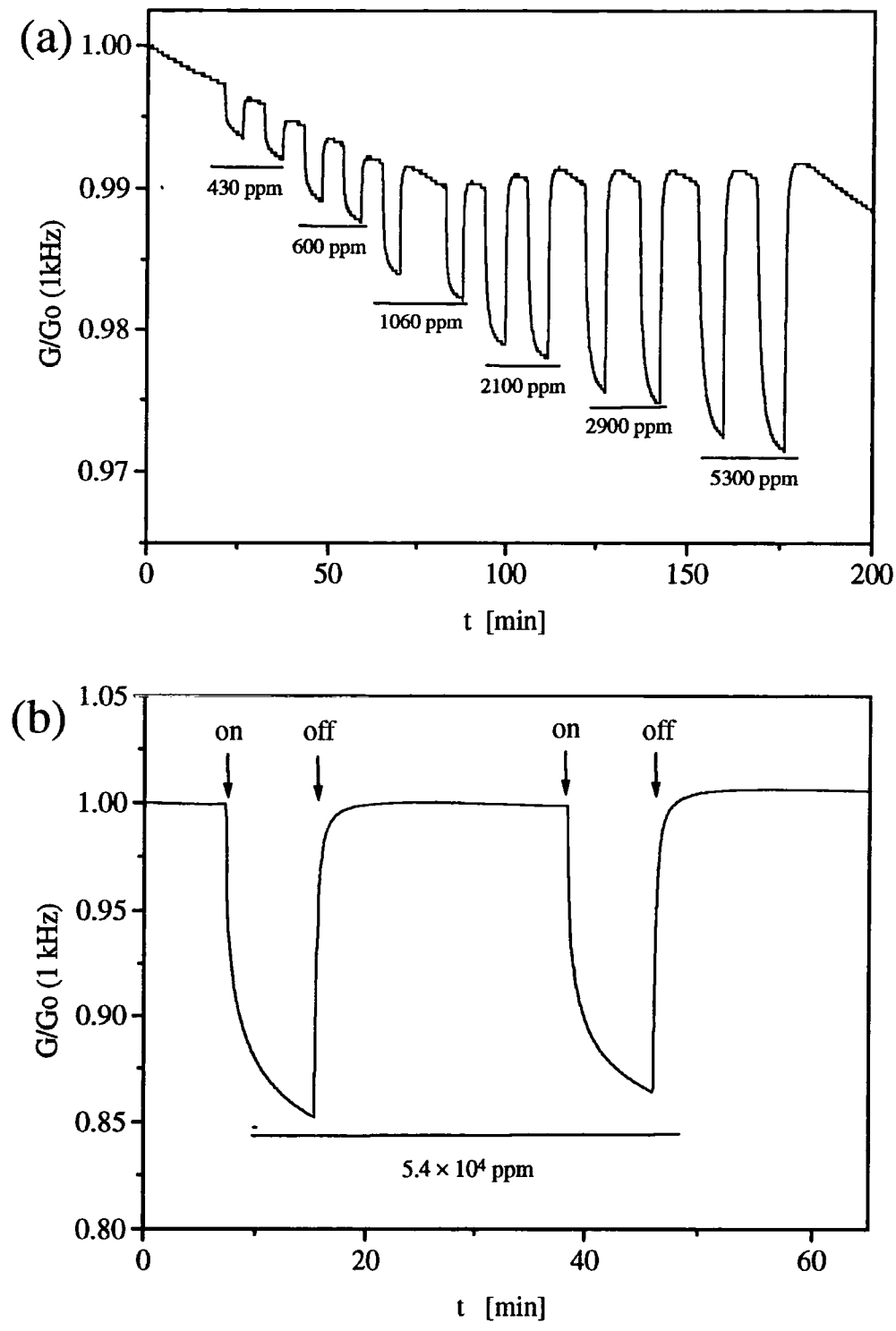

Figure 6.21:(a) & (b) The effect of pulses of increasing concentration of water vapour diluted in N_2 on the conductance (measured at 1 kHz) for a PA/PPy film 19 monolayers thick deposited on an IDE. The data are presented in the form (conductance after exposure)/(conductance before exposure at t = 0) versus time. The concentration is indicated on the graph.

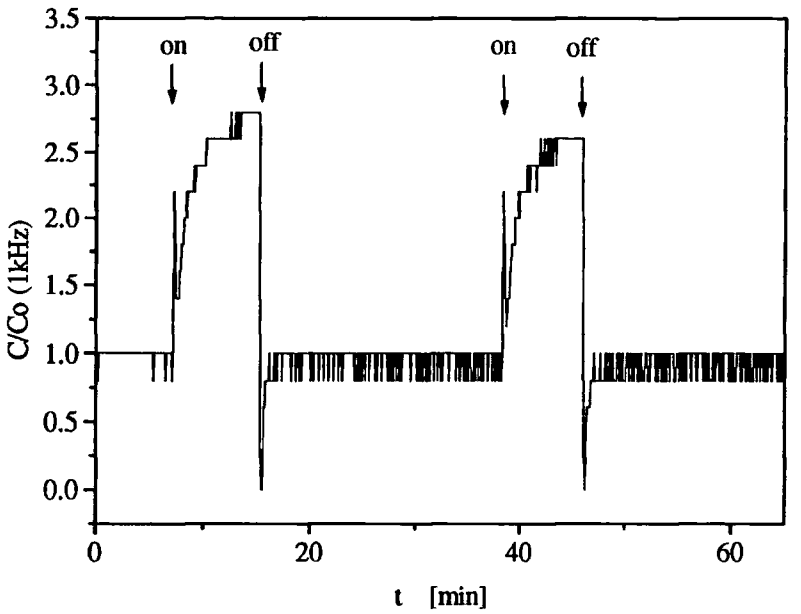

Figure 6.22: The effect of pulses of 2.5% water vapour diluted in N_2 on the capacitance (measured at 1 kHz) for a PA/PPy film 19 monolayers thick deposited on an IDE. The data are presented in the form (capacitance after exposure)/(capacitance before exposure at t = 0) versus time.

Figure 6.22 shows the effect of pulses of 2.5% water vapour on the sample capacitance. The following features are evident: (i) an increase of the capacitance when the sample is exposed to water; (ii) a fast initial response that gradually becomes slower with the capacitance tending to a stable value; (iii) full reversibility; and (iv) a good reproducibility on subsequent exposures. As for the organic vapours, an instrumental effect is noted during the first part of the exposure and the first part of the recovery, giving two spikes.

The effect of 2.5% water on the frequency behaviour of capacitance and conductance is shown in figure 6.23. This measurement reveals an increase of the capacitance (figure 6.23(b)) at all the frequencies investigated. For the conductance (figure 6.23(b)), a decrease is noted over all the frequencies, with a larger difference at lower frequencies.

6.5.3 Interpretation of vapour effects

The use of polypyrrole as a material for gas sensors has been investigated by several workers, mainly in chemiresistive sensors. The conductivity of polypyrrole has been found to be sensitive to both inorganic gases (i.e. NO_2, H_2S, NH_3)[22-24] and to organic vapours [14, 17, 25-34]. Differences in the response to vapours has been shown to depend on the film properties and morphology (related, for example, to different counter ions, deposition techniques and deposition conditions). The change of the DC conductivity has been attributed mainly to a sorption of the vapour into the polymer film with the formation of charge-transfer complexes. For polypyrrole films exposed to high concentrations of organic solvent vapours, swelling [33] and plastification effects [34] have also been observed.

The direction of the electron transfer is determined by the relative magnitude of the electronegativity of the vapour χ_M and the work function of the polymer ϕ [25]. If $\chi_M > \phi$ the vapour is an electron acceptor and if $\chi_M < \phi$ the vapour is an electron donor.

The electronegativity of a molecule is taken as

$$\chi_M = (I_P + E_A)/2 \qquad (6.26)$$

where I_P and E_A are the ionization potential and electron affinity, respectively. χ_M represents the position of the Fermi level relative to vacuum. In the case of most organic compounds $I_P \gg E_A$ and the electronegativity χ_M can be approximated by half of the ionization potential. For the four vapours investigated the ionization potentials are: water $I_P = 12.6$ eV [26], acetonitrile $I_P = 12.2$ eV [35], ethanol $I_P = 10.5$ eV [35] and benzene $I_P = 9.2$ eV [35].

The value of polypyrrole work function was not measured for our sample. In the literature this been shown to depend on the doping level, and a value around 5 eV is usually measured [26]. The decrease of the conductivity of polypyrrole can therefore be

explained by a decrease of the charge carriers (i.e. polarons and bipolarons) due to the transfer of electrons from the vapour molecules to the polymer (polypyrrole is a p-type semiconductor). The decrease of DC conductivity of our film during the exposure to ethanol is in agreement with other results in the literature [17, 26, 27 - 32] where a maximum decrease of 10% (and generally in the range between 2.5% and 10%) was observed for saturated ethanol vapour (i.e. C = 7.6% at T = 298 K). Data in the literature for the other two organic vapours were not found. However, the expected response to acetonitrile should be different from that to ethanol considering the difference in electronegativity.

The sign of the change of conductivity during exposure to water vapour has been shown to depend on the doping level of the polypyrrole [26]. A decrease in conductivity is observed for highly doped polypyrrole while an increase is noted for lightly doped polypyrrole. This suggests that our polypyrrole films are highly doped.

The interpretation of the change of capacitance observed during the exposure to water (not observed for the organic solvents) remains uncertain. A comparison with data in the literature is more difficult. Most of the studies undertaken focus on resistance changes and only few on impedance measurements [14, 17, 36]. Amrani et al. observed similar behaviour for the conductance for organic vapours, with a corresponding change of the capacitance [14], but no results for water vapour were shown. Therefore, it is not clear if the observed change of capacitance is present only during the exposure to water because (i) this effect is greater for water (because of its higher permittivity), or (ii) this is due to a specific interaction between the film and the water. Our interpretation of the measured capacitance is based mainly on an interface effect between the film and the medium above it. We could expect that changes in the relative dimensions of film and electrodes will be very important in determining the magnitude of the interface capacitance and of its dependence on the vapours. However, clarification requires further investigation.

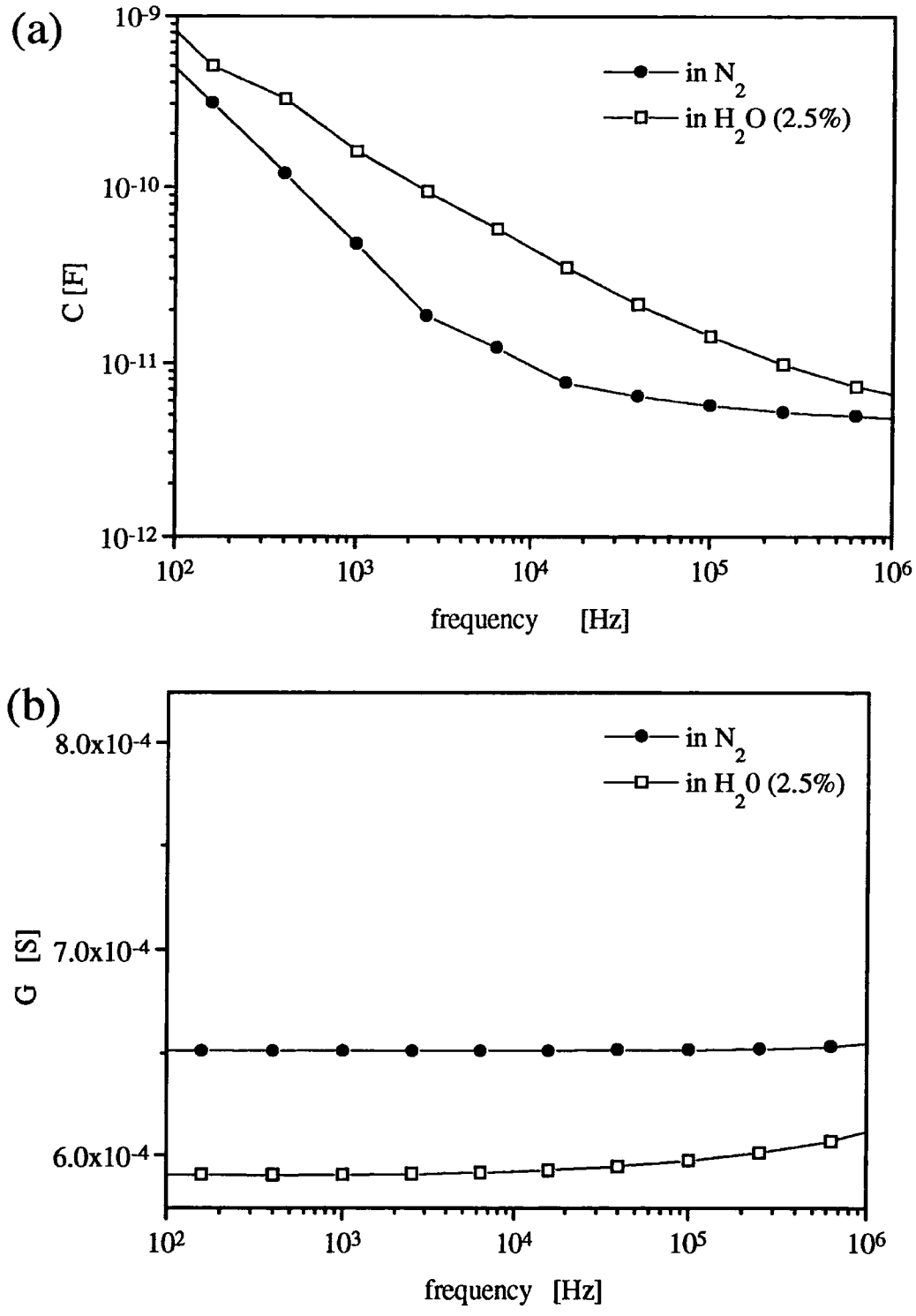

Figure 6.23: (a) Capacitance measured for an IDE covered with an LB film of 19 monolayers of PA/PPy in nitrogen (solid circles) and in 2.5% of water (open squares). (b) Conductance measured for an IDE covered with a LB film of 19 monolayers of PA/PPy in nitrogen (solid circles) and in 2.5% of water (open squares).

6.6 Evaluation of the device for gas sensing applications

In the previous section, results obtained during the exposure of the IDE structure to vapours have been described. Here, we provide a discussion of the device sensitivity, selectivity and stability to evaluate its usefulness as a gas sensor.

As shown in figure 6.18, the dependence of the relative change in conductance on vapour concentration can be described by a power law (equation (6.24)) over the concentration range studied. Considering the sensitivity s as the change of conductance with respect to a unit change (1 ppm) in the vapour concentration, this is given by

$$s = \frac{d|\Delta G|}{dc} = G_o A b c^{b-1} \qquad (6.27)$$

where A and b are the same two parameters of equation (6.24). Therefore, the sensitivity depends on the vapour concentration, and, as shown in figure 6.24, it decreases with increasing the vapour concentration. From figure 6.24, it is evident that the sensitivities to ethanol and acetonitrile are almost the same. This sensitivity is higher than to water for low concentrations but lower for high concentrations. The sensitivity to benzene vapour is low over the range of concentrations measured. The maximum and minimum estimated sensitivity corresponding to 100 ppm and 10^5 ppm, respectively, are reported in table 5 for the four different vapours.

The maximum sensitivity estimated at 100 ppm was used to calculate the minimum detectable concentration. Assuming that the sensitivity will not decrease on decreasing the concentration, an upper limit for the minimum detectable concentration can be estimated by dividing the instrument resolution (1 nS) by the maximum sensitivity (i.e. at 100 ppm), this is reported in table 6.5. It follows that the device should be able to detect concentrations of ethanol and acetonitrile vapours less than 10 ppm.

In terms of the selectivity, two main results need to be considered: (i) the response of the

conductance, over the frequency range of our measurement, was the same; and (ii) a change in the capacitance was only noted for exposure to high concentrations of water. Therefore, measuring the admittance at more than one frequency will not markedly improve the device selectivity, which remains poor. Nevertheless, the observed change in. capacitance to water vapour could be useful considering its ubiquitous presence in the atmosphere.

An improvement in the selectivity of this type of device could probably be obtained by measuring the admittance at higher frequencies (i.e. in the microwave range) where the conductance is not frequency independent (as discussed in paragraph 2.3.3) as shown by other workers [14, 36-38].

Another important factor for a gas sensor is the stability. At the moment long term experiments have not been carried out to investigate this parameter. A preliminary study of the device stability was undertaken by monitoring the conductance during a two weeks period in which the device was exposed repeatedly to the four vapours investigated, and left in a flow of nitrogen for the remaining time. The result is shown in figure 6.25. The conductance decreases by more than 50% of its initial value over the two weeks, with a rapid decrease over the first few days. The behaviour of the conductance versus time was found to be in good agreement with an exponential decay (solid line in figure 6.25), and can be described by the equation

$$G(t) = G_1 + G_2 \exp[-(t/\tau_G)] \qquad (6.28)$$

where G_1 is the value of the conductance for t equal to infinity, G_1+G_2 is the initial value of the conductance (i.e. for t = 0), and τ_G is the time constant of the decay. The value of the parameters estimated from the fit of the data with equation (6.28) were: $G_1 = (2.4 \pm 0.7) \times 10^{-4}$ S, $G_2 = (7.1 \pm 0.6) \times 10^{-4}$ S and $\tau_G = 7 \pm 1$ days

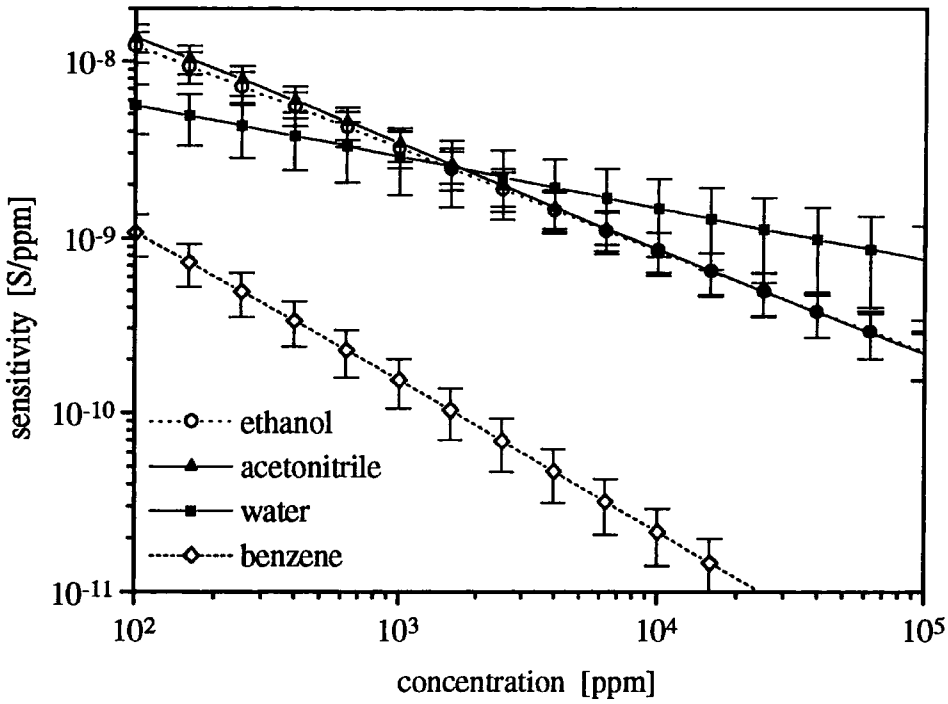

Figure 6.24: Sensitivity of a device consisting of 19 monolayers of PA/PPy deposited on an IDE. The values were calculated using equation (6.27) substituting the values of A and b estimated by the fit of $|\Delta G|/G_o$ versus concentration with equation (6.24) reported in table 6.4.

Vapour	**Maximum sensitivity (at 10^2 ppm)** [S/ppm]	**Minimum sensitivity (at 10^5 ppm)** [S/ppm]	**Minimum detected concentration** [ppm]	**Estimated minimum detectable concentration** [ppm]
Ethanol	$(12 \pm 2)\times10^{-9}$	$(12 \pm 2)\times10^{-11}$	210 ± 10	$< 8 \pm 1$
Acetonitrile	$(14 \pm 2)\times10^{-9}$	$(12 \pm 2)\times10^{-11}$	310 ± 10	$< 7 \pm 1$
Water	$(6 \pm 1)\times10^{-9}$	$(12 \pm 2)\times10^{-11}$	430 ± 10	$< 17 \pm 3$
Benzene	$(11 \pm 3)\times10^{-10}$	$(12 \pm 2)\times10^{-13}$	120 ± 5	$< 90 \pm 25$

Table 6.5: Maximum and minimum sensitivity and minimum detected concentration of a device consisting of 19 monolayers of PA/PPy deposited on an IDE exposed to benzene, acetonitrile, ethanol and water. The maximum and minimum sensitivities were estimated using equation (6.27) substituting the values of A and b from the fit of $|\Delta G|/G_o$ versus concentration with equation (6.24) reported in table 6.4.

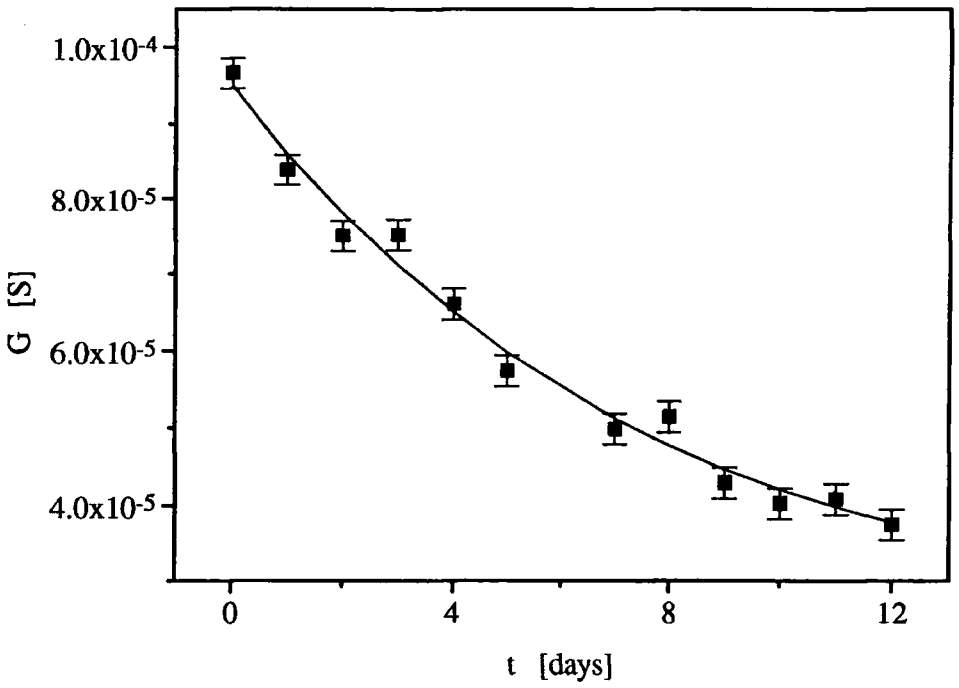

Figure 6.25: Conductance of a device constiting of 19 monolayers of PA/PPy deposited on an IDE versus time during which it was repeatedly exposed to benzene, acetonitrile, ethanol and water. The conductance was measured in the morning before starting the experiments. The sample was left in a flow of nitrogen for the time that it was not exposed to vapours. Points are experimental data, line is the fit using equation (6.28).

6.7 Summary

Thin multilayer films of PPy mixed with fatty acid have been built up using the LB technique followed by two solid state reactions. The structure of the film during the steps of the preparation has been characterised using X-ray diffraction and a surface profilometer.

AC and DC conductivity have been measured over the temperature range 90 - 300 K. A variable range hopping model provided a good description of the DC conductivity whereas the AC behaviour was interpreted in terms of the Cole-Davidson function.

A study of the change of the admittance of multilayer films deposited on IDE during exposure to four different vapours (ethanol, benzene, acetonitrile and water) has been undertaken. The change of the conductance was not dependent on the frequency for all the vapours. A 'real' change of the device capacitance was observed only during exposure to water vapour.

Finally, an evalution of the gas sensing characteristics has been given, with a discussion of the sensitivity, selectivity and stability. The unique response of the device capacitance to water may be useful to discriminate this vapour, but the absolute selectivity of the device remains limited.

References

[1] R.B.Rosner, M.F.Rubner, *Journal of the Chemical Society - Chemical Communications*, **20** (1991) 1449.

[2] A.Paul, D.Sarkar, T.N.Misra, *J.Phys.D: Appl.Phys.*, **28** (1995) 899.

[3] M.C.Petty, *Langmuir Blodgett films: an introduction*, 1996, Cambridge University Press, Cambridge.

[4] G.G.Roberts, *Langmuir-Blodgett films*, 1990, Plenum Press, New York.

[5] R.N.Rosner, M.F.Rubner, *Chem.Mat.*, **6** (1994) 581.

[6] V.Geskin, L.M.Goldenberg, R.Casalini, R.Lazzaroni, J.L.Bredas, M.C.Petty, abstract for *'Forum des microscopies a sonde locale'*, Autrans (France) march 29-31, 1999, in preparation.

[7] D.Schmeisser, H.Naarmann, W.Göpel, *Synthetic Metals*, **59** (1993) 211.

[8] N.Mott, *Conduction in non-crystalline materials*, 1987, Clarendon Press, Oxford.

[9] P.Sheng, E.K.Sichel, J.I.Gittleman, *Phys.Rev.Lett.*, **40** (1978) 1197.

[10] G.Paasch, D.Schmeiber, A.Bartl, H.Naarmann, L.Dunsch, W.Göpel, *Synthetic Metals*, **66** (1994) 135.

[11] A.K.Jonscher, *Universal relaxation law*, 1996, Chelsea Dielectric Press, London.

[12] J.C.Dyre, *J.Appl.Phys.*, **64** (1988) 2456.

[13] J.C.Dyre, *Physical Review B*, **48** (1993) 12511.

[14] M.E.H.Amrani, K.C.Persaud, P.A.Payne, *Meas.Sci.Technol.*, **6** (1995) 1500.

[15] H.E.Endres, S.Drost, *Sensors and Actuators B*, **4** (1991) 95.

[16] A.Jeffrey, *Handbook of mathematical formulas and integrals*, 1995, Academic Press, New York, chapter 12.

[17] F.Musio, M.C.Ferrara, *Sensors and Actuators B*, **41** (1997) 97.

[18] M.Haug, K.D.Schierbaum, H.E.Endres, S.Drost, W.Göpel, *Sensors and Actuators A*, **32** (1992) 326.

[19] H.E.Endres, S.Drost, F.Hutter, *Sensors and Actuators B*, **22** (1994) 7.

[20] K.Alberti, F.Fetting, *Sensors and Actuators B*, **21** (1994) 39.

[21] P.W.Atkins, *Physical Chemistry*, 1994, Oxford University Press, Oxford.

[22] G.Gustafsson, I.Lundström, *Synthetic Metals*, **21** (1987) 203.

[23] M.Penza, E.Milella, M.B.Alba, A.Quirini, L.Vasanelli, *Sensors and Actuators B*, **40** (1997) 205.

[24] F.Selampinar, L.Toppare, U.Akbulut, T.Yalçin, S.Süzer, *Synthetic Metals*, **68** (1995) 109.

[25] D.Blackwood, M.Josowicz, *J.Phys.Chem.*, **95** (1991) 493.

[26] K.Nigorikawa, Y.Kunugi, Y.Harima, K.Yamashita, *Journal of Electroanalytical Chemistry*, **396** (1995) 563.

[27] P.N.Bartlett, S.K.Ling-Chung, *Sensors and Actuators*, **20** (1989) 287.

[28] P.N.Bartlett, S.K.Ling-Chung, *Sensors and Actuators*, **19** (1989) 141.

[29] E.Milella, F.Musio, M.B.Alba, *Thin Solid Films*, **284-285** (1996) 908.

[30] H.V.Shurmer, P.Corcoran, J.W.Gardner, *Sensors and Actuators B*, **4** (1991) 29.

[31] H.Nagase, K.Wakabayashi, T.Imanaka, *Sensors and Actuators B*, **13-14** (1993) 596.

[32] A.C.Partridge, P.Harris, M.K.Andrews, *Analyst*, **121** (1996) 1349.

[33] J.M.Slater, E.J.Watt, N.J.Freeman, I.P.May, D.Weir, *Analyst*, **117** (1992) 1265.

[34] P.Topard, M.Josowicz, *J.Phys.Chem.*, **96** (1992) 7824.

[35] R.C.West, M.J.Astle, *CRC handbook of chemistry and physics*, vol.59, CRC Press, Boca Raton, FL, 1978, pp.E63.

[36] F.Musio, M.E.H.Amrani, K.C.Persaud, *Sensors and Actuators B*, **23** (1995) 223.

[37] M.E.H.Amrani, P.A.Payne, K.C.Persaud, *Sensors and Actuators B*, **33** (1996) 137.

[38] M.E.H.Amrani, R.M.Dowdeswell, P.A.Payne, K.C.Persaud, *Sensors and Actuators B*, **47** (1998) 118.

Chapter 7

Cast polysiloxane films: characterisation and vapour response

7.1 Introduction

In this chapter, a study of the electrical properties of polycyanopropylmethylsiloxane (PCMS) (figure 7.1) on varying the temperature and during the exposure to vapours is presented. First (section 7.2), a description of the film deposition conditions is given. This is followed by a study of the PCMS permittivity (section 7.3) and the effect of exposure to vapours (section 7.4). Finally, (in section 7.5), the sensing characteristics of the device are discussed.

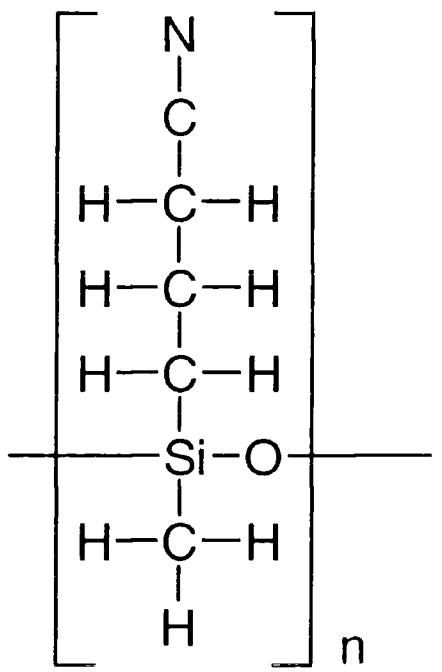

Figure 7.1: The chemical structure of the polycyanopropylmethylsiloxane.

7.2 Film deposition

The PCMS was obtained from Fluorochem (PS906) and used as received. This polymer (figure 7.1) is a modified polysiloxane having the highly polar cyano group (CN) in one of its pendant groups. It is characterised by a low glass-transition temperature due to the high flexibility of the siloxane backbone [1].

For exposure to vapours, the electrode geometry was an interdigitated (ID) structure on top of which the polymer films were deposited. Electrodes were of a gold/platinum blend printed on an alumina substrate (Corintech Ltd.) with geometrical dimensions: separation 250 μm, width 250 μm, height 13 μm and total length 18 cm.

A first attempt to deposit polymer films was undertaken using the spin-coating technique, but the resulting films were not uniform. Moreover, to be able to measure the admittance with a good accuracy quite thick films were required. Therefore, it was preferred to cast the polymer films on the electrodes. Polymer films were deposited by applying 150 μl of a dilute solution (57.3 mg ml^{-1}) of PCMS in dichloromethane in 5 μl drops and waiting about five minutes between consecutive applications to let the solvent evaporate. The thickness, estimated assuming an homogenous distribution of the polymer film on the electrodes, was 80 μm. Thickness measurements by the Alphastep were not successful due to the viscous nature of the film.

Variable temperature measurements were undertaken using a coaxial cell previously calibrated using materials of known permittivity (vacuum, cyclohexane and chloroform). This allowed the determination of the absolute value of the PCMS permittivity. This would otherwise not be possible using ID electrodes because of the dependence of their capacitance upon the films thickness [2].

7.3 Temperature dependence of electrical properties

The admittance measurements were undertaken at the University of Pisa using an HP4194A impedance analyser, based on the same principle of the HP4192A. The permittivity of PCMS was investigated in the range 10^2 - 4×10^7 Hz over the temperature range from 193 K to 298 K. The spectra of the real and imaginary parts of the permittivity at different temperatures are shown in figures 7.2 and 7.3. They reveal the existence of two relaxations: a structural relaxation (or α), whose relaxation time increases more rapidly on decreasing temperature, and a secondary process (β). These are clearly observable in figure 7.4 which shows the estimated contribution of the α and β relaxations separately (dashed and dotted line) together with their sum (full line) and the experimental data (points). As the temperature increases, the α-relaxation shifts toward higher frequencies, where it merges with the β-peak whose position is less dependent on temperature. For high temperatures, a DC conductivity is present, which increases with temperature. The experimental data were conveniently fitted with a superposition of an Havriliak-Negami function (for the α relaxation) and a Cole-Cole function (for the β relaxation) plus a term related to the DC conductivity for high temperatures (>233 K)

$$\varepsilon(\omega) = \varepsilon_\infty + \frac{(\varepsilon_s - \varepsilon_1)}{\left(1+(i\omega\tau_1)^{1-\alpha_1}\right)^{\beta_1}} + \frac{(\varepsilon_1 - \varepsilon_\infty)}{\left(1+(i\omega\tau_2)^{1-\alpha_2}\right)} - i\frac{\sigma_{DC}}{\omega\varepsilon_0} \qquad (7.1)$$

where ε_S is the static permittivity, ε_∞ is the high frequency permittivity, ε_1 is the relaxed permittivity with respect to the α relaxation, σ_{DC} is the DC conductivity, α_1, β_1, τ_1 and α_2, τ_2 are the shape parameters, relaxation times of the α and β relaxations, respectively. At T = 193 K, only the β relaxation is present, and this was analysed using a single Cole-Cole function. The fitting procedure was performed simultaneously for both ε' and ε'' using a computer program [3].

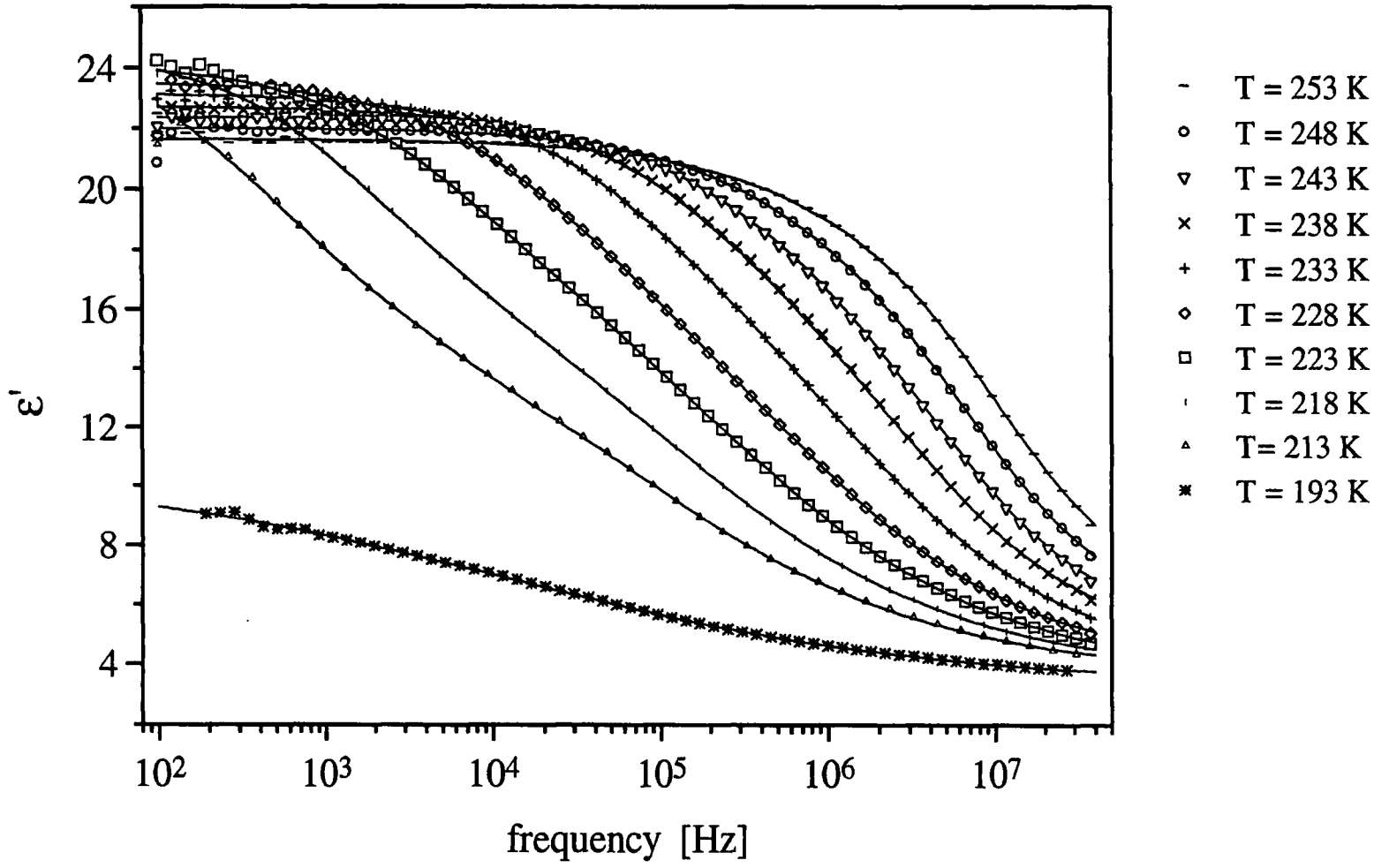

Figure 7.2: Real part of the permittivity versus frequency at different temperatures. Points are experimental (not all displayed). Lines are theoretical fit using equation (7.1), the parameters are reported in table 7.1.

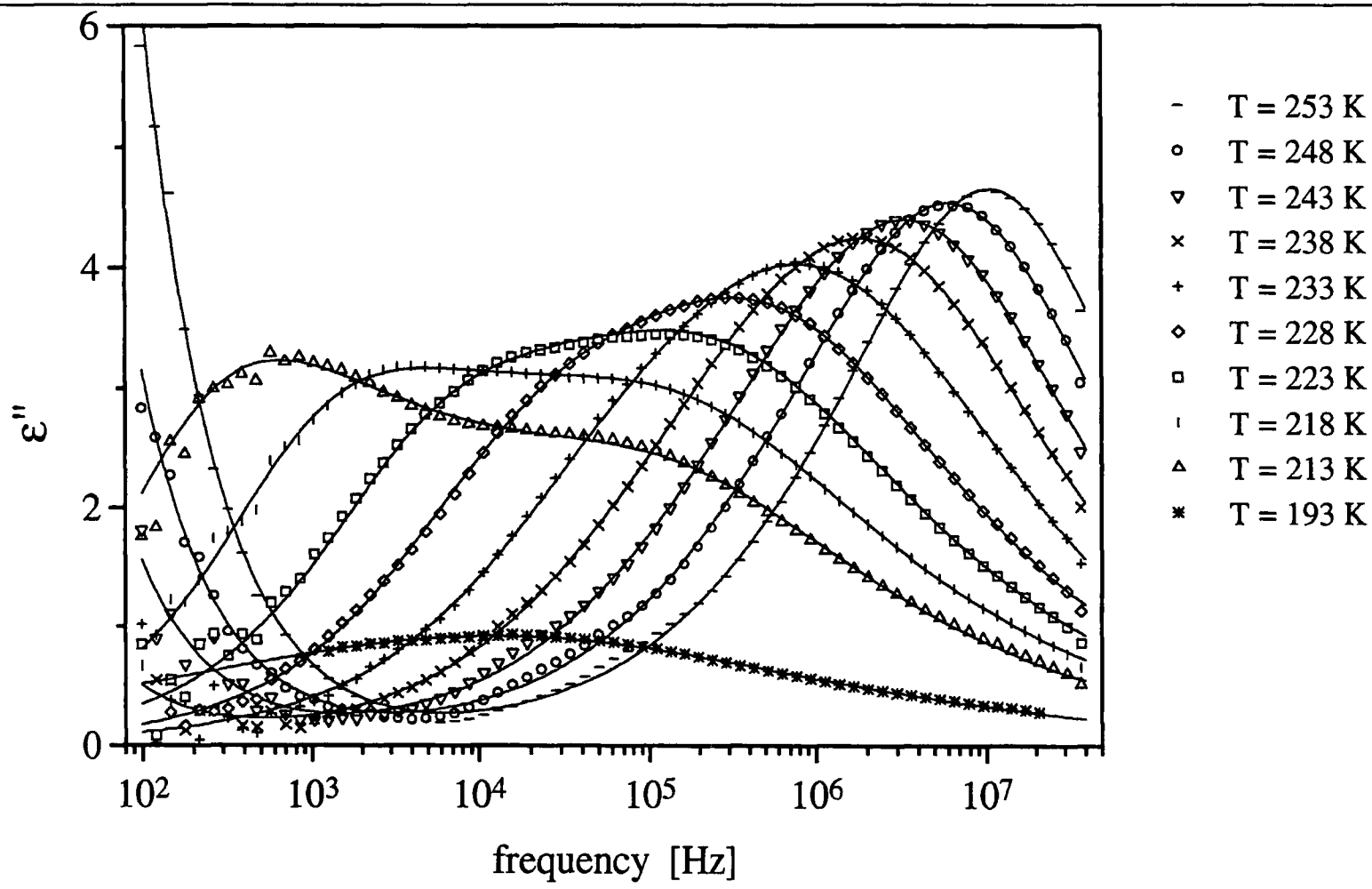

Figure 7.3: Imaginary part of the permittivity versus frequency at different temperatures. Points are experimental (not all displayed). Lines are theoretical fit using equation (7.1), the parameters are reported in table 7.1.

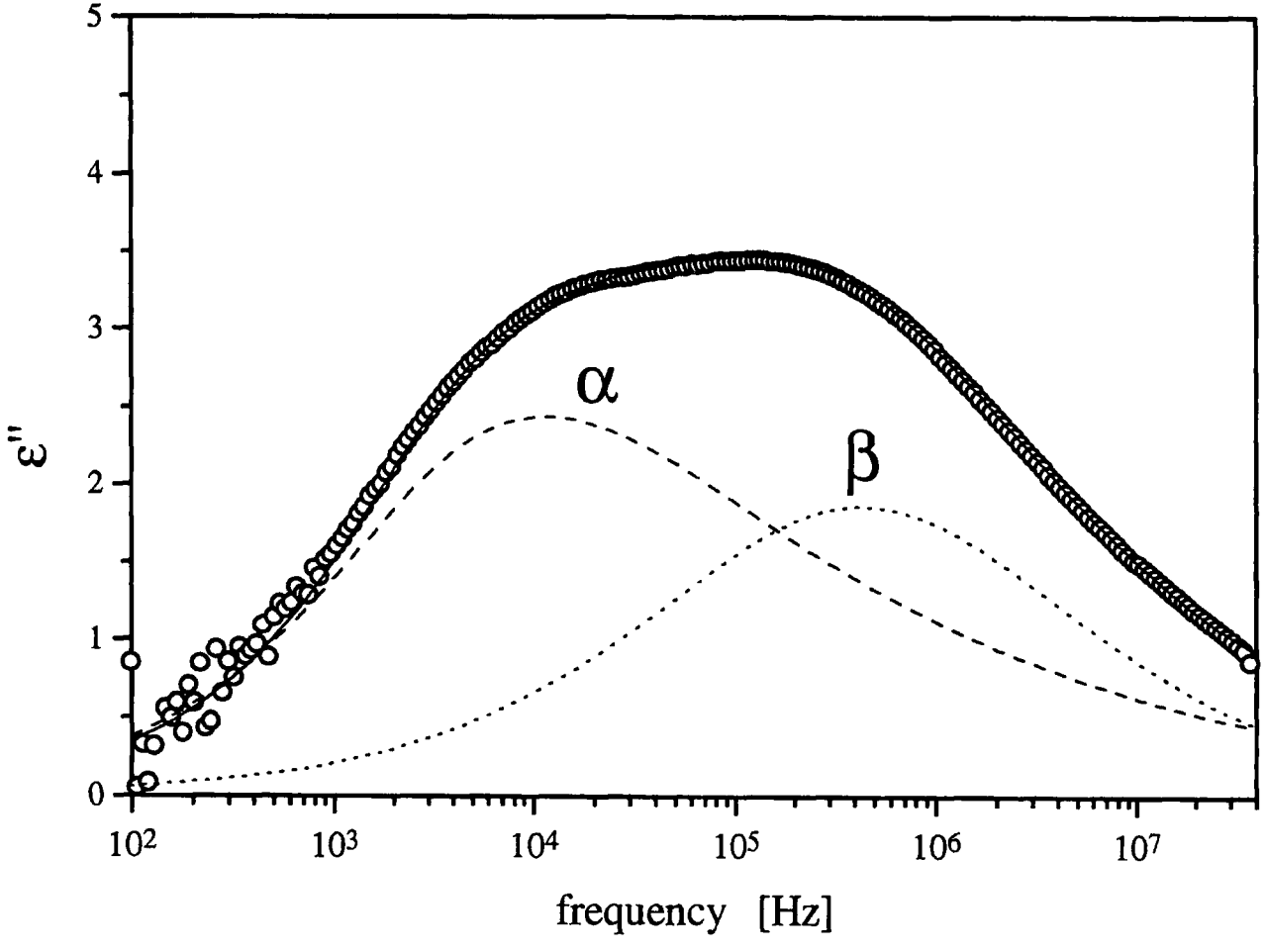

Figure 7.4: Imaginary part of permittivity versus frequency at T = 218 K. Points are experimental. Full line is the theoretical fit using equation (7.1), the parameters are reported in table 7.1. The dotted and dashed lines are the theoretical behaviour of the α and β relaxation, respectively, calculated using the parameters estimated with the theoretical fit.

T [K]	ε_o	ε_1	ε_∞	τ_o [s]	τ_1 [s]	$1-\alpha_1$	β_1	$1-\alpha_2$	σ [S cm^{-1}]
298±0.2	18.3±0.05								$(2.09\pm0.001)\times10^{-8}$
293±0.2	18.6±0.05								$(1.562\pm0.001)\times10^{-8}$
288±0.2	18.9±0.05								$(1.153\pm0.001)\times10^{-8}$
258±0.2	20.9±0.05								$(1.015\pm0.003)\times10^{-9}$
248±0.2	21.66±0.02	15.5±4.6	3.33	$(3.1\pm1.5)\times10^{-7}$	$(14.7\pm0.9)\times10^{-9}$	0.58 ±0.03	0.34±0.1	0.705±0.06	$(3.49\pm0.01)\times10^{-10}$
243±0.2	22.03±0.02	15.55±5.5	3.33	$(4.6\pm2.3)\times10^{-7}$	$(23.6\pm2)\times10^{-9}$	0.615±0.05	0.37±0.2	0.67±0.06	$(1.74\pm0.02)\times10^{-10}$
238±0.2	22.4±0.01	17.5±0.3	3.33	$(8\pm4)\times10^{-7}$	$(42\pm5)\times10^{-9}$	0.7±0.07	0.32±0.1	0.615±0.05	$(8.5\pm0.1)\times10^{-11}$
233±0.2	22.74±0.02	12.69±0.7	3.33	$(14.2\pm6)\times10^{-7}$	$(58.5\pm4)\times10^{-9}$	0.66±0.04	0.415±0.06	0.63±0.05	$(2.5\pm0.2)\times10^{-11}$
228±0.2	23.18±0.02	15.3±1	3.33	$(4.55\pm1.1)\times10^{-6}$	$(13.5\pm1.8)\times10^{-8}$	0.745±0.06	0.46±0.15	0.54±0.01	
223±0.2	23.57±0.04	11.9±1.1	3.33	$(15.5\pm4)\times10^{-6}$	$(21.5\pm2.7)\times10^{-8}$	0.72±0.03	0.34±0.02	0.58±0.02	
218±0.2	24.19±0.03	10.9±0.7	3.33	$(55\pm3)\times10^{-6}$	$(39.5\pm2.5)\times10^{-8}$	0.72±0.01	0.34±0.01	0.555±0.02	
213±0.2	24.61±0.07	10.9±0.4	3.33	$(2.5\pm0.1)\times10^{-4}$	$(70.5\pm5)\times10^{-8}$	0.78±0.01	0.295±0.01	0.535±0.016	
208±0.2	25±0.2	9±0.3	3.33	$(11.5\pm0.5)\times10^{-4}$	$(94\pm5)\times10^{-8}$	0.79±0.02	0.285±0.01	0.53±0.02	
193±0.2		10.45±0.03	3.33±0.02		$(1.32\pm0.02)\times10^{-5}$			0.323±0.002	

Table 7.1: Dielectric parameters estimated by fitting experimental data using equation (7.1) at different temperatures.

The spectra were only analysed in the temperature range 193 K – 253 K because for higher temperatures the maxima of the α and β relaxations tend to be too close to each other and, at the same time, close to the upper limit of our frequency range, introducing a significant error in the theoretical fit. To analyse the data at higher temperatures it would be necessary to measure the permittivity over a wider frequency range, including higher frequencies (i.e. ~GHz). Measurements at higher frequencies would also allow a better estimation of ε_∞. In our measurements it was only possible to evaluate this parameter at low temperatures (i.e. 193 K). In the fitting procedure, at high temperatures, the value of ε_∞ was taken to be constant (assuming ε_∞ was related to the induced polarisation and weakly dependent on the temperature). The values of the parameters obtained by the fitting procedure are listed in table 7.1.

The relaxation times, τ_1 and τ_2 of the α and β relaxation, respectively, are reported in figure 7.5 as a function of 1000/T. The temperature dependence of the average structural relaxation time τ_1 is non-Arrhenius, with an apparent activation energy that increases with decreasing the temperature. This behaviour has been described by the empirical Vogel-Fulcher equation

$$\frac{1}{\tau_1} = \frac{1}{\tau_{01}} \exp\left(-\frac{B}{T - T_0}\right) \tag{7.2}$$

where τ_{01} is the relaxation time in the high temperature limit, B is termed the pseudo activation energy and T_0 corresponds to the temperature for which τ becomes infinite, i.e. the temperature of structural blocking. The values of the parameters obtained by fitting equation (7.2) (full lines in figure 7.5) to the relaxation time τ_1 were

$$\tau_{01} = (1.4 \pm 0.8)\times 10^{-13}\ s^{-1}; \qquad B = (1.5 \pm 0.5)\times 10^{3}\ K; \qquad T_0 = 142 \pm 15\ K$$

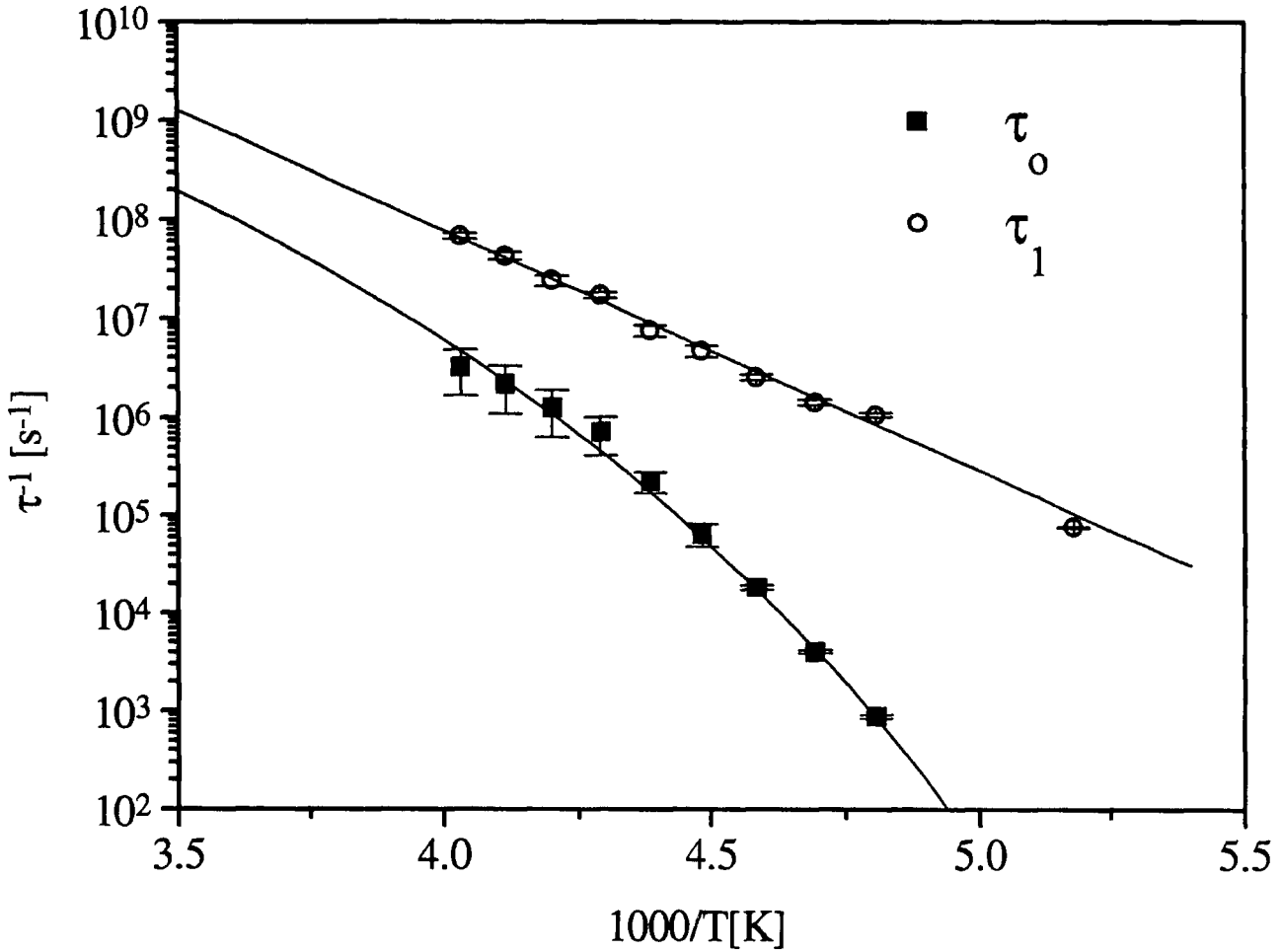

Figure 7.5: The inverse of the relaxation times, τ_1 and τ_2, of the α and β relaxation, respectively, obtained from the best fit of equation (7.1), versus 1000/T. The full lines are the best fit using equation (7.2) and (7.3) for the τ_1 and τ_2, respectively.

The characteristic time of the β relaxation results in good agreement with the Arrhenius law

$$\frac{1}{\tau_2} = \frac{1}{\tau_{02}} \exp\left(-\frac{E_a}{RT}\right) \tag{7.3}$$

where τ_{02} is the relaxation time for $T \rightarrow \infty$, E_a is the activation energy and R is the gas constant. The following values of the parameters were obtained from the fit of τ_2 (full line in figure 7.5) to equation (7.3)

$$\tau_{02} = (8 \pm 5)\times10^{-19}\ s; \qquad E_a = (4.9 \pm 0.1)\times10^{-1}\ eV$$

The temperature dependence of the static dielectric constant ε_S is described by the equation [4, 5]

$$f(\varepsilon_o) = \frac{(\varepsilon_s - \varepsilon_\infty)(2\varepsilon_s + \varepsilon_\infty)}{\varepsilon_s(\varepsilon_\infty + 2)^2} = \frac{N\varepsilon_o}{9k_BT}\mu^2 \tag{7.4}$$

where $f(\varepsilon_o)$ is a function of ε_o defined to indicate the left hand side of equation (7.4) N is the number of molecules per unit volume; μ is the mean dipole moment of each molecule; k_B is the Boltzmann constant. This equation was first derived by Onsager, by considering the long-range dipolar interaction between a polar molecule and its isotropic surroundings (reaction field) in the calculation of the internal field. In this model it is supposed that the particles are spherical and that no specific interactions between these occur [4].

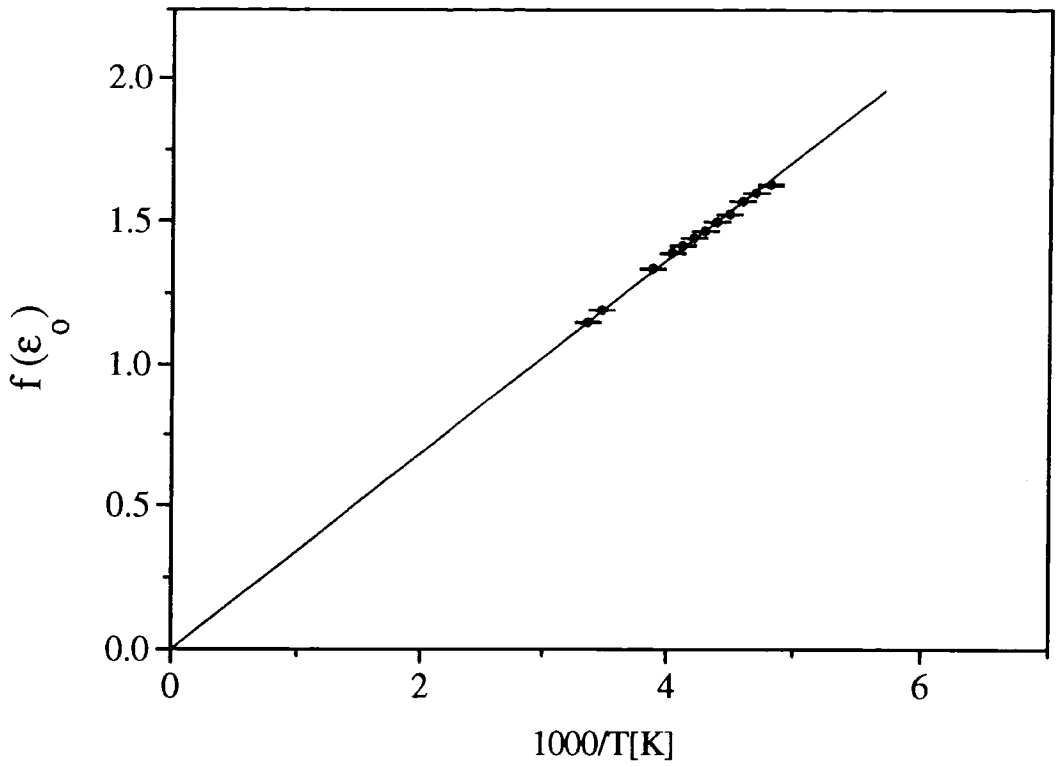

Figure 7.6: Dielectric function $f(\varepsilon_o)$ plotted versus $1000T^{-1}$. Experimental data are points. Full line is a linear fit.

Equation (7.4) predicts that $f(\varepsilon_o)$, depends linearly on the reciprocal of the temperature and approaches zero at very high temperatures. Moreover, the value of ε_∞ should corresponds to the permittivity at a frequency high enough that no orientation polarisation occurs but low enough to include the contributions of the electronic and the atomic polarisation. This value is generally estimated from the refractive index of the material [4]. For the PCMS no refractive index data were found in the literature. Therefore, in the calculation of $f(\varepsilon_o)$ we used the value ε_∞ estimated by the fit to our experimental data. The experimental results are shown in figure 7.6. It is evident that the prediction of a linear behaviour for $f(\varepsilon_o)$ versus T^{-1} is correct and that the linear fit passes through the origin. This line (full line in figure 7.6) gives a slope $(3.426 \pm 0.005)\times10^2\ K^{-1}$.

From the analysis of the shape parameters, α and β, information can be obtained about the low and high frequency tails of the relaxation spectra, characterised by the power law behaviour

$$\varepsilon'' \propto \omega^{m} \qquad \text{for } \omega \ll \omega_0$$

$$\varepsilon'' \propto \omega^{-n} \qquad \text{for } \omega \gg \omega_0$$

where the power law exponent can be estimated as $m_1 = 1 - \alpha_1$, $n_1 = (1 - \alpha_1)\beta_1$, $m_2 = n_2 = 1 - \alpha_2$.

The behaviour of m_1, n_1 and m_2 versus $1000T^{-1}$ are shown in figure 7.7. An increase in m_2 and a decrease in m_1 are noted on increasing the temperature. In contrast, the parameter n_1 does not vary significantly over the temperature range studied and, within experimental error, it is approximately constant. The observed temperature dependence of these parameters means that the time-temperature scaling does not apply to this system over the entire range analysed; i.e. it is not possible to normalise all the spectra in a single curve.

Currently, there is not a universally accepted interpretation of the power law behaviour and of the correlation between the exponent and the molecular properties. However, in a model developed for the interpretation of the dielectric response of polymers, the high frequency part of the relaxation is associated with local-chain dynamics and the low frequency part to a correlation between segments of different molecular chains [6]. The greater dependence of the low frequency exponents (i.e. m_1 and m_2) on the temperature, together with the almost constant value of n_1, indicates that, on varying the temperature, there is mainly a change in the correlation between different chains with almost no changes at the local-chain level. However, for a better understanding of the process it would be necessary to measure the permittivity over a wider frequency range (including the microwave region).

The temperature dependence of the conductivity is shown in figure 7.8. For high temperatures, the conductivity behaviour seems to be thermally activated, with an estimated activation energy $E_a = 0.37 \pm 0.01$ eV. For lower temperatures, approaching the glass transition, a strong decrease of the conductivity is evident. The nature of the observed DC conductivity was attributed to the presence of impurity ions (probably related to the synthesis). The observed temperature behaviour in the proximity of the glass transition was therefore interpreted as a hindering of the ionic diffusion inside the polymer matrix due to the change of the polymer from a viscous to a glassy state.

7.4 Exposure to vapours

In this section, the change of the electrical properties during the exposure to four vapours is discussed. For these measurements, the polymer films were deposited on IDEs (on an alumina substrate) as described in section 7.2.

Admittance measurements were undertaken in the frequency range 10^2 -10^6 Hz. The amplitude of the AC voltage applied to the sample was 1.1 V (RMS).The capacitance of the electrode arrangement, without any film deposited, was 10.5 ±0.1 pF and did not show any variation over the range of frequencies investigated. In this case, the film is isotropic and the equivalent circuit is simpler than for the case of palmitic acid/polypyrrole multilayers. However, it is necessary to take into account the contribution from the substrate (figure 7.9). It has been shown that the capacitance of an ID structure (C_G) coated with a homogeneous film is not a simple function of the film thickness [7, 8]. The electric field distribution, and consequently C_G, depends on the polymer permittivity. Therefore, the permittivity cannot be found directly from the measured admittance, even if the geometrical dimensions of the ID structure and the film thicknesses are accurately known.

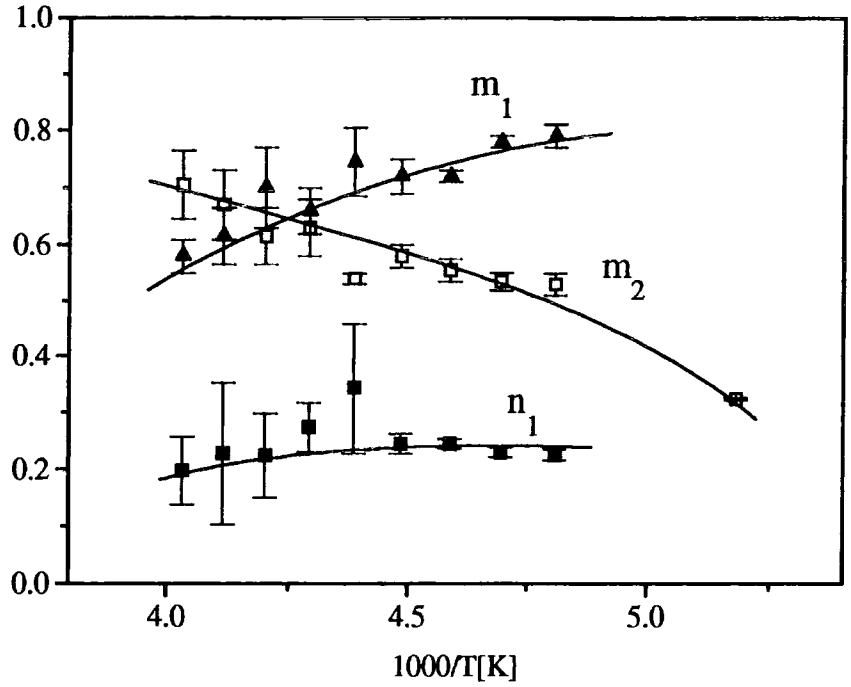

Figure 7.7: Power law exponents of the α-relaxation m_1 and n_1 and of the β-relaxation m_2 versus $1000T^{-1}$. Solid lines are guides for the eye.

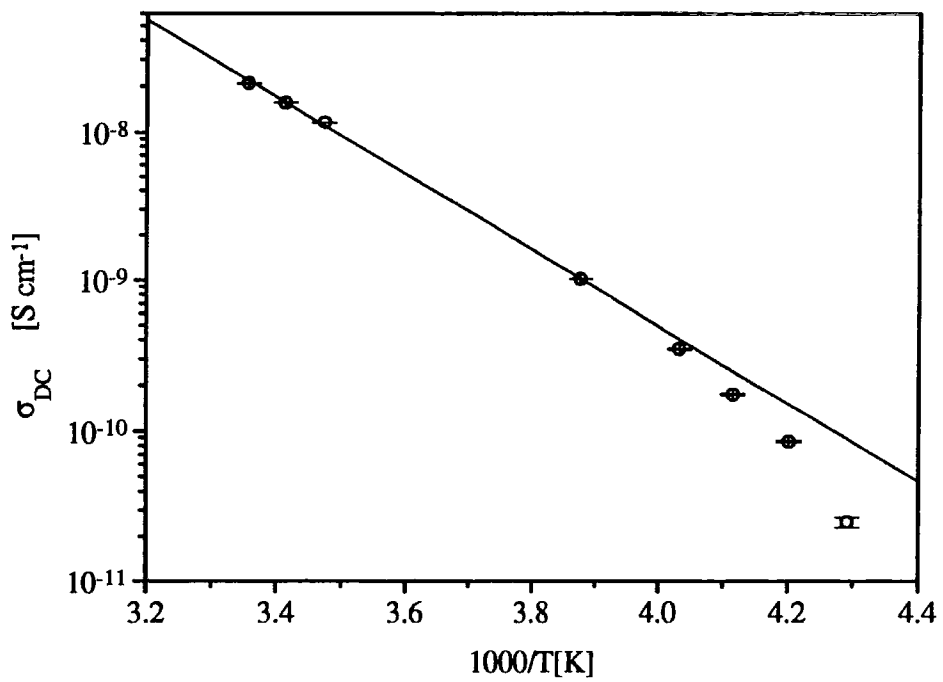

Figure 7.8: DC conductivity versus $1000T^{-1}$. Full line is a linear fit of the high temperature data (first four points).

As discussed in the previous section, the absolute value of the PCMS permittivity was measured using a coaxial cell and it was possible to estimate the value of C_G and check the validity of our equivalent circuit by comparing the two sets of data (from the coaxial cell and those obtained with the IDE at room temperature).

Assuming the equivalent circuit shown in figure 7.9, the admittance of an IDE without and with a homogeneous film deposited on it are, respectively

$$Y_o = Y_{SUB} + i\omega(C_{geom//} + C_{geom\perp}) \tag{7.5}$$

$$Y_1 = Y_{SUB} + i\omega C_G \varepsilon_{PCMS} = Y_{SUB} + i\omega C_G(\varepsilon'_{PCMS} - i\varepsilon''_{PCMS}) \tag{7.6}$$

where Y_{SUB} is the admittance of the substrate, $C_{geom//}$ and $C_{geom\perp}$ are the capacitance in the in plane and out of plane direction of an IDE as discussed in paragraph 6.5, C_G is the capacitance of the IDE with a film on it and ε_{PCMS} is the permittivity of the PCMS.

The capacitance $C_{geom//}$ and $C_{geom\perp}$ can be estimated using equations (6.15) and (6.16) as

$$C_{geom//} = (8.3 \pm 0.1)\times 10^{-2}\ \text{pF} \quad \text{and} \quad C_{geom\perp} = 1.11 \pm 0.01\ \text{pF}$$

Consequently, it was possible to estimate the contribution of the substrate by substituting these values in equation (7.5). Considering that

$$Y_{SUB} = G_{SUB} + i\omega C_{SUB} = C_{geom\perp}(\sigma_{SUB} + i\omega\varepsilon_{SUB}) \tag{7.7}$$

it was possible to estimate $\varepsilon_{SUB} = 7.7 \pm 0.2$, in good agreement with values found in the literature for alumina ($\varepsilon'(10^6\ \text{Hz}) = 4.5\text{-}8.4$) [9]. The conductance without any film was out of our experimental range, therefore it was not possible to estimate σ_{SUB}.

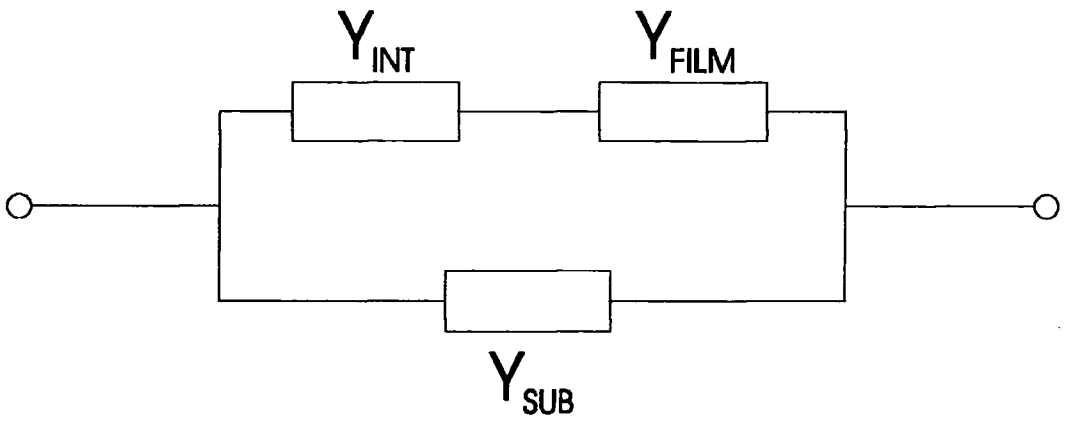

Figure 7.9: Equivalent circuit for an IDE covered with a cast PCMS film. Y_{SUB} is the substrate, Y_{INT} is the electrode/film interface admittance and Y_{FILM} is the film admittance.

By estimating Y_{SUB} and substituting into equation (7.6), it was possible to calculate the geometrical capacitance ($C_G = 0.42 \pm 0.01$ pF, independent of frequency) for the IDE covered with the PCMS film.

Figure 7.10 shows the real and imaginary parts of the permittivity measured using the coaxial cell and the ID electrodes at room temperature. At high frequencies, ε' is almost frequency independent, with a value of 18.2. Below 10^3 Hz a power law of the form $\varepsilon' \propto \omega^{-2}$ is noted that was not evident at lower temperature (figure 7.2). In contrast, ε'' varies below 10^5 Hz as $\varepsilon'' \propto \omega^{-1}$, while at higher frequencies the relationship becomes $\varepsilon'' \propto \omega^p$, with $p < 1$.

The above results may be explained by a superposition of the dielectric response of the polymer film and an interface effect. The former has been discussed in the previous section. At room temperature, the characteristic frequency of the α and β relaxations are

beyond the maximum frequency measured and therefore we observed only a low frequency tail (providing the ω^p dependence) plus the DC conductivity (providing the ω^{-1} dependence of ε'' for low frequencies).

The power law dependence of ε' below 10^3 Hz was attributed to an interface effect. It is unreasonable to assign this phenomenon to the organic film because the dielectric relaxation of polymers for frequencies above and below ω_b is invariably characterised by two power laws with exponents smaller or equal to unity [10], as found in the previous study of the PCMS permittivity at lower temperatures.

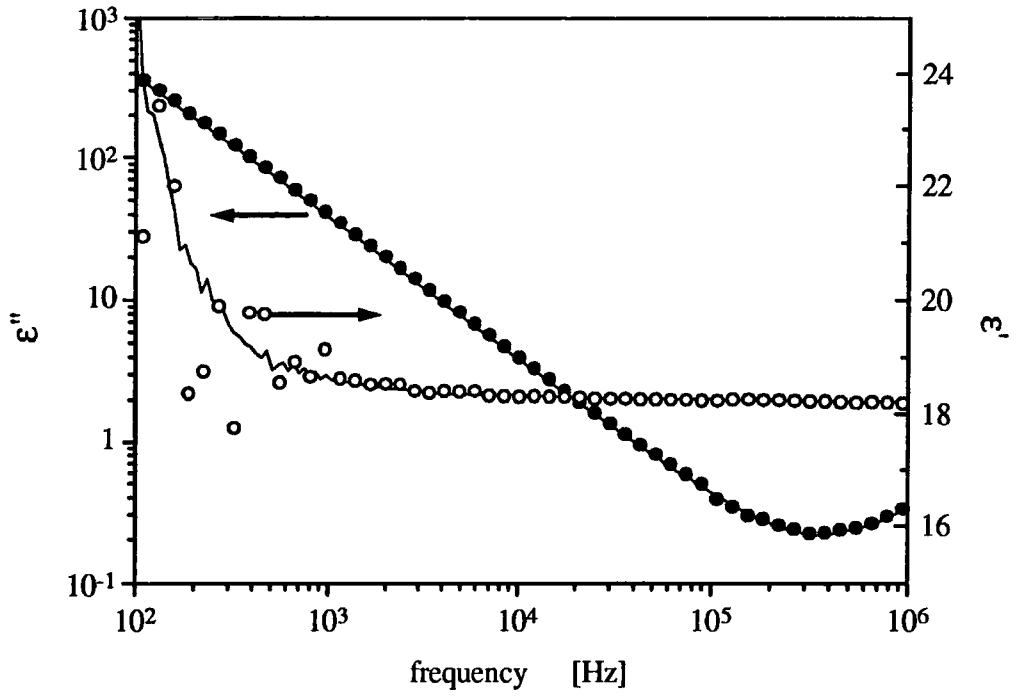

Figure 7.10: Comparison of the real and imaginary parts of the permittivity measured at room temperature for PCMS with ID electrodes (open and solid circles) and with a coaxial cell (solid lines).

The interfacial effect can be modelled by a Maxwell-Wagner dispersion [11]

$$\varepsilon_{MW} = \varepsilon_2 + \frac{(\varepsilon_1 - \varepsilon_2)}{1 + i\omega\tau_{MW}} \tag{7.8}$$

where ε_1 and ε_2 and τ_{MW} are parameters related to the permittivity, conductivity and thickness of the two-layer structure, as discussed in paragraph 2.4. Using this model, we expect that an increase (decrease) in the polymer conductivity will cause a decrease (increase) of the characteristic time τ_{MW} (equation (2.63)) and a consequent shift in the relaxation to higher (lower) frequency.

7.4.1 Exposure to organic solvents vapours

During exposure to the vapours, C_G could not be assumed to remain constant because of the possibility of the film swelling, as observed by other workers [12]. Therefore, the permittivity data in the following section are reported in the form of capacitance (C) and conductance divided by the angular frequency (G/ω). These are proportional to the real and imaginary part of the polymer permittivity, respectively.

Figure 7.11 shows the transient response of C and G/ω, measured at 1 kHz, for a PCMS film exposed to 4.0% ethanol. Both C and G/ω increase on exposure to the organic vapour with a response time of about 10 minutes and a recovery time of about 2 minutes (estimated from the time taken to pass from 10% to 90% of the maximum value and vice-versa when the vapour was turned on and off, respectively). It is evident that the changes induced by the vapour are fully reversible after about 20 minutes. Figure 7.12 shows the effect of exposing the film for four consecutive periods of one minute to 4.0% ethanol separated by 10 minutes of recovery. Reasonable reproducibility is evident.

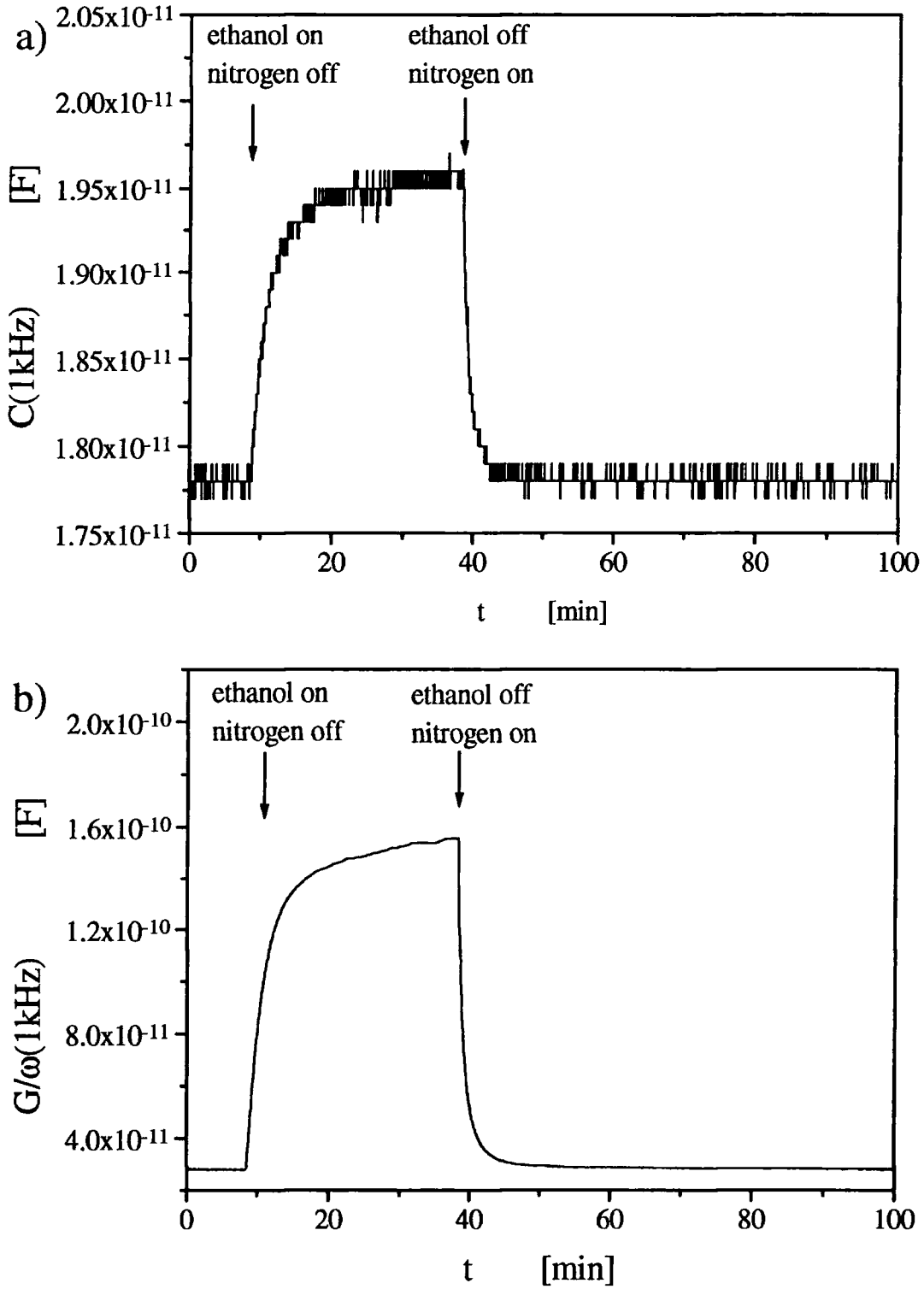

Figure 7.11: Transient behaviour of the capacitance (a) and of the conductance divided by the angular frequency (b) measured at 1 kHz for a PCMS film exposed to a concentration of 4.0% ethanol.

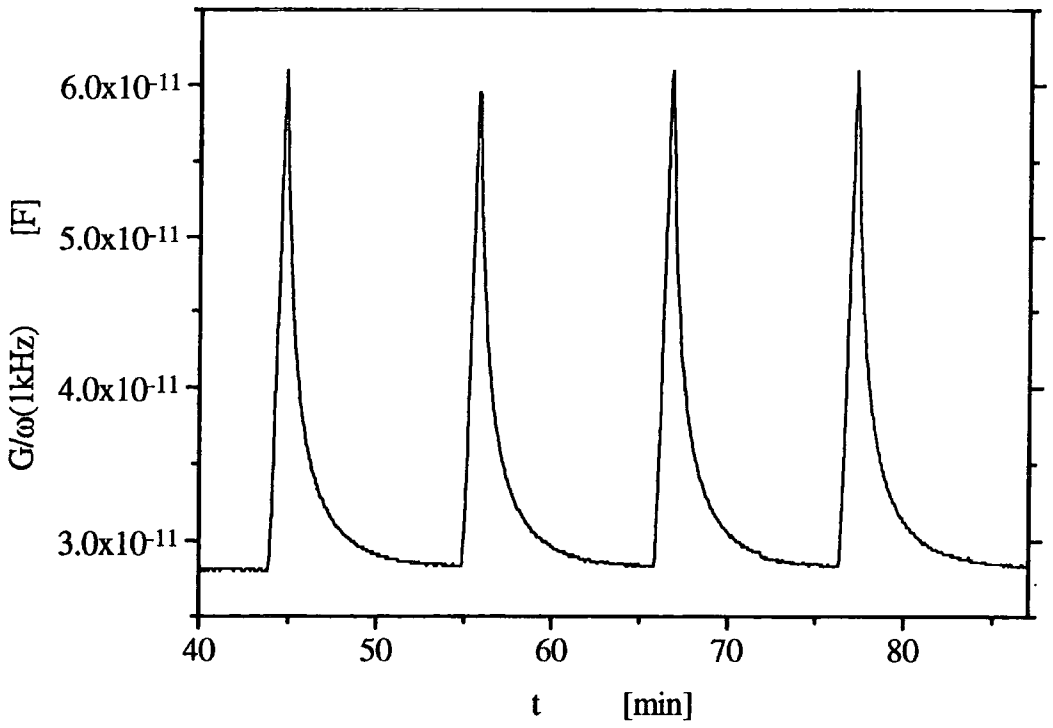

Figure 7.12: Transient behaviour of the conductance divided by the angular frequency measured at 1 kHz for a PCMS film exposed to a concentration of 4.0% ethanol in four consecutive periods of 1 minute, each separated by 10 minutes of recovery.

The frequency dependence of C and G/ω on exposure to benzene and acetonitrile showed similar behaviour to that obtained with ethanol (data not shown).

Figures 7.13a and 7.13b show C and G/ω for a polysiloxane film exposed to three different concentrations of ethanol (2.9%, 4.0% and 5.2%). An increase of G/ω is observed, with no change in the frequency dependence. In contrast, the capacitance shows a large change at lower frequencies. Above 10^4 Hz, C remains almost independent of frequency, but with an increased value with respect to that measured in N_2

Figures 7.14a and 7.14b show the normalised changes in C and G (equal to that of G/ω) on exposure to ethanol. Below 10^3 Hz, the conductance change is frequency independent

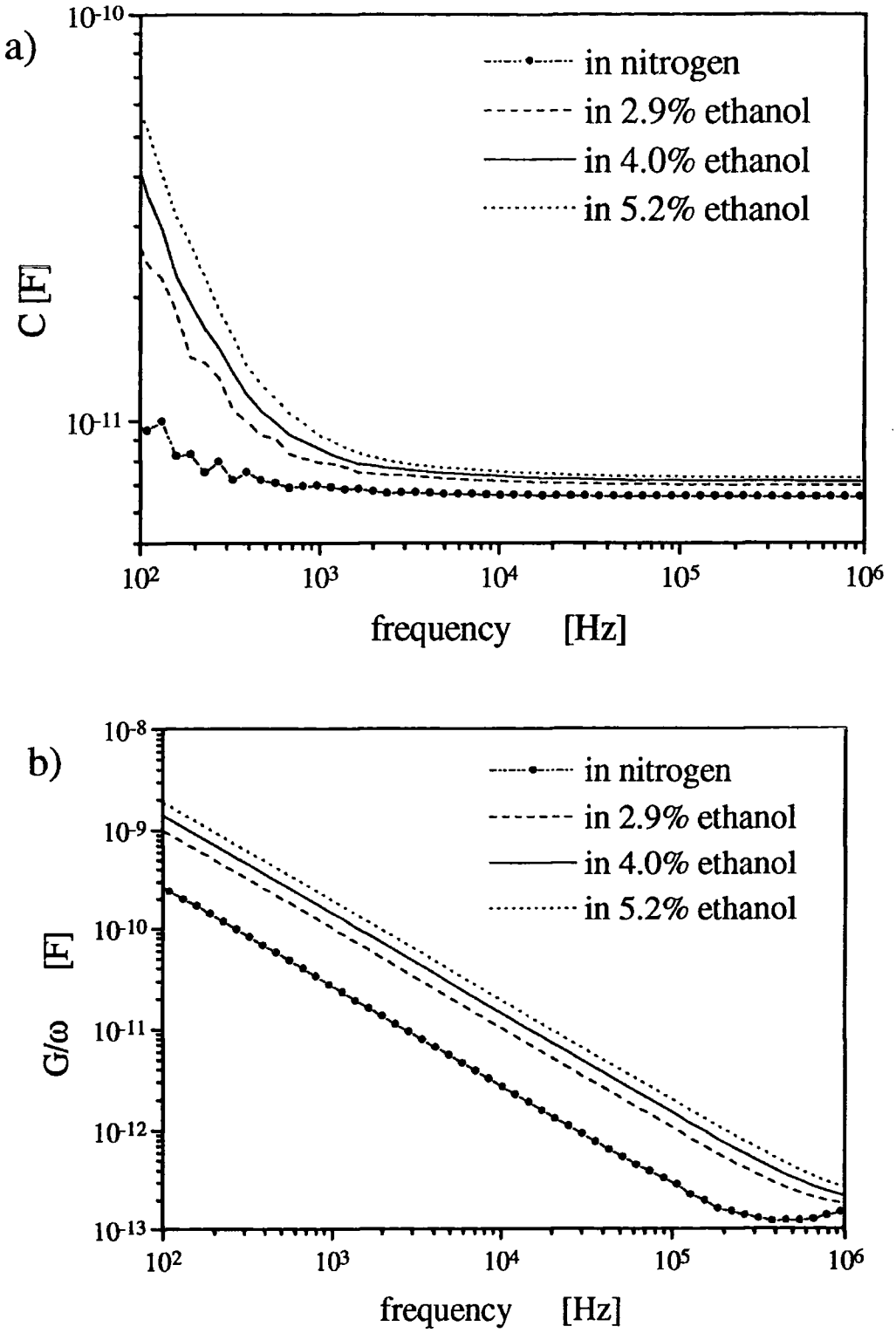

Figure 7.13: Capacitance (a) and conductance over the angular frequency (b) measured at different frequencies for a PCMS film exposed to different concentrations of ethanol vapour and in nitrogen.

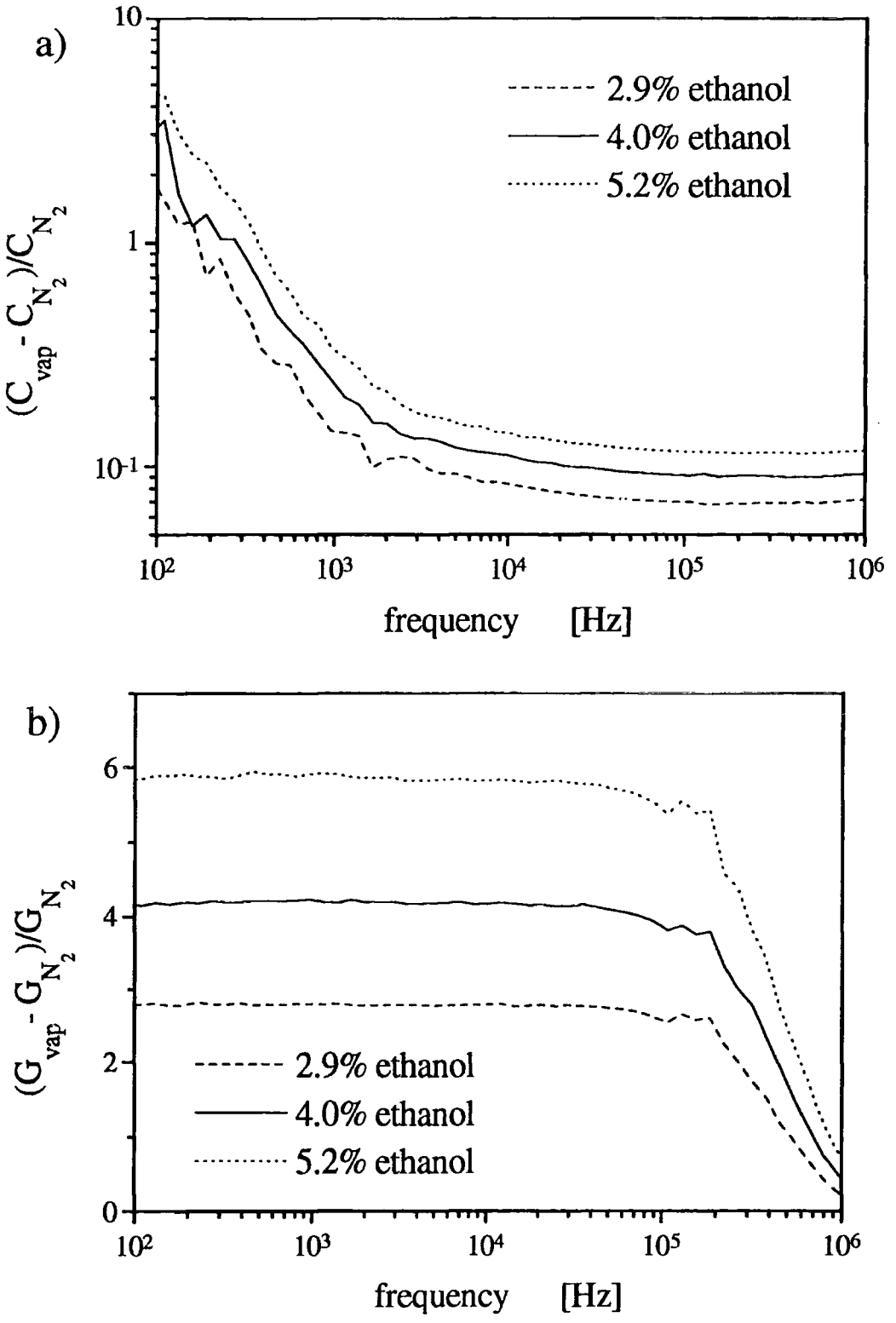

Figure 7.14: Change divided by the initial value in nitrogen of the capacitance (a) and of the conductance (equal to that of G/ω) (b) at different frequencies for a PCMS film exposed to different concentrations of ethanol vapour.

while for high frequency it tends to zero. The lower frequency region corresponds to the case where the contribution of the DC conductivity is much larger than that of the dielectric relaxation. At high frequency, the conductance is dominated by the dielectric relaxation, which appears to be less sensitive to the vapour, and the change tends to zero. The capacitance changes are much greater at lower frequencies (figure 7.14a) and tend to a constant value above 10^4 Hz. Again, lower frequency behaviour can be attributed to an increase in the DC conductivity. This causes a decrease in τ_{MW} (equation (7.8)) with a consequent shift of ε_{MW} to higher frequencies. Above 10^4 Hz, the small changes of the capacitance are related to changes in the polymer permittivity. For the other two vapours similar changes were observed, the only difference was a negative change of the capacitance at high frequency during the exposure to benzene. This will be discussed in paragraph 7.4.3.

In summary, we suggest that the changes in both C and G/ω are dominated by the DC conductivity at low frequencies and related to the dielectric properties of the polymer above about 10^4 Hz.

For a comparison of the sensitivity to different vapours, we calculated the percentage changes in C and G/ω, normalised to the vapour concentration, i.e.

$$\langle \Delta M \rangle = \frac{1}{n} \frac{1}{M_o} \sum_{i=1}^{n} \frac{\Delta M_i}{c_i(\%)} \qquad (7.9)$$

where M is either C or G/ω, n is the number of concentrations used, M_o is the initial value in nitrogen and ΔM_i is the change with respect to the initial value (expressed as a percentage) measured for a concentration $c_i(\%)$. Three concentrations, in the range 1.5% - 7%, were generated for each vapour (including water).

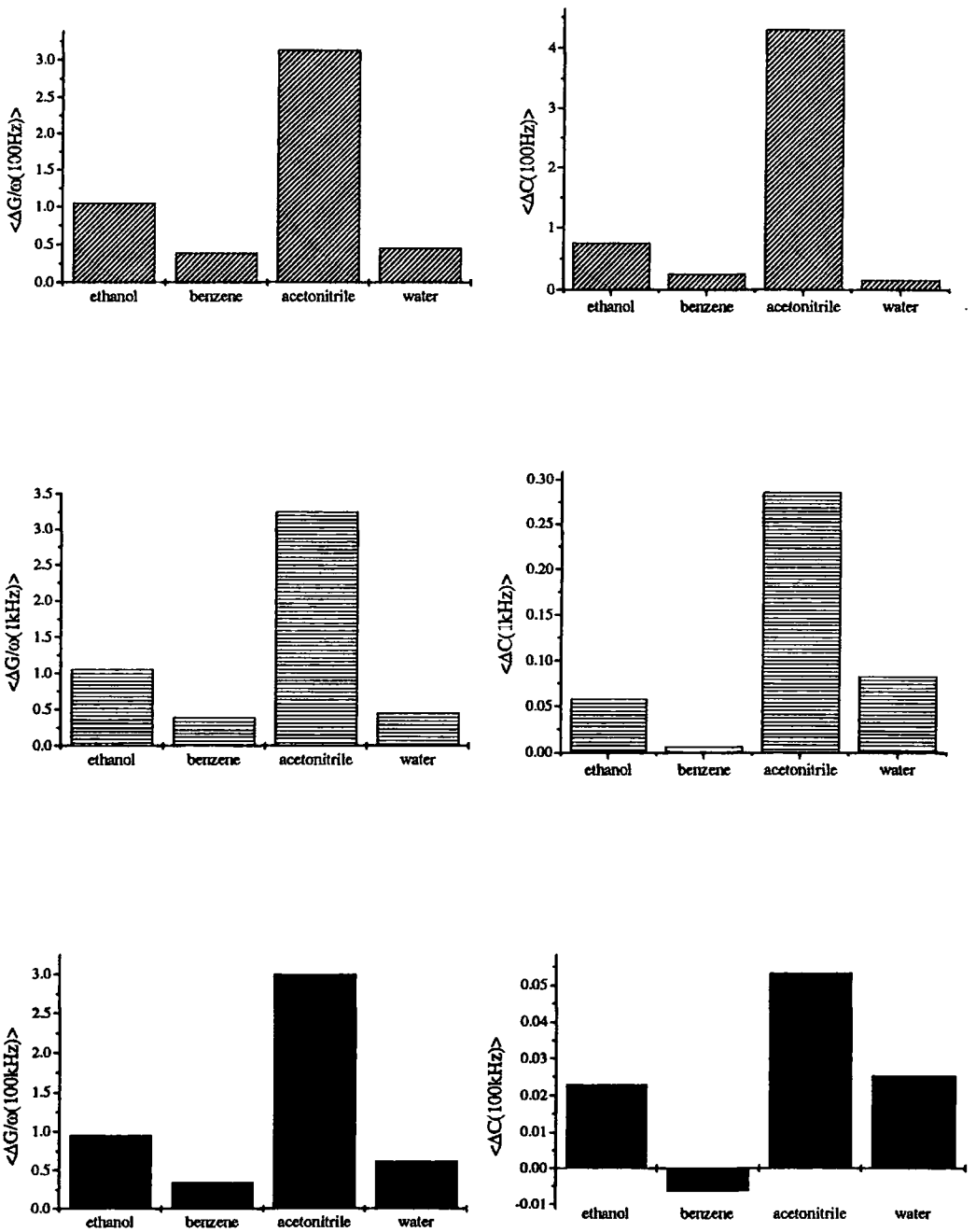

Figure 7.15: Average changes, calculated according to equation (7.9), of the capacitance (on right side) and of the conductance divided by the angular frequency (on the left side), measured at three different frequencies (10^2 Hz, 10^3 Hz, 10^5 Hz) for a PCMS film exposed to four different vapours (ethanol, benzene, acetonitrile and water).

The results at three different frequencies (10^2 Hz, 10^3 Hz and 10^5 Hz) are shown in figure 7.15. For the lowest measurement frequency, there is a good correlation between the changes in C and G/ω. However, at 10^5 Hz the two histograms are quite different.

7.4.2 Exposure to water vapour

During exposure to water no evident differences were observed for the transient behaviour (data not shown), but a different frequency behaviour for the normalised changes was noted. In figures 7.16a and 7.16b, the normalised changes of the capacitance and conductance (equal to that of the conductance over the angular frequency), respectively are shown. It is evident that the conductance change shows a peak around 10^4 Hz which increases with increasing water concentration. The capacitance change shows a smaller increase respect to that observed for ethanol (figure 7.14a) at low frequencies, but comparable with that of ethanol for higher frequencies.

Water seems to have a smaller effect on the change of the DC conductivity with a consequent smaller change of capacitance and conductance at low frequencies but a greater effect on the change of the permittivity of the film. This high frequency effect observed during exposure to water vapour may be explained by the presence of a dielectric relaxation due to the water molecules. The value of the characteristic time of the water relaxation is lower than expected (i.e. not in the microwave range) and may be related to an interaction between the water molecule and the polysiloxane (especially the CN group) with a consequent slowing down of the molecule's orientational motion. This could also be present for the other solvents (i.e. ethanol and acetonitrile) but because of the larger change of the DC conductivity it was not so clearly observable. The effect cannot be attributed to the instrument because it was not observed for low concentrations of benzene (1.5%) for which the change at low frequency is close to that

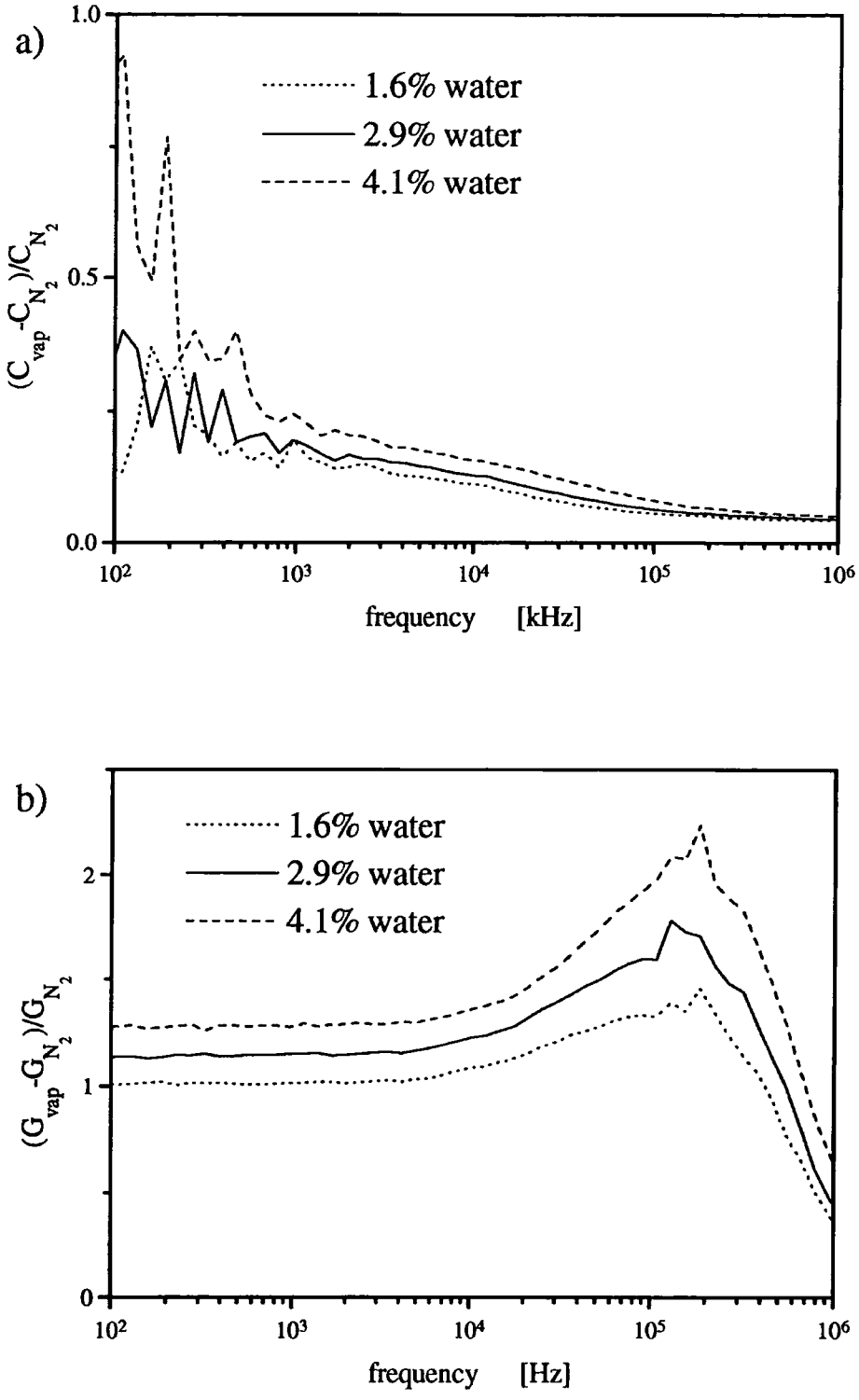

Figure 7.16: Change divided by the initial value in nitrogen of the capacitance (a) and of the conductance (equal to that of G/ω) (b) at different frequencies for a PCMS film exposed to different concentrations of water vapour.

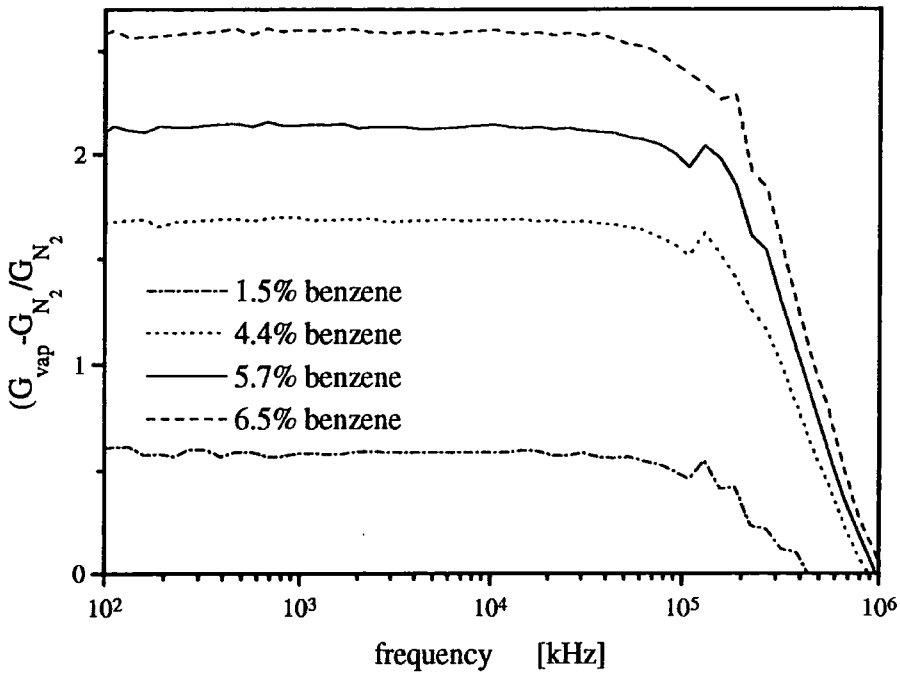

Figure 7.17: Change divided by the initial value in nitrogen of the conductance at different frequencies for a PCMS film exposed to different concentrations of benzene vapour.

of water for low frequency, but no peak was observed around 10^4 Hz as shown in figure 7.17.

7.4.3 Interpretation of the changes observed during exposure to vapours

Other workers have shown that the solubility of different solvents in a PCMS film is correlated with solvents' polarity [8, 13-15]. In particular, the higher the polarity of the molecule, the more vapour will dissolve in a polar polymer such as PCMS. The partition coefficient $f_{p/g}$ for different vapours in PCMS has been measured by a microbalance experiment [13-15]. This parameter is defined [16]

$$f_{p/g} = \frac{c_p}{c_g} \tag{7.10}$$

where c_p and c_g are the concentrations of solvent molecules in the polymer and gas phase, respectively. The solvents used in our experiment were: benzene (non polar), ethanol (μ = 1.69 Debye[17]) and acetonitrile (μ = 3.92 Debye[17]).

An accurate description of the change of the polymer permittivity induced by vapour molecules is a difficult task. The final state will be an heterogeneous system with the vapour molecules distributed inside the polymer film. The effect on the static permittivity should follow a relationship similar to that derived by Maxwell [18, 19] for low volume fractions of spheres of permittivity ε_2 (in our case the vapour molecules) dispersed uniformly (volume fraction v_2 less than 0.1) in a dielectric of permittivity ε_1 (the polymer film)

$$\varepsilon_m = \varepsilon_1 \frac{\left[1 - 2v_2 \frac{(\varepsilon_1 - \varepsilon_2)}{(2\varepsilon_1 + \varepsilon_2)}\right]}{\left[1 + v_2 \frac{(\varepsilon_1 - \varepsilon_2)}{(2\varepsilon_1 + \varepsilon_2)}\right]} \equiv \varepsilon_1 + \frac{3\varepsilon_1(\varepsilon_2 - \varepsilon_1)}{2\varepsilon_1 + \varepsilon_2} v_2 \tag{7.11}$$

where ε_m is the permittivity of the final system. The approximation is valid if the term $(\varepsilon_1 - \varepsilon_2)v_2/(2\varepsilon_1 + \varepsilon_2)$ is small compared to unity and provides a linear dependence of the change of permittivity $(\varepsilon_m - \varepsilon_1)$ on the volume fraction occupied by the dispersed medium.

Assuming that the partition coefficient for PCMS is independent of the vapour concentration, then a linear dependence of the change of capacitance with the vapour concentration is expected [13]. Furthermore, equation (7.11) predicts that if the permittivity of the vapour is smaller than that of the polymer, a negative change of the

capacitance should be observed. In our work, this will be the case for benzene, which explains the decrease of the capacitance at high frequency (figure 7.15). The observed increase of the capacitance at low frequencies during the exposure to benzene is in agreement with the interfacial model described in the previous section and unrelated to the polymer permittivity.

To compare the experimental data with the behaviour expected from equation (7.11), the normalised change in capacitance at 10^5 Hz, as a function of the vapour concentration, for the three organic vapours and the water is shown in figure 7.18. For the range of concentrations studied, the behaviour is approximately linear and in the case of ethanol and benzene, this linear behaviour can be extrapolated to the origin. However, this is not the situation for acetonitrile and water. For the former this may be related to the high polarity of the acetonitrile, resulting in a dependence of the partition coefficient on the vapour concentration [13-15]. In the case of the water, this may be due to the anomalous

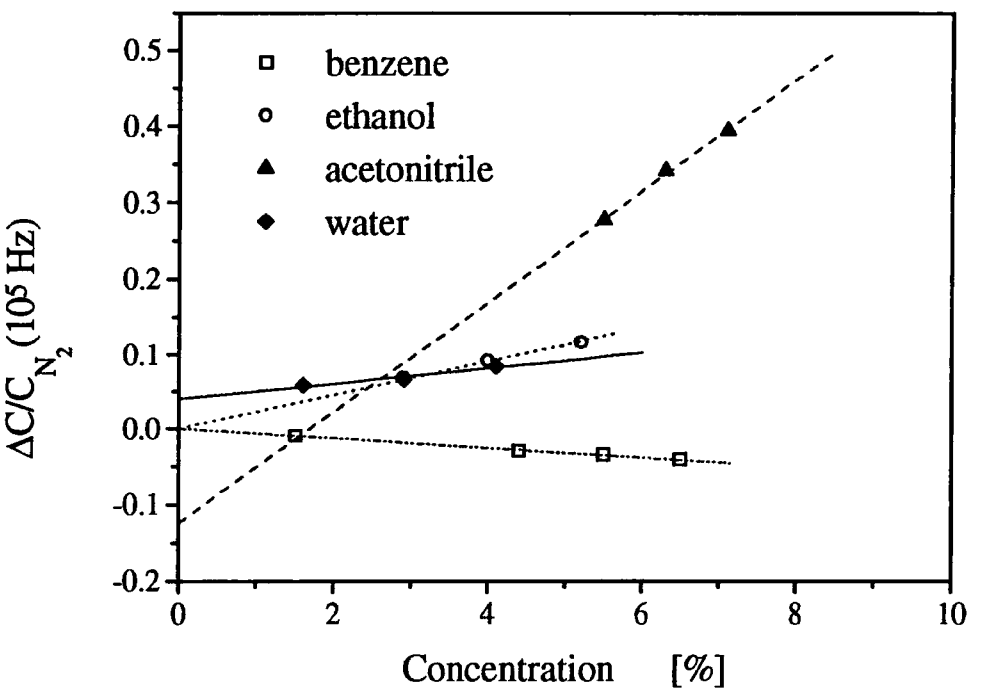

Figure 7.18: Capacitance change divided by the initial value in nitrogen measured at 10^5 Hz for a PCMS film exposed to different concentration of benzene, ethanol, acetonitrile and water. Lines are best linear fits. The error bars were smaller than the size of the data points.

behaviour observed in the capacitance change versus the frequency.

Knowing the partition coefficient of a solvent in a polymer, it is possible to estimate the volume fraction occupied by the solvent molecules. Equation (7.10) can be rewritten

$$\frac{n_{eth}^{(p)}}{V_p} = f_{p/g} \frac{n_{eth}^{(g)}}{V_g} \tag{7.12}$$

where $n_{eth}^{(p)}$ and $n_{eth}^{(g)}$ are the number of moles of ethanol in the polymer and in the gas phase respectively, V_p is the volume of the polymer film and V_g the cell volume. The volume fraction v_2 can be found if the volume of an ethanol molecule is known

$$v_2 = \frac{V_{eth}^{(p)}}{V_p} = \frac{n_{eth}^{(p)}}{V_p} N_A V_{molec} \tag{7.13}$$

where $V_{eth}^{(p)}$ is the total volume occupied by the ethanol inside the polymer, N_A is the Avogadro number and V_{molec} is the volume occupied by an ethanol molecule. Expressing $n_{eth}^{(g)}$ as a function of the vapour concentration in equation (7.12) and substituting into equation (7.13), is possible to write v_2 as

$$v_2 = \frac{V_{eth}^{(p)}}{V_p} = f_{p/g} \frac{n_{eth}^{(g)}}{V_g} n_A V_{molec} = f_{p/g} \frac{cP}{RT} n_A V_{molec} \tag{7.14}$$

where P is the pressure, T is temperature and R is the gas constant. The partition coefficient for ethanol in PCMS $f_{p/g} = 579$ [13]. The volume occupied by an ethanol molecule can be estimated from the density in the liquid phase (under standard conditions) and its molecular weight F_w

$$V_{molec} = \frac{F_w}{d\, n_A} \cong 10^{-1}\ nm^3 \qquad (7.15)$$

Substituting the known values into equation (7.14), the volume fraction occupied by the ethanol inside the polymer was found to be 1.5×10^{-2} c (where the concentration is expressed as a percentage). Using this value for v_2 in equation (7.11), it was finally possible to compare our experimental data with theory

$$\frac{\Delta C}{C_o} = \frac{\varepsilon_m - \varepsilon_1}{\varepsilon_1} = \frac{3(\varepsilon_2 - \varepsilon_1)}{2\varepsilon_1 + \varepsilon_2} v_2 \qquad (7.16)$$

where ΔC is the change of capacitance and C_o is the capacitance in nitrogen. Using $\varepsilon_1 = 18.2$, $\varepsilon_2 = 23.6$ [20] and $v_2 = 1.5\times10^{-2}$ c, $\frac{\Delta C}{C_o} = 4\times10^{-3}$ c. This contrasts with the linear relationship derived from figure 7.18 (dotted line), $\frac{\Delta C}{C_o} = 2.2\times10^{-2}$ c.

The simple theoretical model provides an order of magnitude estimate of the capacitance changes induced by a solvent in a polymer film. The discrepancy between the theory and experiment may be explained by two effects neglected in our calculations. First, the film thickness was assumed constant, ignoring any increase of capacitance due to swelling. Also, no account was taken of any increase in the polymer permittivity due to changes in the orientational ability of the polymer dipoles.

7.5 Evaluation of the device for gas sensing applications

In the former section, the reversible changes in the admittance of devices comprising IDEs coated with PCMS cast films have been discussed. The changes can be explained in terms of a bulk dissolution of the vapours inside the polymer film. To estimate if these

devices could be useful in practical gas-sensing applications, the sensitivity and selectivity are now discussed in more detail.

The average sensitivity (capacitance/concentration or conductance/concentration) for the four different vapours calculated at four different frequencies (100 Hz, 1 kHz, 100 kHz and 1 MHz) are reported in tables 7.2 and 7.3, respectively. From table 7.2, it can be seen that: (i) the sensitivity of the capacitance measurements increases on decreasing the frequency, at 100 Hz being about one order of magnitude greater that at 1 MHz; (ii) the sensitivity is higher for more polar solvents; and (iii) the sensitivity to water vapour is smaller than for polar solvents at low frequencies but the same order of magnitude at higher frequencies. In the case of the sensitivity of the conductance (table 7.3): (i) this is higher for more polar solvent; (ii) it first increases for low frequency and then decreases at high frequency (1MHz) for the solvents; (iii) the conductance increases with frequency for water; and (iv) the sensitivity to water vapour is higher than that to benzene vapour but lower than for the other two solvents at low frequencies.

For each vapour, a minimum detectable concentration was estimated. This corresponded to the concentration for which the observed change would be equal to the instrument resolution (in our case, 0.1 pF and 1 nS). The estimated values are reported in tables 7.2 and 7.3 for the capacitance and conductance, respectively. It is evident that very low concentrations (~ppm) could be detectable using conductance measurements, much lower than using capacitance measurements. However, it is important to note that our experiment was not designed to achieve the maximum possible sensitivity but to study the sensor response over a wide frequency range. A much higher sensitivity could be obtained with a different design and measuring the capacitance at a single frequency [21].

A discussion of the sensor selectivity can be based on average sensitivities calculated using equation (7.9) and reported in figure 7.15. It is evident that, for the lowest frequency, there is a good correlation between the changes in C and G/ω. However, at 100 kHz the two histograms are quite different, suggesting that the conductance and capacitance data over a wide frequency range could provide a useful basis for a selective

sensing system. In particular, the different behaviour observed during the exposure to water could be exploited to discriminate against this vapour. This is particularly important considering that water vapour is present in most of practical sensing situations.

Another important characteristic of a sensor is its long term stability. At this moment no experiments have been carried out over long periods (i.e. months or years). However, the same type of material has been used by other workers and no reference to stability problem have been reported [2, 8, 12-15, 21]. Moreover, a good stability is expected as the interaction mechanism is not based on a 'chemical' reaction between the vapour and the polymer but on a bulk dissolution of the vapour inside the polymer film.

7.6 Summary

The permittivity of PCMS has been measured over the temperature range 298-193 K. The results were interpreted as the superposition of two dielectric relaxations, one attributed to the relaxation of dipoles on the main chain (α relaxation) and the second to the relaxation of the dipoles on the lateral chains (β relaxation). At low temperatures, the two relaxations are clearly separated. On increasing the temperature their characteristic frequencies increase and they merge. At room temperature their characteristic frequencies result higher than the maximum frequency in our range, therefore only the low frequency part of the relaxation is measured. At high temperatures, a DC conductivity, attributed to the presence of impurity ions, was measured.

Cast films of PCMS were deposited on IDE structures for vapour sensing experiments. The electrical admittance of PCMS films on IDE was described in terms of a simple equivalent circuit. Two contributions to the frequency response were noted: from the bulk polymer permittivity; and from the polymer/electrode interface.

	Ethanol		***Benzene***		***Acetonitrile***		***Water***	
Frequency [kHz]	Estimated minimum detectable concentration [ppm]	Measured sensitivity (ΔCap/Δc) [pF/ppm]	Estimated minimum detectable concentration [ppm]	Measured sensitivity (ΔCap/Δc) [pF/ppm]	Estimated minimum detectable concentration [ppm]	Measured sensitivity (ΔCap/Δc) [pF/ppm]	Estimated minimum detectable concentration [ppm]	Measured sensitivity (ΔCap/Δc) [pF/ppm]
10^{-1}	1.3×10^{2}	$(7.48 \pm 0.04)\times10^{-4}$	4×10^{2}	$(2.44 \pm 0.04)\times10^{-4}$	23	$(42.8 \pm 0.04)\times10^{-4}$	6.8×10^{2}	$(1.48 \pm 0.04)\times10^{-4}$
1	2.5×10^{3}	$(4.0 \pm 0.4)\times10^{-5}$	2.5×10^{4}	$(4 \pm 4)\times10^{-6}$	5.1×10^{2}	$(1.97 \pm 0.04)\times10^{-4}$	1.7×10^{3}	$(5.7 \pm 0.4)\times10^{-5}$
10^{2}	6.65×10^{3}	$(1.5 \pm 0.04)\times10^{-5}$	2.4×10^{4}	$(-4.2 \pm 0.4)\times10^{-6}$	2.8×10^{3}	$(3.5 \pm 0.04)\times10^{-5}$	6.2×10^{3}	$(1.6 \pm 0.04)\times10^{-5}$
10^{3}	6.65×10^{3}	$(1.5 \pm 0.04)\times10^{-5}$	2.5×10^{4}	$(-4.0 \pm 0.4)\times10^{-6}$	2.9×10^{3}	$(3.4 \pm 0.04)\times10^{-5}$	6.2×10^{3}	$(1.6 \pm 0.04)\times10^{-5}$

Table 7.2: Sensing characteristics (capacitance) of IDE coated with PCMS cast films, exposed to ethanol/benzene/acetonitrile/water vapours, using admittance spectroscopy. ΔCap is the change of the capacitance corresponding to a change Δc in the vapour concentration.

	Ethanol		*Benzene*		*Acetonitrile*		*Water*	
Frequency [kHz]	Estimated minimum detectable concentration [ppm]	Measured sensitivity (ΔG/Δc) [nS/ppm]	Estimated minimum detectable concentration [ppm]	Measured sensitivity (ΔG/Δc) [nS/ppm]	Estimated minimum detectable concentration [ppm]	Measured sensitivity (ΔG/Δc) [nS/ppm]	Estimated minimum detectable concentration [ppm]	Measured sensitivity (ΔG/Δc) [nS/ppm]
10^{-1}	6	$(171 \pm 1)\times10^{-4}$	16	$(63 \pm 1)\times10^{-4}$	2	$(512 \pm 1)\times10^{-4}$	14	$(73 \pm 1)\times10^{-4}$
1	6	$(175 \pm 1)\times10^{-4}$	15	$(64 \pm 1)\times10^{-4}$	2	$(539 \pm 1)\times10^{-4}$	13	$(74 \pm 1)\times10^{-4}$
10^{2}	5	$(181 \pm 1)\times10^{-4}$	15	$(67 \pm 1)\times10^{-4}$	2	$(570 \pm 1)\times10^{-4}$	8	$(118 \pm 1)\times10^{-4}$
10^{3}	9	$(107 \pm 1)\times10^{-4}$	450	$(2.2 \pm 0.4)\times10^{-4}$	2	$(545 \pm 1)\times10^{-4}$	6	$(169 \pm 1)\times10^{-4}$

Table 7.3: Sensing characteristics (conductance) of IDE coated with PCMS cast films, exposed to ethanol/benzene/acetonitrile/water vapours, using admittance spectroscopy. ΔCap is the change of the capacitance corresponding to a change Δc in the vapour concentration.

The sensitivity of the electrical admittance of a PCMS film to three organic solvents (benzene, ethanol and acetonitrile) and to water vapour was investigated over the frequency range 10^2-10^6 Hz. Reproducible and reversible changes were found for the exposure to all these vapours. The effects were found to be related to the dipole moment of the vapour molecules. A simple model to estimate the capacitance changes induced by different vapours based on their permittivities and partition coefficients has been proposed. Using data from the literature for ethanol, the model predicts the same order of magnitude to that found experimentally. This result could be useful in the selection of polymers for use in sensor array.

Finally, an evaluation of the gas sensing characteristic of this device has been given, with a discussion of the sensitivity and selectivity. During the exposure to water vapour, a distinct frequency behaviour was observed. This could be exploited to eliminate the effect of this vapour in a practical sensor.

References

[1] F.G.A.Stone, W.A.G.Graham, *Inorganic polymers*, 1962, Academic Press, New York, chapter 5.

[2] M.Haug, K.D.Schierbaum, H.E.Endres, S.Drost, W.Göpel, *Sensors and Actuators A*, **32** (1992) 326.

[3] A.Lanini, *Thesis*, 1994, University of Pisa.

[4] C.J.F.Böttcher, *Theory of electric polarization*, vol.I (second edition), 1973, Elsevier Science Publishers, Amsterdam.

[5] A.R.von Hippel, *Dielectrics and waves*, 1962, John Wiley & Sons, New York.

[6] A.Schönhals, E.Schlosser, *Colloid Polym. Sci.*, **267** (1989) 125.

[7] H.E.Endres, S.Drost, *Sensors and Actuators B*, **4** (1991) 95.

[8] M.Haug, K.D.Schierbaum, H.E.Endres, S.Drost, W.Göpel, *Sensors and Actuators A*, **32** (1992) 326.

[9] R.C.West, M.J.Astle, *CRC Handbook of Chemistry and Physics*, 1978, CRC Press Ltd. Florida, vol.59, E60.

[10] A.K.Jonscher, *Universal relaxation law*, 1996, Chelsea Dielectric Press, London.

[11] R.Pethig, *Dielectric and electronic properties of biological materials*, 1979, John Wiley & sons, New York.

[12] W.Nahm, G.Gauglitz, *GIT Fachs.Lab.*, **7** (1990) 889.

[13] K.D.Schierbaum, A.Hielermann, W.Göpel, *Sensors and Actuators B*, **18-19** (1994) 448.

[14] M.Haug, K.D.Schierbaum, G.Gauglitz, W.Göpel, *Sensors and Actuators B*, **11** (1993) 383.

[15] K.D.Schierbaum, A.Gerlach, M.Haug, W.Göpel, *Sensors and Actuators A*, **31** (1992) 130.

[16] J.W.Grate, M.H.Abraham, *Sensors and Actuators B*, **3** (1991) 85.

[17] R.C.West, M.J.Astle, *CRC Handbook of Chemistry and Physics*, 1978, CRC Press Ltd. Florida, vol.59, E63.

[18] J.B.Hasted, *Aqueous dielectrics*, Chapman & Hall, London, 1973, Chapter 5.

[19] B.K.P.Scaife, *Principles of dielectrics*, 1989, Clarendom Press, Oxford, Chapter 4.

[20] Y.Feldman, A.Adrianov, E.Polygalov, I.Ermolina, G.Romanychev, Y.Zuev, B.Milotin, *Rev.Sci.Instrum.*, **67** (1996) 3208.

[21] C.Cornila, A.Hielemann, R.Lenggenhager, P.Malcovati, H.Baltes, G.Noetzel, U.Weimar, W.Göpel, *Sensors and Actuators B*, **24-25** (1995) 357.

Chapter 8

POLY(CUMBSH) LB FILMS: CHARACTERISATION AND VAPOUR RESPONSE

8.1 Introduction

In this chapter, the structural and electrical characterisation and vapour response of LB films of a Schiff co-ordination polymer 5,5′ methylenebis (N-hexadecylsalicydeneamine) (MBSH) are discussed. First, a description of the film deposition conditions and a discussion of the film structure on the basis of studies undertaken by other workers are given (sections 8.2 and 8.3). This is followed by the electrical characterisation of poly(CuMBSH) LB films, both on varying the temperature (section 8.5) and during the exposure to vapours (sections 8.6 - 8.7). Finally, (in section 8.8), an evaluation of the gas sensing characteristics is provided.

8.2 Film deposition

The substrates used for the film deposition were glass microscope slides. These were cleaned in an ultrasonic bath and dried with a flow of nitrogen gas. The substrate was then metal-coated with gold stripes (width 1.4 mm, thickness 500 nm). A second metal strip was deposited on top of the LB film to obtain a sandwich configuration (shown in figure 4.1(b)) that allowed electrical measurements to be made in the out-of-plane direction. This second strip was aluminium (width 0.6 mm, thickness 35 nm). The metals were deposited by thermal evaporation under high-vacuum conditions (~ 10^{-5} mbar).

a)

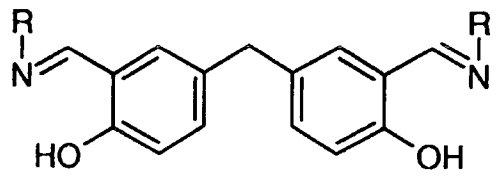

MBSH

b)

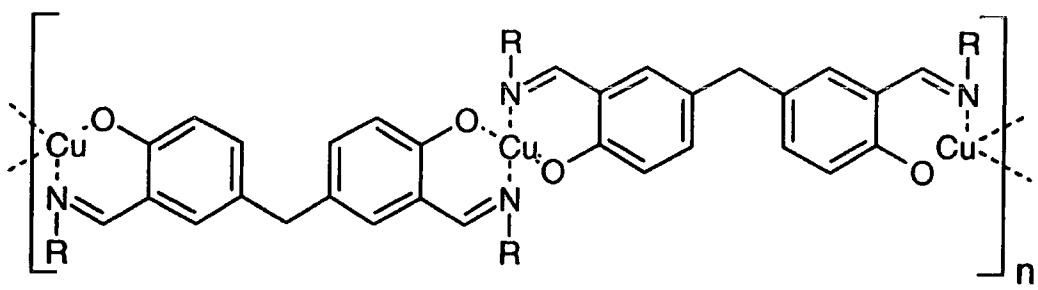

poly(CuMBSH)

$R = C_{16}H_{33}$

Figure 8.1: Structure of (a) 5,5′ methylenebis (N-hexadecylsalicydeneamine) (MBSH); (b) poly(CuMBSH) prepared from MBSH that was spread on a subphase of pure water containing 4.0 mg l^{-1} of copper acetate tetrahydrate.

Poly(CuMBSH) (figure 8.1(b)) films were deposited on the metal-coated substrates using the LB technique, following polymerisation of the 5,5′ methylenebis (N-hexadecylsalicydeneamine) (MBSH) (figure 8.1(a)) monomer on the subphase surface. The synthesis and purification of the monomer were undertaken at the Institut Für Polymerforschung, Dresden (Germany) [1, 2]. 50 µl of the a MBSH monomer solution in chloroform (1 g l^{-1}) was spread on a subphase of pure water containing copper acetate tetrahydrate (4 mg l^{-1}). The layer was left for 15 minutes so that the solvent could evaporate; the film was compressed at 32×10^{-2} nm^2 $molecule^{-1}s^{-1}$ and controlled at 25 mN m^{-1}; floating layers of poly(CuMBSH) were then transferred to substrates. Optimum film transfer (Y-type deposition) was achieved at a dipping speed between 6 and 8 mm min^{-1} with a deposition ratio of 1.0 ± 0.1.

8.3 Film structure

Langmuir layers of MBSH on the surface of different subphases have been studied previously [1, 3, 4]. On pure water, the area occupied by a MBSH molecule was calculated as 0.41 ± 0.1 nm^2. This is almost half that estimated using a space filling molecular model (0.7 ± 0.2) nm^2 (shown in figure 8.2). Such a result suggests that MBSH forms a layer that is more than one molecule in thickness at the air/water interface. Floating layers of pure MBSH could not be transferred to substrates using the LB technique.

On a subphase containing pure water and 4.0 mg l^{-1} copper acetate tetrahydrate, a reaction occurs between the copper ions in the subphase and the floating MBSH monomers. As a result, a Langmuir layer of linked MBSH monomers (by the copper ions) (i.e. poly(CuMBSH)) was formed. In this case, the molecular area was 0.82 ± 0.1 nm^2 per repeat unit (i.e. about twice of that calculated for the MBSH on pure water). This compares well to the figure obtained from the molecular model and that published by Öertel and Nagel [3], suggesting that MBSH reacts with the copper in the

subphase to form a monolayer. In contrast to pure MBSH, poly(CuMBSH) could be easily transferred to a rigid substrate using the LB technique (as discussed in paragraph 8.2).

The thickness of the films was measured by ellipsometry, X-ray diffraction and using an Alphastep profilometer [4, 5]. The measured value was a linear function of the number of layers deposited, showing good reproducibility of the LB film deposition. The average thickness per layer was 2.14 ± 0.05 nm. This is smaller than the length of the hydrophobic side chains of the poly(CuMBSH) molecule ($C_{16}H_{33}$) shown in figure 8.2. One possible explanation is that the side chains are not oriented perpendicular to the subphase, but tilted through about 45° from the vertical [3, 4].

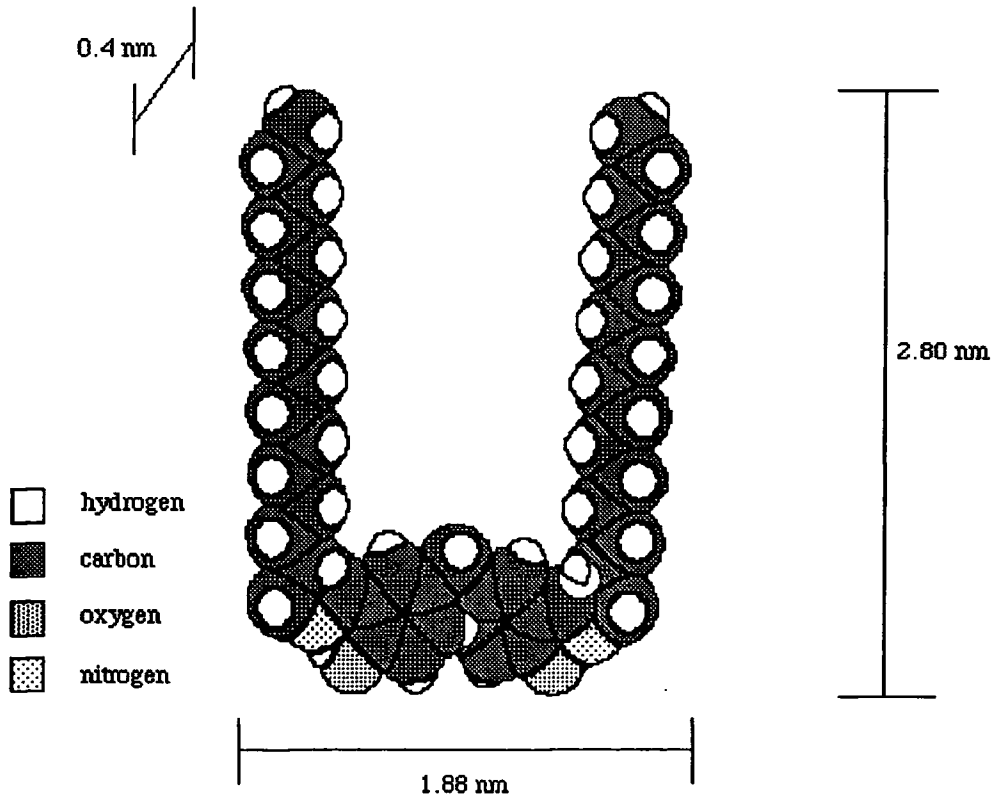

Figure 8.2: Space filling model of the 5,5´ methylenebis (N-hexadecylsalicydeneamine).

8.4 Equivalent circuit and dielectric model

All the samples reported in the electrical studies (varying the temperature and during the exposure to vapour) were 39 layers thick, i.e. 83 ± 2 nm. Below, the equivalent circuit and the dielectric model utilised for the interpretation of the results are described. In the two following sections, the results obtained by varying the temperature and during the exposure to vapours are presented.

An analysis was undertaken by considering the variations of the capacitance and conductance over the frequency range 10^2 - 10^6 Hz. This was preferred to an approach based on complex permittivity, as it was only possible to measure the film's thickness at room temperature and in air. The assumption of a constant thickness under different conditions (temperatures and controlled atmospheres) seemed unreasonable.

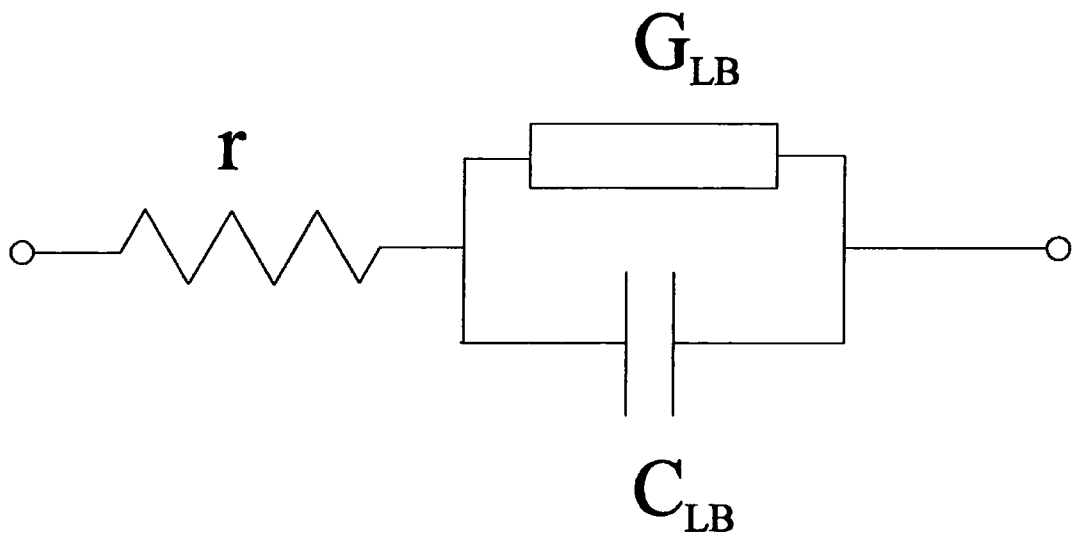

Figure 8.3: The equivalent circuit for the gold/39-layers poly(CuMBSH) LB film/aluminium structure.

The equivalent circuit (figure 8.3) used for the interpretation of our results includes contributions both from the LB film and the electrodes. Other contributions from oxide and leads were negligible (as discussed in paragraph 4.1.2). The LB film was modelled as a capacitance C_{LB} in parallel with a conductance G_{LB}, both frequency dependent. The electrodes were assumed to contribute a resistance r in series with the sample. For the frequency under consideration, the following conditions were satisfied

$$r\,G_{LB} \ll 1 \qquad \omega r\,C_{LB} \ll 1 \tag{8.1}$$

Using equation (4.9), it follows that the measured conductance G and capacitance C are given to a good approximation by

$$G(\omega) \cong G_{LB} + (\omega C_{LB})^2 r \qquad C(\omega) \cong C_{LB} \tag{8.2}$$

G_{LB} and C_{LB} are related, respectively, to the real and imaginary parts of the permittivity (as discussed in paragraph 4.1.2), through the geometrical capacitance of the electrodes C_G

$$G_{LB} = C_G\,\omega\varepsilon''(\omega) \qquad C_{LB} = C_G\,\varepsilon'(\omega) \tag{8.3}$$

The frequency dependence of the permittivity for a dielectric, as discussed in paragraph 2.2.3, is given by the Havriliak-Negami equation (equation 2.29). This describes the power law behaviour observed with polymers for frequencies higher and lower than the characteristic frequency ω_m ($\omega_m = \tau^{-1}$) (equations (2.31) and (2.32)). In terms of capacitance and conductance, these power laws give

$$G_{LB}(\omega) \propto \omega^{1-n} \qquad C_{LB}(\omega) - C_\infty \propto \omega^{-n} \tag{8.4}$$

for $\omega \gg \omega_m$, and

$$G_{LB}(\omega) \propto \omega^{1+m} \qquad C_S - C_\infty - C_{LB}(\omega) \propto \omega^m \qquad (8.5)$$

for $\omega \ll \omega_m$, where C_S and C_∞ are given by the products of the geometrical capacitance C_G with ε_S and ε_∞, respectively.

8.5 Variation of temperature

Figures 8.4 and 8.5 show the conductance and the capacitance of a poly(CuMBSH) LB film at room temperature (T = 297 K) and at T = 235 K. From figure 8.4, it is evident that the room temperature conductance exhibits a power law behaviour with an exponent close to unity for low frequencies and approaching two above 10^5 Hz. The latter was attributed to the electrodes' resistance, as expected from equation (8.2). On decreasing the temperature, figure 8.4 shows that: (i) there is a decrease in the conductance at low frequencies; (ii) the frequency dependence of the low-frequency conductivity decreases with decreasing temperature; and (iii) the temperature dependence of the conductance at high frequencies is very small (in agreement with our interpretation above).

Figure 8.5 shows that there is a decrease in capacitance with increasing frequency. This frequency dependence is much smaller than that exhibited by the conductance. At room temperature, the capacitance varies about 5% over the range of the measurements, corresponding to a change in ε' from 2.42 at low frequencies to 2.31 at high frequencies. In contrast, the conductance varies by about five orders of magnitudes. On reducing the temperature, a decrease in the frequency dependence of the capacitance and a small increase in the capacitance at high frequency are evident from figure 8.5. The latter can be explained by invoking the thermal contraction of the film.

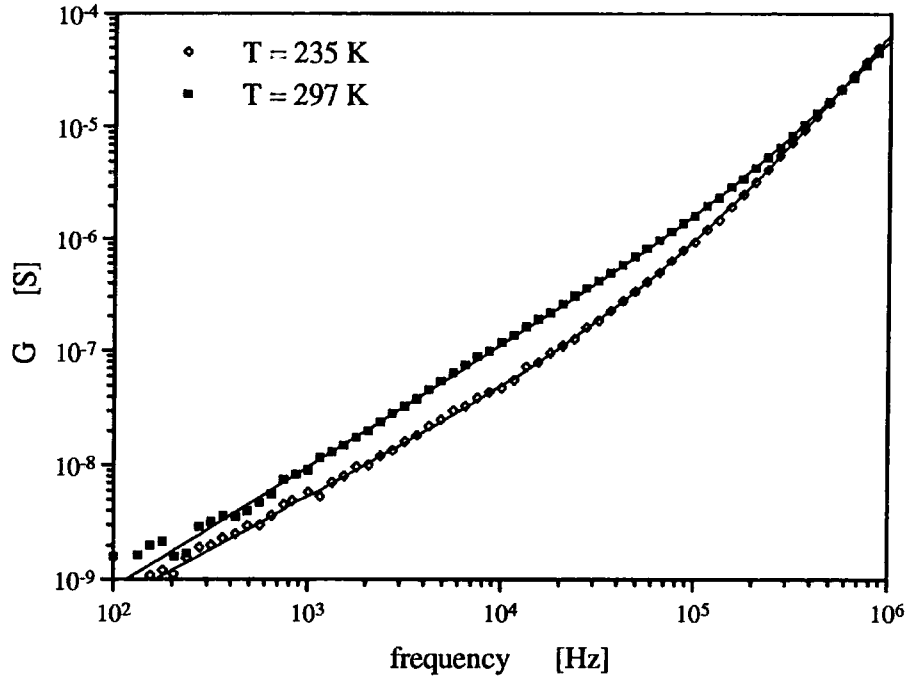

Figure 8.4: The conductance G versus frequency for poly(CuMBSH) LB film. Points are experimental data. Full lines are theory using equation (8.6).

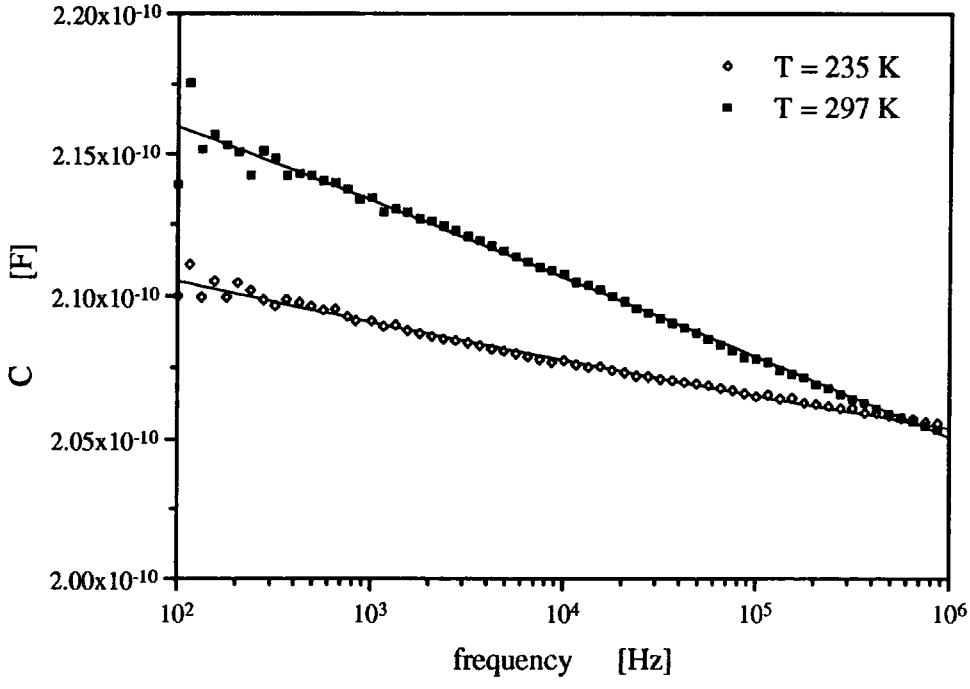

Figure 8.5: The capacitance C versus frequency for poly(CuMBSH) LB film. Points are experimental data. Full lines are theory using equations (8.7).

The data in figures 8.4 and 8.5 can be explained, qualitatively, by invoking an increase in the dielectric relaxation time τ of the LB film as the temperature is reduced (with $\omega_m = \tau^{-1} > 1$ MHz). A detailed analysis using the Havriliak-Negami equation (equation 2.29) is inappropriate because of the very small amplitude of the relaxation ($\varepsilon_S - \varepsilon_\infty$ can be estimated from the room temperature data to be of the order of 0.2) and the complication of the electrodes' resistance. Therefore, the data were fitted using the following expressions, which can be derived from equations (8.2), (8.4) and (8.5)

$$G(\omega) = A\,\omega^s + B\,\omega^2 \tag{8.6}$$

$$\begin{aligned} C(\omega) &= C_\infty + D\,\omega^{-n} \qquad \text{for } \omega \gg \omega_m \\ C(\omega) &= C_S - E\,\omega^m \qquad \text{for } \omega \ll \omega_m \end{aligned} \tag{8.7}$$

where A, B, D and E are constants. The parameter s was chosen to fit the experimental data for G_{LB}. Equations (8.4) and (8.5) reveal that G_{LB} is described by a similar power law both for $\omega \ll \omega_m$ and for $\omega \gg \omega_m$. Estimation of the parameters m and n (defined in equations (8.4) and (8.5)) from s is straightforward, because for $\omega \ll \omega_m$, $s = 1 + m > 1$; and for $\omega \gg \omega_m$, $s = 1 - n < 1$.

The theoretical fits to the capacitance and conductance data were performed separately and, as shown in figures 8.4 and 8.5 (full lines), are in good agreement with the experimental data. The parameters estimated from the best fit for four different temperatures (between T = 298 K and T = 235 K) are presented in table 8.1. For high temperatures (above 270 K), when the condition $\omega \ll \omega_m$ is fulfilled, s is greater then unity. As the temperature is reduced, $\omega \gg \omega_m$ and s became smaller than unity. As expected, the parameter s (equation (8.6)) exhibits a good correlation to the parameters m and n of equations (8.7). At high temperatures ($s > 1$) $s - 1 \equiv m$, whereas for low temperatures ($s < 1$) $s \equiv n$.

T [K]	s	A [$S \times 10^{-12}$]	R [$S \times 10^{-18}$]	n	C_∞ [pF]	D [pF]	m	C_o [pF]	E [pF]
298	1.05 ± 0.005	0.96 ± 0.05	1.12 ± 0.02	-	-	-	$(10 \pm 5)\times10^{-2}$	330 ± 50	100 ± 25
275	1.02 ± 0.006	1.3 ± 0.1	1.50 ± 0.03	-	-	-	$(8 \pm 4)\times10^{-2}$	340 ± 50	125 ± 35
255	0.94 ± 0.004	2.5 ± 0.1	1.56 ± 0.02	0.96 ± 0.01	185 ± 6	35 ± 3	-	-	-
235	0.92 ± 0.01	1.7 ± 0.2	1.58 ± 0.03	0.97 ± 0.02	189 ± 8	32 ± 4	-	-	-

Table 8.1: Exponents estimated from the analysis of the capacitance's and conductance's dependencies on the frequency for four different temperatures. s is the power law exponent estimated for the conductance using equation (8.6), n and m are the power law exponents estimated using equations (8.7). The constants A, B, C_∞, D, C_S and E are defined in equations (8.6) and (8.7).

8.6 Exposure to organic solvent vapours

Figure 8.6 (full line) shows the transient behaviour of the capacitance, measured at 1 kHz, for a film exposed to 3.1% ethanol. Following a rapid initial change, a stable capacitance value is attained after few minutes. The film exhibits complete recovery when the organic vapour is replaced by N_2. The effect of exposing the film for four consecutive periods of 1 min to 3.1% ethanol separated by 10 min recovery is shown in figure 8.7. Reasonable reproducibility is evident. The transient responses to benzene and acetonitrile were found to be similar to that for ethanol (data not shown).

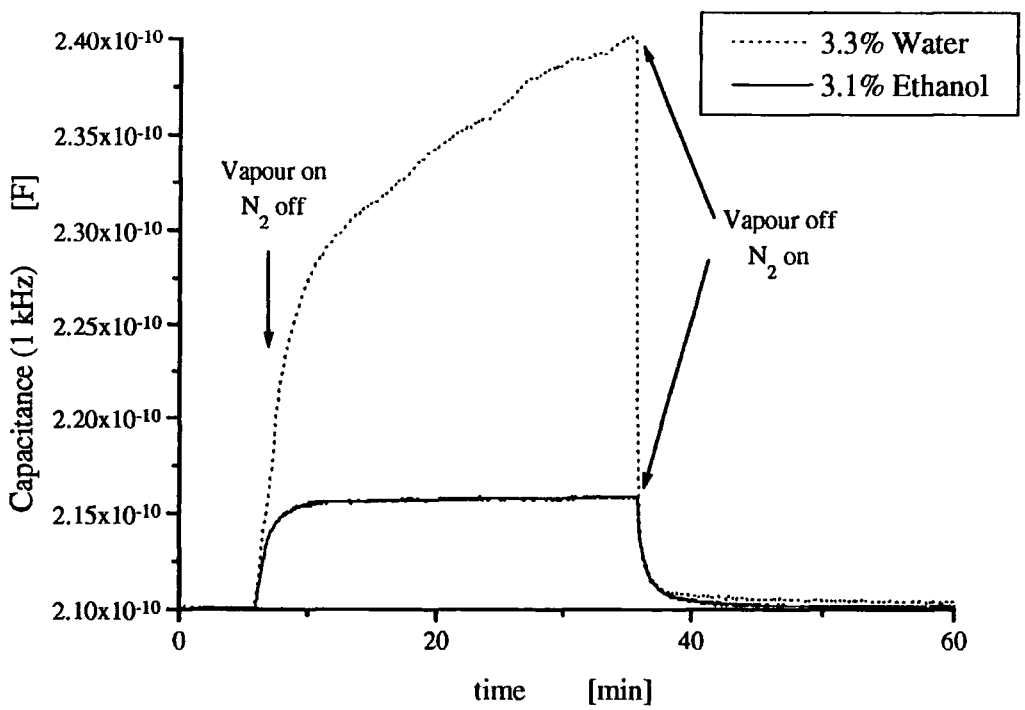

Figure 8.6: The transient behaviour of the capacitance measured at 1 kHz for a poly(CuMBSH) LB film exposed to concentrations of 3.1% of ethanol and 3.3% of water.

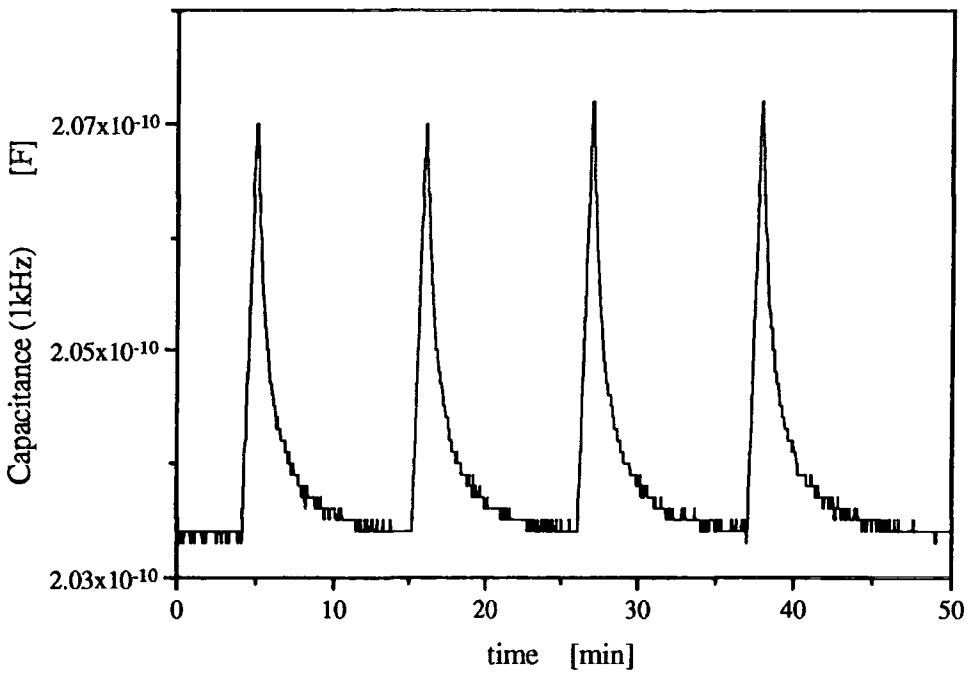

Figure 8.7: The transient behaviour of the capacitance measured at 1 kHz for a poly(CuMBSH) LB film exposed to 3.1% of ethanol for four consecutive periods of 1 min of recovery.

To compare the effects of the different vapours, the data were normalised by dividing the capacitances and conductances in the vapours by the values measured in nitrogen. Figures 8.8 and 8.9 show the results obtained when the LB layers were exposed to various concentrations of acetonitrile, ethanol and benzene.

The capacitance data (figure 8.8) reveal that there is an increase in capacitance on exposure to ethanol and acetonitrile, but a decrease for benzene. Acetonitrile produces the largest change in capacitance. On exposure to all three vapours, an increase in the conductance is noted (figure 8.9), acetonitrile giving a large response at high frequencies.

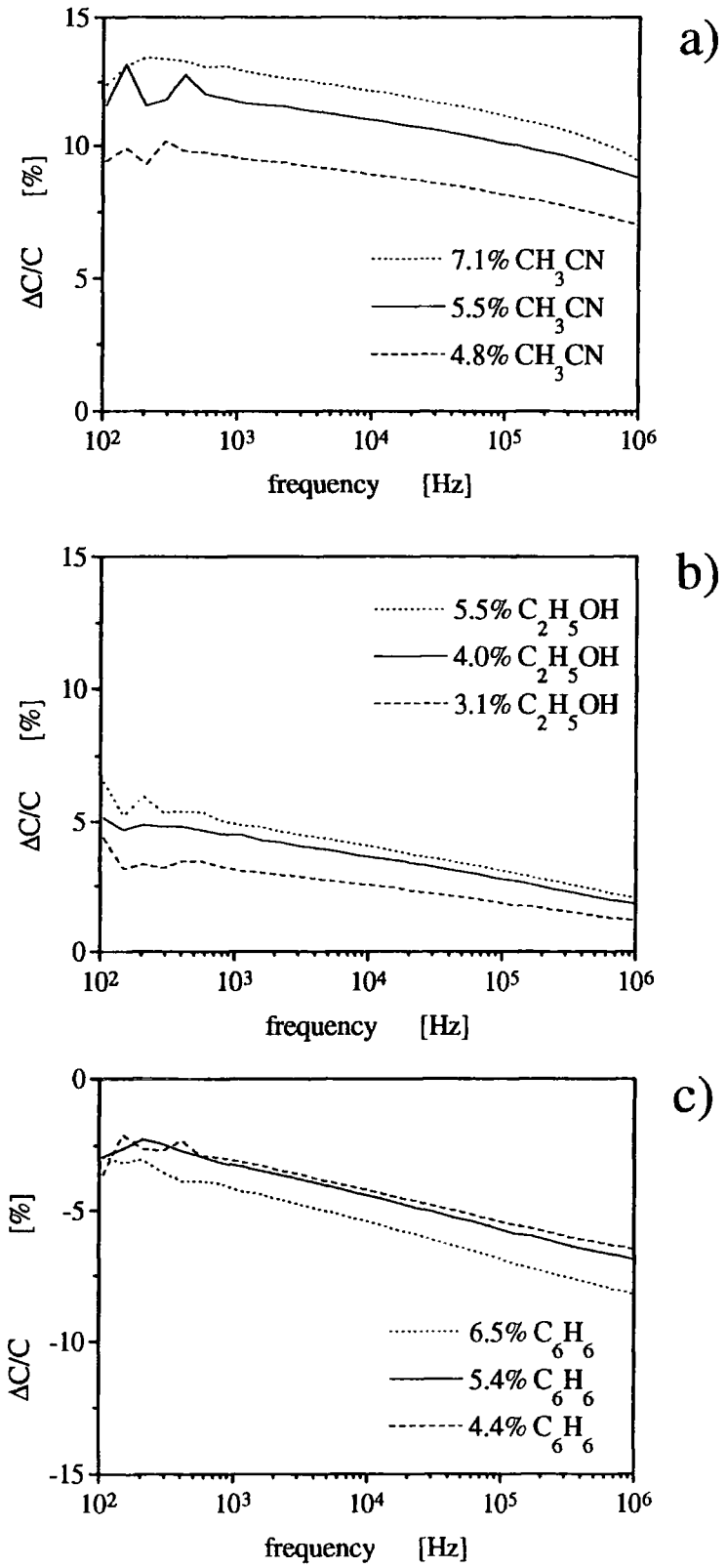

Figure 8.8: The percentage change of the capacitance for a poly(CuMBSH) LB film exposed to various concentrations of acetonitrile (a), ethanol (b) and benzene (c).

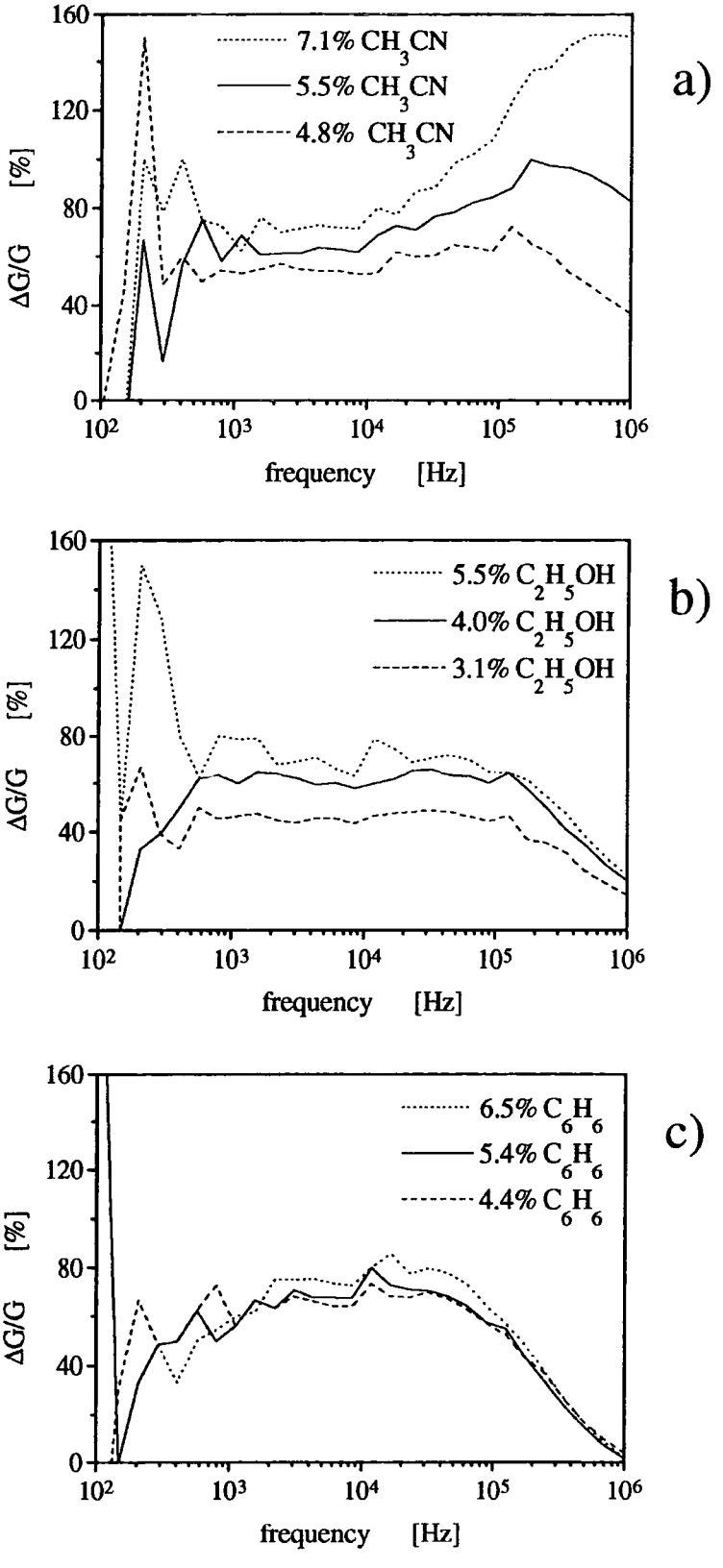

Figure 8.9: The percentage change of the conductance for a poly(CuMBSH) LB film exposed to various concentrations of acetonitrile (a), ethanol (b) and benzene (c).

These data may be understood by considering the dipole moments of the vapour molecules (reported in table 4.1). If the organic solvents dissolve in the bulk of the polymer film figure 8.10(a), with no interaction between the vapour molecules and the polymer, three main effects are expected:

(i) a direct contribution by the vapour molecules to the permittivity of the film (related to their dipole moments);
(ii) a change of the orientational ability of the polymer molecules, induced by the presence of the solvent molecules; and
(iii) a variation of the film's thickness (swelling).

Process (i) will produce both an increase in the measured permittivity at low frequencies ε_S (dependent on the number of molecules dissolved in the film and their dipole moment) and a change in the frequency dependence of the permittivity (given by a superposition of the dielectric relaxations of the vapour molecules and the polymer). The effect of the static permittivity should follow a relationship similar to that derived by Maxwell for low volume fractions of spheres of permittivity ε_2 dispersed in a dielectric of permittivity ε_1 reported in paragraph 2.4 (equation (2.68)).

The relaxation frequencies for the solvents used in this work are in the microwave region at room temperature. Values of the relaxation times τ in the liquid phase for acetonitrile [6] and ethanol [7] are τ = 2-3 ps (at T = 298 K) and τ = 132 ps (at 303 K), respectively (it should also be noted that τ depends on the purity of the solvent). Consequently, if the solvent molecules are not bonded to the polymer, we would not expect to observe a significant change in the frequency behaviour.

A change in the orientational ability of the polymer molecules induced by the presence of the solvent molecules should cause a decrease in the relaxation time τ and a shift of the capacitance (and conductance) versus frequency curve to higher frequencies (similar to that observed for an increase in temperature). The ability of the polymer molecules to

orient themselves along the electrical field direction should also provide an increase in the low-frequency permittivity ε_S. This will give an increase in the relaxation strength ε_S - ε_∞ (also similar to decreasing the temperature). Finally, a change in the film's thickness will result in a change in the absolute values of the measured capacitance and conductance.

The results for benzene (figures 8.8(c) and 8.9(c)), which has zero dipole moment, suggest that the solvent has swollen the film, giving a decrease in the capacitance. However, if this was the only effect , there should be no frequency dependence of the measured value for C and G. The experimental data indicate that there is probably a further contribution from a change in the permittivity of the polymer film, the benzene molecules influencing the dynamics of the orientation of the polymer molecules. An estimate of the degree of swelling can be made by assuming that the permittivity is unchanged

$$\Delta C = \varepsilon' A\left(\frac{1}{t_2} - \frac{1}{t_1}\right) \Rightarrow \frac{\Delta C}{C} = \frac{t_1 - t_2}{t_2} \tag{8.8}$$

where ΔC is the change of the capacitance, A is the electrode area, t_1 is the initial thickness and t_2 is the thickness of the film after exposure to benzene. From equation (8.8), a swelling of a few per cent of the film's thickness is calculated, which is not unreasonable.

For the two other vapours, the observed variations of the capacitance can be explained by assuming that the increase in permittivity will predominate over the film's swelling and that this effect will be greater for molecules having a larger dipole moment. The greater increase in capacitance at low frequencies can be explained by invoking an increase in ε_S due to the high permittivity of the two solvents ($\varepsilon_S = 37.5$ and $\varepsilon_S = 23.6$, respectively, for acetonitrile [6] and ethanol [7]), as expected from equation (2.68).

Because the high frequency conductance is related mainly to the electrodes' resistance, we expect that its variation will tend to zero. This is observed for benzene (figure 8.9(c)). However, the responses for ethanol (figure 8.9(b)) and, in particular, to acetonitrile (figure 8.9(a)) exhibit a different behaviour. The increase in conductance at high frequencies suggests that there is a superposition of the solvent's relaxation on that of the polymer. The greater change observed for acetonitrile is a result of its higher polarity.

8.7 Exposure to water vapour

The response of the poly(CuMBSH) film to water vapour was found to be very different to that for the organic solvents. The transient behaviour of the capacitance measured at 1 kHz is shown in figure 8.7 (dotted line). In contrast to the data for ethanol, given in the same figure, there is no saturation of the capacitance following exposure to water vapour (on the timescale of the experiment). However, the recovery time (measured as the time taken for the response to change from 90% of the maximum output to 10%) is about 0.6 min, compared with a value of about 2.6 min for ethanol. In figures 8.11 and 8.12, the capacitance and the conductance of a polymer film exposed to water (3.3%), after various periods of exposure, are shown. The effects are also significantly greater at lower frequencies. Saturation of the data was not observed, even after 2 h of exposure.

The above indicates that the response mechanism for the polymer LB layer is different for water vapour and organic solvents. Water is not a solvent for poly(CuMBSH) (otherwise we could not use the LB method of thin-film fabrication!). Consequently, we would not expect a strong interaction between the water molecules and the polymer film. This probably accounts for the rapid recovery shown in figure 8.7.

We therefore suggest the following as possible mechanisms to explain the results:

(i) water molecules are adsorbed at the polymer's surface as shown in figure 8.10(b) and the thin water 'layer' provides a capacitance in series with that of the film (as shown in figure 2.4); or

(ii) water diffuses into the polymer matrix forming clusters of molecules, as shown in figure 8.10(c). Charge transport between these clusters would then be possible.

A simple heterogeneous two-layer system, as discussed in paragraph 2.4, can be described in terms of the Debye equation plus an extra term related to the conductivity (frequency independent). The variables ε_S, ε_∞, τ, and σ will be related to the permittivity, conductivity and thickness of the two layer-structure by equations (2.60)-(2.63). In our case, we would expect to observe the high-frequency part of this Maxwell-Wagner interfacial polarisation effect. For $\omega\tau \gg 1$, equation (2.59) gives

$$\varepsilon' \cong \varepsilon_\infty + (\varepsilon_s - \varepsilon_\infty)(\omega\tau)^{-2} \tag{8.9}$$

$$\varepsilon'' \cong (\varepsilon_s - \varepsilon_\infty)(\omega\tau)^{-1} + \sigma(\omega\varepsilon_o)^{-1} \tag{8.10}$$

Such frequency behaviour of the permittivity will correspond to the following frequency dependencies for the capacitance and conductance

$$G(\omega) \cong \text{const} \;; \qquad C(\omega) - C_2 \propto \omega^{-2} \qquad \text{for } \omega \gg \tau^{-1} \tag{8.11}$$

where C_2 is a frequency-independent constant related to the permittivity, conductivity and thickness of the two layers. However, it is evident that these relationships are not consistent with the experimental data shown in figures 8.11 and 8.12.

Mechanism (ii) above has been discussed in paragraph 2.5. This is an example of low frequency dispersion (LFD). In this case, the charge carriers will be ions, from the dissociation of water, that move between clusters of water molecules inside the polymer

matrix. The frequency dependence of the permittivity for LFD can be described by the following equations (that can be derived by equation 2.69)

$$\varepsilon'(\omega) - \varepsilon_a \propto \varepsilon''(\omega) \propto \omega^{n_2-1} \qquad \text{for } \omega \ll \omega_c \qquad (8.12)$$

$$\varepsilon'(\omega) - \varepsilon_a \propto \varepsilon''(\omega) \propto \omega^{n_1-1} \qquad \text{for } \omega \gg \omega_c \qquad (8.13)$$

with $0 < n_2 < 0.5$ and $0.5 < n_1 < 1$, where ω_c is a characteristic frequency, n_1 and n_2 are real numbers and ε_a is the permittivity for frequencies much higher than ω_c. In terms of the capacitance and conductance

$$G_{LB}(\omega) \propto \omega^{n_2} \qquad C_{LB}(\omega) - C_a \propto \omega^{n_2-1} \qquad \text{for } \omega \ll \omega_c \qquad (8.14)$$

$$G_{LB}(\omega) \propto \omega^{n_1} \qquad C_{LB}(\omega) - C_a \propto \omega^{n_1-1} \qquad \text{for } \omega \gg \omega_c \qquad (8.15)$$

where C_a is the product of C_G and ε_a.

The experimental data indicate that the characteristic frequency ω_c for LFD is smaller than our measurement frequencies and the high-frequency power laws (described by equations (8.13) and (8.15)) should be observed.

To test whether the observed behaviour was in agreement with LFD, theoretical fits using the following equations (derived from equations (8.2), (8.14) and (8.15)) for the capacitance and conductance were used

$$G(\omega) = F\omega^{n_1} + H\omega^2 \qquad (8.16)$$

$$C(\omega) = L\omega^{n_1-1} + M\omega^{n_2-1} + C_\infty \qquad (8.17)$$

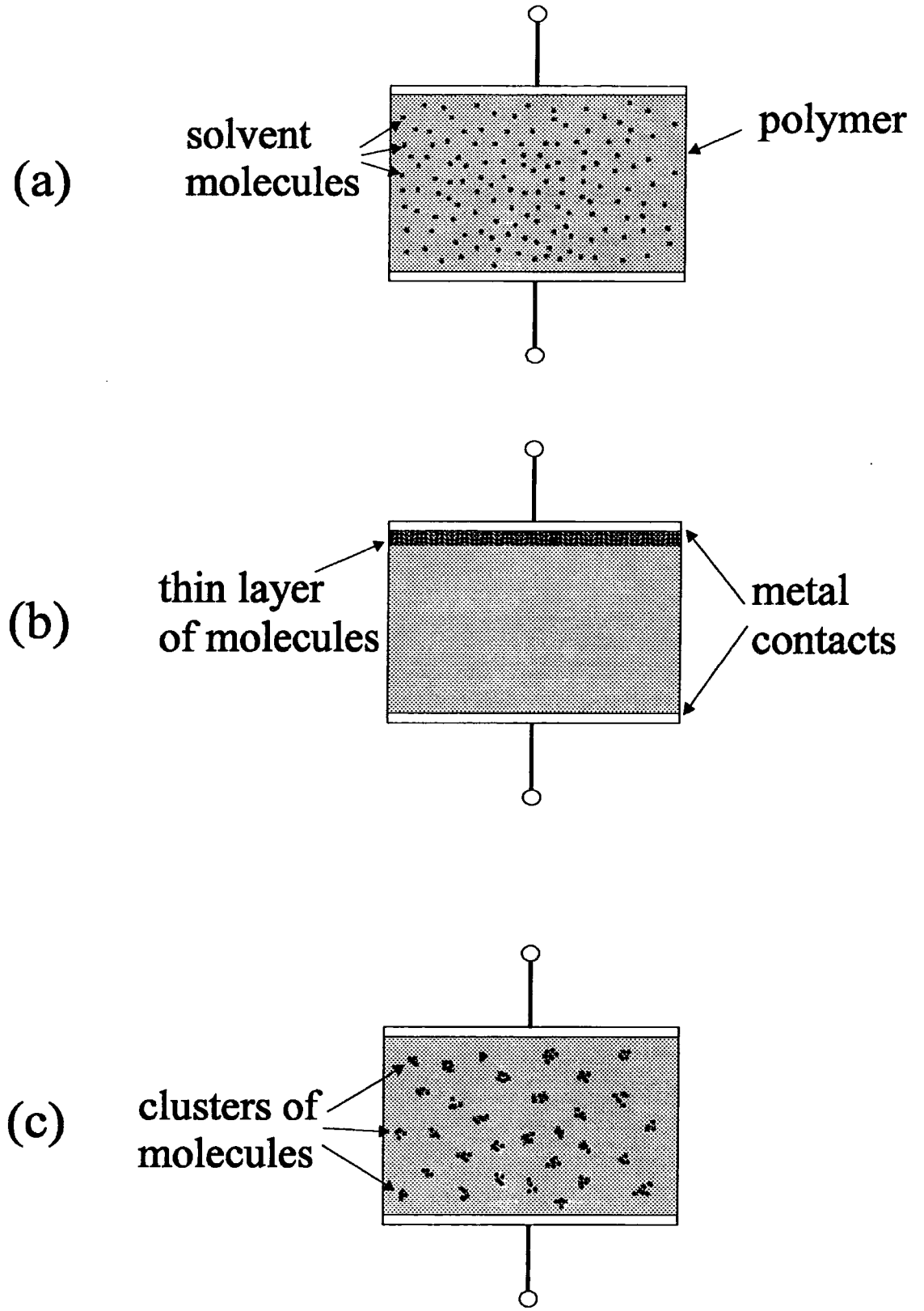

Figure 8.10: Models of vapour sorption by the polymer film: (a) homogeneous bulk dissolution; (b) adsorption; and (c) heterogeneous bulk dissolution.

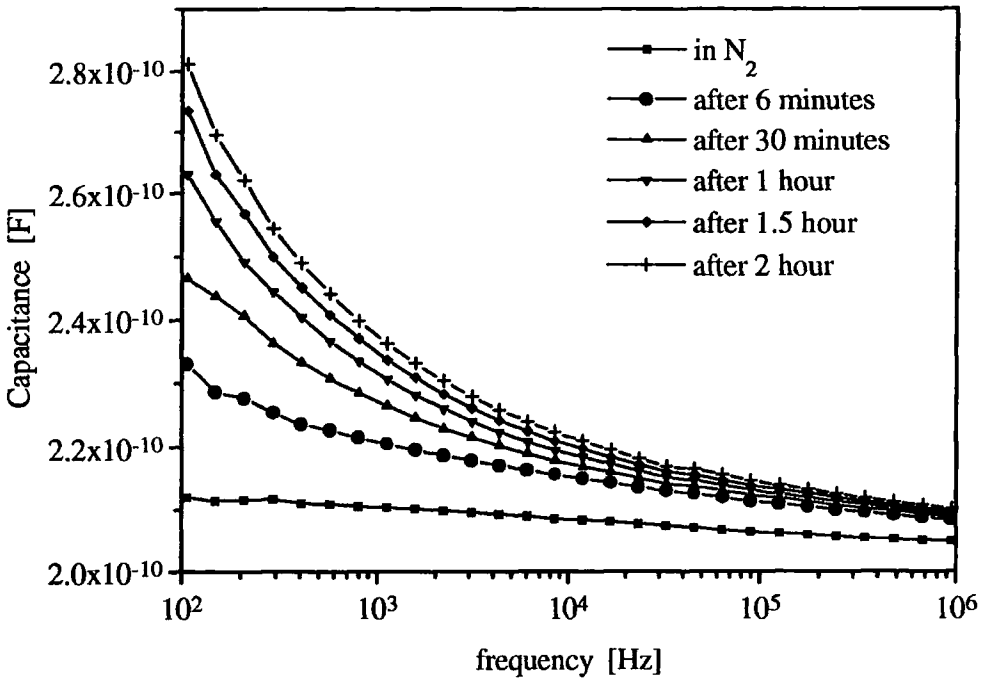

Figure 8.11: The capacitance for a poly(CuMBSH) LB film exposed to water vapour (3.3%). The measurement were taken after various exposure times.

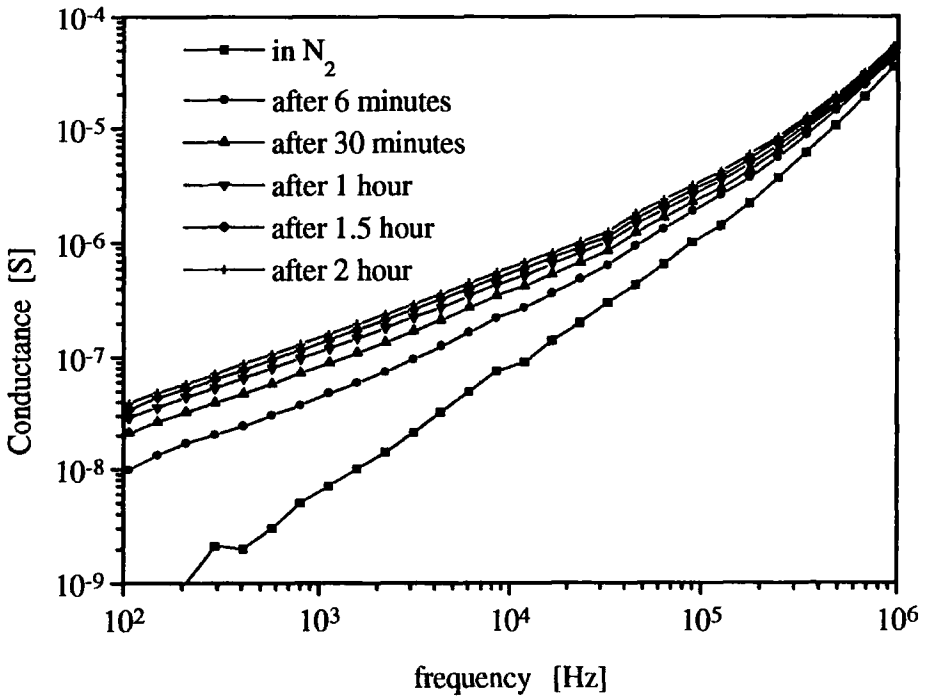

Figure 8.12: The conductance for a poly(CuMBSH) LB film exposed to water vapour (3.3%). The measurements were taken after various exposure times.

As before, the parameters F, H, L and M are frequency-independent constants. Best fits for the case of a thin film of poly(CuMBSH) exposed to water vapour (3.3%) for 2h are shown in figure 8.13 (full lines). The best fit parameters were $F = (6.1 \pm 0.4) \times 10^{-10}$ S, $H = (1.17 \pm 0.03) \times 10^{-18}$ S, and $n_1 = 0.63 \pm 0.01$ for G(ω); and $L = 920 \pm 60$ pF, $M = 37 \pm 5$ pF, $C_\infty = 180 \pm 30$ pF, $n_2 = 0.02 \pm 0.05$, $n_1 = 0.59 \pm 0.04$ for C(ω).

The values of n_1 obtained from the separate fits to the conductance and capacitance data are in excellent agreement and both n_1 and n_2 are in the same range of the values observed in the literature [8]($0 < n_2 < 0.5$ and $0.5 < n_1 < 1$), suggesting that the LFD model can explain our data. However, our measurements really need to be extended to lower frequencies to confirm this.

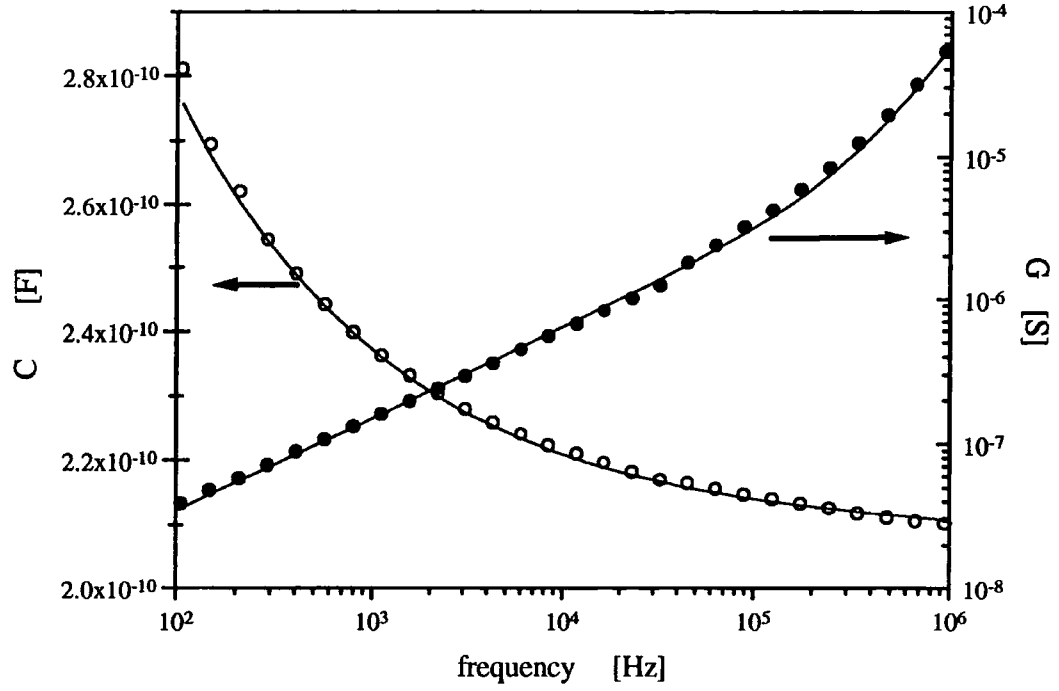

Figure 8.13: The capacitance and conductance for a poly(CuMBSH) LB film exposed to water vapour (3.3%) for 2 h. The full lines are the theoretical fit to the experimental data (points) using equations (8.16) and (8.17).

8.8 Evaluation of the device for gas sensing applications

In the sections above, we have shown that the reversible change in the admittance of a gold/39-layer poly(CuMBSH)/aluminium device on exposure to vapours can be explained in terms of a simple dielectric model. To evaluate if this structure could be useful as a practical gas-sensing device, the sensitivity and selectivity are discussed in more detail.

As noted in section 8.7, exposing the device to water vapour was found to give an 'anomalous' response, with a different transient behaviour, no saturation on the time scale of the experiment and a completely different frequency response. This precluded a direct comparison with the organic vapours. For this reason, the response to water vapour is omitted in the following discussion. However, the unique response may be useful in discriminating water from the other vapours.

The average sensitivity (capacitance/concentration or conductance/concentration) for the three different organic solvent vapours calculated at four different frequencies (1 kHz, 10 kHz, 10^2 kHz and 1 MHz) are given in tables 8.2 and 8.3 for the capacitance and conductance, respectively. From table 8.2, it can be seen that the sensitivity of the capacitance measurements is of the same order of magnitude for each vapour at the four frequencies. On increasing the frequency, the sensitivity for the polar vapours decreases while that for the non polar vapour (benzene) increases. The sensitivity of the conductance (table 8.3) for the polar vapours depends strongly on the frequency, increasing rapidly with increasing frequency. In contrast, the behaviour for benzene is not monotonic. Following an increase at low frequencies ($\nu < 10^2$ Hz), the conductance sensitivity decreases for high frequencies.

For each vapour, the minimum detectable concentration was estimated. This corresponded to the concentration for which the observed change would be equal to the instrument resolution (in our case, 0.1 pF and 1 nS). The estimated values are shown in

tables 8.2 and 8.3 for the capacitance and conductance measurements, respectively. Table 8.3 shows that very small (~ ppm) concentrations of vapours should be detectable by conductance measurements at high frequency. However, this must be confirmed by experiment.

To evaluate the selectivity obtainable at different frequencies, the average percentage changes in C and G divided by the vapour concentration at four different frequencies were evaluated

$$\langle \Delta M \rangle = \frac{1}{n} \frac{1}{M_0} \sum_{i=1}^{n} \frac{\Delta M_i}{c_i(\%)} \qquad (8.18)$$

where M is C or G, n is the number of concentrations used, M_o is the initial value in nitrogen and ΔM_i is the change with respect to the initial value (expressed as a percentage) measured for concentration $c_i(\%)$. The results, for measurements at four frequencies, are shown in figure 8.14. The explanation of the different behaviour has been already elucidated in section 8.6. From a practical sensing viewpoint, it is clear that simultaneous measurements of capacitance and conductance at different frequencies seems to allow a good discrimination between different vapours.

Another important factor for practical applications is the device stability. At this moment, no experiments have been carried out over extended time periods (e.g. months or year). Good stability is anticipated considering that (i) a polymer film should offer a good mechanical strength in view of its structure in which the 'molecular units' are kept together by chemical bonding and not by van der Waals' binding as in a classical LB film, and (ii) the observed changes seem to be related only to a diffusion of the vapours inside the film and not to a chemical reaction that could alter the chemical structure of the film.

	Acetonitrile (d = 3.92 Debye [9])		**Ethanol (d = 1.69 Debye [9])**		**Benzene (d = 0 Debye [9])**	
Frequency [kHz]	Estimated minimum detectable concentration [ppm]	Measured sensitivity (ΔCap/Δc) [pF/ppm]	Estimated minimum detectable concentration [ppm]	Measured sensitivity (ΔCap/Δc) [pF/ppm]	Estimated minimum detectable concentration [ppm]	Measured sensitivity (ΔCap/Δc) [pF/ppm]
1	240	$(4.1 \pm 0.1)\times10^{-4}$	500	$(2.0 \pm 0.06)\times10^{-4}$	760	$(1.3 \pm 0.04)\times10^{-4}$
10	260	$(3.8 \pm 0.1)\times10^{-4}$	620	$(1.6 \pm 0.06)\times10^{-4}$	570	$(1.7 \pm 0.06)\times10^{-4}$
10^2	290	$(3.4 \pm 0.1)\times10^{-4}$	860	$(1.2 \pm 0.04)\times10^{-4}$	450	$(2.2 \pm 0.08)\times10^{-4}$
10^3	350	$(2.8 \pm 0.1)\times10^{-4}$	1400	$(0.7 \pm 0.04)\times10^{-4}$	380	$(2.6 \pm 0.14)\times10^{-4}$

Table 8.2: Sensing characteristics (capacitance) of gold/39-layer LB film poly(CuMBSH)/aluminium device exposed to benzene/ethanol/acetonitrile vapours, using admittance spectroscopy. ΔCap is the change of the capacitance corresponding to a change Δc in the vapour concentration.

	Acetonitrile (d = 3.92 Debye [9])		**Ethanol (d = 1.69 Debye [9])**		**Benzene (d = 0 Debye [9])**	
Frequency [kHz]	Estimated minimum detectable concentration [ppm]	Measured sensitivity (ΔG/Δc) [nS/ppm]	Estimated minimum detectable concentration [ppm]	Measured sensitivity (ΔG/Δc) [nS/ppm]	Estimated minimum detectable concentration [ppm]	Measured sensitivity (ΔG/Δc) [nS/ppm]
1	5×10^{3}	$(2\pm0.1)\times10^{-4}$	5×10^{3}	$(2\pm0.1)\times10^{-4}$	5×10^{3}	$(2\pm0.1)\times10^{-4}$
10	550	$(1.8\pm0.1)\times10^{-3}$	450	$(2.2\pm0.1)\times10^{-3}$	450	$(2.2\pm0.1)\times10^{-3}$
10^{2}	30	$(2.9\pm0.08)\times10^{-2}$	40	$(2.4\pm0.07)\times10^{-2}$	60	$(1.7\pm0.05)\times10^{-2}$
10^{3}	1	1.1 ± 0.03	4	$(2.6\pm0.07)\times10^{-1}$	110	$(9\pm0.2)\times10^{-3}$

Table 8.3: Sensing characteristics (conductance) of gold/39-layer LB film poly(CuMBSH)/aluminium device exposed to benzene/ethanol/acetonitrile vapours, using admittance spectroscopy. ΔG is the change of the conductance corresponding to a change Δc in the vapour concentration.

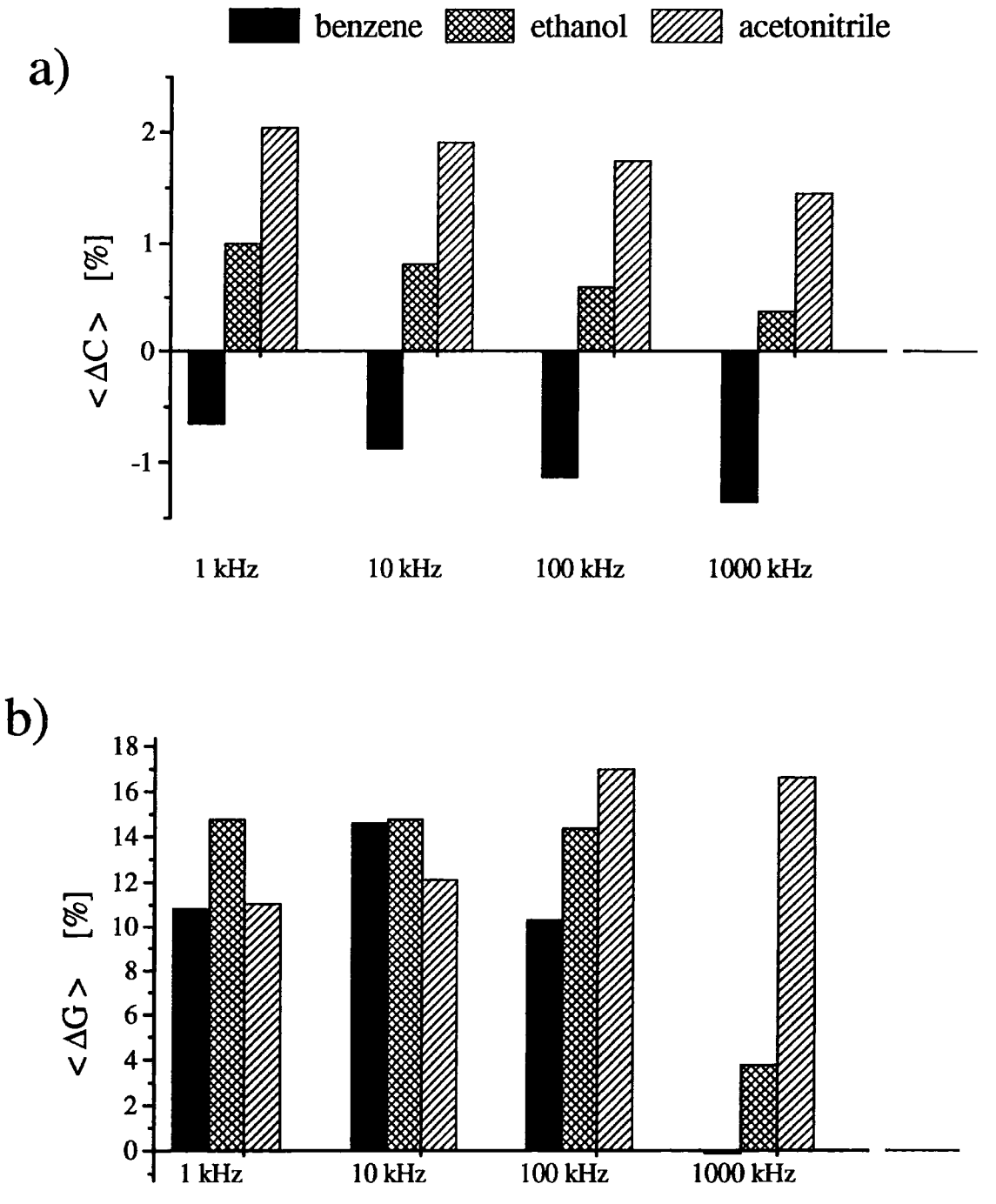

Figure 8.14: Average changes, calculated from equation 8.18, of (a) the capacitance and (b) the conductance measured at four different frequencies for three different vapours.

8.9 Summary

A study of the capacitance and conductance of poly(CuMBSH) LB film has been reported and an interpretation in terms of dielectric relaxation theory has been provided.

Reversible changes in the electrical admittance on exposure to organic vapours (ethanol, acetonitrile and benzene) and to water vapour were observed. For the organic vapours, the results were discussed in terms of the polarity of the vapour molecules; changes in the orientation ability of the polymer molecules, induced by the organic solvent; and swelling of the LB films. Water vapour was found to produce a very different response and a model based on low-frequency dispersion has been suggested.

An evaluation of the device for gas sensing applications has been given, with an estimation of the sensitivity and selectivity of the sensors. The unique response to the water vapour may be a useful way to discriminate it from the other vapours.

References

[1] U.Oertel, J.Nagel, *Thin Solid Films*, **284-285** (1996) 313.

[2] J.Nagel, U.Oertel, *Thin Solid Films*, in press.

[3] J.N.Wilde, *Optical sensing of organic vapours using Langmuir-Blodgett films*, 1998, PhD thesis, University of Durham.

[4] J.N.Wilde, A.J.Wigman, J.Nagel, J.Beeby, B.Tanner, M.C.Petty, *Acta Polymerica*, **49** (1998) 294.

[5] J.N.Wilde, J.Nagel, M.C.Petty, *Thin Solid Films*, in press.

[6] R.H.Cole, J.G.Berberian, S.Mashimo, G.Chryssikos, A.Burns, E.Tombari, *J.Appl.Phys.*, **66** (1989) 793.

[7] Y.Feldman, A.Adrianov, E.Polygalov, I.Ermolina. G.Romanychev, Y.Zuev, B.Milgotin, *Rev.Sci.Instrum.*, **67** (1996) 3208.

[8] A.K.Jonscher, *Universal relaxation law*, 1996, Chelsea Dielectric Press, London.

[9] R.C.West, M.J.Astle, *CRC handbook of chemistry and physics*, vol.59, CRC Press, Boca Raton, FL, 1978, pp.E63.

Chapter 9

CONCLUSIONS AND SUGGESTIONS FOR FURTHER WORK

9.1 Conclusions

An investigation of the electrical behaviour of thin films of four organic compounds has been undertaken. The materials chosen belong to distinct classes of materials: (i) organometallic complexes; (ii) conducting polymers; (iii) polysiloxanes; and (iv) co-ordination polymers. Because of their distinct chemical and physical properties, different techniques were required to form thin films of these compounds.

Thin layers of the tetrabutylammonium $Ni(dmit)_2$ complex mixed with tricosanoic acid (necessary to improve the film quality) were deposited using the LB technique. The AC conductivity was studied both in the in-plane and out-of-plane directions. A high anisotropy in the conductivity was found ($\sigma_{//}/\sigma_{\perp} \sim 10^5$ at 10 Hz) which was attributed to the presence of the fatty acid. The AC conductivity also exhibited different behaviour in the two directions. In the out-of-plane direction, a power law relationship on the frequency $\sigma_{AC} \propto \omega^n$, with n dependent on the amount of fatty acid, was found. However the in-plane conductivity was independent on the frequency. Due to problems of reproducibility over a long period, investigations on vapour sensing were not undertaken using this material.

Thin films of polypyrrole (PPy) mixed with palmitic acid were obtained using the LB technique followed by two solid state reactions. The films' structure was studied using X-ray diffraction, surface profiling and AFM. Although the films were found to possess a high degree of disorder, a large anisotropy in the conductivity was observed

($\sigma_{DC//}/\sigma_{DC\perp}$~$10^7$), indicating that the PPy tends mainly to be located between the layers of fatty acid. The AC and DC conductivities were measured over the temperature range 90 - 300 K. A variable range hopping model provided a good description of the DC behaviour. The AC conductivity was interpreted in terms of a Cole-Davidson function.

For measurements with vapours, thin films of PPy/PA were deposited on IDE structures and exposed to ethanol, acetonitrile, benzene and water vapour. The vapour concentrations were in the range 10^2 - 7×10^4 ppm. Reversible and reproducible changes in the admittance were observed. During exposure to the organic vapours a decrease of the conductance only was observed. in contrast, after exposure to water vapour, a reversible increase of the capacitance was also noted. The observed changes were mainly attributed to a charge transfer process between the polymer and vapour molecules. An evaluation of the gas sensing characteristics of the sensor was given. The device showed a good sensitivity to organic vapours at room temperature but poor selectivity. However, the unique changes of the capacitance observed during the exposure to water vapour could be useful in sensing applications.

The permittivity of polycyanopropylmethylsiloxane (PCMS) was measured over the temperature range 298-193 K. The results were interpreted as the superposition of two dielectric relaxations plus a DC conductivity, attributed to impurity ions. The two relaxations were thought to be associated with dipoles on the main chain (α) and those on the lateral chains (β). At room temperature the two relaxations merged.

Cast PCMS films were deposited on IDEs for the measurement of their vapour sensitivity. Reversible and reproducible changes were observed for benzene, acetonitrile, ethanol and water. These were interpreted in terms of a bulk dissolution of vapour into the polymer film and were found to be related to the dipole moment of the vapour molecules. A simple model to estimate the change of capacitance induced by different vapours based on their permittivities and partition coefficients was proposed. Using data available in the literature for the partition coefficient of ethanol in PCMS, the theoretical

change was found to be the same order of magnitude to that measured in the experiments. The PCMS device showed a quite good sensitivity to the organic vapours together with a selective response at different frequencies, which could be used to distinguish between non-polar and polar solvents. The response to water vapour was found to have a particular frequency behaviour which could prove useful in its discrimination.

The admittance of LB films of a co-ordination polymer 5,5′ methylenebis (N-hexadecylsalicydeneamine) (MBSH) in the out-of-plane direction was measured on varying the temperature over the range 235-298 K. An interpretation in terms of dielectric relaxation theory was provided.

Reversible changes in the admittance during exposure to organic vapours (benzene, acetonitrile and ethanol) and to water vapour were observed. The electrodes used were arranged in sandwich structure (Au/poly(CuMBSH)/Al), and the observed changes were attributed to a bulk dissolution of the vapours inside the films. For the organic vapours, the effects were discussed in terms of the polarity of the vapour molecules, changes in the orientational ability of the polymer molecules, induced by the organic solvent molecules and swelling of the LB films. Water vapour was found to produce a very different response and an explanation based on low-frequency dispersion was suggested. For gas sensing applications, the device showed good sensitivity together with a useful selectivity, arising from the different frequency behaviour. The changes observed during the exposure to water also showed a unique response that could be useful for its discrimination from other vapours.

9.2 Potential of the studied materials for use as gas sensors

A preliminary evaluation of the potential of the materials for use as gas sensors can be given using the results from this thesis. For practical gas sensing applications three key

properties need to be considered. These are: sensitivity, stability and selectivity, which are determined mainly by the chemically sensitive layer present in the device.

For the first material (i.e. the organometallic complex), the reproducibility and the stability of the material deposited using the LB technique does not seem to be very promising for a commercial application. A study of its gas sensitivity was not possible so its potential cannot be discussed further.

The stability of the other three materials seems to be quite good. The best stability was shown by the polysiloxane and co-ordination polymer films. In the case of PPy a slight decrease of the conductivity with aging was observed. However, a study of the longer term stability (in particular using 'non-controlled' atmospheres) is necessary to provide a full assessment of all the materials investigated in this work.

The minimum estimated sensitivities of the other three devices were compared with the maximum exposure limits, fixed from current legislation. The relevant figures are reported in table 9.1. It is evident that none of the three materials would be appropriate for the detection of benzene but all should be able to detect acetonitrile and, with a large margin, ethanol. The sensing layers most widely used in commercial conductometric gas sensors are based on metal-oxides. These can detect low concentrations of organic solvent vapours by changes of their DC conductivity (0.5 ppm of benzene [1], 0.1 ppm of ethanol [2], 1 ppm ethanol [3], 10 ppm benzene [4]). Although AC measurements are suggested as a possible means of increasing selectivity, electrical data were not available in the literature to make a comparison with the organic films [5, 6].

To investigate the selectivity of the devices an investigation using a larger number of vapours would be necessary. From the experiments undertaken the selectivity of the devices seems to be related to the polarity of the vapours. The polypyrrole device was the less selective, exhibiting a frequency independent change of the conductance and a change of the capacitance only during exposure to water vapour. An improved response

for this device may be obtained working over a different range of frequencies. On the other hand, the polysiloxane and co-orditation polymer devices displayed reasonable selectivity. For different vapours a different frequency response in both conductance and capacitance was observed. Therefore, monitoring the change of conductance and capacitance at several frequencies could be exploited to discriminate between vapours.

Considering the overall characteristics of the devices the materials that seem promising for use in gas sensors (based on AC measurements) are the polysiloxane and the co-ordination polymer.

Vapour	Estimated minimum detectable concentration (ppm)			Maximum exposure limits (ppm)	
	PPy/Pa	*PCMS*	*Poly(CuMBSH)*	*Long term*	*Short term*
Benzene	90	15	60	5	15
Acetonitrile	7	2	1	40	60
Ethanol	8	5	4	1000	3000

Table 9.1: Estimated minimum detectable concentrations using the three different devices and maximum exposure limits from the occupational exposure regulation EH40/97. The reported figures of the estimated minimum detectable concentration are the smaller of the values from the different measurements (i.e. capacitance or conductance). The long and short term exposure limits represent the time weighted average concentrations over a period of eight hours and fifteen minutes, respectively. In each reference period the exposure should not exceed three times the short term limit.

9.3 Suggestions for further work

In this work, we have attempted to gain an insight into the physical mechanisms responsible for the observed changes on exposure to vapours. Further understanding may be obtained by measuring other physical parameters. In particular, it would be very useful to know the quantity of vapour dissolved inside the film in relation to the observed changes. This could be estimated by a simultaneous measurement of the change of the mass during vapour exposure.

Moreover, it could be useful to extend the range of frequencies over which the AC measurements were taken. For example, lower frequencies would allow a better analysis of the changes observed during exposure to water vapour for poly(CuMBSH). An extension to higher frequencies would permit the entire relaxation to be observed for PCMS.

Due to limited time, only four different vapours were studied in this work. An extension to a larger number of solvents would provide further information. By choosing different vapours having the same dipole moment, an analysis of the similarities and differences in the observed changes would give an indication of the influence of other vapour characteristics (e.g. molecular dimensions).

An evaluation of the gas sensing characteristics of devices studied in this thesis has been given. From this, it is clear that further optimisation is needed for practical applications.

First, the long term stability (i.e. over months or years) must be measured to understand the limits of the materials used.

Secondly, an increase in the sensitivity is essential for the detection of some important vapours, such as benzene. A higher accuracy in the measurement of the admittance should be obtained by the design of devices operating at a single frequency [7]. The

selectivity of the sensor could be improved by the use of an array of devices (each working at a fixed frequency). However, this approach would require a complicated design for the sensor.

An alternative is to obtain a higher sensitivity for specific vapours (e.g. to benzene). This requires a sensitive material with a greater partition coefficient. One strategy could exploit the results of Haug et al [8]. This showed, by using polysiloxanes with different functional groups, that the partition coefficients are dependent both on the polarity of the functional groups of the polymer and on the organic solvents. In particular, the partition coefficient of non-polar/polar solvents is higher in non-polar/polar polymers.

The array approach has already been exploited in commercial sensor applications (i.e. electronic 'nose') [9-12]. However, such devices invariably use DC resistivity changes and sensing elements that are not particularly specific. The methods outlined above (i.e. using highly selective sensing elements and monitoring admittance changes at different frequencies) should reduce the number of individual sensing elements required in the array and significantly decrease the complexity of the system.

References

[1] S.Nicoletti, I.Elmi, L.Dori, G.C.Cardinali, C.Summonte, M.Leoni, *Eurosensors XII vol.2*, (ed.N.M.White), 1998, IOP Publishing, Bristol, 1017.

[2] H.Pink, L.Treitinger, L.Vité, *Jpn.J.Appl.Phys.*, **19** (1980) 513.

[3] See Figaro Sensors catalogue, model TGS2600.

[4] See Figaro Sensors catalogue, model TGS822.

[5] W.Göpel, K.D.Schierbaum, *Sensors and Actuators B*, **26-27** (1995) 1.

[6] U.Weimar, W.Göpel, *Sensors and Actuators B*, **26-27** (1995) 13.

[7] C.Cornila, A.Hielemann, R.Lenggenhager, P.Malcovati, H.Baltes, G.Noetzel, U.Weimar, W.Göpel, *Sensors and Actuators B*, **24-25** (1995) 357.

[8] M.Haug, K.D.Schierbaum, H.E.Endres, S.Drost, W.Göpel, *Sensors and Actuators A*, **32** (1992) 326.

[9] See Aromascan catalogue, model A32/8.

[10] K.C.Persaud, P.Travers, Intelligent instruments & Computers, July/August (1991) 147.

[11] J.V.Hatfield, P.Neaves, P.J.Hicks, K.Persaud, P.Travers, *Sensors and Actuators B*, **18-19** (1994) 221.

[12] K.C.Persaud, S.M.Khaffaf, J.S.Payne, A.M.Pisanelli, D.H.Lee, H.G.Byun, *Sensors and Actuators B*, **35-36** (1996) 267.

Appendix A

COMPUTER PROGRAMS

All the programs included in this appendix were written in Turbo Pascal. The software was used for acquiring the data from the Impedance Analyser HP4192A by an IEEE488 inteface. The data were measured versus the frequency or at a fixed frequency versus time.

program vric;{program to acquire data from the HP4192A Impedance Analyser using an IEEE488 IOTech interface};
{last modified by R.Casalini, June 1996}

```
uses
ieeeio,Crt,dos,gdriver,gkernel,gwindow,gshell,screen2,vahca
l,printer,graph;

type calfile=array[1..131] of string[12];
     dataarray=array[1..131] of real;


var  grdriver,grmode,error,terminate,a,n,regime,freqcount,
     cycle,rev,j,code:integer;
     C,w,tand,gm,bm,go,bo,freq,rm,xm,z:dataarray;
     disk:text;
     answer:char;
     info,fileinfo1,fileinfo2,filename,rubbish,dataname,
     amplitude,dcbias:string;
     dirinfo:searchrec;
     name:calfile;
     aplot,bplot,cplot:plotarray;
     escape,abort:boolean;
     s,g,i,start:integer;
     scandel:real;
     hour,minute,second,sec100:word;

procedure strip(var data:string);{strips leading nulls from
string}
var c:integer;
     begin
          c:=1;
          repeat;
          c:=c+1;
          until copy(data,c,1)<>chr(0);
          data:=copy(data,c,length(data)-c);
     end;

procedure abortrun(var abort:boolean);
     begin
          if keypressed<>false then begin
          answer:=readkey;
          if (answer='a') or (answer='A') then abort:=true;
     end;
     end;

procedure getdata(var
gm,bm,freq:dataarray;freqcount,cycle:integer);
{waits for 4192A to make measurement and reads data string}
var   data:string;
      code:integer;
```

```
      c,i,cy:integer;
      x,y,z:real;
      hour,minute,second,sec100:word;
begin
abort:=false;
for cy:=1 to cycle do begin
   GetTime(hour,minute,second,sec100);
   writeln(minute,second,sec100);
   for i:=1 to trunc(scandel) do delay(30143);{with i=1 to
25 and delay(30143) waits 5 mins}
   GetTime(hour,minute,second,sec100);
   writeln(minute,second,sec100);
   for c:=1 to freqcount do begin
      {GetTime(hour,minute,second,sec100);}
      {writeln(minute,second,sec100);}
      {for i:=1 to 2 do delay(30143);}{with i=1 to 25 and
delay(30143) waits 5 mins}
      {GetTime(hour,minute,second,sec100);}
      {writeln(minute,second,sec100);}
      x:=0;
      y:=0;
      z:=0;
      if cy=1 then gm[c]:=0;  {zero dataarray element only
for first cycle}
      if cy=1 then bm[c]:=0;
      if abort=false then for i:=1 to 1 do begin
         abortrun(abort);
         if abort=false then begin
            code:=0;
            writeln(ieeeout,'RESET'); {resets GPIB}
            writeln(ieeeout,'OUTPUT
HP;D1FR',freq[c]:1:4,'EN'); {outputs spot freq}
            repeat;
               writeln(ieeeout,'STATUS');  {checks status}
               readln(ieeein,data);        {line for     }
               strip(data);                {measurement  }
            until (copy(data,11,1)='1');{complete sign -
should be character 12!!}
            writeln(IeeeOut,'ENTER HP');{trashes    }
            readln(IeeeIn,data);        {data       }
            writeln(ieeeout,'ENTER HP');
            readln(ieeein,data);
            strip(data);
            writeln(data);
            val(copy(data,4,11),x,code);   {reads data}
            val(copy(data,20,11),y,code);  {into      }
            val(copy(data,33,10),z,code);  {arrays    }
            if code<>0 then writeln('Error in data string
from 4192A.');
            {checks for errors in converting string to
number}
```

```
            gm[c]:=gm[c]+x;
            bm[c]:=bm[c]+y;
            freq[c]:=z;
         end;
      end;
   end;
end;
for c:=1 to freqcount do begin
   gm[c]:=gm[c]/1/cycle;
   bm[c]:=bm[c]/1/cycle;
end;
end;

procedure lowertouppercase(var filename:string);
var  code,n:integer;
     ss:char;
     s:string[1];

begin
   for n:=1 to length(filename) do begin
      s:=copy(filename,n,1);
      ss:=s[1];
      ss:=upcase(ss);
      s:=ss;
      delete(filename,n,1);
      insert(s,filename,n);
   end;
end;


procedure diskwrite(var
disk:text;gm,bm,freq,C,tand,w,rm,xm:dataarray;

freqcount,j:integer;dataname:string);
var i,tt:integer;
    filename,t:string;
    answer:char;
    n,k:integer;
    f:file;

begin
clrscr;
tt:=0;
str(j,t);
repeat
   n:=1;
   filename:=dataname+t;
   lowertouppercase(filename);
   findfirst(filename+'.dat',archive,dirinfo);
   while doserror=0 do begin
      if filename+'.DAT'=dirinfo.name then begin
```

```
          val(t,tt,code);
          tt:=tt+1;          {checks for existing
batch(1..n).dat files}
          str(tt,t);         {and begins numbering from n+1}
          filename:='au'+t;
          n:=0;
       end;
       findnext(dirinfo);
   end;
until n=1;
assign(disk,filename+'.dat');
rewrite(disk);
writeln(disk,'Measured and corrected data, order is
freqcount');
writeln(disk,'and then G, B, frequency, C, tand, w, rm,
xm.');
writeln(disk,freqcount);
for i:=1 to freqcount do begin

write(disk,gm[i],chr(9),bm[i],chr(9),freq[i],chr(9),C[i],ch
r(9));

writeln(disk,tand[i],chr(9),w[i],chr(9),rm[i],chr(9),xm[i])
;
end;
close(disk);
end;

procedure rcompdiskwrite(var
disk:text;gm,bm,freq,C,tand,w:dataarray;

freqcount:integer;r:real;fname:string);
var i:integer;
    filename:string;
    answer:char;

begin
clrscr;
assign(disk,fname+'cmp');
rewrite(disk);
writeln(disk,'R compensated data (',r,' ohms subtracted),
order is freqcount');
writeln(disk,'and then G, B and frequency and then C,tand
and w.');
writeln(disk,freqcount);
for i:=1 to freqcount do begin
   writeln(disk,gm[i],bm[i],freq[i]);
   writeln(disk,C[i],tand[i],w[i]);
end;
close(disk);
end;
```

```
procedure autogetcalfile(archive:byte;var
dirinfo:searchrec;var name:calfile;
                                var go,bo,freq,z:dataarray;var
freqcount,rev:integer);
                                                {automatically reads
in calibration file}
var file_no,col_no,start_page,file_total,code,c:integer;
    number,trash:string;
    funckey:boolean;
    ch:char;

begin
findfirst('*.cal',archive,dirinfo);
file_total:=1;
while doserror=0 do begin
   name[file_total]:=dirinfo.name;
   findnext(dirinfo);
   file_total:=file_total+1;
end;
file_no:=trunc(z[j]);
writeln(file_no);
   assign(disk,name[file_no]);
   reset(disk);
   readln(disk,trash);
   readln(disk,trash);
   readln(disk,trash);
   val(trash,freqcount,code);
   readln(disk,trash);
   val(trash,cycle,code);
   writeln(freqcount,cycle);
   for c:=1 to freqcount do begin
      readln(disk,trash);
      val(copy(trash,1,17),go[c],code);
      val(copy(trash,18,17),bo[c],code);
      val(copy(trash,35,17),freq[c],code);
   end;
   if code<>0 then writeln('Error occurred when reading
calibration file.');
   close(disk);
end;

procedure displaycalfile(archive:byte;var
dirinfo:searchrec;var name:calfile);
var file_no,col_no,start_page,file_total,code,c:integer;
    number,trash:string;
    funckey:boolean;
    ch:char;

begin
findfirst('*.cal',archive,dirinfo);
file_total:=1;
```

```
while doserror=0 do begin
   name[file_total]:=dirinfo.name;
   findnext(dirinfo);
   file_total:=file_total+1;
end;
writeln;
start_page:=0;
clrscr;
file_no:=start_page;
writeln;
writeln('The following are existing calibration files');
writeln;
while (file_no<start_page+72) and (file_no<file_total) do
begin
   for col_no:=1 to 4 do begin
      file_no:=file_no+1;
      if file_no<file_total then write(file_no:3,')
':2,name[file_no]:12,' ');
   end;
   writeln;
end;
end;

procedure correctmeasurements(var
gm,bm,go,bo:dataarray;freqcount:integer);
var c:integer;
begin
for c:=1 to freqcount do begin
   gm[c]:=gm[c]-go[c];
   bm[c]:=bm[c]-bo[c];
end;

end;

procedure calcparameters(var
C,tand,w,rm,xm:dataarray;gm,bm,freq:dataarray;

freqcount:integer);
                        {calculates capacitance, tan delta
and angular freq}
   var i:integer;                    {resistance and
reactance}

   begin
   for i:=1 to freqcount do
     begin
     w[i]:=2*Pi*freq[i]*1000;
     C[i]:=bm[i]/w[i];
     rm[i]:=gm[i]/(gm[i]*gm[i]+bm[i]*bm[i]);
     xm[i]:=bm[i]/(gm[i]*gm[i]+bm[i]*bm[i]);
```

```
      if bm[i]<>0 then tand[i]:=gm[i]/bm[i] else
tand[i]:=999;
      end;
   end;

procedure
displayprintdatafile(filename:string;C,gm,bm,tand,w,freq,rm
,xm:dataarray;

freqcount:integer;fileinfo1,fileinfo2:string);
var freq_no,i,row_no,start_page,start_no,error:integer;
    title:string;
    funckey:boolean;
    ch:char;
begin
start_page:=0;
repeat
   funckey:=false;
   clrscr;
   freq_no:=start_page;
   writeln('Data in file ',filename);
   writeln('Order is G/siemens, B/siemens, freq/kHz, C/F,
tand, w/Hz, R/ohms, X/ohms.');
   writeln;
   while (freq_no<start_page+6) and (freq_no<freqcount+1)
do begin
      for row_no:=1 to 6 do begin
         freq_no:=freq_no+1;
         if freq_no<freqcount+1 then begin
            writeln('G ',gm[freq_no]:11,' B
',bm[freq_no]:11,' F ',freq[freq_no]:11,' C
',c[freq_no]:11);
            writeln('T ',tand[freq_no]:11,' w
',w[freq_no]:11,' R ',rm[freq_no]:11,' X ',xm[freq_no]:11);
         end;
         writeln;
       end;
    end;
    writeln('Press PgUp/PgDn for next/previous screen.');
    writeln('Press P to print.');
    ch:=readkey;
    if ch=#27 then escape:=true;
    if (ch='p') or (ch='P') then funckey:=false;
    if ch=#0 then begin
       ch:=readkey;
       if (ch=#73) and (start_page>=6) then
start_page:=start_page-6;
       if (ch=#81) and (start_page<freqcount+1) then
start_page:=start_page+6;
       if (ch=#73) or (ch=#81) then funckey:=true;
     end;
```

```
      if escape=true then funckey:=false;
until funckey=false;
if (ch='p') or (ch='P') then begin
   title:='Data in file '+filename;
   writeln(lst,title);
   error:=IOResult;
   if error=0 then begin
      writeln(lst,fileinfo1);
      writeln(lst,fileinfo2);
      writeln(lst,freqcount);
      for i:=1 to freqcount do begin
         writeln(lst,gm[i],' ',bm[i],' ',freq[i],' ',C[i],'
',tand[i],' ',w[i]);
      end;
      for i:=1 to 10 do writeln(lst);
   end
   else begin
      writeln('Printer off-line or out of paper.');
      repeat until(KeyPressed);
   end;
end;
end;

procedure
printdatafile(filename:string;C,gm,bm,tand,w,freq:dataarray
;

freqcount:integer;fileinfo1,fileinfo2:string);
   var     i,error:integer;
       title:string;
   begin
   title:='Data in file '+filename;
   {$I-}
   writeln(lst,title);
   error:=IOResult;
   {$I+}
   if error=0 then
      begin
      writeln(lst,fileinfo1);
      writeln(lst,fileinfo2);
      writeln(lst,freqcount);
      for i:=1 to freqcount do
         begin
         writeln(lst,gm[i],' ',bm[i],' ',freq[i],' ',C[i],'
',tand[i],' ',w[i]);
         end;
      for i:=1 to 10 do writeln(lst);
   end
   else
      begin
      writeln('Printer off-line or out of paper.');
```

```
      repeat until(KeyPressed);
    end;
  end;

procedure
printrxdatafile(filename:string;C,gm,bm,tand,w,freq:dataarr
ay;

freqcount:integer;aplot:plotarray;fileinfo1,fileinfo2:strin
g);
   var     n,error:integer;
       title:string;
   begin
   title:='Reactance vs resistance calculated from file
'+filename;
   {$I-}
   writeln(lst,title);
   error:=IOresult;
   {$I+}
   if error=0 then
     begin
        writeln(lst,'Order is X/ohms, R/ohms and
frequency/kHz.');
        for n:=1 to freqcount do
          begin
          writeln(lst,aplot[n,2],' ',aplot[n,1],'
',freq[n]);
          end;
        for n:=1 to 10 do writeln(lst);
     end
     else
        begin
           writeln('Printer off-line or out of paper.');
           repeat until(KeyPressed);
        end;
  end;

procedure
displayrxdata(filename:string;C,gm,bm,tand,w,freq:dataarray
;

freqcount:integer;fileinfo1,fileinfo2:string);
   var     ii,i,iii,iiii,iiiii,error:integer;
       title:string;
       funckey:boolean;
       ch:char;

   begin
   ii:=0;
   repeat
   funckey:=false;
```

```
   clrscr;
   iiiii:=ii;
   writeln;
   writeln('Data in file ',filename);
   writeln('Order is G/S,B/S,freq/kHz and then
C/F,tand,w/Hz.');
   writeln;

       while (ii<iiiii+6) and (ii<freqcount+1) do
       begin
       for iii:=1 to 6 do
       begin
       ii:=ii+1;
       if ii<freqcount+1 then
         begin
         writeln('G ',gm[ii],' B ',bm[ii],' F ',freq[ii]);
         writeln('C ',c[ii],' T ',tand[ii],' w ',w[ii]);
       end;
       writeln;
       end;
       end;
     writeln('Press PgUp/PgDn for next/previous screen.');
     writeln('Press P to print.');
      ch:=readkey;
     if ch=#27 then escape:=true;
     if (ch='p') or (ch='P') then funckey:=false;
     if ch=#0 then
      begin
      ch:=readkey;
      writeln(ii);
      if frac(ii/6)>0 then a:=6;
      if frac(ii/6)=0 then a:=12;
      if (ch=#73) and (ii<=6) then ii:=0;
      if (ch=#73) and (ii>10) then ii:=(6*trunc(ii/6))-a;
      if (ch=#81) and (ii<freqcount+1) then ii:=ii;
      if (ch=#81) and (ii>=freqcount+1) then
ii:=6*trunc(ii/6);
      funckey:=true;
      end;

      if escape=true then funckey:=false;
      until funckey=false;
      if (ch='p') or (ch='P') then
      begin
   title:='Data in file '+filename;
   {$I-}
   writeln(lst,title);
   error:=IOResult;
   {$I+}
   if error=0 then
      begin
```

```
      writeln(lst,fileinfo1);
      writeln(lst,fileinfo2);
      writeln(lst,freqcount);
      for i:=1 to freqcount do
         begin
         writeln(lst,gm[i],' ',bm[i],' ',freq[i],' ',C[i],'
',tand[i],' ',w[i]);
         end;
      for i:=1 to 10 do writeln(lst);
   end
   else
      begin
      writeln('Printer off-line or out of paper.');
      repeat until(KeyPressed);
   end;
   end;
  end;

procedure
plotdata(C,gm,tand,w,freq:dataarray;aplot,bplot,cplot:plota
rray;
                                  freqcount:integer);
              {plots data in graphical form}
  var n,i,error:integer;
               m:string;
               p:char;
             neg:boolean;
    begin
    neg:=false;
    for i:=1 to freqcount do if gm[i]<=0 then neg:=true;
    for i:=1 to freqcount do
      begin
      aplot[i,2]:=C[i];
      aplot[i,1]:=(ln(freq[i]*1000)/2.302585);
      if neg=true then bplot[i,2]:=gm[i];
      if neg=false then bplot[i,2]:=(ln(gm[i]))/2.302585;
      bplot[i,1]:=aplot[i,1];
      cplot[i,2]:=tand[i];
      cplot[i,1]:=aplot[i,1];
      end;
    entergraphic;
    setbackgroundcolor(1);
    defineheader(1,'Dielectric data in file'+filename);
    setheadertotop;
    drawborder;

    findworld(1,aplot,freqcount,1,1);

    drawaxis(1,1,0,30,0,20,0,0,false);

    setwindowmodeoff;
```

```
setcolorblack;
for i:=1 to 600 do
   begin
   for n:=1 to 4 do drawpoint(32+i,314+n);
   for n:=1 to 5 do drawpoint(10+i,320+n);
   end;
   setcolorwhite;
findworld(2,bplot,freqcount,1,1);
drawaxis(1,1,10,30,0,20,0,0,false);
setwindowmodeoff;
setcolorblack;
for i:=1 to 450 do
   begin
   for n:=1 to 4 do drawpoint(112+i,314+n);
   for n:=1 to 5 do drawpoint(96+i,320+n);
   end;
   setcolorwhite;
findworld(3,cplot,freqcount,1,1);
drawaxis(6,1,20,30,0,20,0,0,false);
drawpolygon(cplot,1,freqcount,7,3,0);
resetaxis;
findworld(1,aplot,freqcount,1,1);
 drawpolygon(aplot,1,freqcount,8,3,0);
 resetaxis;
 findworld(2,bplot,freqcount,1,1);
 drawpolygon(bplot,1,freqcount,2,3,0);
drawtext(2,10,1,'CAPACITANCE');
drawtext(10,20,1,'/F  (O)');
if neg=false then
begin
drawtext(80,10,1,'LOG(COND/S)');
drawtext(100,20,1,'(X)');
end;
if neg=true then
begin
drawtext(80,10,1,'CONDUCTANCE');
drawtext(95,20,1,'/S  (X)');
end;
drawtext(172,10,1,'TAN DELTA');
drawtext(185,20,1,'(*)');
m:='FILENAME = '+filename;
drawtext(300,10,1,m);
drawtext(450,10,1,'PRESS P TO PRINT');
drawtext(300,333,1,'LOG ( FREQUENCY/Hz )');
p:=readkey;
if (p='p') or (p='P') then
  begin
  {$I-}
  writeln(lst,'');
  error:=IOResult;
  {$I+}
```

```
      if error=0 then
      begin
      hardcopy(false,6);
      for i:=1 to 10 do writeln(lst);
      leavegraphic;

printdatafile(filename,C,gm,bm,tand,w,freq,freqcount,filein
fo1,

fileinfo2);
      end
      else
      begin
      leavegraphic;
      clrscr;
      writeln('Printer off-line or out of paper.');
      repeat until keypressed=true;
      end
      end
    else
    leavegraphic;
    end;

 procedure alphalist(i:integer;var name:calfile);
    var {swapp:calfile;}
    swapname:boolean;
           c:integer;
       swapp:string;

    begin

    repeat
    swapname:=false;
    for c:=1 to i-2 do
    begin
    if name[c]>name[c+1] then
    begin
    swapp:=name[c+1];
    name[c+1]:=name[c];
    name[c]:=swapp;
    swapname:=true;
    end;
    end;
    until swapname=false;
    end;

procedure getdatafile(archive:byte;var
dirinfo:searchrec;var name:calfile;
                      var
gm,bm,freq,C,tand,w,rm,xm:dataarray;var freqcount:integer;
```

```
                        var fileinfo1,fileinfo2:string; var
i:integer);

var
code,r,a,error:integer;
number,trash:string;
ch:char;
funckey:boolean;

begin
findfirst('*.dat',archive,dirinfo);
i:=1;
while doserror=0 do begin
   name[i]:=dirinfo.name;
   findnext(dirinfo);
   i:=i+1;
end;
findfirst('*.cmp',archive,dirinfo);
while doserror=0 do begin
   name[i]:=dirinfo.name;
   findnext(dirinfo);
   i:=i+1;
end;
findfirst('*.frq',archive,dirinfo);
while doserror=0 do begin
   name[i]:=dirinfo.name;
   findnext(dirinfo);
   i:=i+1;
end;
alphalist(i,name);
end;

procedure
displaydatafile(file_total:integer){(archive,dirinfo,name,g
m,bm,freq,C,tand,w,freqcount,

rm,xm,fileinfo1,fileinfo2)};
var code,i,file_no,col_no,start_page,a,error:integer;
    number,trash:string;
    ch:char;
    funckey:boolean;

begin
start_page:=0;
repeat
   clrscr;
   file_no:=start_page;
   writeln;
   writeln('The following are existing data files.');
   writeln;
```

```
   while (file_no<start_page+72) and (file_no<file_total)
do begin
      for col_no:=1 to 4 do begin
         file_no:=file_no+1;
         if file_no<file_total then write(file_no:3,')
':2,name[file_no]:12,'  ');
      end;
      writeln;
   end;
   writeln('Select a file number.');
   writeln('Press PgUp/PgDn for next/previous screen.');
   number:='';
   ch:=readkey;
   if ch=#27 then escape:=true;
   if ch=#0 then begin
      ch:=readkey;
      if (ch=#73) and (start_page>=72) then
start_page:=start_page-72;
      if (ch=#81) and (start_page<file_total) then
start_page:=start_page+72;
      if (ch=#73) or (ch=#81) then funckey:=true;
   end;
   if (ch>='0') and (ch<='9') then begin
      repeat
         number:=number+ch;
         write(ch);
         ch:=readkey;
      until ch=#13;
      writeln;
      val(number,file_no,code);
      funckey:=false;
      if (file_no<1) or (file_no>file_total-1) then
funckey:=true;
   end;
   if escape=true then funckey:=false;
until funckey=false;
if escape=false then begin
   filename:=name[file_no];
   assign(disk,name[file_no]);
   reset(disk);
   readln(disk,fileinfo1);
   readln(disk,fileinfo2);
   readln(disk,trash);
   val(trash,freqcount,code);
   for i:=1 to freqcount do begin
      readln(disk,trash);
      val(copy(trash,1,17),gm[i],code);
      val(copy(trash,19,17),bm[i],code);
      val(copy(trash,37,17),freq[i],code);
      val(copy(trash,55,17),C[i],code);
      val(copy(trash,73,17),tand[i],code);
```

```
      val(copy(trash,91,17),w[i],code);
      val(copy(trash,109,17),rm[i],code);
      val(copy(trash,127,17),xm[i],code);
   end;
   if code<>0 then writeln('Error occurred when reading
calibration file.');
   close(disk);
end;
end;

procedure
colecole(C,tand,gm,freq:dataarray;freqcount:integer;aplot:p
lotarray);

var code,m,n,i,error:integer;
    d,number:string;
    ch,p:char;
    Xbig,Xsmall,Rbig,Rsmall,minfreq,maxfreq,dummy:real;

begin
clrscr;
minfreq:=0;
maxfreq:=freq[freqcount];
writeln('                          Impedance Plot');
writeln('Enter frequency range.');
write('min frequency(kHz)=');
number:='';
ch:=readkey;
if ch=#27 then escape:=true;
m:=0;
repeat
   m:=m+1;
   if ((ch>='0') and (ch<='9')) or (ch='.') then
number:=number+ch;
   write(ch);
   ch:=readkey;
until ch=#13;
writeln('');
if m=1 then minfreq:=freq[1] else
val('0'+number,minfreq,code);
write('max frequency(kHz)=');
readln(maxfreq);
n:=1;
Xbig:=0;
Xsmall:=0;
Rbig:=0;
Rsmall:=0;
m:=0;
for i:=1 to freqcount do begin
   if (freq[i]>=minfreq) and (freq[i]<=maxfreq) then begin
      m:=m+1;
```

```
      {dummy:=-1/(w[i]*((1+((tand[i])*(tand[i])))*c[i]));}
{ Mike's line}
      dummy:=-bm[i]/(gm[i]*gm[i]+bm[i]*bm[i]);
      if dummy<0 then dummy:=dummy*-1;
      if dummy<>0 then aplot[m,2]:=ln(dummy)/2.302585 else
aplot[m,2]:=Xbig;
      if aplot[m,2]>Xbig then Xbig:=aplot[m,2];
      if aplot[m,2]<Xsmall then Xsmall:=aplot[m,2];

{dummy:=((tand[i])*(tand[i]))/(1+((tand[i])*(tand[i])))/gm[
i];} {Mike's line}
      dummy:=gm[i]/(gm[i]*gm[i]+bm[i]*bm[i]);
      if dummy<0 then dummy:=dummy*-1;
      if dummy<>0 then aplot[m,1]:=ln(dummy)/2.302585 else
aplot[m,2]:=Xbig;
      if aplot[m,1]>Rbig then Rbig:=aplot[m,1];
      if aplot[m,1]<Rsmall then Rsmall:=aplot[m,1];
      if Rsmall=0 then Rsmall:=aplot[m,1];
   end;
end;
entergraphic;
setbackgroundcolor(1);
defineheader(1,'log(-X/ohms) vs log(R/ohms) plot of data in
file'+filename);
setheadertotop;
drawborder;
defineworld(1,Rsmall,Xsmall,Rbig,Xbig);
selectworld(1);
{    findworld(1,aplot,freqcount,1,1);        }
drawaxis(1,1,0,30,0,20,0,0,false);
drawpolygon(aplot,1,m,8,3,0);
drawtext(2,10,1,'LOG(-X/OHMS)');
{    drawtext(10,20,1,'/OHMS');}
d:='FILENAME = '+filename;
drawtext(300,10,1,d);
drawtext(450,10,1,'PRESS P TO PRINT');
drawtext(300,333,1,'LOG(R/OHMS)');
p:=readkey;
if (p='p') or (p='P') then begin
   {$I-}
   writeln(lst,'');
   error:=IOResult;
   {$I+}
   if error=0 then begin
      hardcopy(false,6);
      for i:=1 to 10 do writeln(lst);
      leavegraphic;

printrxdatafile(filename,C,gm,bm,tand,w,freq,freqcount,aplo
t,fileinfo1,
```

```
fileinfo2);
   end
   else begin
      leavegraphic;
      clrscr;
      writeln('Printer off-line or out of paper.');
      repeat until keypressed=true;
   end;
end;
leavegraphic;
end;


procedure
admittanceplot(C,tand,gm,freq:dataarray;freqcount:integer;a
plot:plotarray);

var m,n,i,error:integer;
    d:string;
    p:char;
    Xbig,Xsmall,Rbig,Rsmall,minfreq,maxfreq,dummy:real;
begin
clrscr;
minfreq:=0;
maxfreq:=freq[freqcount];
writeln('Enter frequency range.');
write('min frequency(kHz)=');
readln(minfreq);
write('max frequency(kHz)=');
readln(maxfreq);
m:=0;
n:=1;
Xbig:=0;
Xsmall:=0;
Rbig:=0;
Rsmall:=0;
for i:=1 to freqcount do begin
   if (freq[i]>=minfreq) and (freq[i]<=maxfreq) then begin
      m:=m+1;
      dummy:=bm[i];
      if dummy<0 then dummy:=dummy*-1;
      aplot[m,2]:={ln}(dummy){/2.302585};
      if aplot[m,2]>Xbig then Xbig:=aplot[m,2];
      if aplot[m,2]<Xsmall then Xsmall:=aplot[m,2];
      dummy:=gm[i];
      if dummy<0 then dummy:=dummy*-1;
      aplot[m,1]:={ln}(dummy){/2.302585};
      if aplot[m,1]>Rbig then Rbig:=aplot[m,1];
      if aplot[m,1]<Rsmall then Rsmall:=aplot[m,1];
      if Rsmall=0 then Rsmall:=aplot[m,1];
```

```
   end;
end;
entergraphic;
setbackgroundcolor(1);
defineheader(1,'Admittance plot of data in file'+filename);
setheadertotop;
drawborder;
defineworld(1,Rsmall,Xsmall,Rbig,Xbig);
selectworld(1);
{findworld(1,aplot,freqcount,1,1);}
drawaxis(1,1,0,30,0,20,0,0,false);
drawpolygon(aplot,1,m,8,3,0);
drawtext(2,10,1,'B/S');
{drawtext(10,20,1,'/OHMS');}
d:='FILENAME = '+filename;
drawtext(300,10,1,d);
drawtext(450,10,1,'PRESS P TO PRINT');
drawtext(300,333,1,'G/S');
p:=readkey;
if (p='p') or (p='P') then begin
   writeln(lst,'');
   error:=IOResult;
   if error=0 then begin
      hardcopy(false,6);
      for i:=1 to 10 do writeln(lst);
      leavegraphic;
{printrxdatafile(filename,C,gm,bm,tand,w,freq,freqcount,apl
ot,fileinfo1,fileinfo2);}
    end
    else begin
       leavegraphic;
       clrscr;
       writeln('Printer off-line or out of paper.');
       repeat until keypressed=true;
    end
end
else leavegraphic;
end;


procedure admittancecompensation;
var code,i:integer;
    funckey:boolean;
    number:string;
    ch:char;
    gs,bs,gb,cb:real;

begin
clrscr;
writeln('This routine will compensate for series barrier
phenomena in');
```

```
writeln('the data in file ',filename);
writeln('The data will then be stored in a file with
extension .cmp.');
repeat
   funckey:=false;
   writeln('Enter the value of barrier conductance/S.');
   number:='';
   ch:=readkey;
   if ch=#27 then escape:=true;
   if (ch>='0') and (ch<='9') then begin
      funckey:=true;
      repeat
         number:=number+ch;
         write(ch);
         ch:=readkey;
      until ch=#13;
      writeln('');
      val(number,gb,code);
   end;
   if escape=true then funckey:=true;
until funckey=true;
if escape=false then begin
    repeat
       funckey:=false;
       writeln('Enter the value of barrier
capacitance/F.');
       number:='';
       ch:=readkey;
       if ch=#27 then escape:=true;
       if (ch>='0') and (ch<='9') then begin
          funckey:=true;
          repeat
             number:=number+ch;
             write(ch);
             ch:=readkey;
          until ch=#13;
          writeln('');
          val(number,cb,code);
       end;
       if escape=true then funckey:=true;
    until funckey=true;
    if escape=false then begin
       for i:=1 to freqcount do begin
          gs:=((gm[i]*gb)-(w[i]*w[i]*c[i]*cb))/(gb-gm[i]);
          bs:=((gm[i]*cb)+(gb*C[i]))/(cb-c[i]);
          gm[i]:=gs;
          bm[i]:=bs;
       end;
    end;
end;
assign(disk,copy(filename,1,pos('.',filename))+'cmp');
```

```
rewrite(disk);
writeln(disk,'Compensated data, order is freqcount');
writeln(disk,'and then G, B and frequency and then C,tand
and w.');
writeln(disk,freqcount);
for i:=1 to freqcount do begin
   writeln(disk,gm[i],bm[i],freq[i]);
   writeln(disk,C[i],tand[i],w[i]);
end;
close(disk);
end;

procedure
rxcalc(C,tand,gm,freq:dataarray;freqcount:integer;var
aplot:plotarray);

var n:integer;
begin
for n:=1 to freqcount do begin
   aplot[n,2]:=-1/(w[n]*((1+((tand[n])*(tand[n])))*c[n]));

aplot[n,1]:=((tand[n])*(tand[n]))/(1+((tand[n])*(tand[n])))
/gm[n];
end;
end;

procedure
rcompensation(filename:string;C,gm,bm,tand,w,freq:dataarray
;

aplot:plotarray;freqcount:integer);
var code,i:integer;
    r:real;
    number,fname:string;
    funckey:boolean;
    ch:char;

begin
repeat
   funckey:=false;
   clrscr;
   writeln('This routine will subtract a fixed value of
resitance from');
   writeln('the data in file ',filename);
   writeln('The data will then be stored in a file with
extension .cmp.');
   writeln('Enter the value of resistance (ohms) to be
subtracted.');
   number:='';
   ch:=readkey;
   if ch=#27 then escape:=true;
```

```
   if (ch>='0') and (ch<='9') then begin
      funckey:=true;
      repeat
         number:=number+ch;
         write(ch);
         ch:=readkey;
      until ch=#13;
      writeln('');
      val(number,r,code);
   end;
   if escape=true then funckey:=true;
until funckey=true;
if escape=false then begin
   for i:=1 to freqcount do begin
      aplot[i,2]:=(-
1/(w[i]*((1+((tand[i])*(tand[i])))*c[i])));

aplot[i,1]:=(((tand[i])*(tand[i]))/(1+((tand[i])*(tand[i]))
)/gm[i])-r;
   end;
   for i:=1 to freqcount do begin
      tand[i]:=aplot[i,1]/sqrt(sqr(aplot[i,2]))
   end;
   for i:=1 to freqcount do begin
      gm[i]:=(sqr(tand[i])/(1+sqr(tand[i])))/aplot[i,1];
      bm[i]:=(1/((1+sqr(tand[i]))*aplot[i,2]))*-1;
      C[i]:=bm[i]/w[i];
   end;
   fname:=copy(filename,1,pos('.',filename));

rcompdiskwrite(disk,gm,bm,freq,C,tand,w,freqcount,r,fname);
end;
end;

procedure logsweep;

var strfrq,stofrq,p,pp:real;
    cycle, z,k,s,n,i:integer;
    filename:string;
    freq:dataarray;
    disk:text;
begin
clrscr;
repeat
   n:=1;
   writeln('The frequency points will be stored in .frq
file. Enter file name.');
   readln(filename);
   k:=length(filename);
   if copy(filename,k-3,4)='.frq' then begin
      n:=0;
```

```
      writeln('Do not include .frq in filename');
   end;
   if filename='' then n:=0;
   lowertouppercase(filename);
   findfirst(filename+'.frq',archive,dirinfo);
   while doserror=0 do begin
      if filename+'.FRQ'=dirinfo.name then begin
         writeln('A file with that name already exists.');
         n:=0;
      end;
      findnext(dirinfo);
   end;
until n=1;
writeln('Logarithmic sweep(1) or Linear sweep(2)');
readln(z);
writeln('Enter start frequency in Hz');
writeln('Minimum frequency is 5 Hz');
readln(strfrq);
writeln('Enter stop frequency in Hz');
writeln('Maximum frequency is 13e6 Hz i.e. 13 MHz');
readln(stofrq);
writeln('Enter number of steps for frequency interval');
readln(s);
cycle:=1;
assign(disk,filename+'.frq');
rewrite(disk);
writeln;
writeln(disk,'Frequency regime, frequency in kHz.');
writeln(disk,s+1);
writeln(disk,cycle);
if z=1 then for i:= 0 to s do begin
   p:= (ln(stofrq/1000)-ln(strfrq/1000))/2.303/s;
   pp:=ln(strfrq/1000)/2.303 + p*i;
   freq[i]:=(round(exp(pp*2.303)*1000))/1000;
   writeln(disk,freq[i]:5:6);
end;
if z=2 then for i:=0 to s do begin
   p:=(stofrq-strfrq)/1000/s;
   freq[i]:=strfrq/1000 + p*i;
   writeln(disk,freq[i]:5:6);
end;
close(disk);
writeln('Frequency file has been generated.');
repeat until keypressed;
end;


begin   {*************** main programme*****************}
 grdriver:=detect;
 initgraphic;
 leavegraphic;
```

```
 terminate:=0;
 textbackground(blue);

getdatafile(archive,dirinfo,name,gm,bm,freq,C,tand,w,rm,xm,
freqcount ,

fileinfo1,fileinfo2,i);
 start:=0;
 repeat
 repeat
 if start=0 then screen;
 start:=0;

 clrscr;
 writeln('Select an option.');
 writeln;
 writeln;
 writeln('1) Create calibration file.');
 writeln;
 writeln('2) Measure dielectric data.');
 writeln;
 writeln('3) Plot data file.');
 writeln;
 writeln('4) Print data file.');
 writeln;
 writeln('5) Impedance Plot.');
 writeln;
 writeln('6) Print X vs R.');
 writeln;
 writeln('7) Resistance compensation.');
 writeln;
 writeln('8) Admittance Plot.');
 writeln;
 writeln('9) Print B vs G.');
 writeln;
 writeln('A) Automatic Linear/Logsweep frequency file
generation.');
 writeln;
 writeln('B) Terminate program.');
 for g:=1 to 100 do
   begin
   for s:=1 to 10000 do
    begin
    if keypressed=true then start:=1;
    if start=1 then g:=100;
    if start=1 then s:=10000;
    end;
    end;
 if start=1 then answer:=readkey;
 until start=1;
 start:=0;
```

```
 if answer='b' then answer:='B';
 if answer='a' then answer:='A';
 case answer of
  '1' :
       begin
       {$I-}
       writeln(ieeeout,'ENTER HP');
       readln(ieeein,info);
       error:=IOResult;
       {$I+}
       if error=0 then
       begin
       escape:=false;
       cal4192A;
       start:=1;
       end

       else
       begin
       clrscr;
       writeln('4192A Imedance Analyser is off-line.');
       repeat until keypressed;
       end;
       start:=1;
       end;
  '2' :
       begin
       clrscr;
       writeln('Enter filename for data');
       readln(dataname);
       writeln('Enter required amplitude of a.c. test
signal');
       readln(amplitude);
       writeln('Enter required d.c. bias');
       readln(dcbias);
       writeln('Enter required delay between scans in
minutes');
       writeln('If only one scan is required enter 0');
       readln(scandel);
       scandel:=5*scandel;
       if scandel=0 then scandel:=1;
       writeln(ieeeout,'ENTER HP');
       readln(ieeein,info);
       error:=IOResult;
       if error=0 then begin
          clrscr;
          escape:=false;
          rubbish:='';
          displaycalfile(archive,dirinfo,name);
          writeln('Enter calibration file numbers pressing
return after each number');
```

```
            writeln('Enter * after completing final entry');
            rev:=0;
            while rubbish <> '*' do begin
               rev:=rev+1;
               write(rev,')');
               readln(rubbish);
               val(rubbish,z[rev],code);
            end;
            writeln(rev);
            for j:=1 to rev-1 do begin
               GetTime(hour,minute,second,sec100);
               writeln(minute,second,sec100);
               for i:=1 to 2 do delay(30143);{with i=1 to 25
and delay(30143) waits 5 mins}
               GetTime(hour,minute,second,sec100);
               writeln(minute,second,sec100);

autogetcalfile(archive,dirinfo,name,go,bo,freq,z,freqcount,
rev);
               if escape=false then begin
                  clrscr;
                  writeln('Acquiring data, please wait');
                  writeln('To abort, press "A" and then
wait.');
                  writeln(ieeeout,'OUTPUT
HP;W0F1C3A2V1ZO0ZS0OL'+amplitude+'EN');
                  writeln(ieeeout,'OUTPUT
HP;BI'+dcbias+'EN');
                  getdata(gm,bm,freq,freqcount,cycle);
                  if abort=false then begin

correctmeasurements(gm,bm,go,bo,freqcount);

calcparameters(C,tand,w,rm,xm,gm,bm,freq,freqcount);

diskwrite(disk,gm,bm,freq,C,tand,w,rm,xm,freqcount,j,datana
me);

getdatafile(archive,dirinfo,name,gm,bm,freq,C,tand,w,rm,xm,
freqcount,

fileinfo1,fileinfo2,i);
                  end;
               end;
            end;
         end
         else begin
            clrscr;
            writeln('4192A Impedance Analyser is off-line.');
            repeat until keypressed;
         end;
```

```
        start:=1;
        end;
  '3' :
        begin
        escape:=false;

displaydatafile(i){(archive,dirinfo,name,gm,bm,freq,C,tand,
w,freqcount,

rm,xm,fileinfo1,fileinfo2)};
        if escape=false then
plotdata(C,gm,tand,w,freq,aplot,bplot,cplot,freqcount);
        start:=1;
        end;
  '4':
        begin
        escape:=false;

displaydatafile{(archive,dirinfo,name,gm,bm,freq,C,tand,w,f
reqcount,

rm,xm,fileinfo1,fileinfo2)}(i);
        if escape=false then
displayprintdatafile(filename,C,gm,bm,tand,w,freq,rm,xm,fre
qcount,fileinfo1,

fileinfo2);
        start:=1;
        end;
  '5':
        begin
        escape:=false;

displaydatafile{(archive,dirinfo,name,gm,bm,freq,C,tand,w,f
reqcount,

rm,xm,fileinfo1,fileinfo2)}(i);
        if escape=false then
colecole(C,tand,gm,freq,freqcount,aplot);
        start:=1;
        end;
  '6':
        begin
        escape:=false;

displaydatafile{(archive,dirinfo,name,gm,bm,freq,C,tand,w,f
reqcount,

rm,xm,fileinfo1,fileinfo2)}(i);
        if escape=false then begin
           rxcalc(C,tand,gm,freq,freqcount,aplot);
```

```
printrxdatafile(filename,C,gm,bm,tand,w,freq,freqcount,aplo
t,fileinfo1,

fileinfo2);

getdatafile(archive,dirinfo,name,gm,bm,freq,C,tand,w,rm,xm,
freqcount,

fileinfo1,fileinfo2,i);
        end;
        start:=1;
        end;
  '8':
        begin
        escape:=false;

displaydatafile{(archive,dirinfo,name,gm,bm,freq,C,tand,w,f
reqcount,

rm,xm,fileinfo1,fileinfo2)}(i);
        if escape=false then
admittanceplot(C,tand,gm,freq,freqcount,aplot);
        start:=1;
        end;
  '7':
        begin
        escape:=false;

displaydatafile{(archive,dirinfo,name,gm,bm,freq,C,tand,w,f
reqcount,

rm,xm,fileinfo1,fileinfo2)}(i);
        if escape=false then begin

rcompensation(filename,C,gm,bm,tand,w,freq,aplot,freqcount)
;

getdatafile(archive,dirinfo,name,gm,bm,freq,C,tand,w,rm,xm,
freqcount,

fileinfo1,fileinfo2,i);
           start:=1;
        end;
        end;
  'A':
      begin
      logsweep;

getdatafile(archive,dirinfo,name,gm,bm,freq,C,tand,w,rm,xm,
freqcount,
```

```
fileinfo1,fileinfo2,i);
      start:=1;
      end;
  'B':
       begin
       terminate:=1;
       clrscr;
       writeln('Bye bye.');
       end;
       end;
 until terminate=1;
end.
```

Program Sense5;
{programm for data acquisition and display data from HP4192A digital Impedance Analyser by IEEE488 IOTech}
{Aquisition of C and G versus time at 1kHz}
{The data are saved on disk and displyed on the screen}
{R.Casalini, March 1997}

```
uses ieeeio, Crt, dos, graph;

var
    IeeeOut,IeeeIn                                  : text;
    dvm1,points,aver1,j                             : integer;
    graphdriver, graphmode,x                        : integer;
    impC,impG,scale_pointC,scale_pointG             : real;
    instr1,cmdstr                                   : string;
    data,stardata,Cy,Gy                             : string;
    C_string,G_string                               : string;


procedure initialization_ieee;

begin
         {Initialization of the ieee488}

     Assign(IeeeOut,'IeeeOut'); Rewrite(IeeeOut);
     Assign(IeeeIn,'IeeeIn'); Reset(IeeeIn);
     RawMode(IeeeOut);
     RawMode(IeeeIn);
     IOCTL; {invoke ioctl procedure}
     Writeln(IeeeOut,'RESET');
     Writeln(IeeeOut,'FILL ERROR');
end;

procedure read_data;

var

code             :integer;

begin

     {writeln(IeeeOut,'RESET');}
     {writeln(IeeeOut,'OUTPUT HP;D1EN');}
     writeln(IeeeOut,'ENTER HP');
     readln(IeeeIn,data);
     stardata:=data;
     Cy:=copy(data,6,10); {take capacitance values}
     Gy:=copy(data,22,10); {take G values}
     val(Cy,impC,code);
     val(Gy,impG,code);
```

```
     str(impC,C_string);
     str(impG,G_string);
end;

procedure set_page;

var

     a,b,x_ticks,data_point,x_label,x_labelo      :integer;
     y_ticks                                      : real;
     x_string,y_string,x_stringo                  : string;

begin
     setbkcolor(8);
     setcolor(15);
     textcolor(15);
     setviewport (0,0,getmaxx,getmaxy,clipon);
     settextstyle (defaultfont,horizdir,1);
     settextjustify (centertext,centertext);
     moveto (25,10);
     lineto (25,310);
     lineto (625,310);
     a:=1;

     for a :=1 to 6 do
               begin
                    x_ticks := a * 100;
                    moveto(x_ticks+25,313);
                    lineto(x_ticks+25,307);
                    x_label := x_ticks+(600*(j-1));
                    x_labelo:= 0+(600*(j-1));
                    str (x_label,x_string);
                    str (x_labelo,x_stringo);
                    outtextxy (25,320,x_stringo);
                    outtextxy (x_ticks+20,320,x_string);
               end;

     b:=1;
     for b :=1 to 5 do
               begin
                    y_ticks := getmaxx;
                    str (y_ticks,y_string);
                    moveto (25,310-(75*b));
                    lineto (28,310-(75*b));
                    outtextxy(15,160,'0');
                    outtextxy(11,10,'2%');
                    outtextxy(14,310,'-2%');
               end;

 end;
```

```
procedure display_data;


 var
     x_point, y_pointC, y_pointG          : longint;
     y_offsetC,y_offsetG                  : longint;
     yC,yG                                : real;
     points_stringC,points_stringG        : string;

begin

          x_point := x + 25  ;
          yC:=10*(scale_pointC-impC)/scale_pointC;
          yG:=1600*(scale_pointG-impG)/scale_pointG;
          str(yC,points_stringC);
          str(yG,points_stringG);
          y_offsetC:=trunc(yC);
          y_offsetG:=trunc(yG);
          y_pointC:=(y_offsetC)+160;
          y_pointG:=(y_offsetG)+160;
          putpixel(x_point,y_pointC,5);
          putpixel(x_point,y_pointG,14);
          outtextxy(240,460,'Hit any key to stop reading');
          outtextxy(425,460,' data from the DVM.');
end;

var
  i,s,loop,r,d                          : integer;
  inpdel,del                            : real;
  f                                     : text;
  c                                     : char;
  fullname,filename,start_point         : string;
  hour,minute,second,sec100             : word;
  g,rescale                             : real;
  hou,min,sec,sec1                      : word;

begin

initialization_ieee;

{set HP4192A, W0 manual sweep, F1 ouput diplays A/B/C, C3
parallel mode, }
{V1 average on, ZO0 zero open off, ZS0 zero short off, FR1
freq. 1kHz,}
{A4 disply A C, B3 display B G, }

writeln(ieeeout,'RESET'); {reset GPIB}
writeln(ieeeout,'OUTPUT HP;F1FR1EN');
writeln(ieeeout,'OUTPUT HP;A4B3EN'); {read G and C}

  clrscr;
```

```
  writeln('Enter the integer value for the required
frequency of readings,');
  write('[ in seconds] :- ');
  readln(inpdel);
  writeln;
  write('Enter the number of data points to be sampled :');
  readln(points);
  writeln;
  writeln('Enter Filename to be saved under (without
extension)....');
     readln(filename);
     fullname :='C:\riccardo\pascal\data\' +filename+'.dat';
     assign(f,fullname);
     rewrite(f);


             {measurement start}

gettime(hour,minute,second,sec100);
writeln('Start time=', hour,':',minute,':',second);
hou:=hour;min:=minute;sec:=second;sec1:=sec100;

graphdriver:=detect;
initgraph(graphdriver,graphmode,'');


         {*****Read in first data point initially****}


  delay(1410);
  aver1:=1;
  x:=0;
  j:=1;
  read_data;
  append(f);
  writeln(f,impC,impG);
  close(f);
  set_page;
  start_point:= stardata;
  scale_pointC:= impC;
  scale_pointG:= impG;
  display_data;
  aver1:=2;

          {*****Read rest of data points with delay****}

 repeat
       d:=1;

       repeat
             delay(1410);
```

```
            d:=d+1;
        until d > inpdel;

        read_data;
        append(f);
        writeln(f, impC,impG);
        close(f);
        display_data;
        aver1:=aver1+1;
        x:=x+1;
        rescale := aver1/(380*j);

        if rescale > 1 then
                    begin
                         clearviewport;
                         x:=0;
                         j:=j+1;
                         set_page;
                    end;

 until (aver1 > points) or (keypressed);

  closegraph;
  writeln(ieeeout,'LOCAL');
  writeln(ieeeout,'FINISH');
  writeln;
  gettime(hour,minute,second,sec100);
  writeln('Start time =' ,hou,':',min,':',sec,':',sec1);
  writeln('End time  = ',hour,
':',minute,':',second,':',sec100);
  writeln(aver1 - 1,' data points collected');
  writeln('Delay time between acquisition =',inpdel);
  writeln;
  writeln('Start values: ', start_point);
  writeln;
  writeln('The data has been saved in ',filename,'.dat');

end.

     {End of Program}
```

Appendix B

PUBLICATIONS

R.Casalini, L.M.Goldenberg, C.Pearson, M.R.Bryce, M.C.Petty, ' An electrical impedance study of Langmuir-Blodgett films containing a tetrabutylammonium Ni(dmit)(2) complex', *Journal of Physics D-Applied Physics*, **30** (1997) 2928-2931

R.Casalini, L.M.Goldenberg, C.Pearson, B.K.Tanner, M.C.Petty, 'The electrical behaviour of multilayer polypyrrole films', *Journal of Physics D-Applied Physics*, **31** (1998) 1504-1510.

R.Casalini, J.Nagel, U.Oertel, M.C.Petty, 'The effect of organic vapours on the permittivity of a co-ordination polymer Langmuir-Blodgett film', *Journal of Physics D-Applied Physics*, **31** (1998) 3146-3153.

R.Casalini, J.Nagel, U.Oertel, M.C.Petty, 'Impedance spectroscopy of thin films of a co-ordination polymer: application to the detection of organic vapours', *Eurosensors XII vol.1* (ed. N.M.White), 1998, IOP Publishing, Bristol, 135-138.

R.Casalini, M.Kilitziraki, D.Wood, M.C.Petty, 'Sensitivity of the electrical admittance of a polysiloxane film to organic vapours', *Sensors and Actuators B*, in press.

R.Casalini, J.N.Wilde, J.Nagel, U.Oertel, M.C.Petty, 'Organic vapour sensing using thin films of a co-ordination polymer: comparison of electrical and optical techniques', *Sensors and Actuators B*, in press.